

**PALACKÝ UNIVERSITY OLMOUC**

Faculty of Science

Department of Cell Biology and Genetics



**CARVONE IS AN ATYPICAL NEGATIVE ALLOSTERIC  
MODULATOR OF ARYL HYDROCARBON RECEPTOR**

**Ph.D. Thesis**

Author: **Mgr. Karolína Ondrová**  
Study program: P1527 Biology  
Study branch: Molecular and Cell Biology  
Form of study: Present  
Supervisor: **prof. RNDr. Zdeněk Dvořák, DrSc. et Ph.D.**  
Submitted: 29<sup>th</sup> May 2023

Olomouc 2023

I hereby declare that this presented Ph.D. thesis is based on my research conducted in the Department of Cell Biology and Genetics, Faculty of Science, Palacký University Olomouc, in the period from September 2017 to May 2023. Co-authors agree with the inclusion of the published results.

Olomouc, 29th May 2023

.....

Mgr. Karolína Ondrová

## **ACKNOWLEDGEMENT**

Firstly, I would like to express my special gratitude to my supervisor Prof. RNDr. Zdeněk Dvořák, DrSc. Ph.D., for the opportunity to join his research team and be a part of several valuable projects. Thank you for your helpful guidance, time, advice, support, and passion for science in making my graduate studies productive. I learned much more than that I had ever hoped for. I am grateful to all my colleagues from the Department of Cell Biology and Genetics for their help and their friendly and pleasant working environment. My special thanks go to my friend and colleague, Mgr. Barbora Vyhřídálová, Ph.D., for huge support. Any attempt at any level could not have been satisfactorily completed without the support of my parents and family who have always been there. Finally, I would like to thank my husband for a lot of advice and understanding.

The research presented in this thesis was financially supported by the following grants: NV19-05-00220 by the Czech Health Science Council, PrF 2018-005, PrF 2019-003, PrF 2020-006, PrF 2021-005, and PrF 2022-009 by student grant projects IGA of Palacký University.

**The data presented in this thesis are contained in the following publications:**

Dvořák, Z., **Pouliková, K.**, Mani, S. (2021). Indole scaffolds as a promising class of the aryl hydrocarbon receptor ligands. *Eur J Med Chem*, 215: 113231. **[IF 7.088]**.

**Ondrová K.**, Zůvalová I., Vyhřídálová B., Krasulová K., Miková E., Vrzal R., Nádvořník P., Nepal B., Kortagere S., Kopečná M., Kopečný D., Šebela M., Rastinejad F., Pu H., Sural M., Rolfes KM., Haarmann-Stemmann T., Li H., Mani S., Dvořák Z. (2023). Monoterpenoid aryl hydrocarbon receptor allosteric antagonists protect against ultraviolet skin damage in female mice. *Nat Commun* 14: 2728. **[IF<sub>2021</sub> 17.694]**.



**Bibliographical identification:**

First name and surname: Mgr. Karolína Ondrová  
Title: Carvone is an atypical negative allosteric modulator of aryl hydrocarbon receptor  
Type of thesis: Ph.D.  
Department: Department of Cell Biology and Genetics  
Supervisor: prof. RNDr. Zdeněk Dvořák, DrSc. et Ph.D.  
The year of presentation: 2023

**Abstract:**

Human aryl hydrocarbon receptor (AhR) is a ligand-activated transcription factor that is a key regulator of human physiology and pathophysiology. Existing AhR antagonists bind to the orthosteric sites. However, allosteric inhibition has not yet been discovered, and was previously thought to be untenable. Dietary monocyclic monoterpenoid carvones were identified as the first non-competitive antagonists of AhR, and we characterized the structural and functional consequences of their binding to AhR. Carvones were found to bind allosterically in the bHLH/PAS-A region of AhR domains and did not displace radiolabeled ligands from binding to AhR. Carvones do not influence the translocation of ligand-activated AhR into the nucleus, but inhibit the heterodimerization of AhR with its canonical partner aryl hydrocarbon receptor nuclear translocator (ARNT) and the subsequent binding of AhR to the CYP1A1 promoter. As a proof of concept, we demonstrated physiologically relevant AhR antagonism by carvones *in vivo* in mice. The selective targeting of AhR by carvones, regardless of the type of bound ligand, provides opportunities for treating AhR-modified diseases.

**Keywords:** Aryl hydrocarbon receptor, antagonism, monoterpenoid, carvone, allosteric binding site

**Number of pages:** 134

**Number of appendices:** 2

**Language:** English

## **Bibliografická identifikace**

Jméno a příjmení:	Mgr. Karolína Ondrová
Titul:	Karvon je atypickým negativním alosterickým modulátorem aryl uhlovodíkového receptoru
Druh práce:	Ph.D.
Pracoviště:	Katedra buněčné biologie a genetiky
Školitel:	prof. RNDr. Zdeněk Dvořák, DrSc. et Ph.D.
Rok odevzdání:	2023

## **Abstrakt:**

Lidský aryl uhlovodíkový receptor (AhR) je ligandem aktivovaný transkripční faktor, který hraje důležitou roli v lidské fyziologii a patofyziologii. Mnoho známých antagonistů se váže na ortosterická místa receptorů, zatímco alosterická inhibice AhR nebyla dosud popsána a dříve byla považovaná za nedosažitelnou. Monocyklické monoterpenoidy karvony pocházející ze stravy byly v této práci poprvé identifikovány jako nekompetitivní antagonisté AhR a byly charakterizovány strukturální a funkční důsledky jejich vazby na AhR. Bylo zjištěno, že karvony se alostericky váží v oblasti bHLH/PAS-A domén AhR a zároveň nevytěsňují radioaktivně značené ligandy z vazby na AhR. Karvony neovlivňují translokaci ligandem aktivovaného AhR do jádra, ale inhibují heterodimerizaci AhR s jeho kanonickým partnerem ARNT a následnou vazbu AhR do promotoru CYP1A1. Karvony vyvolaný AhR antagonismus byl demonstrován také *in vivo* na myších. Selektivní cílení AhR za pomoci karvonů bez ohledu na typ přítomného ligandu by mohlo poskytnout příležitost pro léčbu chorobných procesů, do jejichž regulace je AhR zapojen.

**Klíčová slova:** Aryl uhlovodíkový receptor, antagonismus, monoterpen, karvon, alosterické vazebné místo

**Počet stran:** 134

**Počet příloh:** 2

**Jazyk:** Angličtina

## TABLE OF CONTENTS

INTRODUCTION.....	13
AIMS .....	14
THEORETICAL PART.....	15
1 Aryl hydrocarbon receptor .....	15
2 AhR signaling .....	16
2.1 Canonical genomic AhR signaling .....	17
2.2 Non-canonical genomic AhR signaling.....	18
2.3 Non-genomic AhR signaling.....	20
2.4 Negative-feedback regulation of AhR activity.....	21
2.5 AhR-ARNT-HIF1 $\alpha$ signaling .....	23
3 Physiological and pathophysiological processes involving the AhR .....	25
3.1 Role of AhR in physiological processes .....	25
3.2 Role of AhR in pathophysiological processes .....	27
4 Receptor theory.....	29
4.1 Agonism and antagonism .....	31
5 AhR ligands.....	34
5.1 Xenobiotic AhR ligands .....	34
5.1.1 Environmental pollutants .....	35
5.1.2 Dietary ligands.....	39
5.1.3 Drugs.....	43
5.1.4 Other AhR-active xenobiotic ligands.....	45
5.2 Endogenous AhR ligands.....	49
5.2.1. Microbial ligands.....	51
5.2.2 Ultraviolet light-produced AhR ligands.....	53
6 Essential oils .....	55
6.1 Essential oils and AhR .....	55
6.2 Carvone .....	57
EXPERIMENTAL PART .....	59
7 Materials.....	59
7.1 Biological materials .....	59
7.2 Compounds and reagents.....	60
8 Methods .....	62
8.1 Cytotoxicity test (MTT) .....	62
8.2 Reporter gene assay.....	62

8.3	Quantitative real-time polymerase chain reaction qRT-PCR .....	63
8.4	Simple western blotting by Sally Sue™ .....	64
8.5	7-ethoxyresorufin-O-deethylase activity (EROD) .....	65
8.6	Radioligand binding assays .....	65
8.7	Intracellular distribution of AhR .....	67
8.8	Protein immunoprecipitation assay .....	67
8.9	Chromatin immunoprecipitation assay .....	68
8.10	Protein kinase C inhibition assay .....	68
8.11	KINOMEScan™ profiling .....	69
8.12	Tyrosine-protein phosphatases non-receptor type inhibition assays .....	69
8.13	HSP90 fluorescence competitive binding assay.....	69
8.14	Molecular modeling and Docking .....	70
8.15	Thermal shift assay .....	71
8.16	Cellular thermal shift assay .....	72
8.17	Microscale thermophoresis .....	72
8.18	Covalent functionalization of the AhR with azido-S-carvone .....	74
8.19	Animal experiments .....	75
8.20	Statistics .....	76
9	RESULTS.....	77
9.1	Cytotoxicity of carvone .....	77
9.2	The effect of carvone and AhR agonists on transcriptional activity of AhR... 77	
9.3	The effect of S-carvone on agonist-inducible AhR activity .....	79
9.4	Down-regulation of AhR target genes by carvones .....	83
9.5	Influence of carvone on AhR cellular functions .....	88
9.6	Binding of carvones to the AhR.....	91
9.7	Carvone binds to AhR but not ARNT .....	95
9.8	Carvone does not inhibit the transcriptional activity of ARNT .....	100
9.9	S-carvone does not inhibit protein kinases.....	101
9.10	Carvone does not interact with AhR-related off-targets.....	102
9.11	Carvone antagonize Ahr in mouse skin.....	104
	DISCUSSION.....	107
	CONCLUSION .....	112
	REFERENCES.....	114
	CURRICULUM VITAE.....	132

## ABBREVIATIONS

<sup>3</sup> H	tritium; radioactive isotope of hydrogen
3-MC	3-methylchlorantrene
3-MI	3-methylindole
6BIO	6-bromoindirubin-30-oxime
ACE2	angiotensin-converting enzyme 2
AhR	aryl hydrocarbon receptor
AhRR	aryl hydrocarbon receptor repressor
Ala	alanine
AR	androgen receptor
ARNT	aryl hydrocarbon receptor nuclear translocator
ATP	adenosine triphosphate
BaP	benzo[a]pyrene
bHLH	basic helix-loop-helix
BRCA1	breast cancer gene 1, tumor suppressor
CBP	CREB-binding protein
CDK	cyclin D–cyclin-dependent kinase
cDNA	complementary DNA
CH223191	2-methyl-2H-pyrazole-3-carboxylic acid
ChIP	chromatin immunoprecipitation
cMaf	transcription factor cellular viral musculoaponeurotic fibrosarcoma
COVID-19	coronavirus disease 2019
c-Rel	subunit of nuclear factor-κB, transcription factor
CRL4	cullin 4-RING ubiquitin ligase
CUL4B	cullin-RING ligase 4B complex
Cxcl5	C-X-C motif chemokine 5
CYP	cytochrome P450
DAPI	4',6-diamino-2-phenylindole
DEX	dexamethasone
dFICZ	6,12-diformylindolo[3,2-b]carbazole
DFX	deferoxamine mesylate
DIM	3,3'-diindolylmethane
DMBA	7,12-dimethylbenz[a]anthracene
DMEM	Dulbecco's modified Eagle's medium
DMSO	dimethyl sulfoxide
DNA	deoxyribonucleic acid
DRE	dioxin responsive element
DRE-luc	pGL-4.27- dioxin responsive element reporter plasmid
DSS	dextran sodium sulfate
E2F	transcription factor
E3	ubiquitin-ligase
EC <sub>50</sub>	half-maximal effective concentration
EC <sub>80</sub>	80 % of the maximal agonist effect
EDTA	ethylenediaminetetraacetic acid
EFSA	European Food Safety Authority
E <sub>MAX</sub>	maximal effective concentration
EO	essential oil
ER	estrogen receptor
EROD	7-ethoxyresorufin-O-deethylase

ER $\alpha$	estrogen receptor alpha
ER $\beta$	estrogen receptor beta
FAK	focal adhesion kinase
FBS	fetal bovine serum
FICZ	6-formylindolo[3,2-b]carbazole
FKK2	di(1H-indol-2-yl)(pyridin-4-yl)methanol
FKK9	1-(1-(ethoxymethyl)-1H-indol-2-yl)-2-(1H-indol-2-yl)-1-(pyridin-4-yl)ethan-1-ol
GAPDH	glyceraldehyde-3-phosphate dehydrogenase
GNF351	N-(2-(1H-indol-3-yl)ethyl)-9-isopropyl-2-(5-methyl pyridine-3-yl)-9H-purin-6-amine
GR	glucocorticoid receptor
GSK3iXV	Pyridocarbazolo-cyclopentadienyl Ruthenium complex GSK3 inhibitor XV
GST	glutathione S-transferases
HaCaT	human immortalized keratinocytes
HAHs	halogenated aromatic hydrocarbons
H/E	hematoxylin/eosin
HEPES	4-(2-hydroxyethyl)-1-piperazineethanesulfonic acid
HIF-1	hypoxia-inducible factor 1
HIF-1 $\alpha$	alpha subunit of hypoxia-inducible factor 1
HIF1 $\beta$	beta subunit of hypoxia-inducible factor 1
HRP	horseradish peroxidase
HSP90	90 kDa heat shock protein
I3C	indole-3-carbinol
IC <sub>50</sub>	half-maximal inhibitory concentration
ICZ	indolo [3,2-b] carbazole
IEL	intraepithelial lymphocyte
IL	interleukin
ILC	innate lymphoid cell
ILC3	innate lymphoid cell type 3
ITE	2-(1'H-indole-3'-carbonyl)-thiazole-4-carboxylic acid methyl ester
K <sub>D</sub>	equilibrium dissociation constant
K <sub>i</sub>	equilibrium inhibitor dissociation constant
KLF6	Krüppel-like factor 6
Leu	leucine
LH75	primary human hepatocytes
LXA <sub>4</sub>	lipoxin A4
LXB <sub>4</sub>	lipoxin B4
Lys	lysine
MEM	minimum essential medium
MNF	3'-methoxy-4'-nitroflavone
MTT	3-[4,5-dimethylthiazole-2-yl]-2,5-diphenyltetrazolium bromide
N <sub>3</sub>	azide group
NaCl	sodium chloride
NAD(P)H	nicotinamide adenine dinucleotide (phosphate)
NC-XRE	non-consensus xenobiotic-responsive elements
NES	nuclear export sequence
NF- $\kappa$ B	nuclear factor- $\kappa$ B
NK	natural killer cells

NLS	nuclear localization sequence
NRF2	erythroid 2-related factor 2
p21 <sup>cip1</sup>	cyclin-dependent kinase inhibitor 1
p23	23 kDa co-chaperone
p27 <sup>Kip1</sup>	cyclin-dependent kinase inhibitor 1B
p50	50 kDa subunit of nuclear factor-κB
p52	52 kDa subunit of nuclear factor-κB
p53	tumor suppressor p53
PAH	polycyclic aromatic hydrocarbon
PAI-1	plasminogen-1 activator inhibitor
PARP	poly(ADP-ribose) polymerase
PAS	Per-Arnt-Sim domain
PBS	phosphate buffered saline
PCB	polychlorinated biphenyl
PCR	polymerase chain reaction
PD98059	2-(2'-amino-3'-methoxyphenyl)-oxanaphthalen-4-one
PGBB3	prostaglandin B3
Phe	phenylalanine
PKC	protein kinase C
PPAR $\gamma$	peroxisome proliferator-activated receptor $\gamma$
PR	progesterone receptor
pRB	hypophosphorylated form retinoblastoma protein
Pro	proline
PTP1B	protein tyrosine phosphatase 1B
PTPN11	protein tyrosine phosphatase non-receptor type 11
PTPN6	protein tyrosine phosphatase non-receptor type 6
PY108	(1H-indol-3-carbonyl) picolinonitrile
PY109	(1H-indol-3-yl) (6- (trifluoromethyl) pyridin-2-yl) methanone
qRT-PCR	quantitative real-time polymerase chain reaction
RB	retinoblastoma protein
RelA	subunit of nuclear factor-κB, transcription factor
RelB	subunit of nuclear factor-κB, transcription factor
RNA	ribonucleic acid
Rplp0	ribosomal protein lateral stalk subunit P0
RT	room temperature
RT-PCR	reverse transcription polymerase chain reaction
RXR $\alpha$	retinoid X receptor alpha
SD	standard deviation
SB216763	3-(2,4-Dichlorophenyl)-4-(1-methyl-1H-indol-3-yl)-1H-pyrrole-2,5-dione
SDS	sodium dodecyl sulfate
SDS-PAGE	sodium dodecyl sulfate–polyacrylamide gel electrophoresis
SIM	single-minded proteins
siRNA	small interfering RNA
SOS1	son of sevenless
Src	tyrosine-protein kinase Src
SULT	sulfotransferase
TCDD	2,3,7,8-tetrachlorodibenzodioxin
TCDF	2,3,7,8-tetrachlorodibenzofuran
TEACOP	trace-extended aromatic condensation product

TEF	toxic equivalency factor
Th17	T-helper 17 cell
TIPARP	TCDD Inducible Poly(ADP-Ribose) Polymerase
TMF	6,2',4'-trimethoxyflavone
Treg	regulatory T cells
Tris	tris(hydroxymethyl)aminomethane
Trp	L-tryptophan
TSA	thermal shift analyses
TSU-16	(Z)-3-[(2,4-dimethylpyrrol-5-yl)methylidene]-2-indolinone
Tyr	tyrosine
UGT	UDP glucuronosyltransferases
UV	ultraviolet
VAF347	[4-(3-chloro-phenyl)-pyrimidin-2-yl]-(4-trifluoromethyl-phenyl)-amine
VEGF	vascular endothelial growth factor
XAP2	AIP or ARA9; hepatitis B Virus X-associated protein 2
XRE	xenobiotic-responsive elements



## INTRODUCTION

The aryl hydrocarbon receptor (AhR), a ligand-activated transcription factor, is a critical target for treating several diseases. Whereas agonists are used to treat atopic dermatitis or inflammatory bowel disease, AhR antagonists have been proposed as therapeutic strategies for viral diseases, such as Zika, COVID-19, and cancer. Existing antagonists are ligand-dependent and have limited clinical use. However, ligand-independent AhR antagonists have not been identified. Therapeutic targeting of AhR has been neglected for several years, mainly because of the negative stigma that it is a receptor that mediates dioxin toxicity. With the growing knowledge of the physiological and pathophysiological roles of AhR, researchers have focused on breaking this paradigm. Majority of current drugs are designed to bind directly to primary active orthosteric sites, leading to the modification of enzyme or receptor functions. Targeting allosteric sites is an emerging approach to drug discovery.

It is likely that the most significant activation of AhR by ligands originates from food sources. Recently, the essential oils of dill, caraway, and spearmint were found to antagonize AhR and the common components responsible for this effect, S- and R-carvone, were identified. However, the underlying molecular mechanism remains unclear. This study focused on elucidating the antagonistic effects of carvones on AhR by applying a series of complementary mechanistic experiments. Selective targeting of AhR activity may be beneficial for modulation of intestinal immunity, chemoprotection, and chemoprevention of the skin.

## **AIMS**

The aim of this study was to investigate the antagonistic effects of carvones on the AhR.

1. *In vitro* mechanism of the carvone antagonist effects on AhR.
2. *In vivo* antagonistic effects of carvone on AhR-dependent function.

# THEORETICAL PART

## 1 Aryl hydrocarbon receptor

The aryl hydrocarbon receptor (AhR) is a ligand-activated transcription factor that belongs to the family of basic-helix-loop-helix Per-Arnt-Sim (bHLH/PAS) transcription factors. This receptor was discovered as the first xenosensor to mediate the induction of aryl hydrocarbon hydroxylase using polycyclic hydrocarbons (Nebert et al., 1972) and halogenated polyaromatics (Poland et al., 1976). AhR can be activated by structurally diverse synthetic and naturally occurring chemicals, as described in detail in Chapter 5. AhR is highly expressed in the human and mouse lungs, liver, kidney, spleen, and placenta (Abel et Haarmann-Stemmann, 2010).

The AhR gene is located on chromosome 7p15, and the human AhR protein consists of 848 amino acid residues (Micka et al., 1997). The structure of AhR includes some functional domains. At the N-terminal, AhR contains the bHLH domain, which is responsible for DNA binding and protein–protein interactions. This is followed by the PAS domain, which consists of two structural repeats, PAS-A and PAS-B. They contribute to dimer formation via a heterodimerization partner known as AhR nuclear translocator (ARNT) and chaperone proteins, such as heat shock protein 90 (HSP90). Moreover, the PAS-B domain contained ligand-binding site. The C-terminal domain contains three subdomains: enriched acidic (glutamate/aspartate) subdomain, enriched glutamine subdomain and subdomain enriched with serine, threonine, and proline, which are responsible for transcriptional activation after DNA binding (Larigot et al., 2018). The structure of the AhR protein is shown in Figure 1.

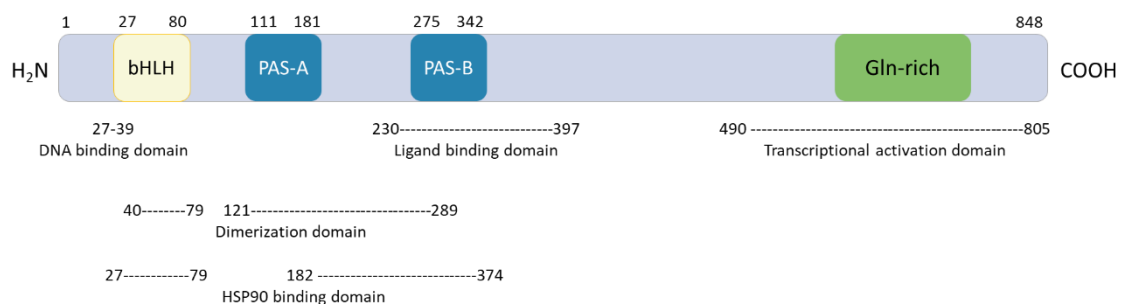


**Figure 1: Aryl hydrocarbon receptor functional domains** (Malorni et al., 2012).

## 2 AhR signaling

AhR controls the transcription of a wide variety of genes involved in the xenobiotic metabolism, immune homeostasis, cell cycle, cell differentiation, and energy metabolism (Vyhlidalova et al., 2020b). The inactive form of AhR resides in a complex form with p23 (23 kDa co-chaperone), XAP2 (hepatitis B Virus X-associated protein 2; also known as AIP or ARA9), and two molecules of the chaperone protein HSP90 in the cytosol. Studies have suggested that Src tyrosine kinase is also a member of this complex (Larigot et al., 2018; Rothhammer et Quintana, 2019; Wang et al., 2020). This chaperone complex maintains AhR in a high-affinity state for ligand binding and prevents proteasomal degradation of AhR (Denison et Nagy, 2003; Petrusis et Perdew, 2002). Upon ligand binding, the chaperone complex dissociates, and AhR undergoes a conformational change that exposes nuclear localization sequences (NLSs), resulting in the translocation of AhR into the nucleus. Subsequently, AhR heterodimerizes with the AhR nuclear translocator (ARNT/HIF1 $\beta$ ) (see Chapter 2.4) or other non-canonical factors (see Chapter 2.2) and binds to the specific DNA recognition sites, thereby inducing the expression of AhR-target genes. In addition to AhR-induced genomic effects, it can also act in a non-genomic manner (Holme et al., 2019). Following the transcription of downstream genes, the nuclear export sequence (NES) present in the AhR is responsible for the AhR export from the nucleus to the cytoplasm, where AhR is subjected to proteasomal degradation in the 26S proteasome (Ma et Baldwin, 2000).

AhR activation is influenced by ligand-binding and post-translational modifications, particularly phosphorylation. AhR phosphorylation plays an important role in the transformation of inactive AhR into an active AhR-ARNT dimer (Li et Dougherty, 1997) and affects the binding activity of the heterodimer to the DNA promoter region (Puga et al., 2002). It is catalyzed by protein kinase C (PKC) and mitogen-activated protein kinases (MAPKs) (Delescluse et al., 2000; Henklova et al., 2008). Phosphorylation of the co-chaperone HSP90 subunits in the AhR complex at amino acids Ser225 and Ser254 of HSP90 $\beta$  and Ser230 of HSP90 $\alpha$  has been shown to modulate the formation of a functional cytosolic AhR complex (Ogiso et al., 2004). Furthermore, phosphorylation

of serine residues in the NLS sequence inhibits ligand-dependent nuclear AhR import (Ikuta et al., 2004; Puga et al., 2009).

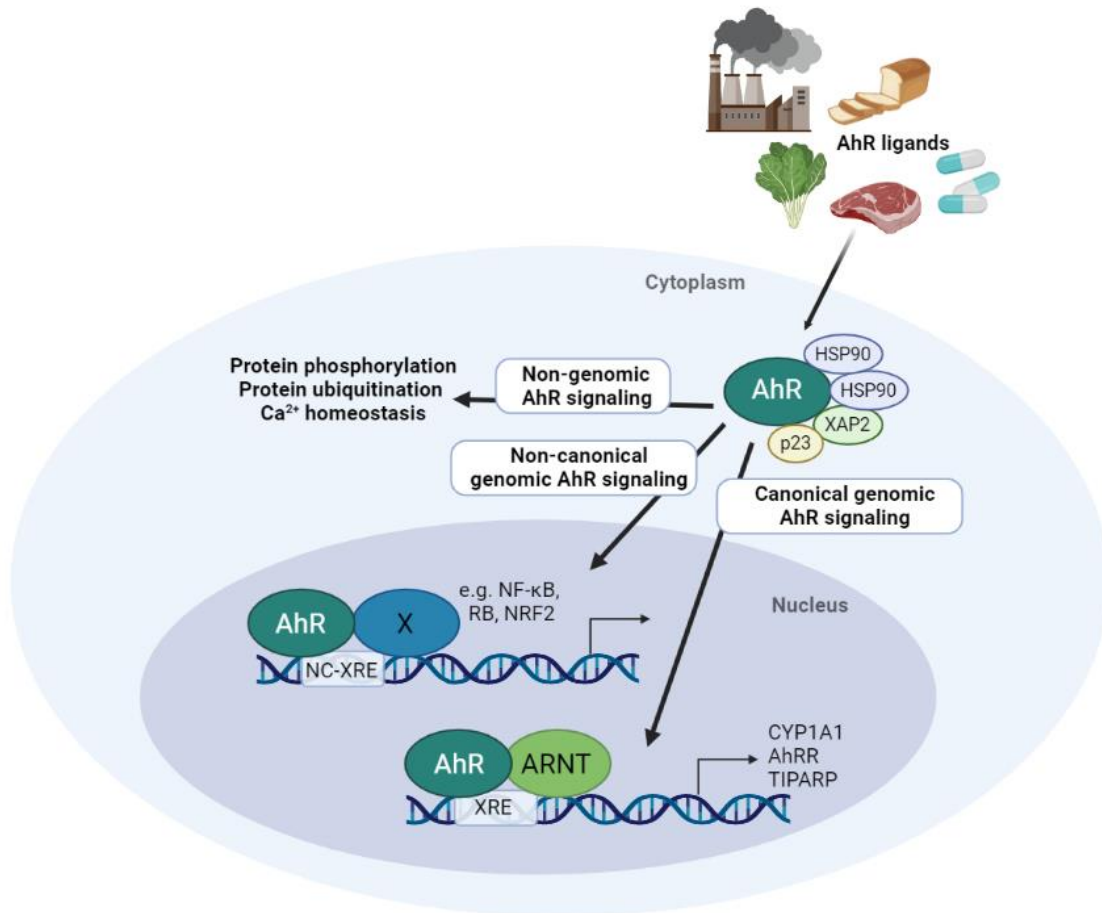


Figure 2: AhR signaling pathway (Holme et al., 2019).

## 2.1 Canonical genomic AhR signaling

Upon ligand binding, AhR translocates into the nucleus and forms an active high-affinity DNA-binding heterodimer with ARNT, which binds to specific DNA recognition sites, multiple xenobiotic response elements (XREs), also known as dioxin response elements (DREs), upstream of cytochrome P450 (CYPs), and other AhR-responsive genes (Denison et Nagy, 2003). AhR target genes include CYP1A1, CYP1A2, CYP1B1, UDP glucuronosyltransferases (UGTs), glutathione S-transferases (GSTs) (Vogel et al., 2020), AhR repressor (AhRR), 2,3,7,8-tetrachlorodibenzodioxin (TCDD) inducible poly(ADP-ribose) polymerase (TIPARP), and son of sevenless (SOS1) (Denison et al., 2011). The specific DRE/XRE sequence, 5'-TNGCGTG-3', is highly evolutionarily

conserved. Nucleotide substitution in this region causes a multiple-fold reduction in AhR affinity for the response elements (Yao et Denison, 1992). In addition, AhR can affect gene expression through its ability to function as a coactivator for other nuclear transcription factors (Denison et Faber, 2017), such as the estrogen receptor (ER) (Gottel et al., 2014; Matthews et Gustafsson, 2006) and glucocorticoid receptor (GR) (Dvorak et al., 2008; Wang et al., 2009).

## **2.2 Non-canonical genomic AhR signaling**

The non-canonical AhR pathway is characterized by the binding of a heterodimerization partner other than ARNT to the AhR (Wright et al., 2017). AhR can interact with proteins (Denison et al., 2011), such as nuclear factor- $\kappa$ B (NF- $\kappa$ B) (Kim et al., 2000; Tian et al., 2002), Krüppel-like factor 6 (KLF6) (Wilson et al., 2013), nuclear factor erythroid 2-related factor 2 (NRF2) (Esser et Rannug, 2015; Miao et al., 2005), hypophosphorylated retinoblastoma protein (pRB) (Levine-Fridman et al., 2004), and transcription factor c-Maf (Nguyen et al., 2013). The heterodimer binds to a non-consensus XRE (NC-XRE), defined by the repeated tetranucleotide motif (5'-GGGA-3') (Huang et Elferink, 2012).

The AhR-NF- $\kappa$ B crosstalk can affect diverse cellular processes, including adaptive and innate immunity, inflammatory responses, cell differentiation, proliferation, and apoptosis (Vogel et Matsumura, 2009). NF- $\kappa$ B consists of five subunits (p50, p52, RelA, RelB, and c-Rel); of which, RelA and RelB can interact with AhR (Vogel et al., 2007). Dimerization of AhR with the NF- $\kappa$ B subunit RelA is transcriptionally inactive in CYP1A1 and interleukin-6 (IL-6) gene activity. In contrast, heterodimer AhR-RelB is capable of binding to the DRE, inducing transcription of the CYP1A1 gene, as well as binding to RelBAhRE binding sites that activate NF- $\kappa$ B target genes, such as chemokines, primarily IL-8 (Vogel et Matsumura, 2009). AhR also cooperates with c-Maf to control immune response. AhR-c-Maf complexes induce transcription of IL-10 and IL-21 (Nguyen et al., 2013).

NRF2 expression can be modulated by ligand-activated AhR; conversely, AhR expression can be modulated by the NRF2 signaling pathway. Both AhR and NRF2 are the key regulators of the cytoprotective responses

to environmental stress. AhR primarily regulates the expression of biotransformation phase I enzymes, whereas NRF2 regulates biotransformation phase II enzymes (GSTs and UGTs) and phase III transporters (multidrug resistance-associated proteins). Shin et al. reported that pharmacological activation of NRF2 induces *AhR* mRNA and mRNA expression of AhR-target genes *in vitro* (Shin et al., 2007). In addition, 2,3,7,8-tetrachlorodibenzodioxin (TCDD), the most effective xenobiotic AhR inducer (Denison et Nagy, 2003), activates NRF2 activity in an AhR-dependent manner, leading to the induction of NRF2 target genes, including *Nqo1* and *Gsta1* (Yeager et al., 2009).

The transition from G1 to S phase of the cell cycle is controlled by the phosphorylation of retinoblastoma protein (RB) by some CDK (cyclin-dependent kinase) complexes, which release RB from the RB-E2F complex, leading to the increased expression of E2F-dependent cell cycle genes. In the presence of AhR agonists, two mechanisms of AhR-dependent cell cycle arrest have been proposed. Ligand-activated AhR binds RB-E2F and inhibits RB release, resulting in repression of E2F-dependent gene expression. In addition, ligand-activated AhR complexed with ARNT can bind RB and induce the CDK2 inhibitor *p27<sup>kip1</sup>* gene expression. In both cases, AhR-RB interactions lead to G1/S phase cell cycle arrest (Denison et al., 2006). Cell cycle arrest is also associated with the induction of the CDK inhibitor *p21<sup>CIP1</sup>*, whose transcriptional induction is triggered by the complex AhR-KLF6 (Huang et Elferink, 2012; Wilson et al., 2013). The association between AhR and KLF6 also induces the expression of plasminogen activator inhibitor-1 (PAI-1, *serpine1*) (Jackson et al., 2015).

## 2.3 Non-genomic AhR signaling

AhR has also been shown to control cellular processes through non-genomic signaling pathways by affecting protein phosphorylation, ubiquitination, and regulation of calcium ion levels (Grosskopf et al., 2021; Holme et al., 2019; Quintana et Sherr, 2013). Majority of the AhR-active environmental compounds are lipophilic, and the accumulation of chemicals in the membrane affects the plasma membrane organization in human endothelial cells. A rapid and transient increase in intracellular calcium concentration was observed following treatment with benzo[a]pyrene (BaP) (Mayati et al., 2012), TCDD (Puga et al., 1992), and organic diesel exhaust particle extract (Brinchmann et al., 2018).

Ohtake et al. (2007) identified AhR as a ligand-dependent E3 ubiquitin ligase, part of the atypical cullin-RING ligase 4B complex (CUL4B<sup>AhR</sup>), whereby AhR functions as a substrate-specific adapter to target proteins for ubiquitination and proteasomal degradation (Ohtake et al., 2007). The discovery of the CUL4B<sup>AhR</sup> complex suggests that the adverse effects of AhR ligands on sex hormone signaling can be attributed to the increased degradation of sex steroid receptors through the E3 ubiquitin ligase activity of AhR (Ohtake et al., 2009). AhR-dependent protein degradation has been observed for the ER (Wormke et al., 2003), peroxisome proliferator-activated receptor  $\gamma$  (PPAR $\gamma$ ) (Dou et al., 2019), and the androgen receptor (AR) (Ghotbaddini et Powell, 2015). On the other hand, ligand binding to AhR can lead to the functional activation of Src tyrosine kinase by releasing it from the AhR complex. Activation of Src can be rapidly accompanied by the activation of MAP kinases or phosphorylation of the E3 ubiquitin ligase c-CBL and degradation of spleen tyrosine kinase SYK through the AhR-c-Src-c-Cbl pathway, which consequently inhibits osteoclastogenesis and bone destruction in arthritis (Grosskopf et al., 2021; Jia et al., 2019). Activation of Src can also lead to the activation of the focal adhesion kinase FAK and by the modification of the cell adhesion properties by disrupting the focal adhesion points (Larigot et al., 2018; Tomkiewicz et al., 2013).



## 2.4 Negative-feedback regulation of AhR activity

The AhR function is regulated by a negative feedback mechanism. The following strategies were employed: a) CYP1-catalysed degradation of the AhR-activating ligand, b) Repression of AhR transactivation by AhRR, and c) induced degradation of AhR through TIPARP-mediated ribosylation (Figure 3).

AhR activation induces CYP1 enzymes that oxidize AhR ligands, leading to their metabolic clearance and detoxification (Schiering et al., 2017; Wincent et al., 2012). Deletion of CYP1 enzymes delays ligand metabolism, resulting in increased AhR signaling *in vivo* (Schiering et al., 2017).

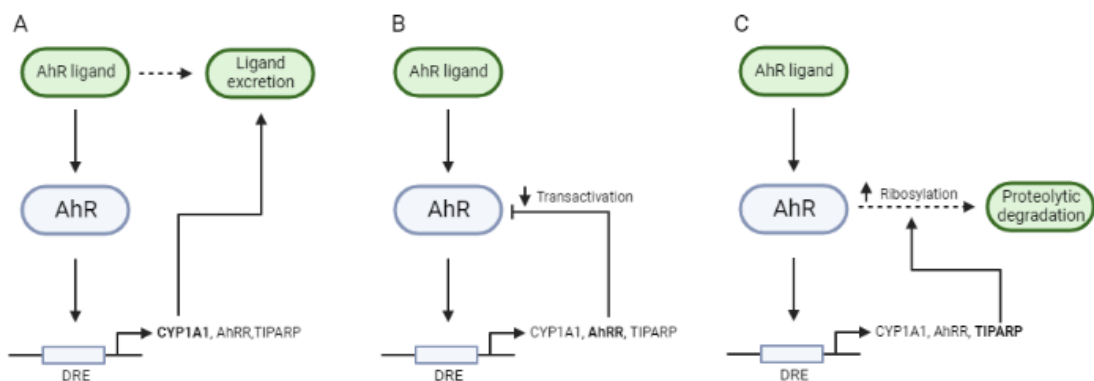


**Figure 3: Mechanisms for negative-feedback regulation of AhR activity. PANEL A:** CYP1-catalysed degradation of AhR-activating ligands. **PANEL B:** Repression of AhR transactivation by AhRR. **PANEL C:** Induced AhR degradation through TIPARP-mediated ribosylation. (Stockinger et al., 2021).

AhR also induces the expression of its competitive repressor AhRR. AhRR competes with AhR for ARNT binding (Figure 4). The AhRR–ARNT dimer binds to XRE but does not trigger transcription, thereby blocking AhR transcriptional activity (Matthews, 2012). Similar to AhR, AhRR belongs to the bHLH/PAS protein family but lacks functional ligand-binding and transactivation domains (Vogel et Haarmann-Stemmann, 2017).

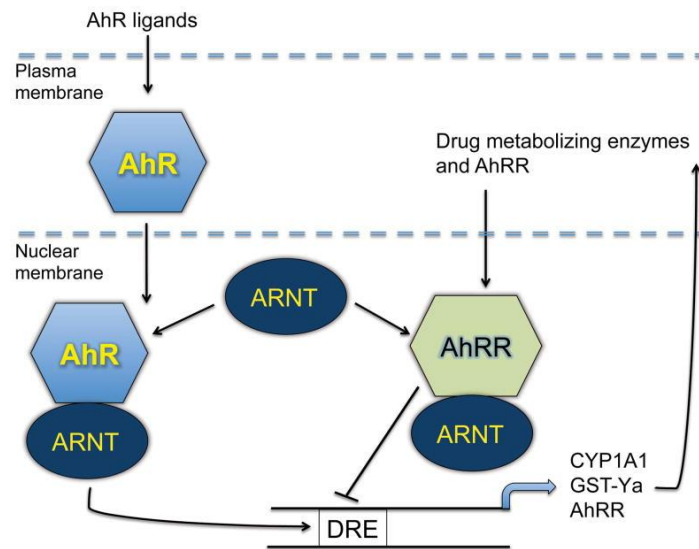


**Figure 4: Repression of the canonical AhR signaling pathway by AhRR.** Adopted from (Vogel et Haarmann-Stemmann, 2017).

The AhR target gene, TIPARP, has also been reported to be a part of a negative feedback loop that regulates AhR activity (Matthews, 2012). ADP-ribosylation is a ubiquitous post-translational protein modification that is important for multiple cellular activities, including transcription, proliferation, DNA repair, and apoptosis. The synthesis of poly-ADP-ribose polymers is catalyzed by members of the poly(ADP-ribose) polymerase (PARP) family (MacPherson et al., 2013). *In vivo* studies have revealed that TIPARP-knockout mice have an increased susceptibility to a dioxin-induced wasting syndrome, steatohepatitis, lethality, and impaired AhR-mediated antiviral innate defense (Ahmed et al., 2015; Stockinger et al., 2021). Downregulation of TIPARP levels by siRNA led to the increased expression of *CYP1A1* and *CYP1B1* mRNA and, simultaneously, inhibited the proteasomal degradation of AhR after TCDD treatment. In contrast, TIPARP overexpression significantly reduced the level of CYP1 enzyme levels. These effects were not been observed in other members of the PARP family. Therefore, TIPARP is considered to be a selective repressor of AhR activity (MacPherson et al., 2013).

## 2.5 AhR-ARNT-HIF1 $\alpha$ signaling

Hypoxia-inducible factor 1 (HIF-1) is a heterodimeric transcription factor that belongs to the bHLH/PAS protein family. It consists of an oxygen-regulated  $\alpha$ -subunit HIF-1 $\alpha$  and a constitutively expressed  $\beta$ -subunit HIF-1 $\beta$  (Ziello et al., 2007). HIF-1 regulates genes involved in oxygen homeostasis and directs the migration of mature endothelial cells to a hypoxic environment by regulating vascular endothelial growth factor (VEGF) (Dery et al., 2005; Hewitson et Schofield, 2004). Importantly, HIF-1 $\beta$  is identical to the vertebrate protein, ARNT (Dery et al., 2005). ARNT, also designated as HIF-1 $\beta$ , heterodimerizes with the alpha subunits of HIF-1, -2, and -3 (Rankin et Giaccia, 2008). Under hypoxia, the HIF- $\alpha$  subunits are stabilized and translocated to the nucleus. They form a heterodimer with ARNT, which activates transcription by recruiting the transcriptional activators p300 and CREB-binding protein (CBP) to hypoxia response elements located within the regulatory elements of VEGF (Rankin et Giaccia, 2008).

The important role of ARNT in both the AhR and HIF-1 $\alpha$  signaling pathways has been demonstrated, suggesting possible crosstalk between these two signaling pathways (Figure 5). Hypoxia can cause HIF-1 $\alpha$  to take over the ARNT for itself, thereby inhibiting the activation of the AhR transcriptional response to the AhR ligand. Conversely, exposure to AhR ligands may attenuate HIF-1 $\alpha$ -mediated reactions under hypoxia. Nie et al. showed that TCDD significantly reduced the hypoxia-mediated reporter gene activity, and the hypoxia response inducers, deferoxamine and cobalt chloride, inhibited AhR-mediated CYP1A1 enzyme activity in B-1 cells (Nie et al., 2001). In addition, Gassmann et al. reported that hypoxia inhibits AhR-mediated CYP1A1 mRNA expression in Hepa1 cells (Gassmann et al., 1997).

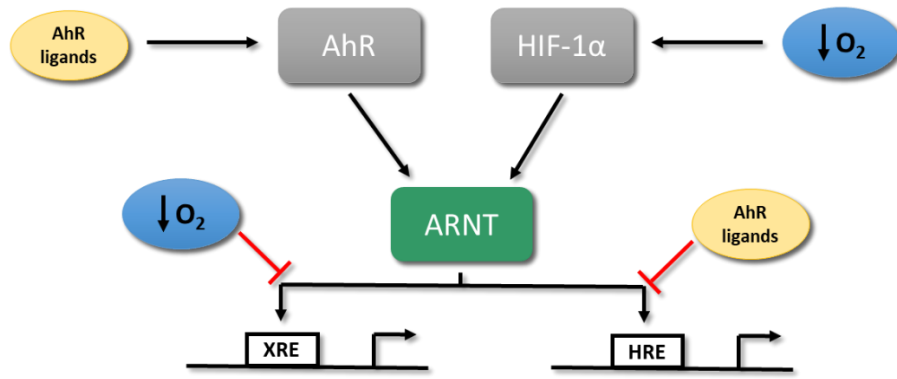


**Figure 5: Crosstalk of AhR-ARNT-HIF1 $\alpha$  signaling.** (Vorrink et Domann, 2014).

## **3 Physiological and pathophysiological processes involving the AhR**

AhR has long been considered a transcriptional mediator of xenoprotective and drug-metabolizing genes (Dvorak et al., 2021). However, AhR has been found to regulate various genes, such as p21<sup>CIP1</sup>, p27<sup>KIP1</sup>, c-jun, junD, Bax, IL-6, IL-22, PAI-1, among others (Bock et Köhle, 2006; Jackson et al., 2015; Rothhammer et Quintana, 2019), suggesting that AhR is involved in multiple physiological and pathological processes, and the therapeutic targeting of AhR is an emerging issue.

### **3.1 Role of AhR in physiological processes**

AhR plays a role in diverse physiological processes, such as circadian rhythm, detoxification, cell proliferation and differentiation, reproduction, and vascular, hematopoietic, and nervous development (Kewley et al., 2004; Larigot et al., 2018; Rothhammer et Quintana, 2019). Studies in AhR-deficient mice have revealed an important role of AhR in the development and functioning of various organs. AhR-deficient mice exhibit hepatic and skin defects and abnormalities in vascular and hematopoietic development (Barouki et al., 2007). *In vivo*, altered AhR signaling increases postnatal mortality, slows growth, reduces fertility, and causes liver pathology (Harrill et al., 2013; Rothhammer et Quintana, 2019; Walisser et al., 2004). Abnormal AhR expression can disrupt proliferation and differentiation into various hematopoietic lineages and their transformation into terminal hematopoietic phenotypes (Angelos et Kaufman, 2018). AhR inhibition, as well as AhR gene deletion using the CRISPR/Cas9 system, enhances the proliferation and differentiation of natural killer cells from human embryonic stem cells, whereas AhR hyperactivation suppresses the development of hematopoietic progenitor cells and accelerates their differentiation into more mature hematopoietic lineages (Angelos et Kaufman, 2018; Angelos et al., 2017).

Ligand-dependent AhR signaling pathway controls cell proliferation. The effects of AhR ligands on the induction or inhibition of cell proliferation likely

depend on the other signals received during the G1 and G1/S phases (Puga et al., 2002). AhR activation has been shown to lead to cell cycle arrest in several cell models. Bar Hoover et al. showed that TCDD treatment of human breast cancer cells induces G1 cell cycle arrest (Bar Hoover et al., 2010). In addition, experiments with rat liver tumor cell lines revealed that TCDD delayed G1/S progression in 5 L hepatoma cells (Weiss et al., 1996). Moreover, the AhR target gene induction levels were observed to vary at different stages of the cell cycle. MCF-7 cells showed up to 6-fold higher inducibility of CYP1A1 and CYP1B1 after incubation with BaP in the S-phase than that in the G1-phase (Hamouchene et al., 2011).

AhR is an essential regulator of the gut innate immune system and is responsible for the intestinal barrier function and microbial homeostasis (Chen et al., 2020). AhR is expressed by different immune cells, such as intraepithelial lymphocytes (IELs), regulatory T cells (Tregs), T-helper 17 (Th17) cells, innate lymphoid cells (ILCs), macrophages, dendritic cells, and neutrophils (Nieves et al., 2022). The human gut microflora produces a wide range of AhR-active microbial metabolites (see Chapter 5.2.1), which often show low affinity for AhR. Such low endogenous levels of AhR activation have been shown to be beneficial in the maintenance of immune health and intestinal homeostasis (Vrzalova et al., 2022). Under physiological conditions, AhR agonism in IEC can directly increase barrier function by strengthening junctional complexes, increasing goblet cell expansion and mucus production, and promoting epithelial cell regeneration, which aid in intestinal repair (Stockinger et al., 2021; Zelante et al., 2013). In addition, ILC3s and Th17 cells express IL-22 in an AhR-dependent manner. IL-22 promotes antimicrobial activity, increases mucus production, improves barrier function, and promotes wound healing (Nieves et al., 2022; Wyatt et Greathouse, 2021). Furthermore, the AhR-dependent release of IL-10 from Treg cells may also promote goblet cell expansion and stem cell differentiation (Nieves et al., 2022). Moreover, AhR activation modulates immunity through interactions with the NF- $\kappa$ B signaling pathway, leading to the expression of several cytokines and chemokines (Vogel et Matsumura, 2009).

### 3.2 Role of AhR in pathophysiological processes

AhR has an important role in the incidence, onset, and progression of pathophysiological processes and diseases including infection, inflammation, diabetes, cardiovascular diseases, and carcinogenesis (Bock, 2018; Larigot et al., 2018; Rothhammer et Quintana, 2019). The involvement of AhR in carcinogenesis has been demonstrated in many studies describing its pro- and anti-tumor functions in several types of cancer (Kolluri et al., 2017; Murray et al., 2014). The underlying mechanisms of AhR action in cancer include the inhibition of functional expression of tumor suppressors (such as p53 and BRCA1) (Romagnolo et al., 2015; Seifert et al., 2009), promotion of stem cell transformation, and angiogenesis (Roman et al., 2009; K. P. Singh et al., 2011), as well as alteration of cell cycle and apoptosis (Yin et al., 2016). Majority of studies on AhR have focused on the effects of TCDD on tumor formation. Long-term chronic cytotoxicity studies in rodents have reported that TCDD is a hepatocarcinogen (Knerr et Schrenk, 2006). Exposure to AhR ligands and increased AhR expression have been associated with many types of cancer (Kolluri et al., 2017; Wang et al., 2020), and potential therapeutic effects have been observed using AhR antagonists (DiNatale et al., 2012; Parks et al., 2014). Currently, two AhR antagonists, BAY2416964 and IK-175, have entered phase 1 clinical trials to assess the tolerability and toxicity of AhR-targeting agents in patients with incurable solid cancers (Paris et al., 2021). Furthermore, off-target AhR-active pharmaceuticals such as tranilast, flutamide, hydroxytamoxifen, and omeprazole or their derivatives have been found to have AhR-dependent anticancer effects (Safe et al., 2017). Dysregulation of diet-derived L-tryptophan (Trp) metabolites and the associated lack of endogenous AhR ligands have been observed in inflammatory bowel disease (Lamas et al., 2016), celiac disease (Lamas et al., 2020), and irritable bowel syndrome (Mars et al., 2020). Pharmacological activation of AhR leads to the improvement of inflammatory diseases, mainly through increased IL-22 transcription (Lamas et al., 2016; Zelante et al., 2013). Dextran sodium sulfate (DSS)-induced colon inflammation is inhibited by multiple AhR ligands, including TCDD (Kawai et al., 2017; N. P. Singh et al., 2011). Currently, there are rationally designed heterocyclic AhR agonist drugs (e.g., indole-based PY109) for treating inflammatory bowel

disease. PY109 increased the production of IL-22 in a murine model of DSS-induced colitis and in human T cells from patients with inflammatory bowel disease (Chen et al., 2020). Grycová et al. tested a series of highly potent AhR agonists derived from bacterial indothiazinones and observed substantial anticolic effects of ITE-CONHCH<sub>3</sub> *in vivo* in mice (Grycová et al., 2022). Furthermore, dietary pelargonidin and its glycosides are AhR agonists (Kamenickova et al., 2013a; Kamenickova et al., 2013) that can attenuate inflammatory bowel disease symptoms through AhR (Biagioli et al., 2019; Ghattamaneni et al., 2020). Ligand-dependent activation of AhR can also modulate cutaneous pathological processes. Naturally occurring compounds have been successfully used for topical treatment of atopic dermatitis. A bacterial stilbenoid, tapinarof, have successfully passed phase 2b randomized clinical trials as topical therapies for atopic dermatitis (Paller et al., 2021) and plaque psoriasis (Stein Gold et al., 2021).

AhR has been identified as a host factor for Zika and is linked to multiple congenital disabilities, including microcephaly. Inhibition of AhR boosts antiviral immunity and reduces the *in vivo* replication of this virus (Giovannoni et al., 2020). AhR is also activated by infection with various coronaviruses. Pharmacological inhibition of AhR by CH223191 suppresses the *in vivo* replication of HCoV-229 and SARS-CoV-2 viruses, which cause the common cold and COVID-19 disease (Giovannoni et al., 2021). Additionally, cigarette smoke (a source of AhR ligands) is generally believed to be harmful and smokers may be at a higher risk of infection. However, there is lower numbers of SARS-CoV-2 positive cases among smokers than that among non-smokers and cigarette smoke extract treatments were surprisingly found to suppress the expression of angiotensin-converting enzyme 2 (ACE2), an entry point enzyme into cells for selected coronaviruses, in HepG2 cells. Treatment with AhR agonists, including 6-formylindolo[3,2-b]carbazole (FICZ) and omeprazole, decreases the expression of ACE2 via AhR activation, resulting in suppression of SARS-CoV-2 infection in mammalian cells (Tanimoto et al., 2021).



## 4 Receptor theory

In biochemistry and pharmacology, the parameters of the relationship between receptors, ligands, and cellular responses are quantified. The term receptor in pharmacology refers to a protein located on the cytoplasmic membrane, in the cytoplasm, or in the cell nucleus, which binds small molecules (ligands) (Rang, 2001). Ligand binding to the receptor is governed by the law of mass action, which is based on the dynamic nature of chemical equilibria. Ligand binding is affected by several factors. Ligands and receptors must collide with the correct orientation and energy. The interaction is reversible, and the rate of ligand-receptor complex formation or dissociation depends on the number of receptors, ligand concentration, and the association and dissociation rate constants (Rang, 2001). The ability of a drug to bind to a receptor is called affinity, and it is numerically expressed by the equilibrium dissociation constant  $K_D$ .  $K_D$  represents the concentration of ligand required to occupy 50% of the receptor population. The lower the  $K_D$ , the higher is the affinity of the ligand for the receptor. The relationship between occupancy and drug concentration is determined by the fractional occupancy curve (Figure 6).

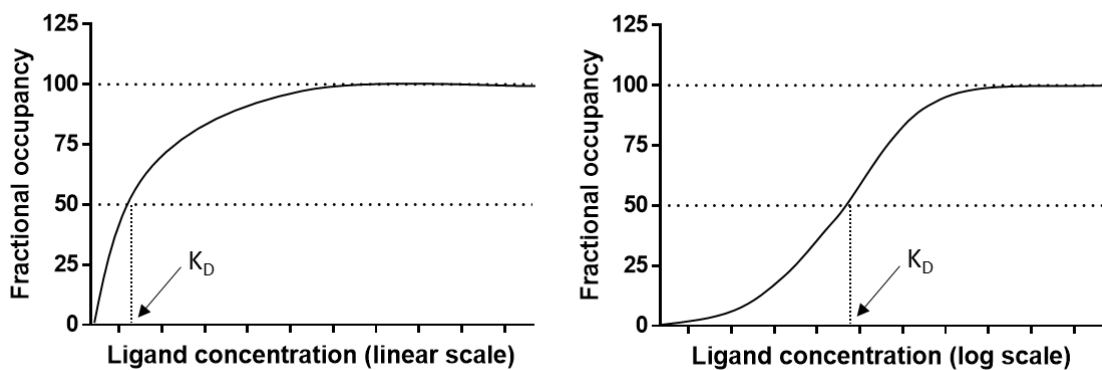


Figure 6: Fractional occupancy curve – linear and logarithmic scales.

The fractional occupancy of the receptor and the affinity of the ligand for the receptor were studied as radioactively labeled ligands. However, if a radioligand was unavailable, a competitive binding assay was performed. It measures the binding of a labeled ligand to a target protein in the presence of a second competing but unlabeled ligand. The concentration of the competing

ligand (inhibitor) that displaces 50% of the labeled ligand from binding to the receptor is called the  $IC_{50}$  (half-maximal inhibitory concentration). Based on the knowledge of  $IC_{50}$  values, we can also calculate the equilibrium dissociation inhibition constant  $K_i$ , which is the ligand concentration that binds 50% of the receptor binding sites in the absence of a labeled ligand. The equation of Cheng and Prusoff's equation was used to determine the  $K_i$  values (Dvorak et Cvek, 2011).

$$K_i = \frac{IC_{50}}{1 + \frac{[ligand]}{K_D}}$$

Figure 7: Cheng-Prusoff equation.

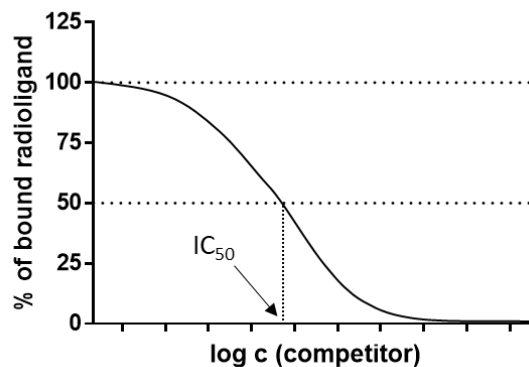


Figure 8: Competitive binding curve.

The receptor theory also determines the dose-response relationship. From the linear and logarithmic expression of the dose-response curve, we obtained two parameters:  $E_{MAX}$  value (maximal effective concentration) and  $EC_{50}$  value (half-maximal effective concentration). At a certain drug concentration, the maximum cellular response was reached, and the cellular response no longer increased, which corresponds to the  $E_{MAX}$  value. The concentration at which half of the  $E_{MAX}$  is reached is called the  $EC_{50}$ . The lower the  $EC_{50}$  value, the higher is the potency of the ligand, which causes a measurable functional change (Dvorak et Cvek, 2011).

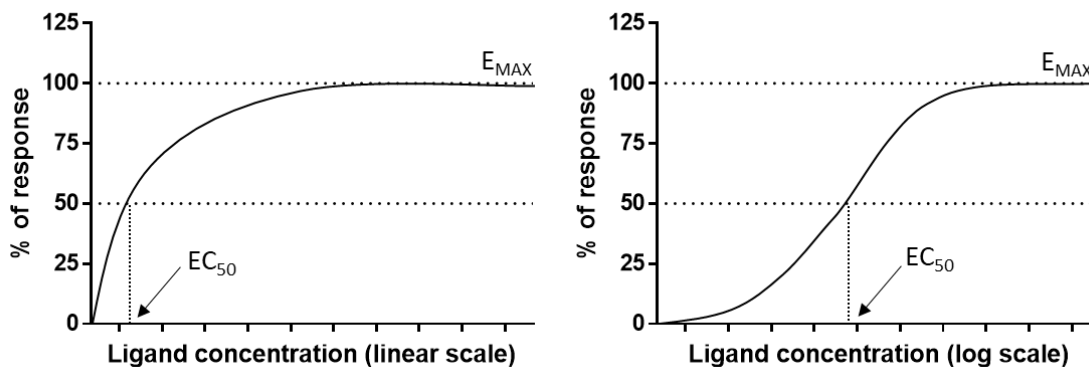
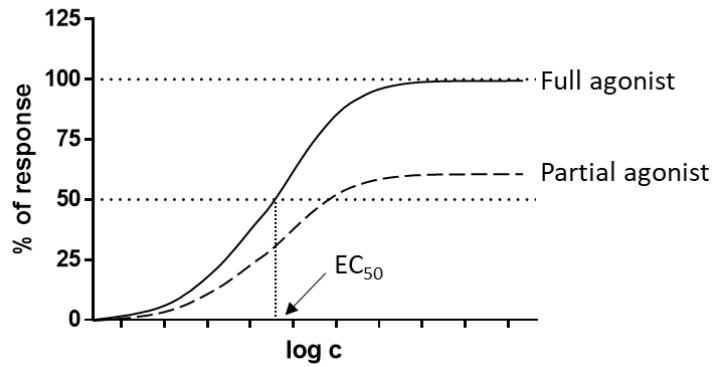


Figure 9: Dose-response curve: linear and logarithmic scales.

## 4.1 Agonism and antagonism

Although the affinity defines the ability of a ligand to bind to a receptor, it does not reveal the functional consequences of this interaction. In contrast, intrinsic efficacy includes the ability of a ligand to bind to a receptor and elicit a functional response. It is also called intrinsic activity and expresses the relative maximal effect of a substance in comparison with a natural endogenous ligand or model ligand of the receptor (Berg et Clarke, 2018; Dvorak et Cvek, 2011). Based on their intrinsic activity, we divided the ligands into:

- Super agonist: elicits a higher response than endogenous ligands; efficacy is higher than that of an endogenous agonist.
- Full agonists produce a maximal effect and possess high efficacy and activity, identical to those of endogenous ligands. Both the methods achieved the same  $E_{MAX}$  values.
- Partial agonists produce submaximal responses even at maximal receptor saturation and have intermediate efficacy. Its efficacy is lower than that of the endogenous agonists.
- Antagonist: does not elicit any response. It has an affinity for the receptor (blocks the receptor) but has no efficacy.
- Inverse agonist: reduce the level of constitutive activation of the receptor and produce a qualitatively opposite effect; efficacy is inverse (Dvorak et Cvek, 2011; Rang, 2001).



**Figure 10: Dose-response curve: full and partial agonism.**

Receptor antagonism can be divided into several groups: competitive, noncompetitive, and irreversible antagonism. Competitive antagonists bind to the same site on a receptor as do ligands/agonists but occupy the site without activating the effector mechanism and have zero efficacy. Competitive antagonism can be reversible or irreversible. Competitive antagonists compete for the receptor binding, and their action can be reversed by increasing agonist concentration (Pleuvry, 2004). In the dose-response curve, a competitive antagonist combined with an agonist shifted to the right without a change in  $E_{MAX}$ .

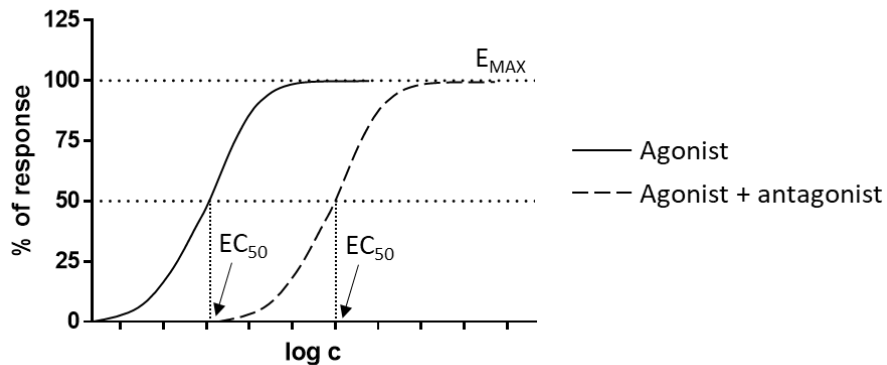


**Figure 11: Competitive antagonism.**

Non-competitive antagonists bind to or close to the ligand-binding domain, thereby hindering ligand binding without changing the conformation or binding to the allosteric site (other than the ligand's active site) on the receptor and inhibiting the cellular response through a conformational change. This type

of antagonism is also considered insurmountable; therefore, it cannot be disturbed by excess agonists. Noncompetitive antagonists reduce the magnitude of the maximal response; however, the  $EC_{50}$  value remains unchanged (Dvorak et Cvek, 2011).

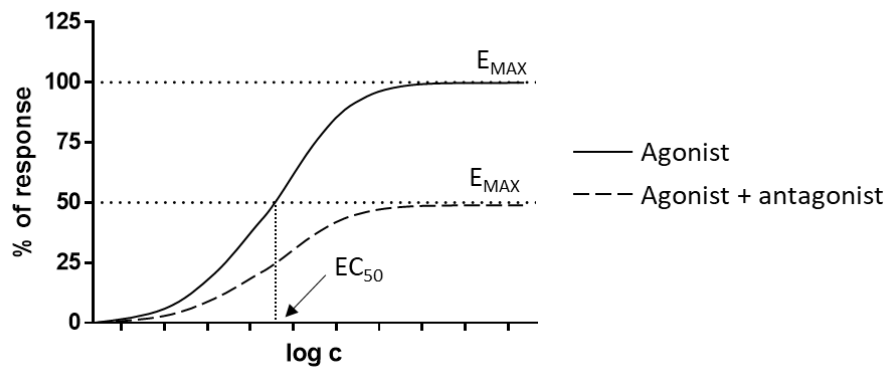


**Figure 12: Non-competitive antagonism.**

An uncompetitive antagonist binds to the receptor only in the presence of an already-bound ligand. Irreversible antagonists bind irreversibly to the receptor, usually through covalent bonds resulting in a reduced number of receptors capable of binding agonists. The addition of another agonist is ineffective and the only way to restore the original concentration is to synthesize a *de novo* receptor (Pleuvry, 2004).

To assess antagonism in cell-based bioassays, increasing concentrations of antagonist were combined with a competitive agonist at a constant concentration, and the suppression of agonist action indicated antagonism. Neale et al. recommended an  $EC_{80}$  agonist concentration when assessing antagonism. The  $EC_{80}$  concentration showed less variability than  $EC_{50}$  (Neale et Leusch, 2015).

## 5 AhR ligands

Structurally diverse ligands bind to AhR, causing ligand-, species-, and tissue-specific AhR-dependent biological and toxicological effects. Majority of the substances are organic hydrophobic, planar, and polycyclic compounds, and the affinity of AhR ligands is influenced by many factors, particularly the shape, size, and polarity of the molecule (Denison et al., 2011). A large number of AhR-active substances are known, and their numbers are constantly increasing. Currently, all the reported AhR ligands, both agonists and antagonists, are orthosteric ligands. AhR orthosteric ligands bind to a ligand-binding pocket and can be divided into three structurally distinct groups based on their interactions. AhR orthosteric ligands include full agonists, partial agonists, and competitive antagonists (Giani Tagliabue et al., 2019). Although allosteric ligands have several advantages over orthosteric ligands, these are not yet known (Meijer et al., 2019). Allosteric ligands are frequently receptor-selective because they may target less conserved regions on receptors than orthosteric ligands (Meijer et al., 2019; Smelcerovic et al., 2019). Allosteric ligands do not compete with ligands for the receptor, allowing allosteric modulators to be used at lower concentrations, resulting in fewer side effects (Meijer et al., 2019). Beneficial properties suggest potential for allosteric modulators in drug discovery (Foster et Conn, 2017; Gentry et al., 2015; Changeux et Christopoulos, 2016; Lisi et Loria, 2017; Taly et al., 2014). However, research on allosteric inhibitors is limited because specific assay formats for target ligand screening are lacking and allosteric sites are often difficult to identify (Meijer et al., 2019; Nussinov et Tsai, 2013).

### 5.1 Xenobiotic AhR ligands

AhR was originally identified as an environmental sensor of xenobiotic chemicals. These include industrial chemicals, environmental pollutants, herbal ingredients, drugs, pesticides, cosmetics, flavors, fragrances, and food additives (Patterson et al., 2010).

### **5.1.1 Environmental pollutants**

Environmental pollutants are chemicals with harmful effects on living organisms. They can be of natural (such as ash, soot, sulfur dioxide, volcanic, and combustion gases) or synthetic (such as pesticides, herbicides, and fungicides) origin (Stejskalova et al., 2011).

#### **Polycyclic Aromatic Hydrocarbons**

Polycyclic aromatic hydrocarbons (PAHs) are a large group of aromatic hydrocarbons with two or more condensed benzene rings. PAHs originate from natural sources, such as forest fires, pastures, oil seeps, and volcanic eruptions as well as from anthropogenic sources, such as exhaust gases, combustion of wood, coal tar, garbage, by-products of industrial production, lubricating oils and oil filters, combustion of solid municipal waste and oil stains, grilled food, and cigarette smoke (Stejskalova et al., 2011). For example, PAHs include naphthalene, biphenyl, fluorene, anthracene, phenanthrene, phenalene, tetracene, chrysene, triphenylene, pyrene, pentacene, perylene, BaP, 3-methylchloranthrene (3-MC), benz[a]anthracene, and benzo[c]phenanthrene. Chemical structures of the commonly studied PAHs are shown in Figure 13. PAHs are promutagens that can form reactive products capable of chemically modifying DNA and inducing tumors. They are metabolized by UGTs, GSTs, sulfotransferases, NAD(P)H quinone oxidoreductase 1, aldo-ketoreductase, enzymes of the CYP1 family (such as CYP1A1, CYP1A2, and CYP1B1), and epoxide hydrolases, which are considered important detoxifying and activating systems for these carcinogens (Shimada, 2006). One of the most important AhR-active PAHs is BaP, which is produced by incomplete combustion of organic matter. BaP-related cancer was first detected in the 18th century, when scrotal cancer occurred in chimney sweeps in England. In the 19th century, other occupation-associated tumors were detected among fuel industry workers (Ling et al., 2004). BaP is a carcinogen metabolized in mammals to benzo(a)pyrene-7,8-diol-9,10-epoxide, leading to the formation of DNA adducts that induce tumor growth (Ling et al., 2004). 3-MC is produced by burning

organic compounds and other PAHs; it is genotoxic and a potent carcinogen for human cells (Stejskalova et al., 2011).

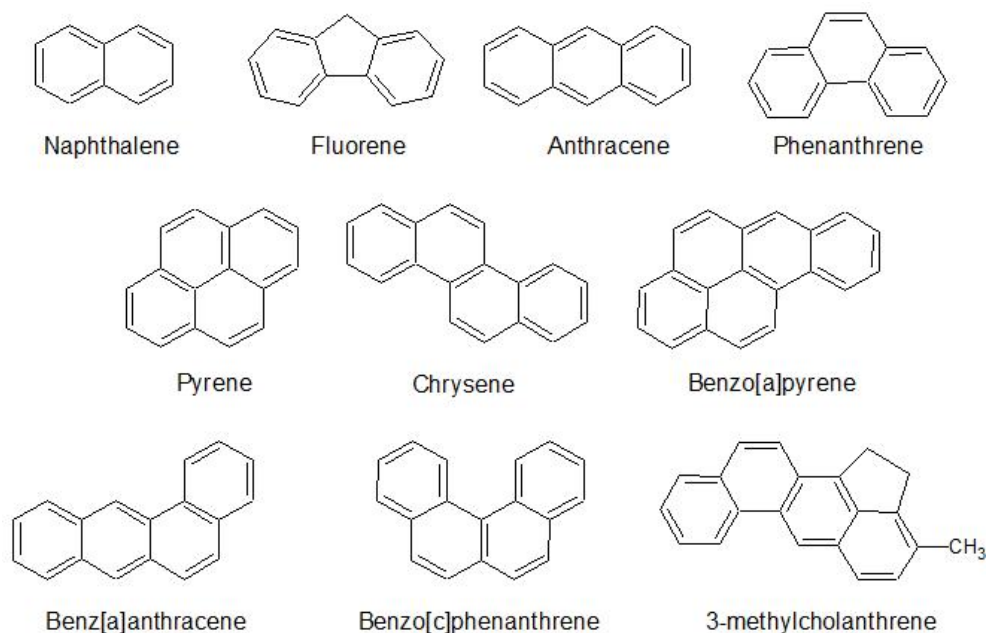


**Figure 13: Chemical structures of selected polycyclic aromatic hydrocarbons.**

### **Polychlorinated Biphenyls**

Polychlorinated biphenyls (PCBs) are synthetic organic substances in which the hydrogen atoms on the biphenyl skeleton are replaced by chlorine atoms. This group includes 209 isomers, but only a few of them are used in industry (Stejskalova et al., 2011). Their affinity for AhR depends on the number and position of chlorine atoms on biphenyl. Non-dioxin-like PCBs contain at least two chlorine atoms at their ortho positions. In contrast, the most potent AhR ligands among PCBs are dioxin-like PCBs, which can adopt a coplanar structure because they have zero or one chlorine atom at the ortho position (Hamers et al., 2011). Owing to their advantageous properties (such as chemical stability and heat resistance), PCBs are used in the industry as capacitors, transformer oils, hydraulic fluids, lubricating oils, organic diluents, and plasticizers (Safe, 1993; Stejskalova et al., 2011). As their spread has not been regulated by protective measures to prevent their formation and entry into the environment, their residues have been identified in air, water, aquatic and marine sediments, fish and wildlife, human adipose tissue, serum, and milk (Safe, 1993).



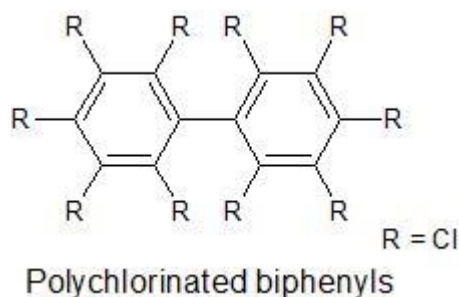


**Figure 14: Chemical structure of polychlorinated biphenyls.**

### **Halogenated dioxins and related compounds**

Halogenated dibenzo-p-dioxins, dibenzofurans, azo(xy)benzenes, and naphthalenes are structurally related AhR agonists. They arise from industrial processes, such as the imperfect combustion of organic substances, paper bleaching, and by-products of the production of chlorinated herbicides. AhR-active halogenated compounds are shown in Figure 15. Dioxins, which are the most potent AhR activators, are a group of toxic polychlorinated organic heterocyclic compounds derived from dibenzo[1,4] dioxins. These substances are widespread contaminants found in the air, soil, aquatic sediments, and living organisms (Stejskalova et al., 2011). Among these, TCDD is the most potent AhR agonist with a high affinity. The half-life of TCDD in humans is approximately 10–20 years, because of its accumulation in the body, particularly in adipose tissue, making it one of the most toxic substances (Joffin et al., 2018). For dioxin-like compounds, the World Health Organization derived toxic equivalency factors (TEFs) expressing their relative AhR-mediated toxicity compared to TCDD (Van den Berg et al., 2006).

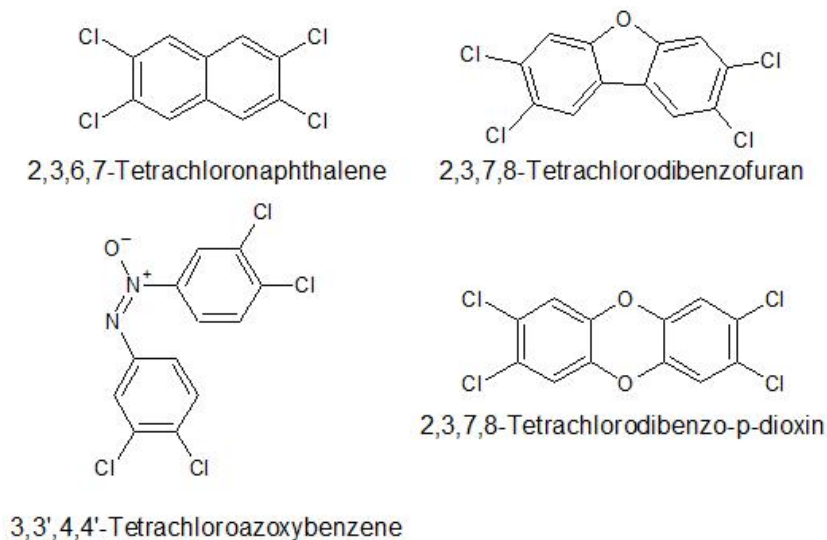


**Figure 15: Chemical structures of the selected AhR-active halogenated compounds.**

## Pesticides

Takeichi et al. identified 11 out of 200 pesticides with AhR-mediated transcriptional activity (acifluorfen-methyl, bifenox, chlorpyrifos, isoxathion, quinalphos, chlorpropham, diethofencarb, propanil, diuron, linuron, and prochloraz). Specifically, three herbicides (propanil, diuron, and linuron) with a common chemical structure exhibited stronger agonist activity than other pesticides, but they are relatively weak AhR inducers and ligands compared to TCDD (Takeuchi et al., 2008). In addition, the insecticide parathion is an AhR activator (Vrzal et al., 2015), and carbaryl, a carbamate insecticide, has also been demonstrated to be a weak AhR ligand and inducer of AhR-dependent gene expression (Denison et al., 1998).

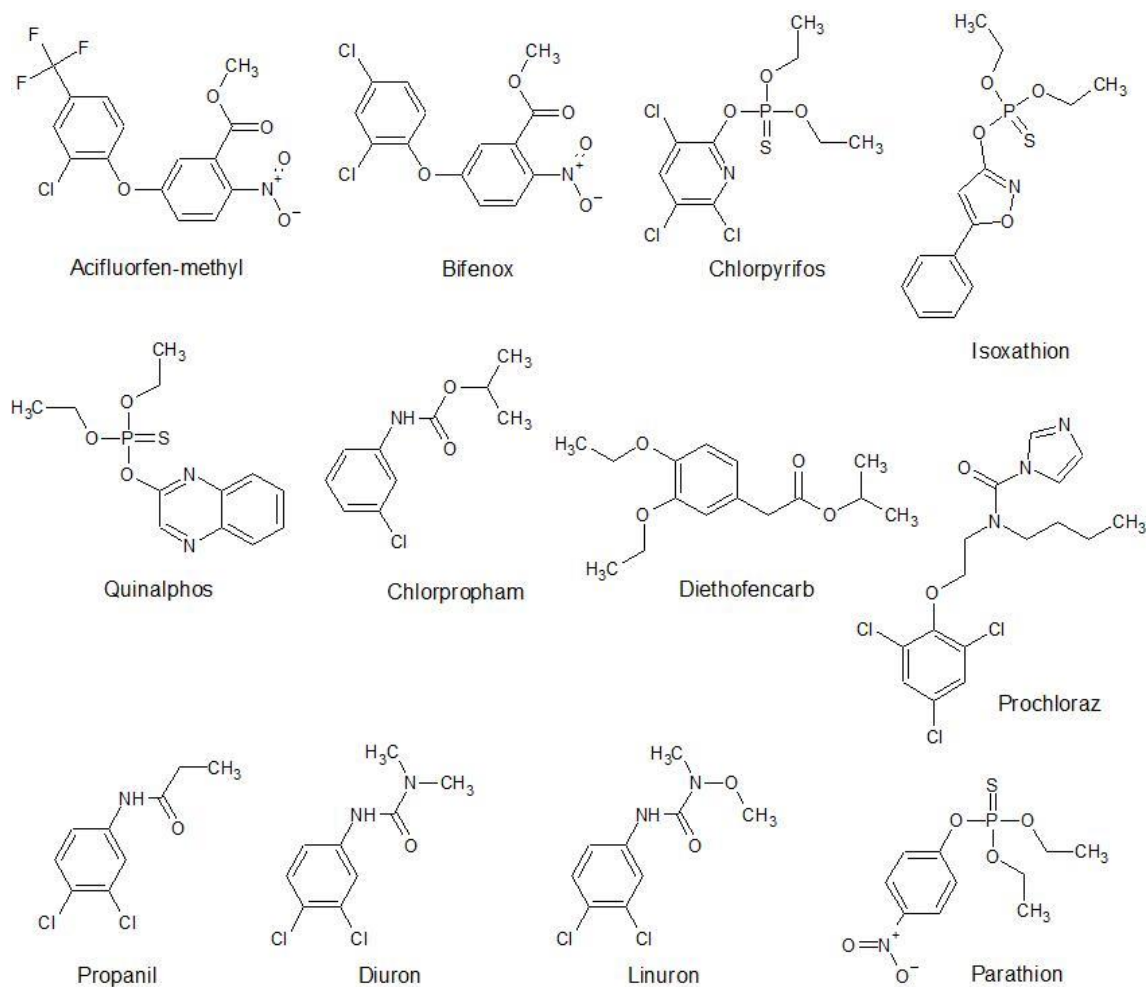


**Figure 16: Chemical structures of the selected AhR-active pesticides.**

## 5.1.2 Dietary ligands

### Polyphenols

Polyphenols are naturally occurring compounds that are found largely in fruits, vegetables, and cereals. In food, polyphenols may contribute to bitterness, astringency, color, flavor, odor, and oxidative stability (Pandey et Rizvi, 2009). Polyphenols are divided into four classes: phenolic acids, stilbenes, lignans, and flavonoids. Flavonoids include flavones, flavanols, also called catechins, flavanones, and isoflavones (Stejskalova et al., 2011). Chemical structures of the selected AhR-active polyphenols are shown in Figure 17.

Generalization of structure-activity relationships is not possible when studying flavonoids as AhR modulators (Goya-Jorge et al., 2021). For example, diosmin, diosmetin (Ciolino et al., 1998b), biochanin A (Bialesova et al., 2015;

Dunlap et al., 2017; Kaur et Badhan, 2017), formononetin (Bialesova et al., 2015; Dunlap et al., 2017), and 4',5,7-Trimethoxyisoflavone (Park et al., 2019) have been identified as AhR agonists. By contrast, PD98059 (Reiners et al., 1998; Shin et al., 2005), tangeretin (Arivazhagan et Subramanian, 2015), and genistein (Dunlap et al., 2017; Froyen et Steinberg, 2016) are AhR antagonists. Several flavonoids exhibit both agonist and antagonist activity during AhR transcriptional activation. For instance, chrysin acts as an AhR agonist (Kaur et Badhan, 2017; Ronnekleiv-Kelly et al., 2016) but can also suppress dioxin toxicity (Ashida, 2000). Similarly, apigenin exhibited agonist activity against AhR transcriptional activation (Kaur et Badhan, 2017) and demonstrated an inhibitory effect on TCDD-mediated AhR induction (Ashida, 2000). Furthermore, flavones (Ashida, 2000; Kaur et Badhan, 2017), flavanol (Ashida, 2000), flavanone (Ashida, 2000; H. Ashida et al., 2000), galangin (Quadri et al., 2000; Zhang et al., 2003), kaempferol (Jin et al., 2018), and quercetin (Hitoshi Ashida et al., 2000) (Amakura et al., 2008; Ashida, 2000) show AhR agonist and antagonist activities.

In addition to flavonoids, the polyphenolic compounds exhibit AhR activity. Polyphenol curcumin, known as a yellow pigment in turmeric, exerts inhibitory effects on BaP-induced AhR activation, nuclear translocation, and DNA binding, which lead to a reduction in CYP1A gene transcription, decreased protein expression, and CYP1A1/2 enzyme activity *in vivo* (Garg et al., 2008). The stilbene derivative resveratrol is a competitive antagonist of AhR that inhibits CYP1A1 gene expression *in vitro* (Ciolino et al., 1998a) and inhibits the transactivation of several dioxin-inducible genes, including CYP1A1 and IL-1 $\beta$ , both *ex vivo* and *in vivo* (Casper et al., 1999). Fukuda et al. discovered that chlorophyll and carotenoid lutein in green tea can act as AhR antagonists of AhR (Fukuda et al., 2004). Moreover, green tea components, epigallocatechin gallate and epigallocatechin are the most potent AhR antagonists in green tea (Palermo et al., 2003).

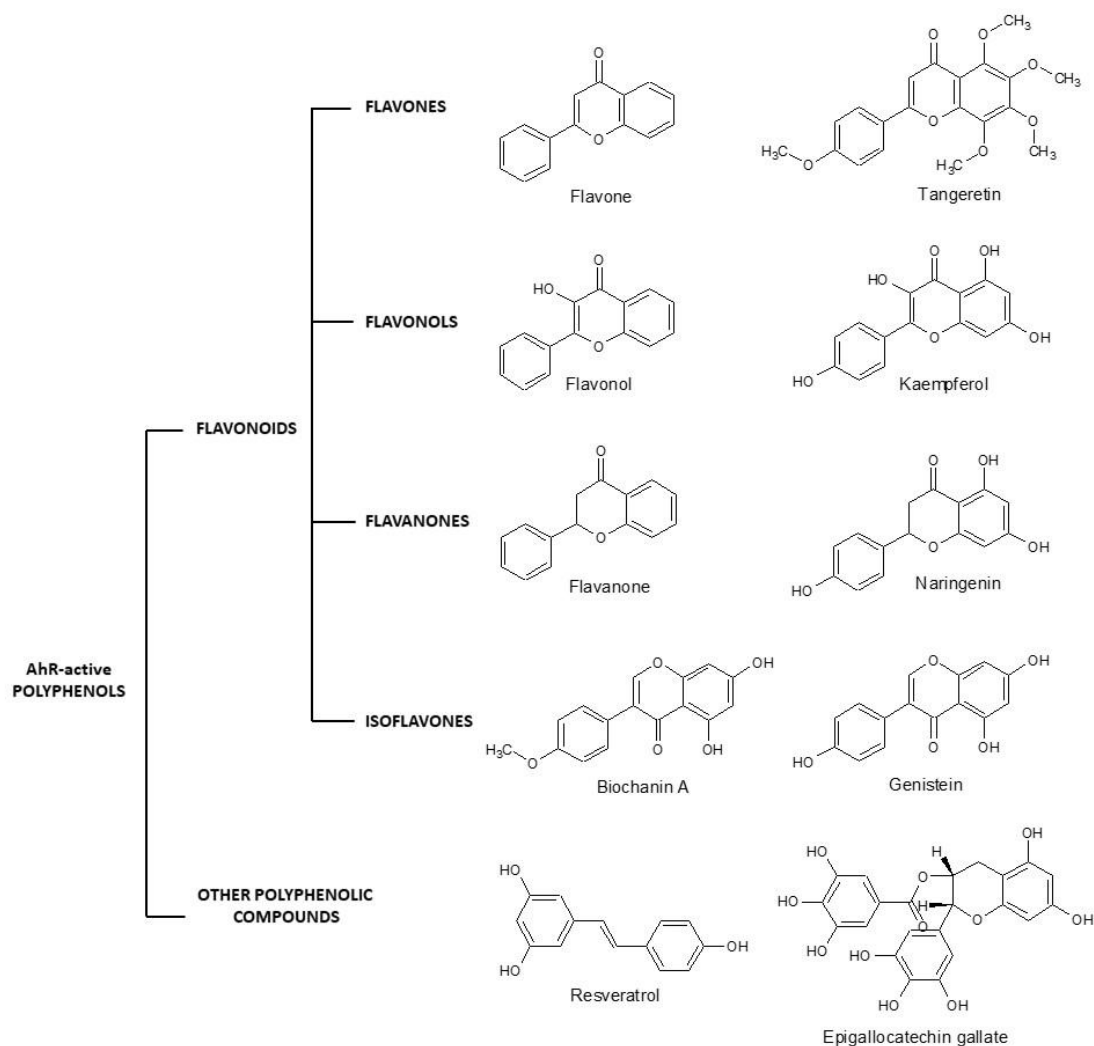


**Figure 17: Chemical structures of the selected AhR-active polyphenols.**

## Alkaloids

Alkaloids are complex organic molecules containing heterocyclic nitrogen rings. They are produced by many different organisms, including animals and microbes, but a particularly diverse range of alkaloids is produced by plants (Twyman et al., 2003). The alkaloids were also evaluated for their ability to activate AhR-dependent gene expression. For example, harman, an aromatic  $\beta$ -carboline alkaloid, induces CYP1A1 gene (El Gendy et El-Kadi, 2010). Moreover, rutaecarpine, anomontine, and xestomanzamine A increased the expression of the AhR target genes, CYP1A1 and AhRR (Haarmann-Stemmann et al., 2010). Berberine, an isoquinoline alkaloid, can activate AhR; however, it is accompanied by inactivation of the catalytic activity of CYP1A1

enzyme at concentrations that exceed *in vivo* concentrations (Vrzal et al., 2005). The fungal alkaloid schizocommunin is an AhR activator that induces CYP1A1, CYP1B1, and UGT1A gene expression in human hepatic and lung cells (Filip et al., 2019).

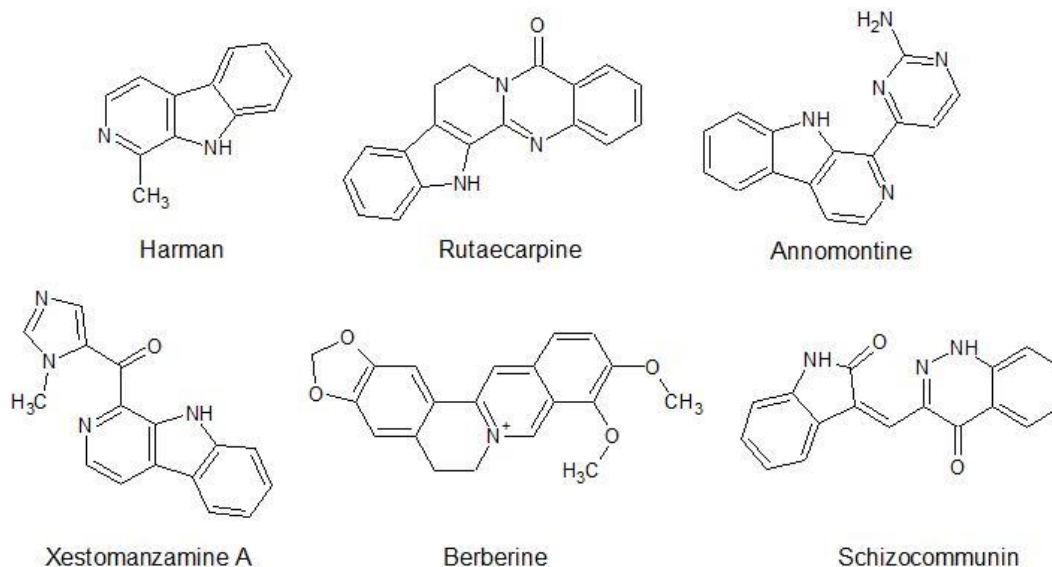


**Figure 18: Chemical structures of the selected AhR-active alkaloids.**

### Other dietary AhR ligands

Cruciferous vegetables contain glucosinolate glucobrassicin and its various derivatives, such as neoglucobrassicin, which are dietary precursors of AhR-active compounds. During digestion, glucobrassicin is converted into indole-3-carbinol (I3C), an AhR ligand and agonist. Subsequently, I3C undergoes a series of condensation reactions, resulting in a production of AhR-active indole derivatives, including 3,3'-diindolylmethane (DIM), indolo[3,2-b]carbazole (ICZ), 2-(Indol-3-yl-methyl)- 3,3'-diindolylmethane and 5,6,11,12,17,18-Hexahydrocyclonona[1,2-b:4,5-b':7,8-b''] triindole (Bjeldanes et al., 1991; Chen et al., 1996). Similarly, dietary neoglucobrassicin is converted to N-methoxyindole-3-carbinol, which is also an AhR agonist (Dvorak et al., 2021; Stephensen et al., 2000). The potential anticancer properties of I3C have also been investigated. I3C upregulates the classical AhR-regulated monooxygenases (Loub et al., 1975). Oral administration of I3C increases hepatic monooxygenase activity, suggesting that I3C is converted into AhR agonists in the acidic environment of the stomach (Bradfield et Bjeldanes, 1987).

Ascorbigen, an indole ring-containing degradation product of glucobrassicin, has been demonstrated to be an AhR activator and CYP1A1 gene inducer in various cell lines (Stephensen et al., 2000). Furthermore, selected heterocyclic aromatic amines derived from cooked food activate AhR and induce the expression of AhR-regulated genes. This group includes 3-amino-1,4-dimethyl-5H-pyrido[4,3-b]indole, 3-amino-1-methyl-5H-pyrido[4,3-b]indole, 2-amino-9H-pyrido[2,3-b]indole, and 2-amino-3-methyl-9H-pyrido[2,3-b]indole (Sekimoto et al., 2016). Natural marine products are important sources of AhR ligands. Several marine brominated indoles and brominated (methylthio) indoles act as AhR ligands and agonists (DeGroot et al., 2015).

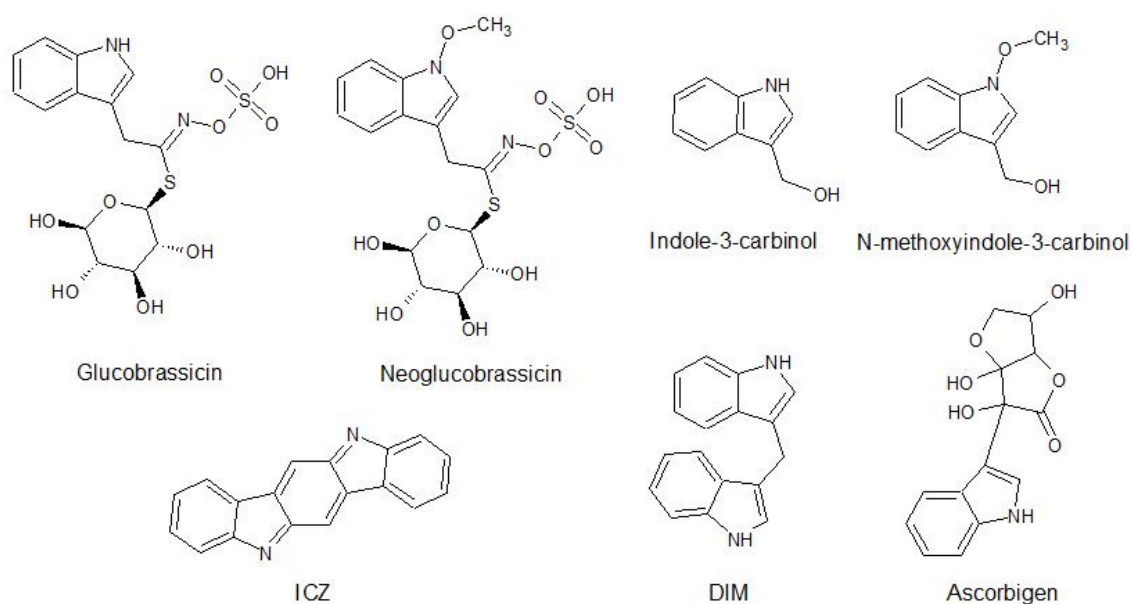


**Figure 19: Chemical structures of the selected AhR-active dietary ligands.**

### 5.1.3 Drugs

Benzimidazole derivatives (omeprazole and lansoprazole) are proton pump inhibitors that suppress gastric acid secretion. The chemical structure of omeprazole does not correlate with the classical structural requirements for planar and polycyclic AhR ligands. Omeprazole can promote AhR nuclear translocation and its association with ARNT (Clissold et Campoli-Richards, 1986; Stejskalova et al., 2011). Importantly, these drugs are administered as racemic mixtures and have enantiospecific effects on AhR, which may be a significant finding for clinical use (Novotna et al., 2014). Also, dihydropyridine calcium

channel blockers (such as benidipine, isradipine, and felodipine) are used as anti-hypertensives and in the treatment of angina pectoris, drugs display enantiospecific effects on AhR (Stepankova et al., 2016). Several AhR-active drugs contain an indole core in their chemical structure. For instance, the antimigraine triptan drugs avitriptan and donitriptan have been reported to be low-affinity ligands and weak agonists of AhR (Vyhlidalova et al., 2020b). Receptor tyrosine kinase inhibitors semaxinib and sunitinib are AhR agonists that induce AhR-regulated genes (Maayah et al., 2013; O'Donnell et al., 2017). The anticancer drug indisulam acts as an AhR antagonist that induces ARNT degradation through CRL4<sup>DCAF15</sup> E3 ligase (Kim et al., 2020). Vemurafenib also acts as an AhR antagonist, thereby inducing the expression of proinflammatory cytokines and chemokines (Hawerkamp et al., 2019). Clinically used AhR-active drugs, such as tranilast or flutamide, may be effective AhR-dependent chemotherapies for treating breast and pancreatic cancers (Safe et al., 2017). The purity of the drugs was also worth considering. For example, impurities contained in the antifungal drug ketoconazole are potent activators of the human AhR. These findings may have implications for the role of ketoconazole in chemoprevention and/or skin damage, including in AhR (Grycova et al., 2015).



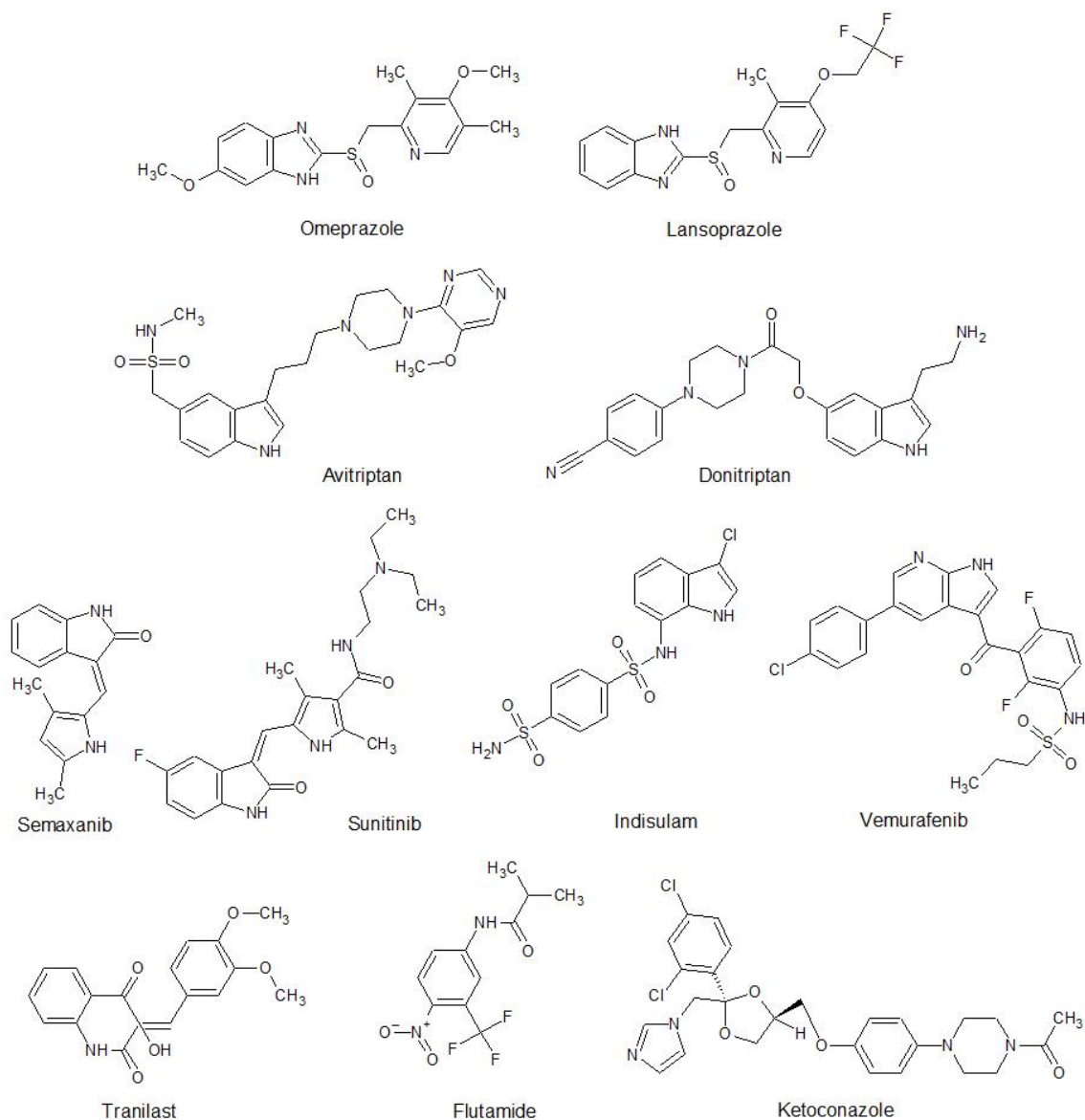


**Figure 20: Chemical structures of the selected AhR-active drugs.**

#### 5.1.4 Other AhR-active xenobiotic ligands

TSU-16, an inhibitor of the tyrosine kinase of the vascular endothelial growth factor receptor-2, is a potent activator of AhR. It is mainly metabolized by CYP1A2 in human liver microsomes and it increases *CYP1A1* and *CYP1A2* mRNA levels in human hepatocytes with similar potency of 3-MC (Matsuoka-Kawano et al., 2010). SB216763, an inhibitor of glycogen synthase kinase (GSK), is a partial agonist of AhR (Braeuning et Buchmann, 2009). In addition, the GSK inhibitors 6BIO and GSK3iXV have been described as AhR full agonists (Briolotti et al., 2015). Dual inhibitors of GSK and cyclin-dependent kinases,

indirubin-3'-monoxime and isoindigo, have been identified as AhR agonists (Nishiumi et al., 2008; Peter Guengerich et al., 2004).

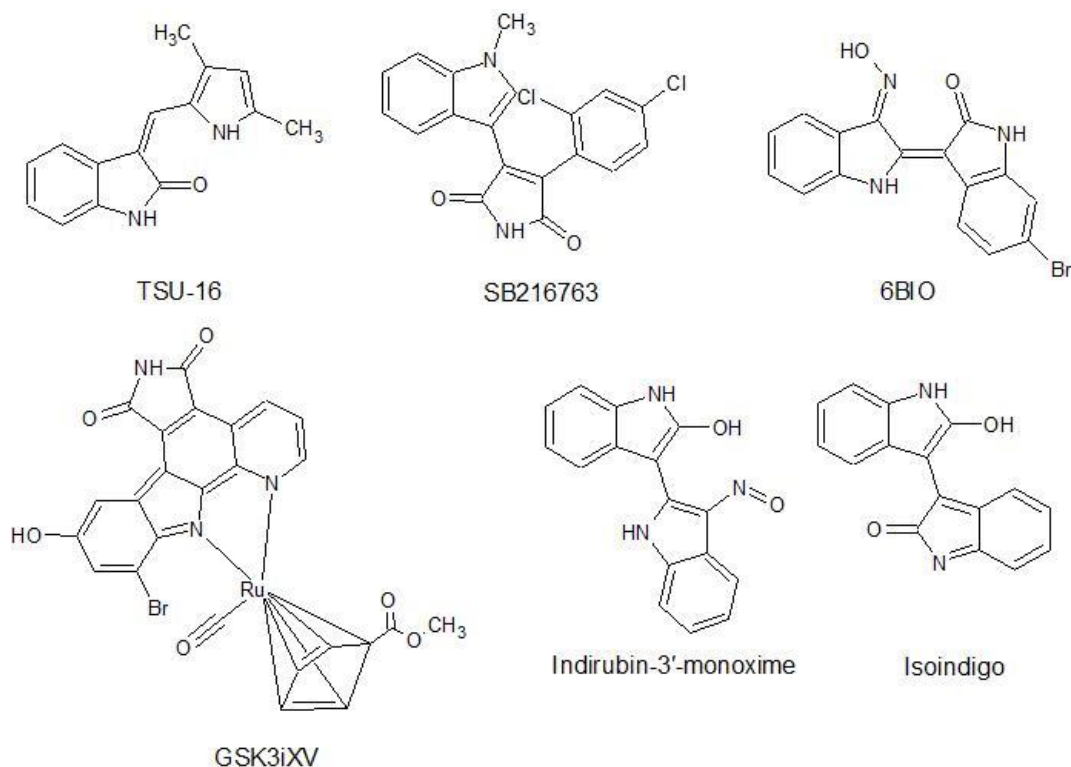


**Figure 21: Chemical structures of the selected AhR-active kinase inhibitors.**

Synthetic flavonoids TMF (6,2',4'-trimethoxyflavone) and MNF (3'-methoxy-4'-nitroflavone) are AhR antagonists that can reduce TCDD-induced binding of AhR to DNA (Lu et al., 1995; Murray et al., 2010). In contrast to TMF, MNF shows species differences, acting as an AhR antagonist in mice but as an agonist in guinea pigs (Henry et Gasiewicz, 2008). Another synthetic flavone,  $\beta$ -naphthoflavone, induces AhR-mediated CYP1A gene expression and inhibits CYP1A1 gene expression induced by AhR agonists through competitive interactions for binding with AhR (Merchant et al., 1992; Sinal et al., 1999; Stejskalova et al., 2011).

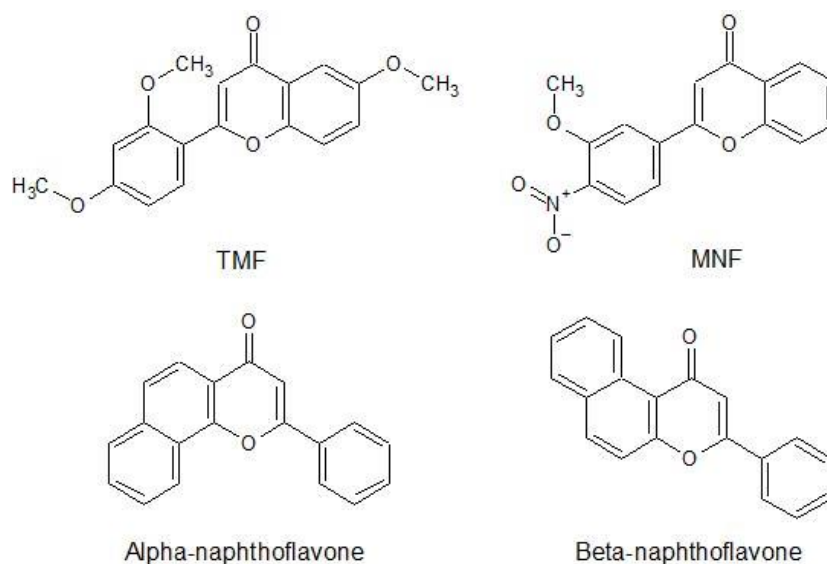


**Figure 22: Chemical structures of the selected AhR-active synthetic flavonoids.**

AhR-active compounds also include bisphenol A (Vrzal et al., 2015) and environmental pollutants from halogenated carbazoles that display the AhR-agonist activities. Tetrasubstituted chloro/bromocarbazoles are among the most active compounds (Riddell et al., 2015). A series of halogen-, alkyl-, or carbomethoxy-group-bearing mono- and bi-substituted indirubins and tryptanthrines, particularly 3-bromotryptanthrin, 3,9-dibromotryptanthrin, 5,5'-dichloroindirubin, and 6,6'-dibromoindirubin, were found to be human AhR agonists (Mexia et al., 2019).

Simple methylated and methoxylated indoles have been identified as AhR ligands. The AhR agonists are 4-methylindole, 5-methylindole, 6-methylindole, 7-methoxyindole, and 2,5-dimethylindole. In contrast, 3-methylindole, 2,3-dimethylindole, 2,3,7-trimethylindole, 6-methoxyindole, and 5-methoxy-2-methylindole have been characterized as antagonists (Stepankova et al., 2018). Moreover, 3-methylindole acts as a partial agonist of the AhR (Rasmussen et al., 2016). In addition, the indole derivative 2,2'-aminophenyl indole was identified as a ligand and potent AhR agonist (Gutierrez et al., 2016).

The synthetic compound GNF351 (N-(2-(1H-indol-3-yl)ethyl)-9-isopropyl-2-(5-methyl pyridine-3-yl)-9H-purin-6-amine) has been characterized as a high-affinity AhR ligand and antagonist (Smith et al., 2011).

In addition, VAF347 ([4-(3-chloro-phenyl)-pyrimidin-2-yl]-(4-trifluoromethyl-phenyl)-amine) binds to the AhR protein, consequently inducing AhR-driven signaling (Stejskalova et al., 2011).

Comprehensive studies have been conducted to rationally design AhR-active compounds. Chen et al. synthesized a chemical library of structurally distinct indole and indazole compounds and characterized several highly potent AhR modulators. The most potent drugs were PY109 ((1H-indol-3-yl) (6-(trifluoromethyl) pyridin-2-yl) methanone) and PY108 (6- (1H-indol-3-carbonyl) picolinonitrile), which exhibited the desired pharmacokinetic effects and low toxicity with a promising effect as anticolicitis agents (Chen et al., 2020). The AhR-active compound, CH223191 (2-methyl-2H-pyrazole-3-carboxylic acid (2-methyl-4-o-tolylazo-phenyl)-amide), was also identified via chemical library screening (Kim et al., 2006). CH223191 is a selective AhR modulator that inhibits TCDD and halogenated aromatic hydrocarbons (HAHs) but not other AhR agonists, such as PAHs, flavonoids, or indirubin. This preferential antagonism is explained by the hypothesis that there are significant differences in the binding of AhR agonists in the ligand-binding pocket (Stejskalova et al., 2011). Symmetrical dihalogenated diindolyl methanes (including 4,4'-dichloro and 6,6'-dichloro 5,5'-dibromo-diindolylmethane) are weak AhR agonists (McDougal et al., 2000). A series of 2,3'-substituted diindolylmethanes derived from a malassezin scaffold was also examined for AhR activity. The methyl substituent at 1'-N significantly increased AhR activity. In contrast, the 2-formyl group is not critical in some diindolylmethanes (Winston-McPherson et al., 2014). Wincent et al. designed and synthesized a series of indolocarbazole-based compounds with core structures of diindole-selenopyrans and thiopyrans. For example, 5H-Thiopyrano[2,3-b:6,5-b']diindole and 5H-Selenopyrano[2,3-b:6,5-b']diindole are highly potent AhR agonists (Wincent et al., 2009b). Wu et al. tested the 6- and N-substituted derivatives of 6-formylindolo[3,2-b]carbazole (FICZ). They identified 5-methyl-FICZ as a more AhR-active substance than parental FICZ (Wu et al., 2020). Recently, a series of AhR-active indole-containing asymmetric aromatic triarylmethanes was designed and synthesized by employing an innovative microbial metabolite mimicry approach. These compounds harbor an indole moiety and pyridinyl and phenyl sulfonyl

building blocks. The most active AhR agonists, FKK2 (di(1H-indol-2-yl)(pyridin-4-yl)methanol) and FKK9 (1-(1-(ethoxymethyl)-1H-indol-2-yl)-2-(1H-indol-2-yl)-1-(pyridin-4-yl)ethan-1-ol), have medium potency and relative efficacy, comparable to that of TCDD (Dvorak et al., 2020a; Dvorak et al., 2020b).

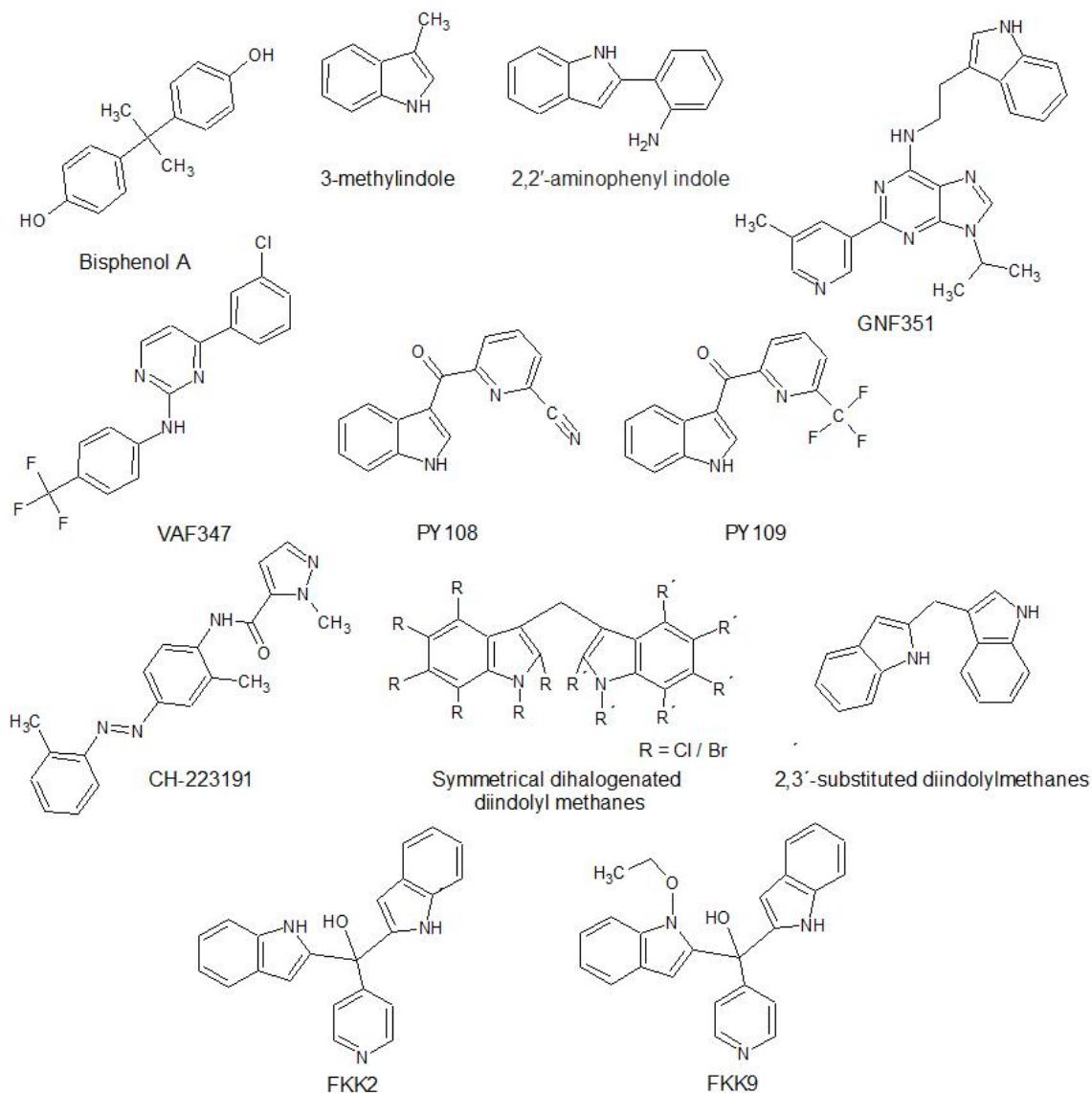


**Figure 23: Chemical structures of the selected AhR-active compounds.**

## 5.2 Endogenous AhR ligands

Endogenous ligands are naturally occurring small molecules endogenously synthesized in higher organisms (Murray et al., 2010; Nguyen et Bradfield, 2008). Endogenous ligands often have moderate to low affinities for AhR (Gasiewicz et al., 1996; Henry et al., 2010), and such low endogenous

levels of AhR activation have been shown to be beneficial in maintaining immune health and intestinal homeostasis (Vrzalova et al., 2022).

Two isomeric condensed oxindoles, indigo and indirubin, are highly potent endogenous activators of the AhR, found in human urine and bovine serum (Adachi et al., 2001). Some studies have indicated that indigoids can also exhibit antagonistic effects at lower concentrations in mammalian cells (Nishiumi et al., 2008).

The heme metabolites biliverdin and hemin most likely induce CYP1A1 gene transcription indirectly by acting as precursors for endogenous bilirubin production through normal heme metabolic pathways (Sinal et Bend, 1997).

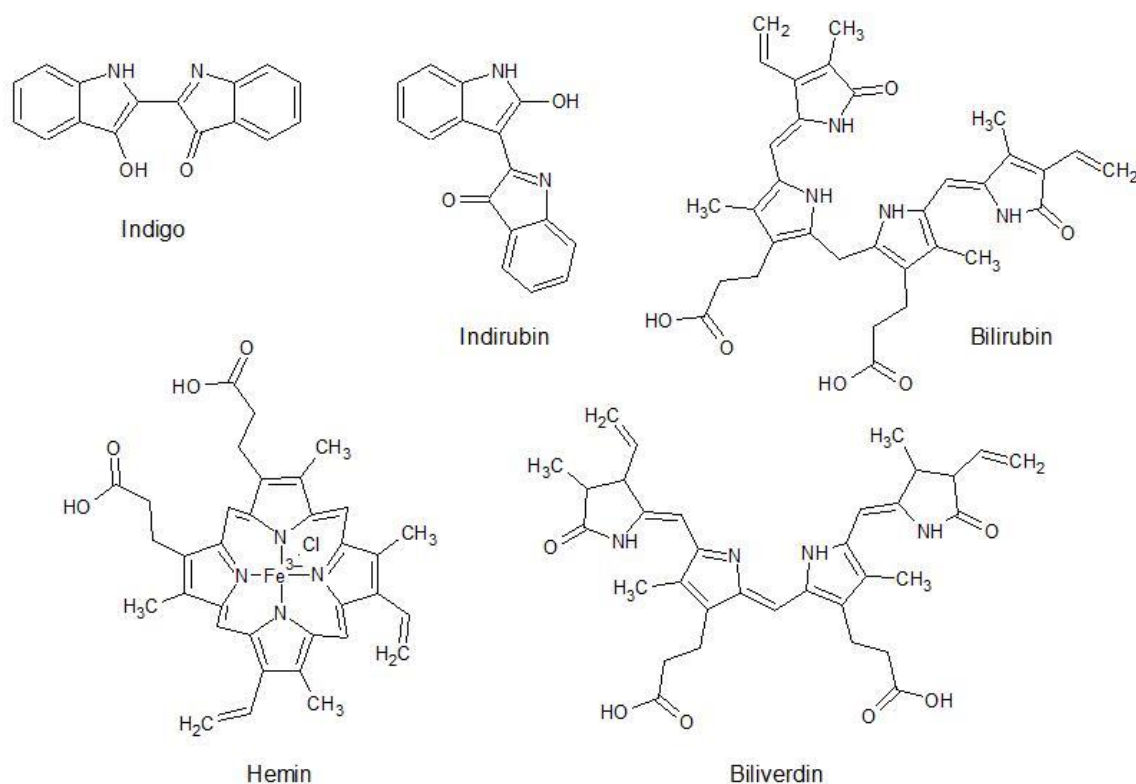


**Figure 24: Chemical structures of the selected AhR-active indigoids and heme metabolites.**

Eicosanoids are oxygenated products of the metabolism of twenty-carbon fatty acids, particularly arachidonic acid. Until the discovery of lipoxin A4 (LXA<sub>4</sub>), no acyclic ligand with affinity for AhR was known. LXA<sub>4</sub> contains neither rings nor a fully planar geometry, and is a negatively charged molecule at physiological pH, making it dramatically different from the classical AhR ligands.

The structurally similar molecule, lipoxin B4 (LXB<sub>4</sub>), does not show any appreciable affinity for AhR. LXA<sub>4</sub> induce transcription of AhR-dependent genes (Bennett et Gilroy, 2016; Schaldach et al., 1999). Selected prostaglandins, namely prostaglandin B3 (PGB3), analogously named PGD3, PGF3 $\alpha$ , PGG2, PGH1, and PGH2, are weak agonists of AhR. They stimulate AhR transformation and DNA binding *in vitro* and induce AhR-dependent reporter gene expression in mouse hepatoma cells (Seidel et al., 2001).

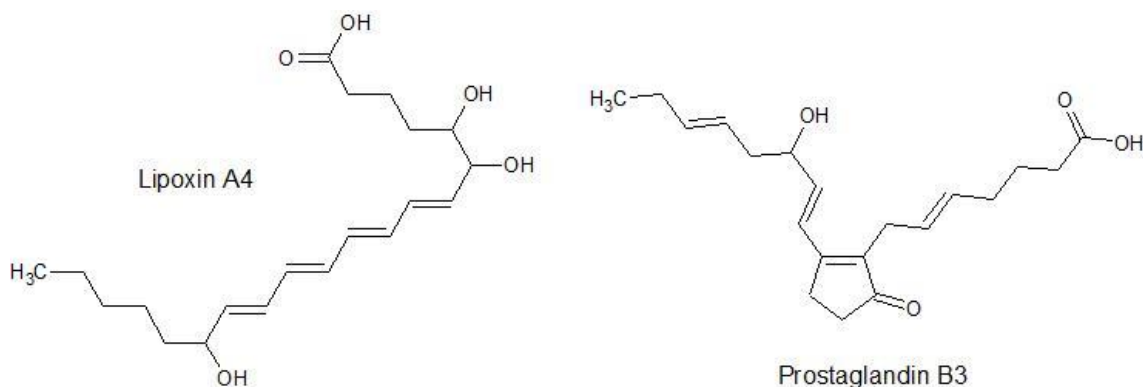


**Figure 25: Chemical structures of the selected AhR-active eicosanoids.**

### 5.2.1. Microbial ligands

The human physiological microbiota is a rich source of tryptophan (Trp)-derived AhR ligands, both in the skin and intestine (Dvorak et al., 2021). Majority of dietary Trp is metabolized by the kynurenine pathway (Hoglund et al., 2019). Kynurenine has long been considered to be an AhR agonist. A recent study provided evidence that kynurenine acts as an AhR pro-ligand and that its closely related condensation products, called trace-extended aromatic condensation products (TEACOPs), are highly potent agonists of the AhR (Seok et al., 2018). Moreover, Trp metabolites, such as kynurenic acid and xanthurenic acid, have been described as ligands and agonists of AhR (Michaudel et al., 2022). Vyhřídálová et al. examined the effects of microbial intestinal catabolites of Trp, including indole, tryptamine, and indole-3 substituted catabolites of Trp, on AhR activity. All the studied catabolites acted as low-potency AhR agonists, but their effects on AhR varied significantly, as they exhibited different AhR activities in terms of potency and affinity. The most efficacious agonists are indole, 3-methylindole, tryptamine, indole-3-pyruvate, indole-3-acrylate,

and indole-3-acetamide (Vyhlidalova et al., 2020a). Another endogenous and potent AhR indole-scaffold ligand is ITE (2-(1'H-indole-3'-carbonyl)-thiazole-4-carboxylic acid methyl ester), which was isolated from porcine lung (Song et al., 2002). Dong et al. recently revealed the presence of AhR agonists 2-oxindole and 3-methyl-2-oxindole in human feces (Dong et al., 2020). Moreover, the microbial production of FICZ (Smirnova et al., 2016), triptanthrin (Magiatis et al., 2013), pityriazepin (Mexia et al., 2015), and malassezin (Wille et al., 2001) by the opportunistic cutaneous pathogen *Malassezia* has been described. FICZ is also produced from precursors (such as indole-3-pyruvate) formed by the intestinal microbiota, implying that FICZ is a dual endogenous and microbial AhR ligand (Dvorak et al., 2021; Rannug, 2020). In addition, pigmented bacterial virulence factors from *Pseudomonas* and *Mycobacterium* strains have been shown to bind to and activate AhR. AhR activation leads to virulence factor degradation and regulated cytokine and chemokine production (Moura-Alves et al., 2014)



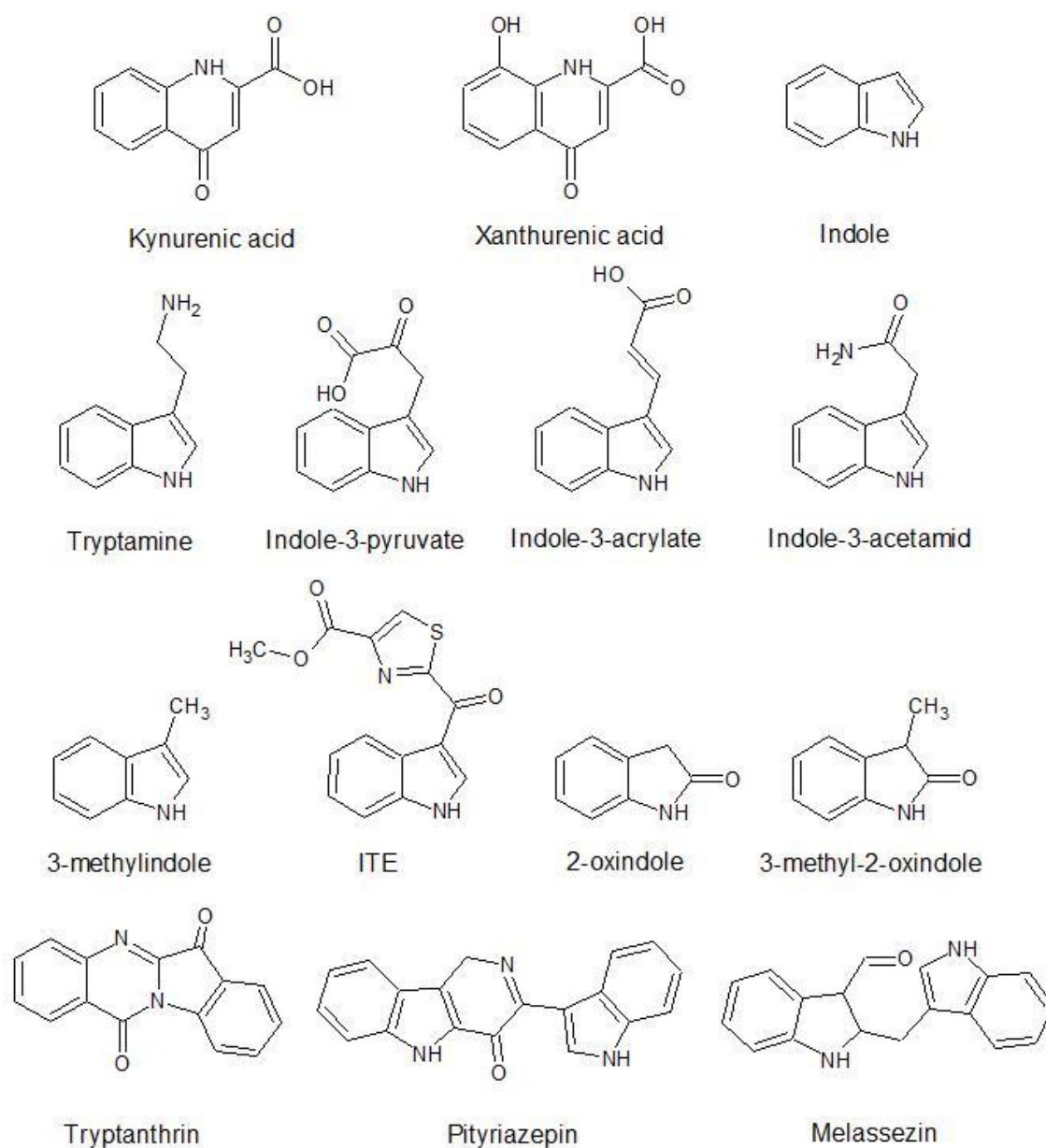


**Figure 26: Chemical structures of the selected AhR-active microbial ligands.**

### 5.2.2 Ultraviolet light-produced AhR ligands

Ultraviolet (UV) irradiation of Trp generates compounds with high affinity for AhR, such as FICZ and 6,12-diformylindolo[3,2-b]carbazole (dFICZ) (Stejskalova et al., 2011). Sulfoconjugates of phenolic metabolites of FICZ are present in human urine, indicating that FICZ is a potent, naturally occurring activator of the AhR signaling pathway and may be the key substrate of the CYP1 and sulfotransferase SULT1 family of enzymes (Wincent et al., 2009a). FICZ has also been identified in the skin of individuals with a non-infectious skin disorder

called vitiligo (Schallreuter et al., 2012). It is worth noting that these compounds are structurally similar to a dietary indole ligand indolo[3,2-b]carbazole (ICZ), which is also an AhR active compound (Stejskalova et al., 2011; Wei et al., 1998).



**Figure 27: Chemical structure of tryptophan-related AhR-active compounds.**

## 6 Essential oils

Essential oils (Eos, also called volatile or ethereal oils) are aromatic oily liquids obtained from plants (Burt, 2004). The term “essential oil” was likely invented by the Swiss medical reformer and alchemist Paracelsus von Hohenheim in the 16th century. He named the effective component of the drug Quinta essential (Burt, 2004). EOs are used for their broad biological effects and are also known for their antiseptic, bactericidal, virucidal, fungicidal, and overall healing properties (Bakkali et al., 2008). EOs are commonly used in classical, complementary, and alternative medicine (such as aromatherapy, antiseptics, carminatives), cosmetics (perfumes), household cleaning products, and food and gastronomy industries (food and drink flavoring and coloring and preservatives) (Bartonkova et Dvorak, 2018b).

EOs are multicomponent mixtures of volatile compounds, the final effects of which include the aggregated activities of the individual components (Bartonkova et Dvorak, 2018b). EOs usually consist of two to three main components at high concentrations and from 20–60 other substances in small amounts (Bakkali et al., 2008). EOs are mainly composed of terpenes, terpenoids, and phenolic compounds (El-Shemy, 2020). Furthermore, EOs contain esters, ethers, alcohols, aldehydes, hydrocarbons, and carboxylic acids (Tongnuanchan et Benjakul, 2014). The presence of phenylpropanoid derivatives gives the EOs a distinct taste, aroma, and spiciness (El-Shemy, 2020). EOs can be obtained through expression, fermentation, dry distillation, microwave extraction, enfleurage, resin tapping, and solvent extraction (Burt, 2004; Tongnuanchan et Benjakul, 2014); however, steam distillation is the most commonly used method for the commercial production of EOs (Burt, 2004).

### 6.1 Essential oils and AhR

Owing to the increasing consumption of EOs from culinary herbs and spices in gastronomy, where several cookbooks and recipes are available, there is a growing interest in their research. The intake of EOs and their components is important; therefore, they deserve attention in terms of endocrinology, pharmacology, and toxicology (Bartonkova et Dvorak, 2018b).

Many dietary compounds have been found to be AhR ligands, which can cause food-drug interactions and thus affect human physiology and health. For example, the suppressive effect of caraway extract on the dioxin-dependent expression of AhR-regulated genes in rat hepatoma cells is known (Naderi-Kalali et al., 2005). Ligustilide, the main component of EO of lovage, suppresses BaP-induced CYP1A1 gene expression and subsequent skin damage via the NRF2 pathway (Wu et al., 2014). Eugenol, a major component of EO of clove, is an activator of AhR, which induces the nuclear translocation of AhR and the expression of AhR target genes, resulting in cell cycle inhibition and proliferation in keratinocytes (Kalmes et Blomeke, 2012; Kalmes et al., 2006). Eugenol inhibited AhR-mediated 7,12-dimethylbenz[a]anthracene (DMBA)-induced DNA damage in MCF-7 cells (Han et al., 2007). Moreover, hepatic levels of CYP1A1 were reduced in eugenol-treated rats, whereas the expression of hepatic UDP glucuronosyltransferase family members UGT1A6, UGT1A7, and UGT2B1 increased (Iwano et al., 2014). Bartonkova et Dvorak examined the effects of 31 EOs of culinary herbs and spices on the transcriptional activity of AhR, and investigated the individual and combined effects of the major constituents (>10%) of AhR-active EOs. Of the 31 EOs tested, 14 were AhR inactive. AhR-active compounds were sorted into full agonists (cumin, jasmine, vanilla, bay leaf), partial agonists (cloves, dill, thyme, nutmeg, oregano), and antagonists (tarragon, caraway, turmeric, lovage, fennel, spearmint, star anise, and anise). However, EOs are multicomponent mixtures, and their effect on transcriptional activity is the result of a combination of compounds that may be additive, synergistic, or opposite. An example is the AhR activity of the EOs of jasmine and vanilla. Both have strong AhR-agonist effects; however, the same effect is not caused by any of their major components, implying either the effect of minor constituents or the effect of a mixture. A different effect was observed for the EOs of basil and tarragon, which contained a similar percentage of estragole as a major constituent (more than 70%). Whereas the EO of basil was AhR-inactive, the EO of tarragon antagonized AhR. This phenomenon might be explained by the combined effects of estragole and the other constituents of both EOs (Bartonkova et Dvorak, 2018b)

## 6.2 Carvone

Carvone (2-methyl-5-(1-méthylethenyl)-2-cyclohexen-1-one;  $C_{10}H_{14}O$ ) is a monoterpene naturally present in the EO of caraway (*Carum carvi*), dill (*Anethum graveolens*), and spearmint (*Mentha spicata*). It exists in two enantiomeric forms: R-(–)-carvone and S-(+)-carvone. These two optical isomers produce different biological responses, especially toward olfactory receptors. S-carvone has a caraway-like spicy aroma with a medium intensity, whereas R-carvone has a sweet minty medium-strength odor (Morcia et al., 2016). Anosmia is observed in approximately 8% of the population of (R)-(–)-carvone, suggesting enantioselective odorant receptors (Geithe et al., 2017).

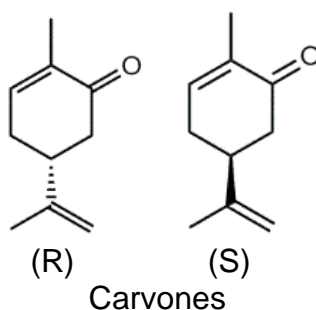


**Figure 28: Structure of R/S-carvone.**

Carvone is extensively used in the food industry (such as chewing gum, flavoring), cosmetics (such as perfumes), hygiene and care (such as toothpaste oral care products, soaps), herbalists, and pharmaceutical preparations. Wrigley patented the use of carvone in fruity bubble chewing gums (US Patent Number 5158790). R-carvone increases sweetness and prolongs the taste of chewing gum (Morcia et al., 2016). Carvone-rich EO from dill supports the production of gastric juices (which improve digestion, act against bloating, relieve cramps in the intestines and stomach) and regulates elevated blood cholesterol levels (Suresh et al., 2012). Furthermore, S-carvone blocked high-fat diet-induced weight gain and fat accumulation in the liver (Alsanea et Liu, 2017). Carvones also exhibit neuroprotective (de Sousa et al., 2007; Faliagkas et al., 2015), antidiabetic (Alsanea et Liu, 2017), and antifungal effects (Boni et al., 2016). Carvone is also used in agriculture as a crop protection and germination agent during tuber storage (Morcia et al., 2016), and as an environmentally friendly

product against parasites and insecticides (Franzios et al., 1997). Moreover, the addition of carvone to parathion, a highly toxic organophosphate insecticide, increased the effect of insecticide by more than 90% (Gupta et al., 2012). Carvones also exhibit neuroprotective (de Sousa et al., 2007; Faliagkas et al., 2015), antidiabetic (Alsanea et Liu, 2017), and antifungal effects (Boni et al., 2016).

Bartonkova et al. were the first to identify carvone as an AhR antagonist. Carvone-rich EOs of caraway, spearmint, and dill inhibited the TCDD-inducible AhR activity to 10% of its initial activity. A similar degree of the inhibition was achieved by the major constituents S-carvone and R-carvone. Antagonist activity was also observed in the mixtures of major constituents. Hence, the inhibitory activities of EOs of caraway and spearmint EOs against AhR are likely caused by their constituents, S-carvone and R-carvone, respectively (Bartonkova et Dvorak, 2018b). Ćavar Zeljković et al. tested the antiviral activity of Lamiaceae essential oils and their monoterpenes and monoterpenoids against SARS-CoV-2. Carvone-rich EOs and carvone inhibited SARS-CoV-2 in infected Vero 78 cells. Carvone can also be used as a therapy for COVID-19, particularly in topical applications of the airway mucosa or in inhalation therapy for viral respiratory infections, where biologically relevant concentrations could be achieved (Ćavar Zeljković et al., 2022).

# EXPERIMENTAL PART

## 7 Materials

### 7.1 Biological materials

#### Cell lines

The human hepatoma cell line HepG2 (ECACC No. 85011430), intestinal human colon adenocarcinoma cells LS180 (ECACC No. 87021202), human immortalized keratinocytes HaCaT (kindly donated by P. Boukamp, Leibniz-Institut für umweltmedizinische Forschung Düsseldorf, Germany), human embryonic kidney cells HEK293T (ECACC No. 12022001), African green monkey kidney fibroblast-like COS-7 cell line (ECACC No. 87021302) transiently transfected with pGL-4.27-DRE reporter plasmid (DRE-luc), and stably transfected reporter gene cell line AZ-AHR derived from human hepatoma cells HepG2 (expressing endogenous AhR and transfected construct containing several AhR binding sites upstream of a luciferase reporter gene (development described previously in (Novotna et al., 2011)) were cultured in Dulbecco's modified Eagle's medium (DMEM) supplemented with 10% of fetal bovine serum (FBS), 100 U/mL streptomycin, 100 µg/mL penicillin, 4 mM L-glutamine, 1% non-essential amino acid, and 1 mM sodium pyruvate. Mouse hepatoma cells Hepa1c1c7 (ECACC No. 95090613) were cultured in minimum essential medium (MEM) without nucleosides with 2mM glutamine and 10% FBS. Primary human hepatocytes, Hep200571 (male, 77 years, unknown ethnicity) and Hep220993 (female, 76 years, Caucasian), were purchased from Biopredic International (Rennes, France). Primary human hepatocytes, LH75 (female, 75 years old, Caucasian), were prepared at the Faculty of Medicine, Palacky University, Olomouc. The tissue acquisition protocol complied with the regulations issued by the "Ethical Committee of the Faculty Hospital Olomouc, Czech Republic" and Transplantation Law #285/2002 Coll. The cells were cultured in the ISOM medium. Cells were maintained at 37°C and 5% CO<sub>2</sub> in a humidified incubator.

#### Bacterial cultures

Rosetta 2 (DE3) competent *Escherichia coli* cells and T7 Express competent *E. coli* cells were purchased from Novagen (Merck KGaA; Darmstadt, Germany).

## Animals

Six-week-old female C57BL/6 mice which were purchased from Jackson Laboratories (Bar Harbor, Maine; # 000664) were co-housed for acclimatization at the vivarium for one week prior to experiments. Housing conditions: 14 hour light/ 10 hour dark cycle; temperature: 20-22 °C; humidity: 30-70%; diet: LAB Diet #5058. The experiments were approved by the Institutional Animal Care and Use Committee of the Albert Einstein College of Medicine (New York, NY, USA; Protocol #00001405). They were performed with the following institutional and national guidelines (Percie du Sert et al., 2020).

## 7.2 Compounds and reagents

S-carvone (sc-239480, purity 99.4%, Lot L0613), R-carvone (sc-293985, purity 99.7%, Lot H1015), D-limonene (sc-205283, Lot F1314), indole (sc-257606, purity 98.4%, Lot J0918), 3-methylindole (sc-256535, purity 99.9%, Lot E0418), indirubin (sc-201531A, purity 96.5%, Lot B1513) were purchased from Santa Cruz Biotechnology (Santa Cruz, CA, USA). BaP (B1760, Lot SLBS0038V, purity 99%), FICZ (SML1489, Lot 0000026018, purity 99.5%), staurosporine (S4400, purity 98%), deferoxamine mesylate (DFX; D9533, purity 92.5%), dexamethasone (DEX; D4902, Lot 112K12845, purity 98%), dimethyl sulfoxide (DMSO; D8418), DMEM, MEM, FBS, non-essential amino-acids, L-glutamine, penicillin, streptomycin, TRI Reagent®, Triton X 100, D-luciferin, coenzyme A, adenosine triphosphate (ATP), MTT (3-[4,5-dimethylthiazole-2-yl]-2,5-diphenyltetrazolium bromide; M2128; purity 98%), bovine serum albumin and protease inhibitor cocktail (5056489001) were purchased from Sigma-Aldrich (Prague, Czech Republic). TCDD (RPE-029) was purchased from Ultra Scientific (North Kingstown, RI, USA), and 2,3,7,8-tetrachlorodibenzofuran (TCDF; Amb17620425, Lot 51207-31-9) was purchased from Ambinter (Orléans, France). Radio-labeled [<sup>3</sup>H]-TCDD (ART 1642, lot 181018, purity 98.6%) was purchased from American Radiolabeled Chemicals (St. Louis, MO, USA). Bio-Gel® HTP Hydroxyapatite (1300420, Lot 64079675) and QC Colloidal Coomassie S stain (1610803) were purchased from Bio-Rad Laboratories (Hercules, CA, USA). M-MuLV Reverse Transcriptase (M0253) and Random Primer 6 (S1230S) were acquired from New



England Biolabs (Ipswich, MA, USA). LightCycler® 480 Probes Master (04707494001), LightCycler® 480 SYBR Green I Master (04707516001), and EDTA-free cComplete™ protease inhibitor cocktail (11873580001) were purchased from Roche Diagnostic Corporation (Prague, Czech Republic). The UPL probes and oligonucleotide primers were designed by the Universal Probe Library Assay Design Center and synthesized by Sigma-Aldrich (Prague, Czech Republic). KicQ start probes were acquired from Sigma-Aldrich (Prague, Czech Republic). WesternSure® PREMIUM Chemiluminescent Substrate (926-95000) was purchased from LI-COR Biotechnology (Lincoln, NE, USA). Simple western blotting reagents from Sally Sue™ were acquired from ProteinSimple (San Jose, CA). The Pierce™ Co-Immunoprecipitation Kit (26149), PowerUp SYBR Green Master Mix (A25742), NuPAGE Bis-Tris protein gels, and B-PER Complete Bacterial Protein Extraction Reagent (90079) were obtained from Thermo Fisher Scientific (Waltham, MA, USA). Lysis buffer (E4030) and the Nano-Glo HiBiT lytic detection system (N3040) were purchased from Promega (Madison, WI, USA). VectaShield® Antifade Mounting Medium was purchased from Vector Laboratories (Newark, CA, USA), SimpleChIP Plus Enzymatic Chromatin IP kit (Magnetic Beads, 9005) from Cell Signaling Technology (Danvers, MA, USA), PKC Kinase Activity Assay Kit (ab139437) from Abcam (Cambridge, UK), SYPRO orange dye (S6650) from Invitrogen (Waltham, MA, USA), Denerase from c-LEcta (Leipzig, Germany), and RED-tris-NTA 2<sup>nd</sup> generation dye from NanoTemper Technologies GmbH (München, Germany).

## **Antibodies**

Anti-CYP1A1 mouse monoclonal antibody (Santa Cruz Biotechnology, sc-393979, A-9, LOT C0217); anti-β-actin mouse monoclonal antibody (Cell Signalling Technology, 3700S, LOT 15, 8H10D10); anti-ARNT 1 mouse monoclonal antibody (Santa Cruz Biotechnology, sc-17812, G-3, LOT B2306); anti-AhR mouse monoclonal antibody (Santa Cruz Biotechnology, sc-133088, A-3, LOT 1718); anti-His-tag mouse monoclonal antibody (Invitrogen, MA1-21315, LOT WH326875); anti-FLAG-tag rabbit monoclonal antibody (Cell Signaling Technology, 14793S, LOT 5); Phospho-Histone H2A.X rabbit monoclonal antibody (Cell Signaling Technology, CST9718); Alexa Fluor 488

labeled anti-AhR mouse monoclonal antibody (Santa Cruz Biotechnology, sc-133088 , LOT AF488); anti-AhR rabbit monoclonal antibody (Cell Signaling Technology, D5S6H, LOT 83200); horse anti-mouse secondary HRP-linked antibody (Cell Signaling Technology, 7076S, LOT 34); goat anti-rabbit secondary HRP-linked antibody (Cell Signaling Technology, 7074P2, LOT 30); goat anti-mouse secondary HRP- linked antibody (Protein Simple, PN 042-205, LOT 86063).

## **8 Methods**

### **8.1 Cytotoxicity test (MTT)**

The human cancer AZ-AHR cells were seeded at 96-well plates at a density of 25 000 cells/well and incubated for 4 and 24 h with AhR agonists at concentrations ranging from 10 pM to 100  $\mu$ M (TCDD up to 100 nM) or carvone at concentrations ranging from 10 nM to 1 mM, vehicle (DMSO; 0.1% v/v), and Triton X-100 (1%, v/v). Thereafter, the medium was removed, and the cells were washed with 1x phosphate buffered saline (PBS) and incubated with 0.3 mg/mL MTT solution in a volume of 100  $\mu$ L/well. The reaction was stopped by removing the MTT solution and adding 60  $\mu$ L of DMSO. Absorbance was measured spectrophotometrically at 540 nm using a Tecan Infinite M200 Pro plate reader (Schoeller Instruments, Czech Republic). The data were expressed as a percentage of cell viability, where 100% represented the lowest tested concentration, whose effect was comparable to the negative control, and 0% represented positive control, respectively.

### **8.2 Reporter gene assay**

Stably transfected gene reporter AZ-AHR cells were used to evaluate the transcriptional activity of AhR (Novotna et al., 2011). Cells were seeded in 96-well culture plates at a density of 25 000 cells/well and incubated for 4 and 24 h with the tested compounds, carvone, vehicle (DMSO; 0.1% v/v), and AhR agonists (agonist mode) or their combinations (antagonist mode). Thereafter, the cells were washed with 1 $\times$  PBS and lysed using a Reporter Lysis Buffer according to the manufacturer's instructions. Luciferase activity was

measured using a Tecan Infinite M200 Pro plate reader (Schoeller Instruments, Czech Republic).

### **8.3 Quantitative real-time polymerase chain reaction qRT-PCR**

LS180, HepG2, and HaCaT cells were seeded in 6-well plates at a density of  $1 \times 10^6$  cells/well and incubated for 24 h with AhR agonists at  $EC_{80}$  concentrations or in their combination with carvone at concentrations ranging from 10  $\mu$ M to 1 mM and vehicle (DMSO; 0.1% v/v). Primary human hepatocytes were stabilized 24 h after delivery. Thereafter, the cells were treated with the AhR agonists, carvone, and their combinations for 24 h. Total RNA was isolated using TRI Reagent® according to the manufacturer's instructions. RNA concentration was determined using a Nanodrop Lite Spectrophotometer (Thermo Fisher Scientific, USA), and cDNA was synthesized from 1  $\mu$ g of total RNA using M-MuLV Reverse Transcriptase and Random Primers 6 at 42°C for 60 min and diluted in 1:4 ratio using PCR grade water. qRT-PCR was performed on Light Cycler® 480 Instrument II (Roche Diagnostic Corporation, Prague, Czech Republic) UPL Probes Library, using the following program: an activation step at 95°C for 10 min; followed by 45 cycles of PCR (denaturation at 95°C for 10 s; annealing with elongation at 60°C for 30 s). KiCqStart Probes were subjected to the following program: an activation step at 95°C for 20 s, followed by 45 cycles of PCR (denaturation at 95°C for 5 s; annealing with elongation at 58°C for 30 s). The experiments were performed in triplicate. Data were processed using the delta-delta  $C_t$  method and normalized per glyceraldehyde-3-phosphate dehydrogenase (GAPDH) as a housekeeping gene.

For animal experiments, cDNA was synthesized from 2  $\mu$ g of total RNA using a High Capacity cDNA Reverse Transcription Kit (#4368814, Thermo Fisher Scientific, USA). qRT-PCR was performed using PowerUp SYBR Green Master Mix on a ViiA Y Real-Time PCR System (Thermo Fisher Scientific, USA).

The levels of individual mRNAs were determined using the probes and primers listed in Table 1.

**Table 1: Primers and probes used in qRT-PCR**

Gene	Primers and probes	Supplier
GAPDH	probe: GAPDH-UPL60	Universal Probes Library, Roche
	fw: CTCTGCTCCTCTGTTTCGAC	
	rev: ACGACCAAATCCGTTGACTC	
CYP1A1	probe: CYP1A1-UPL33	
	fw: CCAGGCTCCAAGAGTCCA	
	rev: GATCTTGGAGGTGGCTGCT	
GAPDH	probe: [6FAM]ACTAACCTGCGCTCCTGCCTCGAT[OQA]	KiCqStart®
	fw: GAAGGAAATGAATGGGCAGC	
	rev: TCTAGGAAAAGCATCACCCG	
PAI-1	probe: [6FAM]GTGGCCTCCTCATCCACAGCTGTCA[OQA]	
	fw: GCTGCAGAAAGTGAAGATCG	
	rev: GTCCATGATGATCTCCTCGG	
AhRR	probe: [6FAM]AAACCCAGAGCAGACACCCGAGCCA[OQA]	
	fw: GAGATGAAAATGAGGAGCGC	
	rev: TTTTACTTTTGCATCCGCGG	
GAPDH	fw: AGGTGAAGGTCGGAGTCA	Eurofins Genomics
	rev: GGTCATTGATGGCAACAA	
VEGF	fw: TGCAAAAACACAGACTCGCG	
	rev: TGTCACATCTGCAAGTACGTTTCG	
mRplp0	fw: CGTCCTCGTTGGAGTGACAT	Thermo Fischer Scientific
	rev: TAGTTGGACTTCCAGGTGCGC	
mCXCL5	fw: TGCCCTACGGTGGGAAGTCAT	
	rev: AGCTTTCTTTTTGTCACTGCC	
mCYP1A1	fw: CTCTTCCCTGGATGCCTTCAA	
	rev: GGATGTGGCCCTTCTCAAATG	
mIL-1b	fw: CAGGCAGGCAGTATCACTCA	
	rev: AGGTGCTCATGTCCCTCATCC	

#### 8.4 Simple western blotting by Sally Sue™

HepG2, HaCaT, and LS180 cells were seeded at 6-well culture plates in the density of  $1 \times 10^6$  cells/well and incubated for 24 h with AhR agonists TCDD, BaP, and FICZ, applied in their EC<sub>80</sub> concentrations or their combination with carvone at concentrations ranging from 10  $\mu$ M to 1 mM and vehicle (DMSO; 0.1% v/v). Thereafter, the cells were washed with ice-cold PBS, scraped, and centrifuged at  $1500 \times g/3$  min/RT. Total protein extract was isolated from pellets using ice-cold lysis buffer (150 mM NaCl, 10 mM Tris pH 7.2, 1% (v/v) Triton X-100, 0.1% (w/v) SDS, 1% (v/v) sodium deoxycholate, 5 mM EDTA, anti-protease cocktail, and anti-phosphatase cocktail). The mixture was centrifuged at  $13\ 000 \times g/15$  min/4°C. The supernatant was collected,

and the protein concentration was determined using the Bradford reagent. Detection of CYP1A1 and  $\beta$ -actin proteins the Sally Sue™ Simple Western system using Compass Software version 2.6.5.0 (ProteinSimple™, USA). Immuno-detection was performed using a primary antibody against CYP1A1 (sc-393979, dilution 1:100; Santa Cruz Biotechnology, USA) and  $\beta$ -actin (3700S, dilution 1:100; Cell Signaling Technology, USA). Detection was performed using an HRP-conjugated secondary antibody (PN 042-205, undiluted, Protein Simple), followed by reaction with a chemiluminescent substrate.

### **8.5 7-ethoxyresorufin-O-deethylase activity (EROD)**

AZ-AHR cells were plated in 96-well culture dishes at a density 25 000 cells/well. Cells were incubated for 24 h with vehicle (DMSO; 0.1% v/v), TCDD (13.5 nM), or TCDD (13.5 nM) with S-carvone (1 mM). After washing with PBS, the medium containing 7-ethoxyresorufin (8  $\mu$ M) and dicoumarol (10  $\mu$ M) was added to the cells. To inhibit CYP1A1 catalytic activity, AZ-AHR cells were pre-incubated with TCDD (13.5 nM). Thereafter, S-carvone (1 mM, 100  $\mu$ M, 10  $\mu$ M, and 1  $\mu$ M) in a mixture with the CYP1A1 substrate was applied to the cells. After 30 min of incubation at 37°C, an aliquot of 75  $\mu$ L of the medium was mixed with 125  $\mu$ L of methanol, and fluorescence was measured in a 96-well plate with 530 nm excitation and 590 nm emission filters, using a Tecan Infinite M200 Pro plate reader (Schoeller Instruments, Czech Republic).

### **8.6 Radioligand binding assays**

Aryl hydrocarbon receptor: Cytosol from Hepa1c1c7 cells was isolated as previously described (Denison et al., 2002). Cytosolic proteins (2 mg/mL) were incubated for 2 h at room temperature in the presence of 2 nM [<sup>3</sup>H]-TCDD and S-carvone (1  $\mu$ M, 10  $\mu$ M, 100  $\mu$ M, 1000  $\mu$ M), FICZ (10 nM; positive control), DEX (100 nM; negative control), or vehicle (DMSO; 0.1% v/v; corresponding to specific binding of [<sup>3</sup>H]-TCDD = 100%). Ligand binding to the cytosolic proteins was determined using a hydroxyapatite-binding protocol and scintillation counting. Specific binding of [<sup>3</sup>H]-TCDD was determined as the difference between the total and non-specific (TCDF; 200 nM) reactions. Five independent

experiments were performed, and the incubations and measurements were performed in triplicates for each experiment (technical replicates).

A radioligand binding assay counter-screen (with 100  $\mu$ M and 1000  $\mu$ M S-carvone) was performed on a series of human recombinant steroids and nuclear receptors at Eurofins Panlabs Discovery Services Taiwan (New Taipei City, Taiwan) and Eurofins Cerep SA (Poitiers, France).

Glucocorticoid receptor (GR; NR3C1) is an endogenous receptor in IM-9 cells. The model ligand was 1.5 nM [ $^3$ H]-dexamethasone, and the non-specific competitor was 10  $\mu$ M triamcinolone. The incubation period was 6 h at 4°C.

Androgen receptor (AR; NR3C4): Endogenous receptor in LNCaP cells. The model ligand was 1 nM [ $^3$ H]-methyltrienolone and the non-specific competitor was 1  $\mu$ M testosterone. The incubation period was 24 h at 4°C.

Progesterone receptor (PR; NR3C3): endogenous receptor in T47D cells. The model ligand was 0.5 nM [ $^3$ H]-progesterone, and the non-specific competitor was 1  $\mu$ M promegestone. The incubation period was 20 h at 4°C.

Estrogen receptor alpha (ER $\alpha$ ; NR3A1): Recombinant receptor expressed in sf9 cells. The model ligand was 0.5 nM [ $^3$ H]-estradiol, and the non-specific competitor was 1  $\mu$ M diethylstilbestrol. The incubation period was 2 h at room temperature.

Estrogen receptor beta (ER $\beta$ ; NR3A2): Recombinant receptor expressed in sf9 cells. The model ligand was 0.5 nM [ $^3$ H]-estradiol, and the non-specific competitor was 1  $\mu$ M diethylstilbestrol. The incubation period was 2 h at 25°C.

Peroxisome proliferator-activated receptor gamma (PPAR $\gamma$ ; NR1C3): Recombinant receptor expressed in *E. coli*; the model ligand was 5 nM [ $^3$ H]-rosiglitazone, and the non-specific competitor was 10  $\mu$ M rosiglitazone. The incubation period was 2 h at 4°C.

Retinoid X receptor alpha (RXR $\alpha$ ; NR2B1): Recombinant receptor expressed in sf9 cells. The model ligand was 5 nM [ $^3$ H]-9-cis-retinoic acid, and the non-specific competitor was 3  $\mu$ M 9-cis-retinoic acid. The incubation period was 1 h at 4°C.

## 8.7 Intracellular distribution of AhR

Immunofluorescence assays were performed as previously described (Stepankova et al., 2018). LS180 cells were seeded on chamber slides (ibidi GmbH, Germany) and cultured for 2 days. Cells were then treated for 90 min with carvone (1000  $\mu$ M) in combination with vehicle (DMSO; 0.1% v/v) or the AhR agonists TCDD (20 nM), BaP (7  $\mu$ M), or FICZ (8 nM). After the treatment, washing, fixation, permeabilization, and blocking, the cells were incubated with Alexa Fluor 488 labeled primary antibody against the AhR (sc-133088, dilution 1:500, Santa Cruz Biotechnology, USA) in 0.5% bovine serum albumin at 4°C overnight. The next day, nuclei were stained with 4',6-diamino-2-phenylindole (DAPI), and cells were enclosed in VectaShield® Antifade Mounting Medium (Vector Laboratories Inc., USA). The AhR translocation into the nucleus was visualized and evaluated using fluorescence microscope IX73 (Olympus, Japan). The whole staining protocol was performed in two independent experiments with technical duplicates (for all tested compounds). The AhR translocation was evaluated visually based on the distinct signal intensity of the AhR antibody in the nucleus and cytosol. For percentage calculation, approximately 100 cells from at least four randomly selected fields of view in each replicate were used.

## 8.8 Protein immunoprecipitation assay

LS180 cells were plated at 60 mm Petri dishes at the density  $4 \times 10^6$  cells/dish and incubated with carvone (1000  $\mu$ M) in combination with vehicle (DMSO; 0.1% v/v) or the AhR agonist TCDD (20 nM), BaP (7  $\mu$ M), and FICZ (8 nM), their  $EC_{80}$  from 4 h treatment, for 90 min at 37°C. A Pierce™ Co-Immunoprecipitation Kit was used, and the protein immunoprecipitation assay was performed according to the manufacturer's instructions. Briefly, the cells were washed with ice-cold PBS, lysed, and centrifuged at  $13\,000 \times g$  for 10 min at RT. Twenty five micrograms of AhR antibody (sc-133088; Santa Cruz Biotechnology, USA) were covalently coupled to the resin for 120 min at room temperature. The antibody-coupled resin was incubated with the cell lysate overnight at 4°C. The next day precipitate was eluted. In parallel with the total parental lysates, eluted protein complexes were

diluted in delivered sample buffer and resolved on 8% SDS-PAGE gels, followed by western blot analysis and immuno-detection with ARNT 1 antibody (sc-17812, dilution 1:250, Santa Cruz Biotechnology, USA) and AhR antibody (sc-133088, dilution 1:500, Santa Cruz Biotechnology, USA). Chemiluminescent detection was performed using an HRP-conjugated anti-mouse secondary antibody (7076S, dilution 1:2000, Cell Signaling Technology, USA) and WesternSure® PREMIUM Chemiluminescent Substrate using a C-DiGit® Blot Scanner (LI-COR Biotechnology, USA).

## 8.9 Chromatin immunoprecipitation assay

This assay was performed as previously described (Stepankova et al., 2018). Briefly, HepG2 cells were seeded in a 60-mm dish, and the following day they were incubated with carvone (1000  $\mu$ M) in combination with vehicle (DMSO; 0.1% v/v) or the AhR agonists TCDD (20 nM), BaP (7  $\mu$ M), and FICZ (8 nM) for 90 min at 37°C. The procedure followed the manufacturer's recommendations for the SimpleChIP Plus Enzymatic Chromatin IP Kit. Immunoprecipitation was performed using an anti-AhR rabbit monoclonal antibody (D5S6H; Cell Signaling Technology, USA).

RT-PCR reaction was performed using SYBR Green dye and CYP1A1 promoter primers (5'-AGCTAGGCCATGCCAAAT-3', 5'-AAGGGTCTAGGTCTGCGTGT-3').

## 8.10 Protein kinase C inhibition assay

Protein kinase C (PKC) inhibition was assayed in lysates from HepaG2 cells, using a PKC Kinase Activity Assay Kit. Cells were grown to 90% confluence in a 60 mm dish. After removing the medium, 1 mL of lysis buffer (Promega) was applied for 10 min on ice. The cells were scraped, sonicated, and centrifuged at 15 000  $\times g$ /15 min/4°C (Eppendorf Centrifuge 5415R; Eppendorf, UK). Then, 3  $\mu$ L of cell lysate was mixed with 297  $\mu$ L of Kinase Assay Buffer and aliquoted 40  $\mu$ L into 0.5 mL microtubes. These aliquots were mixed with 1/100 stock solutions of carvone to obtain the final concentrations of 10  $\mu$ M, 100  $\mu$ M, and 1000  $\mu$ M. DMSO (1% v/v) and staurosporine (1  $\mu$ M) were used as the negative and positive controls, respectively. The reaction was initiated by adding



10  $\mu$ L reconstituted ATP, and the rest of the procedure was performed according to the manufacturer's instructions. The absorbance was measured at 450 nm using a microplate reader (Infinite M200; TECAN, Austria). The results are expressed as the percentage of the negative control. The cell lysate was stored at  $-80^{\circ}\text{C}$  and used for performing three independent experiments.

### **8.11 KINOMEscan™ profiling**

The KINOMEscan™ screening platform (ScanMAX assay) employs a proprietary active-site-directed competition binding assay that quantitatively measures the interactions between test compounds (here 100  $\mu$ M S-carvone) and 468 human protein kinases (Fabian et al., 2005). The assay was performed by the Eurofins DiscoverX Corporation (Fremont, CA, USA).

### **8.12 Tyrosine-protein phosphatases non-receptor type inhibition assays**

The catalytic activity of PTPN11/SHP2 and PTPN6/SHP1 was measured using recombinant enzymes incubated with vehicle (DMSO, 0.1% v/v), PTP1B inhibitor (33.3  $\mu$ M), and S-carvone (100  $\mu$ M; 1000  $\mu$ M). Phosphatase activity was monitored as a time-course measurement of the increase in the fluorescence signal from the fluorescent substrate (6,8-difluoro-4-methylumbelliferyl phosphate) and the initial linear portion of the slope (signal/min) was analyzed. The assays were performed by Reaction Biology Corporation (Malvern, PA, USA).

### **8.13 HSP90 fluorescence competitive binding assay**

The HSP90 fluorescence competitive binding assay is based on the competition between fluorescently labeled geldanamycin for binding to HSP90. The fluorescent substrate binds to the ATP-binding pocket of HSP90; therefore, an ATP-competitive inhibitor was found in this assay. The assay was performed by Reaction Biology Corporation (Malvern, PA, USA).

## 8.14 Molecular modeling and Docking

The full-length three-dimensional structure of the human AhR has not yet been resolved. The structure available in the alpha-fold database consists of several unstructured regions that are unsuitable for understanding the binding modes of carvones. Furthermore, a recent effort by Bourguet's group has resulted in a high-resolution cryo-EM structure of the indirubin-bound HSP90-XAP2-AhR complex (Gruszczuk et al., 2022) but could not be used to understand the binding mode of carvones, as the cryo-EM studies failed to resolve the coordinates for the 270 residues from the N-terminal region. The crystal structure complex of a construct of human AhR with a truncated mouse ARNT has been solved (PDB code: 5NJ8) (Schulte et al., 2017). Because the solved structure did not contain the ligand-binding domain of AhR, it was modeled based on the neuronal PAS-1 protein (PDB code: 5SY5) (Wu et al., 2016), as previously described (Stepankova et al., 2018). The molecular structures of the carvones were modeled using the ligand builder module of the Molecular Operating Environment (MOE ver. 2018; Chemical Computing Group, Montreal, Canada). The molecules were energy-minimized and the geometry was optimized for docking studies. Because carvones occupy a small volume and have the potential to bind to nearly any binding pocket, we utilized a triage-based approach to finalize the predicted binding pocket. We screened the PAS-B domain of AhR containing the binding pockets for TCDD, FICZ, BaP, CH-223191, vemurafenib, dabrafenib, PLX7904, PLX8394, and resveratrol as detailed in (Corre et al., 2018), and our newly developed methylindoles (Stepankova et al., 2018). Pockets containing TCDD were used as control for each docking. All docking screening experiments were performed using GOLD version 5.2 (Cambridge Crystallographic Data Centre, Cambridge, UK) (Jones et al., 1995). The complexes were ranked using the default option of GOLD SCORE, and the best-ranking complexes were visualized using MOE. The molecules were also docked to the AhR derived from the AhR-ARNT complex. The S-carvone-bound AhR was then energy-minimized and subjected to molecular dynamics simulation with a production run of 10 ns. The docked protein complex of AhR protein with S-carvone was incorporated into an aqueous rectangular box with dimensions of 106 nm × 106 nm × 106 nm. Potassium chloride (0.15 M) was added with extra

ions to neutralize the excess charges. The water molecules were modeled as TIP3P water. The initial minimization and equilibration were carried out on our local server using the NAMD software (Version 2.15) and CHARMM36 force field. The force field for the ligand was generated using CHARMM General Force Field (CGenFF) program version 2.5.1. The production simulation was conducted on the Anton2 supercomputer at the Pittsburgh Supercomputing Center for 400 ns with a 2.5 fs time step. Simulations were run in the NPT ensemble at 310 K and 1 bar using a Nose-Hoover thermostat and the MTK barostat. The cutoff distances for the non-bonded interactions were determined automatically using Anton2. Structural snapshots were taken at 10 ns, 100 ns, and 250 ns, and the binding mode of carvone was assessed to determine binding specificity.

### **8.15 Thermal shift assay**

Human AhR, encoding amino acid residues 112-272 (domain PASA), was subcloned into the pMKH vector to produce a his6-TEV-hAHR(PASA) construct. The plasmid was transformed into Rosetta (DE3) cells, and the protein was expressed in LB media. Cells were dissolved in lysis buffer containing 20 mM Tris (pH 8.0), 500 mM NaCl, 5% glycerol, 5 mM imidazole, and a protease inhibitor cocktail. The supernatant was collected after sonication and centrifugation, and then passed through a Ni-NTA His-bind resin (#70666-5, Millipore). The resin was washed thrice with lysis buffer, The proteins were eluted with 200 mM imidazole in lysis buffer. The purified protein was passed through a gel filtration column (HiLoad 16/600 Superdex 75) to remove the aggregated proteins and imidazole. The His tag was removed by TEV cleavage, and the final hAHR(PASA) protein was pooled in size-exclusion chromatography with a Bis-Tris Propane buffer (20 mM Bis-Tris Propane, pH 8.0, 150 mM NaCl). For the thermal shift assay, 50 nL of the compound was transferred into a 384-well plate using an Echo 555 liquid handler (Labcyte), and then 5  $\mu$ L of protein solution was added to each well in a microplate dispenser (#5840300, Thermo Scientific). The protein solution was prepared by diluting hAHR(PASA) protein to 0.1 mg/mL in Bis-Tris Propane buffer, and then add SYPRO orange dye was added to a final concentration of 8 $\times$ . The plate was centrifuged at 1000  $\times$  g for 10 s and incubated at room temperature for 30 min before being

transferred to a QuantStudio 7 Flex Real-Time PCR machine (Applied Biosystems). Melt curves were generated by heating the plate from 25°C to 95°C by applying a gradient of 0.1°C/s. Data were analyzed using the protein thermal shift software v1.4 (Applied Biosystems).

### **8.16 Cellular thermal shift assay**

Human AhR, encoding amino acid residues 112-272 (domain PASA), was subcloned into the pBiT3.1-N vector to produce a HiBiT-hAHR(PASA) construct. HEK293T cells were cultured in Dulbecco's Modified Eagle Medium (DMEM) media (#31966-021, Gibco) at 37°C, 5% CO<sub>2</sub>. The plasmid was transfected into HEK293T cells using Lipofectamine 3000 (L3000001, Invitrogen) and the cells were grown to 60–80% confluence. Cells were harvested 3 days after transfection. The cells were washed twice with ice-cold PBS, scraped, and suspended in Bis-Tris Propane buffer containing protease inhibitor cocktail. The cells were sonicated, and the supernatant was collected after centrifugation. The cell lysate was diluted to 0.3 mg/mL for further analysis. The compound solution (50 nL in DMSO) was transferred to a 384-well plate with an Echo 555 liquid handler (Labcyte), and 5 µL of the cell lysate was added to each well. The plate was spun at 1000 × *g* for 10 s and incubated at room temperature for 30 min. The plate was heated in a PCR thermal cycler (Bio-Rad, C1000 Touch) at a gradient of 38–62°C for 3 min. Denatured proteins were removed by spinning the plates at 4300 × *g* for 15 min, and soluble HiBiT-hAHR(PASA) protein was detected using the Nano-Glo HiBiT lytic detection system, according to the manufacturer's protocol.

### **8.17 Microscale thermophoresis**

A codon-optimized fragment of human AhR encoding amino acid residues 23–273 was synthesized and cloned into pET28b(+) using NdeI and BamHI restriction sites to express an N-terminally fused 6×His-tag. A codon-optimized fragment of mouse Arnt encoding amino acid residues 85–345 was synthesized and cloned into pETDuet-1 using BamHI and HindIII restriction sites, expressing N-terminally fused 6×His-tag or using NcoI and HindIII restriction sites, expressing N-terminally FLAG-tag (GenScript, Leiden, Netherlands).

The truncated versions of AhR and Arnt were selected based on the previously published data (Puyskens et al., 2020; Schulte et al., 2017). Both constructs were coexpressed in Rosetta 2 (DE3) *E. coli* cells. Protein production was induced with 1 mM isopropyl- $\beta$ -thiogalactopyranoside, and cells were grown at 20°C in LB medium overnight. Cells were lysed at 30 kpsi using a One-Shot cell lyser (Constant Systems Ltd.), and an EDTA-free cOmplete™ protease inhibitor cocktail was added. B-PER complete bacterial protein extraction reagent and erase were added to the lysate. Protein heterodimers were partially purified using HisPur Cobalt columns (Thermo Fisher Scientific) to obtain solutions in a final buffer containing 20 mM HEPES (pH 7.0), 300 mM NaCl, and 5% (w/v) glycerol. The presence of AhR and Arnt proteins was verified by Western blot using anti-His-tag (MA1-21315, dilution 1:1000; Invitrogen) and anti-FLAG-tag (14793S, dilution 1:1000; Cell Signaling Technology) antibodies. Lysates from *E. coli* were separated through electrophoresis on precast NuPAGE Bis-Tris protein gels and visualized using Coomassie Brilliant Blue staining. Excised gel pieces with protein bands corresponding to the expected molecular masses of recombinant AhR and Arnt were processed using the previously described in-gel digestion and peptide extraction protocols (Shevchenko et al., 2006), and the recombinant proteins were identified using nanoflow liquid chromatography of peptides coupled to tandem mass spectrometry (Petrovska et al., 2014).

The protein fractions were concentrated to 2 mg.mL<sup>-1</sup> using 10 kDa filters (Amicon) and stored at 5°C for 10 days. Microscale thermophoresis was used to determine S-carvone and D-limonene binding to human 6×His-tagged AhR in a complex with FLAG-Arnt. The protein (200 nM) was fluorescently labeled using a RED-tris-NTA 2<sup>nd</sup> generation dye and a 1:1 dye/protein molar ratio in the reaction buffer (20 mM Tris-HCl, pH 7.4) supplemented with 150 mM NaCl and 0.075% Tween-20. The ligands were then dissolved in ethanol (max. 0.5% of the final concentration of the reaction mixture). Measurements were performed on a Monolith NT.115 instrument (NanoTemper Technologies GmbH) at 25°C with 3 s/22 s/2 s laser off/on/off times, continuous sample fluorescence recording in premium capillaries, using an excitation power of 90% and a high MST power mode. The normalized fluorescence  $\Delta F_{\text{norm}}$  [%] as a function of the ligand concentration was analyzed and was found to reflect ligand-binding interactions.

In experiments using AhR mutants (Y76A and Y76F), the above described procedure was applied, using the wt-His-hAhR(23-273) plasmid as a template for site-directed mutagenesis (GenScript, Leiden, Netherlands).

### **8.18 Covalent functionalization of the AhR with azido-S-carvone**

N<sub>3</sub>-S-carvone was synthesized according to a previously published procedure (Figure 51) (Xu et al., 2019). His-AhR(23-273)/FLAG-Arnt(85-345) was co-expressed in T7 Express *E. coli* cells as described above and reconstituted (0.5 mg/mL) in 20 mM phosphate buffer (pH 7.0) using 10 kDa filters (Amicon). The protein was mixed with 10 mM N<sub>3</sub>-S-carvone and photoactivated using a 3UV lamp (Thermo Fisher Scientific) for 1 h at 365 nm and 2 mW.cm<sup>-2</sup> intensity. The reaction mixture was resolved using SDS-PAGE, and the gel was stained with QC Colloidal Coomassie S stain. The protein bands of the recombinant His-AhR(23-273) segment were excised from the gel slab, and their contents were subjected to in-gel digestion with SOLu trypsin (Merck, Steinheim, Germany) after a reduction, followed by the carbamidomethylation of thiol groups (Shevchenko et al., 2006). Peptides from the digests were purified using ZipTip-C18 pipette tips (Merck-Millipore, Carrigtwohill, Ireland) and analyzed using MALDI-TOF/TOF MS and MSMS on an ultrafleXtreme instrument equipped with a Smartbeam II Nd:YAG laser (Bruker Daltonik, Bremen, Germany). Peptide samples (0.5 µL) were deposited on an MTP AnchorChip 384 BC MALDI target (Bruker Daltonik) using a standard dried droplet technique with an α-cyano-4-hydroxycinnamic acid matrix (5 mg/mL in 50% acetonitrile containing 0.1% trifluoroacetic acid). Calibration spots on the target were made using Peptide Calibration Standard II (Bruker Daltonik) and the same matrix. The instrumental setups for acquiring the mass spectra and tandem mass spectra were the same as those described previously (Petrovska et al., 2014). MS and MSMS data were processed using flexAnalysis 3.4 and BioTools 3.1 (Bruker Daltonik). Database searches (against the Swiss-Prot protein sequence database) were performed using ProteinScape 3.1 (Bruker Daltonik) and Mascot Server 2.4 (Matrix Science, London, UK) or using PEAKS Studio X (Bioinformatics Solutions, Waterloo, ON, Canada). The mass error

tolerances for the MS and MSMS data-based searches were 25 ppm and 0.5 Da, respectively.

### **8.19 Animal experiments**

Six-week-old female C57BL/6 mice are inbred, active, and had nearly equivalent starting weights/overall body habitus, therefore, mice were randomly picked without prior knowledge of baseline weight from each cage and assigned to control versus treatment group(s) in a consecutive manner. No randomization software was used. Since this is an exploratory analysis to generate the hypothesis that carvones protect against AhR mediated UV-damage as an in vivo “proof-of-concept” for its antagonist actions on ligand-activated AhR, a priori sample size calculations for the treatment groups and controls were not conducted. Instead, given the technical difficulty of managing more than 3 mice per treatment group for the UV studies, we performed all the experimental groups in two installments spread over time using  $n = 3/\text{treatment group}$ . Thus, in total, we obtained  $n = 6$  mice/treatment, which was included in the analyses. Experiments with RT-qPCR analysis endpoints were performed separately from experiments with H&E endpoints. No mice died or had sickness to preclude and replace the sample. Mouse ears were irradiated with short-wave UV 254 nm light (distance:  $\sim 1$  cm; absorbed dose:  $360 \text{ mJ/cm}^2$ ) using a Spectronics ENF-240C Handheld UV Lamp (Spectronics Corp., Melville, NY, USA). Chemicals were dissolved in acetone and topically applied to the skin (mouse ear). (i) BaP ( $1 \mu\text{g}$ ) was applied in two doses (0 h, 16 h); (ii) S-carvone ( $960 \mu\text{g}$ ) was applied 1 h before the first BaP dose; (iii) UV irradiation was applied at 0 h and -1 h. In each mouse, the left and right ears were exposed to different treatments, thereby providing internal individual controls for comparative treatments, and each animal then represents a biological repeat. The ears were collected at 24 h, and RNA was isolated using TRI Reagent® (Carlsbad, CA, USA, #15596026). Note: In these experiments, mouse positioning relative to the UV lamp is critical to get even exposures across entire ear, so this was optimized individually for each mouse. Adjustments of distance from the source and time of exposure will also need to be optimized for a given mouse since that natural ear positioning and curvature is different from each mouse.

*Ear histology & immunohistochemistry:* Following auricectomy, the ear tissue was rinsed, fixed in 10% buffered formalin for 24 h, and embedded in paraffin. Slices (3 mm) were cut and, for sun (UV)-burned cell scoring purposes, stained with hematoxylin-eosin. The sunburn cell count was performed by HL in a single blinded manner; the slides were decoded only after the cell count was determined. Immunohistochemical staining against gamma-H2AX-Ser139-P was performed using P-Histone H2AX primary antibody (Cell Signaling, CST9718, 1:800). Bond Polymer Refine Detection (Leica Biosystems) was used according to the manufacturer's protocol. After staining, sections were dehydrated, and film cover-slipped using a TissueTek-Prisma and Coverslipper (Sakura). Whole-slide scanning (40x) was performed on an Aperio AT2 (Leica Biosystems). Immunohistochemistry was carried out at HistoWiz, Inc. (New York City, NY, USA). Note: In these studies, ear embedding needs to be adjusted and the cut level appropriate to obtain an accurate representation of the entire "continuous" auricular epithelium. This was optimized for each mouse ear through repeated embedding and cuts adjusted to obtain a continuous epithelial layer.

## **8.20 Statistics**

All statistical analyses, as well as the calculations of half-maximal effective concentration ( $EC_{50}$ ),  $EC_{80}$ , and half-maximal inhibitory concentration ( $IC_{50}$ ) were performed using GraphPad Prism 8 for Windows (GraphPad Software, La Jolla, CA, USA). The numbers of independent repeats and technical replicates are stated in the corresponding figure legends for all the experiments. Where appropriate, data were processed using one-way analysis of variance (ANOVA) followed by Dunnett's test or Student's *t*-test. Results with  $p < 0.05$  were considered significant. The  $EC_{50}$ ,  $EC_{80}$ , and  $IC_{50}$  values were calculated using the nonlinear regression with the least-squares fitting method. The R-squared value was checked in all the calculations and did not drop below 0.9. The inhibition constant ( $K_i$ ) was calculated using the Cheng-Prusoff equation (Cheng et Prusoff, 1973). In an animal experiment, the normality of the data was analyzed by Shapiro-Wilk test, the outliers were detected by Grubbs test, and the significance was determined by Mann-Whitney non-parametric test.



## 9 RESULTS

### 9.1 Cytotoxicity of carvone

The cytotoxicity of carvone in AZ-AHR cells was determined using an MTT assay after 4 and 24 h. No significant decrease in cell viability was observed. Based on the cytotoxicity data, gene reporter assays with carvone were performed at concentrations of up to 1 mM (Figure 29).

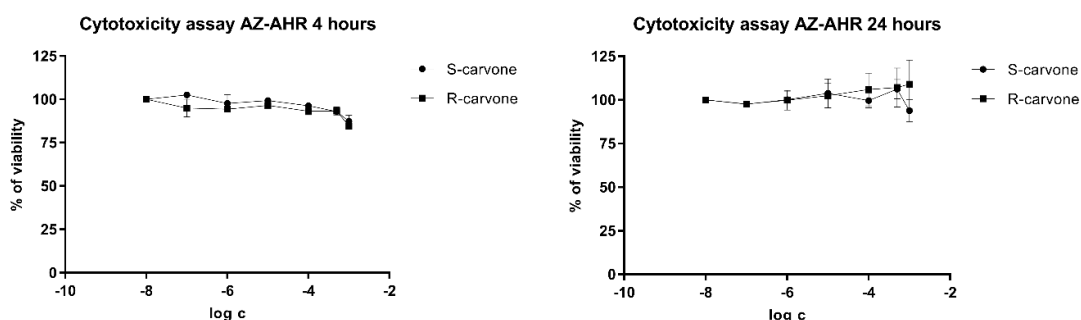


**Figure 29: Cytotoxicity of carvone.** AZ-AHR cells were incubated with carvone at concentrations ranging from 10 nM to 1 mM for 4 and 24 h. In parallel, the cells were treated with the vehicle (DMSO; 0.1% v/v; negative control) and Triton X-100 (1%, v/v; positive control). Data are presented as a mean values  $\pm$  standard deviation (SD) from three independent cell passages. Incubation and measurements were performed in four technical replicates. The percentage of cell viability achieved at the lowest concentration of the tested substance was comparable to that of the negative control.

### 9.2 The effect of carvone and AhR agonists on transcriptional activity of AhR

A wide range of AhR agonists, including TCDD, BaP, FICZ, indirubin, indole, and 3-methylindole (3-MI), have been used to investigate the effects of carvone on AhR transcriptional activity. AZ-AHR cells were incubated with carvone or AhR agonist for 4 or 24 h. AhR full agonists caused a concentration-dependent increase in AhR-mediated luciferase activity, and the  $EC_{50}$  and  $EC_{80}$  were determined (Figure 30). Carvones do not activate AhR. Moreover, a concentration-dependent decrease in luciferase activity with carvone was observed at 4 h, indicating antagonism of the AhR activators present in the medium (Figure 31).

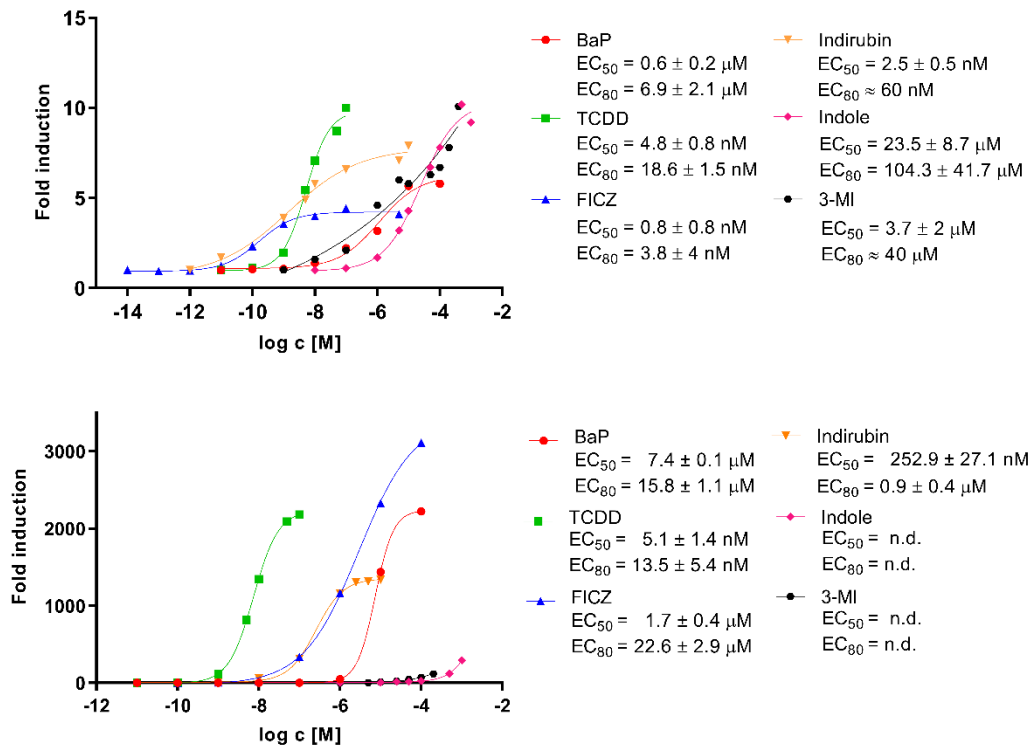


**Figure 30: Effect of AhR agonists on AhR transcriptional activity.** AZ-AHR cells were incubated for 4 or 24 h with vehicle (DMSO; 0.1% v/v) and AhR agonists (TCDD, BaP, FICZ, indirubin, indole, and 3-MI). Representative graphs from one cell passage are shown. EC<sub>50</sub> and EC<sub>80</sub> values are presented as a mean mean ± SD from three independent cell passages and measurements were performed in four technical replicates. Data are expressed as a fold-increase in luciferase activity over control cells.

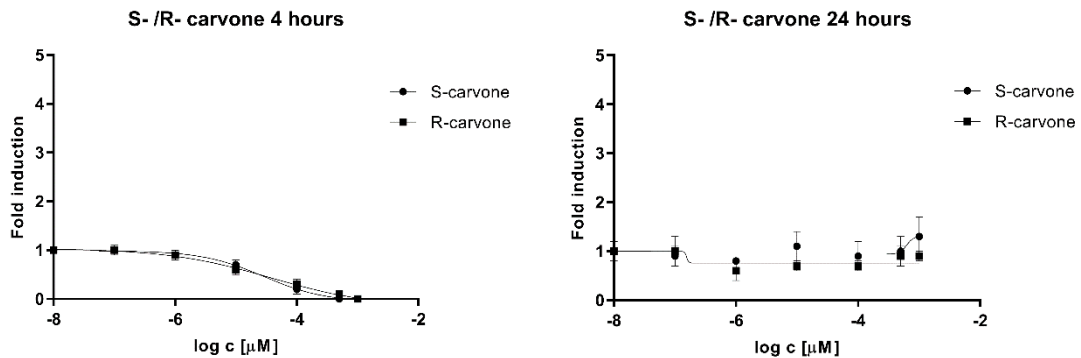
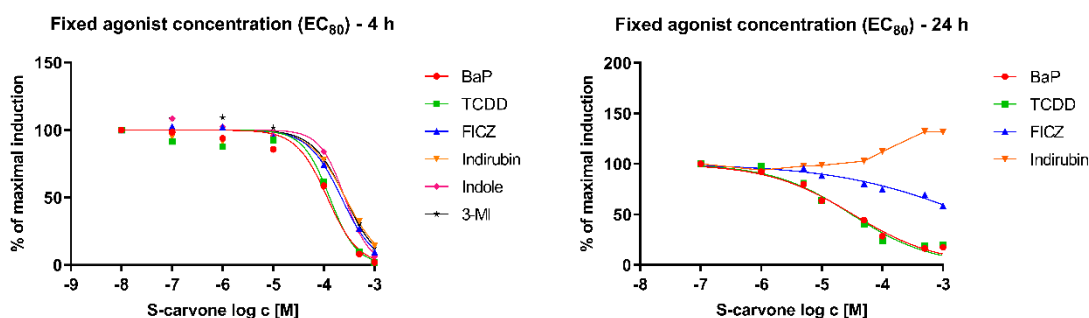


**Figure 31: Effect of S/R-carvone on AhR transcriptional activity.** AZ-AHR cells were incubated for 4 or 24 h with S/R-carvone at concentrations ranging from 10 nM to 1 mM. Data are shown as a mean ± SD from three independent cell passages and they are expressed as a fold increase in luciferase activity over control cells. Measurements were performed in four technical replicates.

### 9.3 The effect of S-carvone on agonist-inducible AhR activity

The effects of S-carvone on agonist-inducible AhR activity were examined in AZ-AHR cells co-incubated with fixed concentrations of TCDD, BaP, FICZ, indirubin, indole, or 3-MI (corresponding to their EC<sub>80</sub> values) and increasing concentrations of carvones for 4 and 24 h. After 4 h of incubation, carvone displayed a concentration-dependent antagonistic effect on AhR activation by all the agonists. After 24 h of incubation, carvone antagonized the BaP- and TCDD-activated AhR. In contrast, carvone did not inhibit FICZ-activated AhR and potentiated the activation of AhR by indirubin (Figure 32). The values of IC<sub>50</sub> and K<sub>i</sub> values were calculated using GraphPad and Cheng-Prusoff equations, respectively.



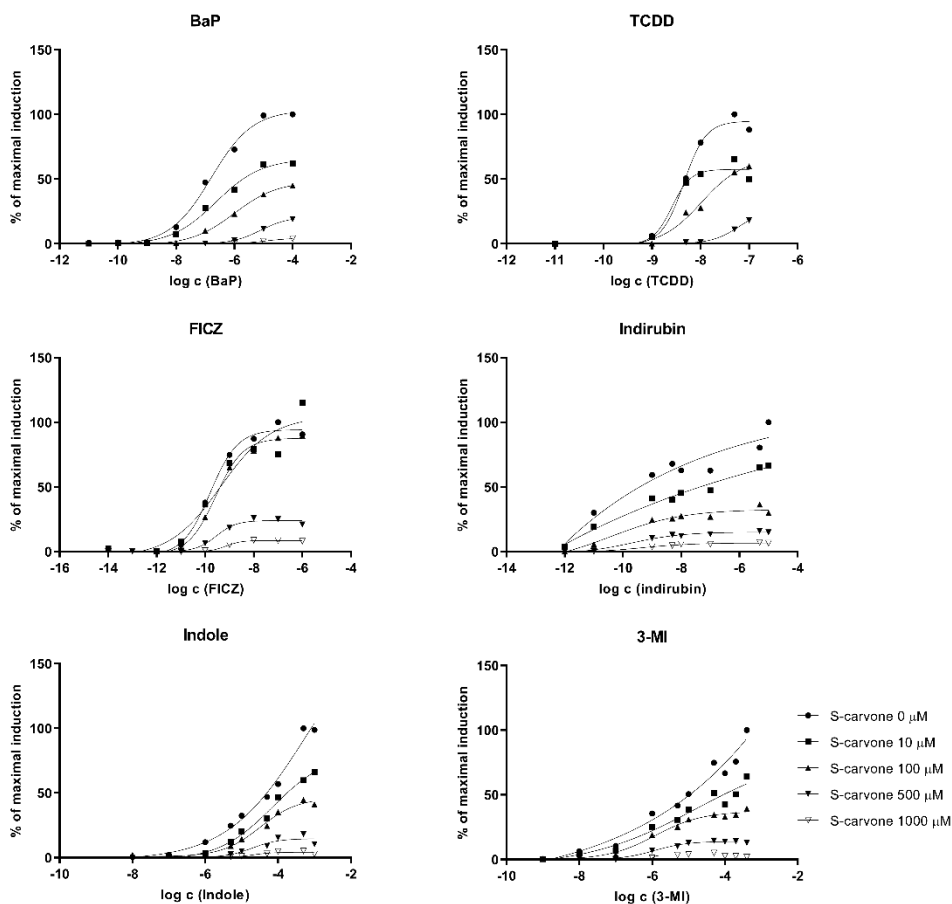
	K <sub>i</sub> [μM]			
	S-carvone		CH223191	
	4 h	24 h	4 h	24 h
BaP	11.4 ± 3.6	12.3 ± 4.3	0.4 ± 0.1	5.2 ± 0.5
TCDD	27.1 ± 5.7	7.7 ± 1.6	0.1 ± 0.03	0.03 ± 0.005
FICZ	38.7 ± 11.5	-	0.7 ± 0.3	-
Indirubin	10.8 ± 2.0	-	-	-
Indole	47.7 ± 27.9	-	0.3 ± 0.1	-
3-MI	22.9 ± 11.7	-	1 ± 0.6	-

**Figure 32: Effect of S-carvone on agonist-inducible AhR activity.** AZ-AHR cells were incubated for 4 and 24 h in combination with fixed EC<sub>80</sub> concentrations of AhR agonists and increasing concentrations of S-carvone, ranging from 100 nM to 1 mM. Representative graphs from one cell passage are shown. Values IC<sub>50</sub> and K<sub>i</sub> values from two independent cell passages are indicated in the table. Measurements were performed in five technical replicates. Data are expressed as a percentage of the maximal induction of the lowest tested S-carvone concentration.

Furthermore, the mechanism underlying AhR antagonism was analyzed. AZ-AHR cells were incubated with fixed concentrations of S-carvone (0  $\mu\text{M}$ ; 10  $\mu\text{M}$ ; 100  $\mu\text{M}$ ; 500  $\mu\text{M}$ ; 1000  $\mu\text{M}$ ) combined with increasing concentrations of individual AhR agonists. We observed a gradual decrease in  $E_{\text{MAX}}$  and a slight decline in  $EC_{50}$  with increasing concentrations of carvones for each agonist tested at both incubation times (Figure 33). These data imply that carvones exhibit either (insurmountable) non-competitive, irreversibly competitive, or uncompetitive antagonism. As carvones at a given concentration antagonized both high and low concentrations of all agonists to a similar degree (Table 2), an uncompetitive mechanism can be ruled out. The inhibition of luciferase catalytic activity was excluded (Figure 34).

Fixed concentration of S-carvone with increasing concentration of AhR agonists

**A 4 h**



**B 24 h**

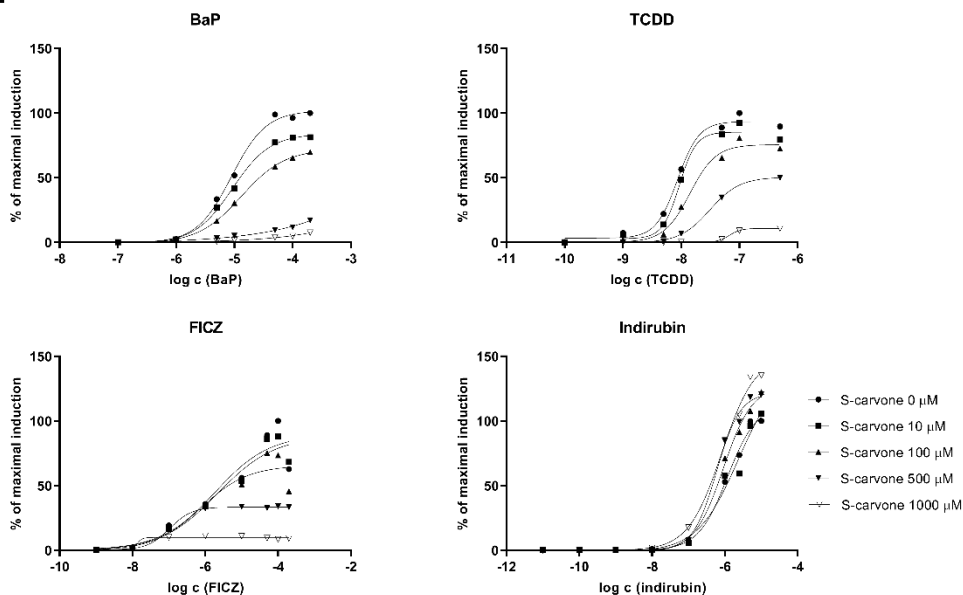


**Figure 33: Non-competitive antagonism of S-carvone.** AZ-AHR cells were incubated for 4 or 24 h with fixed concentrations of S-carvone (0, 10, 100, 500, and 1000 μM) and increasing concentrations of AhR agonists. Representative graphs from one cell passage are shown. The EC<sub>50</sub> values are indicated in the graph. Experiments were performed in three independent cell passages and incubation and measurements were performed in four technical replicates.

Representative experiments from one cell passage are shown in the plots and they are expressed as a percentage of maximal induction. **PANEL A:** 4 h of treatment. **PANEL B:** 24 h of treatment

**Table 2: Reporter gene assays for AZ-AHR.** Inhibition of ligand-inducible AhR activity by S-carvone was calculated from the plots shown in Figure 33 B, as follows: % of inhibition at  $c_x = 100 \cdot (1 - (\% \text{ of max. Induction at } c_x) / (\% \text{ of max. Induction at } c_0))$ .

% of inhibition		S-carvone				
		0 $\mu\text{M}$	10 $\mu\text{M}$	100 $\mu\text{M}$	500 $\mu\text{M}$	1000 $\mu\text{M}$
FICZ	100 nM	0%	15%	29%	44%	77%
	1 $\mu\text{M}$	0%	13%	25%	55%	82%
	10 $\mu\text{M}$	0%	17%	28%	57%	88%
	50 $\mu\text{M}$	0%	21%	30%	55%	90%
	100 $\mu\text{M}$	0%	22%	32%	53%	91%
	200 $\mu\text{M}$	0%	23%	33%	50%	91%
BaP	5 $\mu\text{M}$	0%	18%	45%	89%	95%
	10 $\mu\text{M}$	0%	19%	44%	92%	97%
	50 $\mu\text{M}$	0%	19%	37%	90%	96%
	100 $\mu\text{M}$	0%	19%	33%	87%	95%
	200 $\mu\text{M}$	0%	18%	31%	84%	93%
TCDD	5 nM	0%	39%	60%	93%	100%
	10 nM	0%	14%	55%	89%	99%
	50 nM	0%	8%	24%	62%	97%
	100 nM	0%	8%	20%	53%	90%
	500 nM	0%	8%	19%	46%	88%

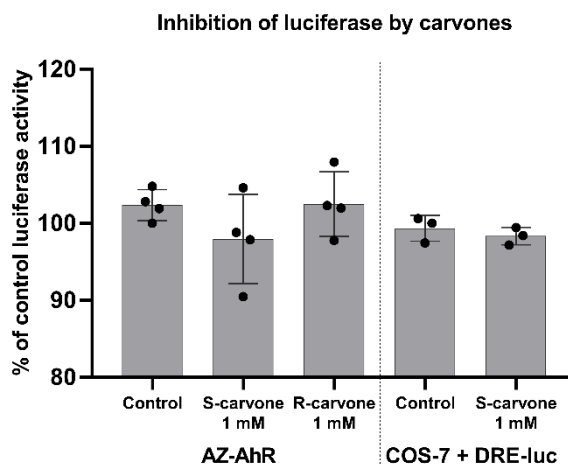
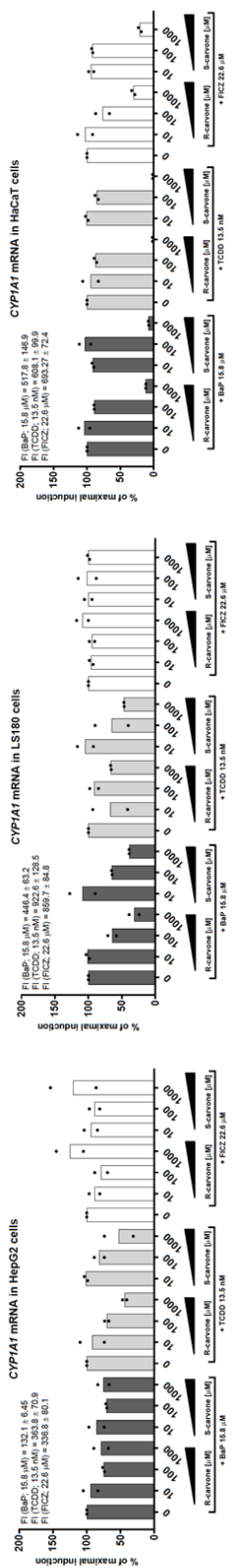


**Figure 34: Inhibition of luciferase catalytic activity.** Stably transfected AZ-AHR and COS-7 cells transiently transfected with the DRE-luc reporter plasmid were incubated for 24 h with 20 nM TCDD. Cells were lysed, and the lysate containing luciferase was incubated for 30 min with carvones (1 mM) or vehicle (control). The bar graph shows the mean  $\pm$  SD of three/four consecutive cell passages. Incubation and measurements were performed in triplicate. The bar graph shows the percentage of luciferase activity relative to that of the control.

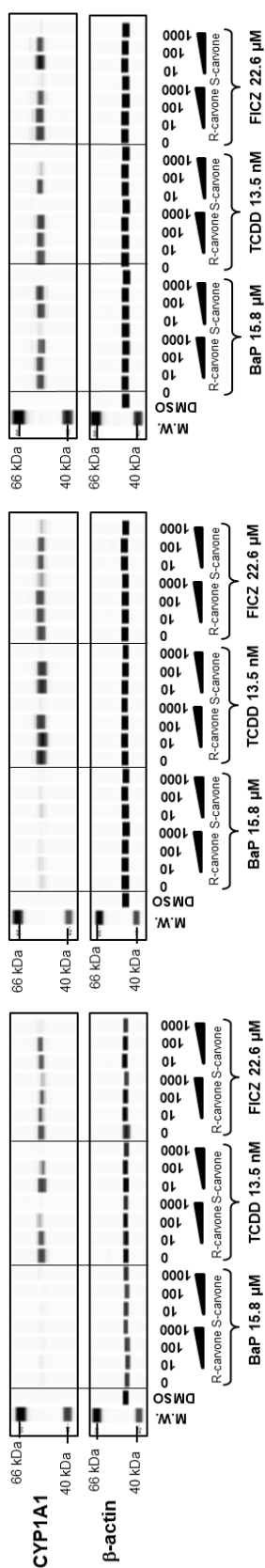
## 9.4 Down-regulation of AhR target genes by carvones

The effects of carvone on *CYP1A1* mRNA and protein levels were tested using a complementary set of human cell lines (HepG2, LS180, HaCaT cells, and primary human hepatocytes). S- and R-carvone inhibited ligand-inducible expression of *CYP1A1* mRNA and protein in a cell type-specific and ligand-selective manner. Induction of *CYP1A1* mRNA and protein by TCDD was inhibited by both carvones in all the cell types; BaP in LS180, HaCaT, and human hepatocytes and FICZ in HaCaT cells and human hepatocytes (Figure 35 and 37). Induction of *CYP1A* genes by AhR agonists in primary human hepatocytes is shown in Figure 36.

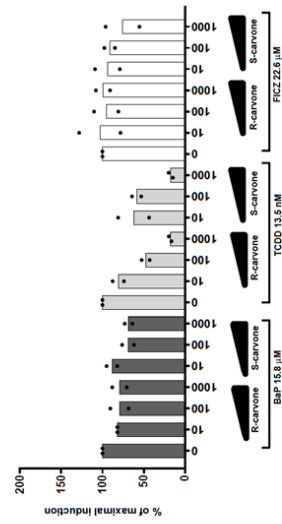
**A**



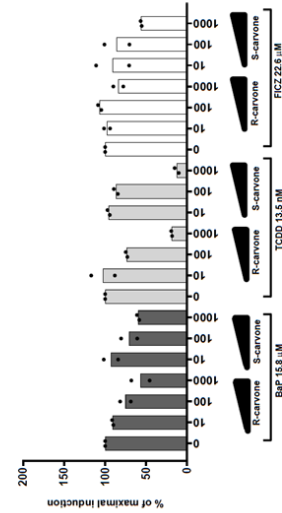
**B**



Normalization per model inducers, HepG2 cells



Normalization per model inducers, LS180 cells



Normalization per model inducers, HaCaT cells

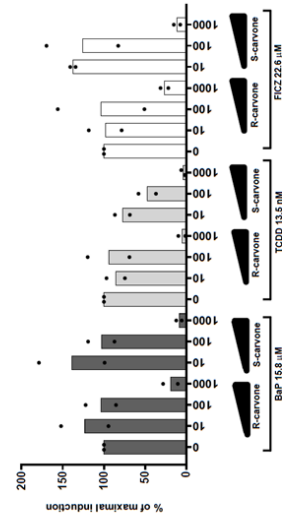


**Figure 2**

**Figure 35: Downregulation of CYP1A1 mRNA and protein in human cell lines by carvonnes.** HepG2, LS180, and HaCaT cells were incubated for 24 h with S/R-carvone (0–1000 μM) in the



presence of AhR agonists TCDD, BaP, and FICZ, applied in their EC<sub>80</sub> concentrations. Incubation and measurement were performed in triplicates. **PANEL A:** RT-PCR analysis of *CYP1A1* mRNA; results are expressed relative to agonist in the absence of carvones (100%). Data are shown as a mean from two independent cell passages. The results were normalized to GAPDH as the housekeeping gene. The absolute values of *CYP1A1* mRNA fold induction (F.I.) by model agonists are indicated in the text inserted in bar graphs from each cell line. **PANEL B:** Quantitative automated western blot analysis using SallySue of the *CYP1A1* protein. Representative SallySue data from one cell passage are shown. Bar graphs at the bottom show quantified *CYP1A1* protein normalized per  $\beta$ -actin. Data are expressed as a mean from two independent cell passages and they are expressed relative to agonist in the absence of carvones (100%).

### Expression of *CYP1A1* and *CYP1A2* mRNAs in primary human hepatocytes

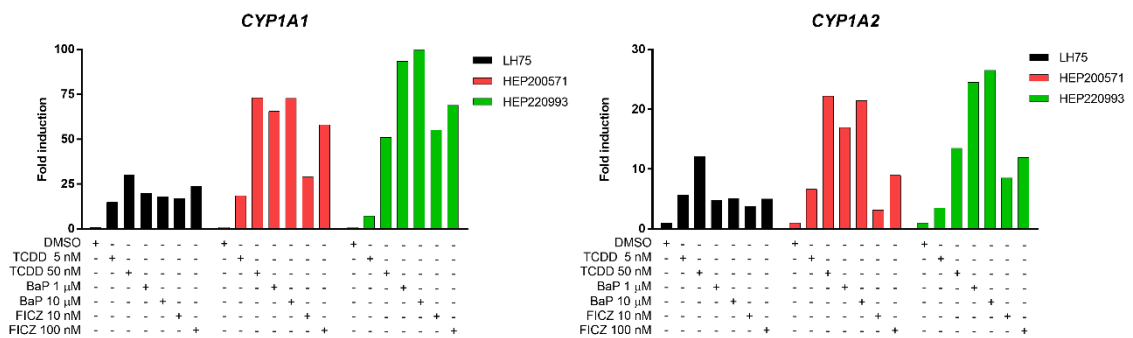


**Figure 36: Induction of *CYP1A* genes by AhR agonists in primary human hepatocytes.** Human hepatocyte cultures from three tissue donors (LH75, HEP200571, and HEP220993) were incubated with AhR agonists TCDD (5 nM, 50 nM), BaP (1 μM, 10 μM) and FICZ (10 nM, 100 nM) for 24 h. The data were normalized to GAPDH as the housekeeping gene.

## Expression of *CYP1A1* and *CYP1A2* mRNAs in primary human hepatocytes

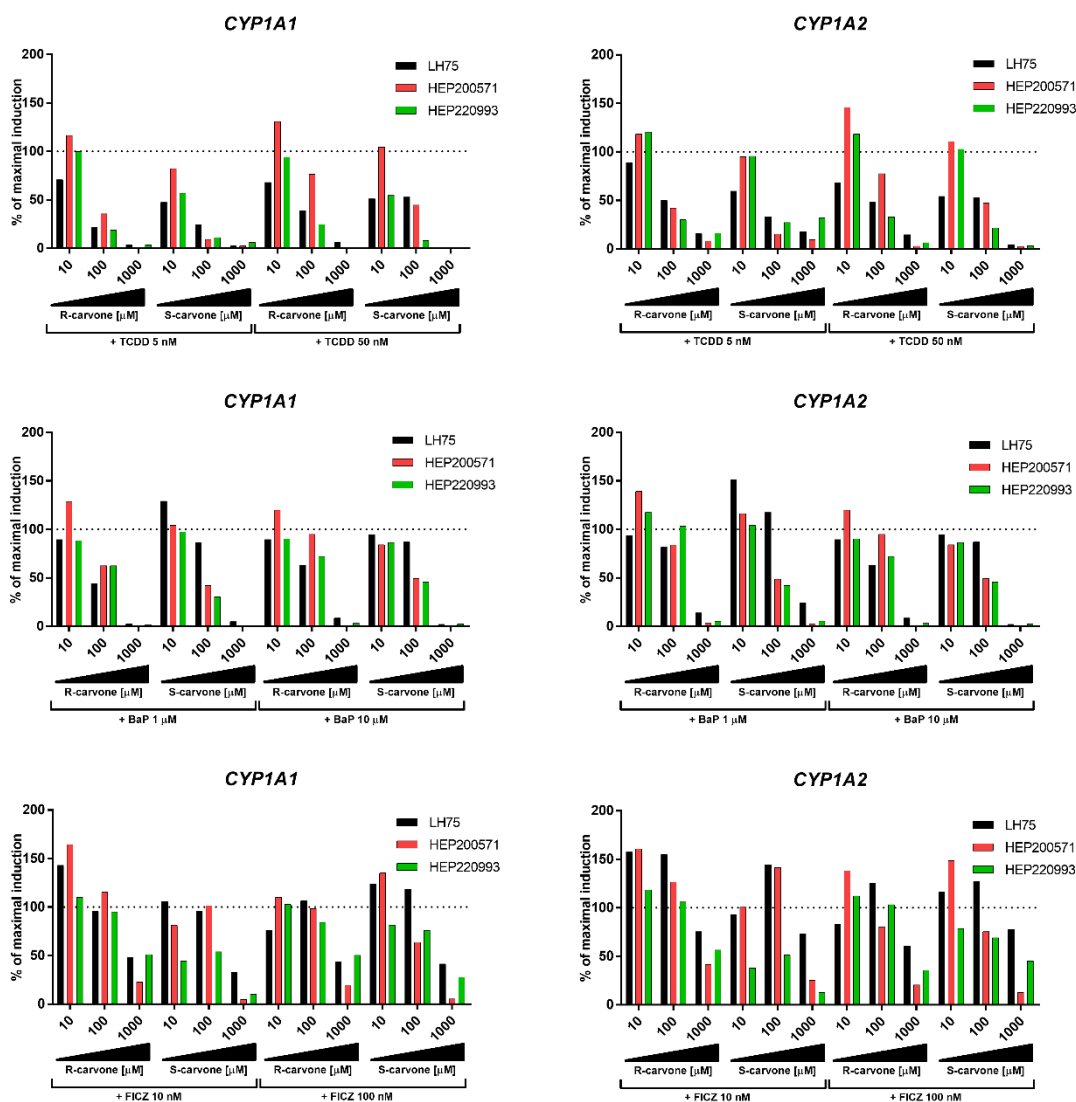


**Figure 37: Downregulation of *CYP1A1* and *CYP1A2* mRNAs in primary human hepatocyte cultures.** Human hepatocyte cultures from three tissue donors (LH75, HEP200571, and HEP220993) were incubated with carvones (10 μM, 100 μM, and 1000 μM) in the presence of AhR agonists TCDD (5 nM, 50 nM), BaP (1 μM, 10 μM) and FICZ (10 nM, 100 nM) for 24 h. the data were normalized to GAPDH as the housekeeping gene.

We also tested the effect of S-carvone on AhR receptor-regulated EROD catalytic activity. The TCDD-inducible EROD catalytic activity was significantly decreased by S-carvone in AZ-AHR cells, but carvones did not inhibit *CYP1A1* enzyme activity itself (Figure 38).

### CYP1A catalytic activity (EROD) in AZ-AHR cells

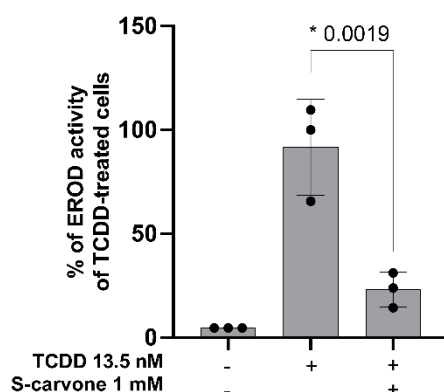


**Figure 38: Effect of S-carvone on CYP1A1 enzyme activity.** AZ-AHR cells were incubated for 24 h with a vehicle (DMSO; 0.1% v/v), TCDD (13.5 nM), or TCDD combined with S-carvone (1–1000  $\mu$ M). Data are shown as a mean  $\pm$  SD from three consecutive cell passages and are expressed as the percentage of fluorescence in TCDD-treated cells. Incubation and measurement were performed in triplicates. \* = value significantly different from positive control ( $p < 0.05$ ) and  $p$ -value is indicated in the graph.

In addition to CYP1A1, carvones downregulated additional canonical and non-canonical AhR target genes. Downregulation of the TCDD/BaP/FICZ-inducible canonical gene CYP1A2 was observed in primary human hepatocytes (Figure 37). Carvones inhibited TCDD-inducible *AhRR* mRNA expression and downregulated the non-canonical AhR target gene, PAI-1 (Figure 39).

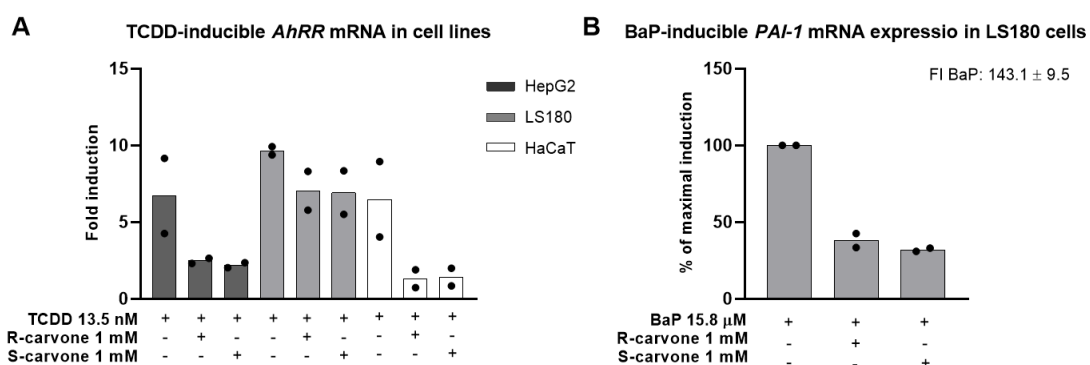


**Figure 39: Downregulation of *AhRR* and *PAI-1* mRNA by carvones.** **PANEL A:** LS180, HepG2, and HaCaT cells were incubated for 24 h with TCDD (13.5 nM) in the presence or absence of carvones (1 mM). Data are presented as the mean from two consecutive cell passages. The results were normalized to GAPDH as the housekeeping gene and they are expressed as fold induction per vehicle-treated cell. **PANEL B:** LS180 cells were incubated for 24 h with BaP (15.8  $\mu$ M) in the presence or absence of carvones (1 mM). Data are presented as the mean from two consecutive cell passages. The results were normalized to GAPDH as the housekeeping gene and they were expressed as a relative to BaP in the absence of carvones (100%). The absolute value of *PAI-1* mRNA fold induction (F.I.) by BaP is indicated in the text inserted into the bar graph.

## 9.5 Influence of carvone on AhR cellular functions

Subsequently, the effect of carvone on individual cellular events throughout the AhR signaling pathway was analyzed. The TCDD, BaP, and FICZ triggered AhR translocation from the cytosol to the nucleus, whereas carvones did not influence this process. Additionally, carvones did not trigger AhR nuclear translocation (Figure 40). Quantification of AhR nuclear translocation using immunofluorescence is shown in Table 3.

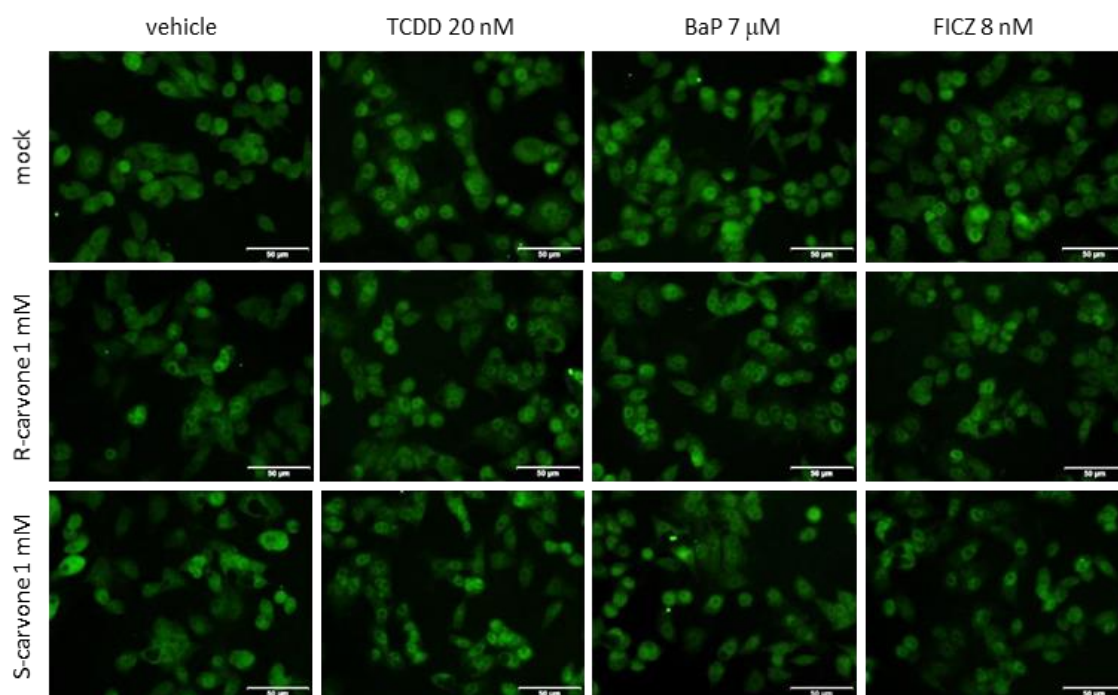


**Figure 40: Nuclear translocation of the AhR is not influenced by carvones.** LS180 cells were incubated for 90 min with carvones (1 mM) in combination with vehicle (DMSO; 0.1% v/v) or AhR agonists TCDD (20 nM), BaP (7  $\mu$ M), and FICZ (8 nM). Microscopic specimens were prepared using Alexa Fluor 488 labeled primary antibody against AhR and DAPI. The AhR expression was visualized and evaluated using fluorescence microscopy. Experiments were performed in two consecutive cell passages with all tested compounds in duplicate. Representative images are shown.

**Table 3: Nuclear translocation of AhR – quantification using immunofluorescence.** LS180 cells were treated for 90 min with S/R-carvones combined with the vehicle or AhR agonists TCDD, BaP, and FICZ. Intracellular AhR was visualized using an Alexa Fluor 488 labeled primary antibody. The staining protocol was performed in duplicate in two independent experiments. AhR translocation was evaluated visually based on the distinct signal intensity of the AhR antibody in the nucleus and cytosol. For the percentage calculation, approximately 100 cells from at least four randomly selected fields of view in each replicate were used. The relative ligand efficiency was calculated as follows:

$$\text{relative ligand efficiency} = 100 \times \frac{(\#AhR \text{ positive nuclei})_{LIGAND+CARVONE} - (\#AhR \text{ positive nuclei})_{DMSO}}{(\#AhR \text{ positive nuclei})_{LIGAND} - (\#AhR \text{ positive nuclei})_{DMSO}}$$

		# of cells	# of fields of vision	# of AhR positive nuclei	% of AhR positive nuclei	Relative ligand efficiency (%)
<b>DMSO</b>	Exp #1	359	3	16	4.5	n.a.
	Exp #2	438	4	6	1.3	n.a.
<b>TCDD 20 nM</b>	Exp #1	550	5	235	43.1	100
	Exp #2	453	4	198	43.6	100
<b>BaP 7 μM</b>	Exp #1	446	4	143	31.9	100
	Exp #2	486	4	158	32.6	100
<b>FICZ 8 nM</b>	Exp #1	494	4	176	35.3	100
	Exp #2	470	4	188	40.9	100
<b>R-carvone 1 mM</b>	Exp #1	445	4	18	4.0	n.a.
	Exp #2	429	4	2	0.5	n.a.
<b>R-carvone + TCDD</b>	Exp #1	437	4	212	48.6	90
	Exp #2	491	4	193	39.5	97
<b>R-carvone + BaP</b>	Exp #1	454	4	144	32.0	101
	Exp #2	396	4	169	42.3	107
<b>R-carvone + FICZ</b>	Exp #1	481	4	191	40.0	109
	Exp #2	496	5	191	38.7	102
<b>S-carvone 1 mM</b>	Exp #1	570	5	23	4.0	n.a.
	Exp #2	428	4	6	1.5	n.a.
<b>S-carvone + TCDD</b>	Exp #1	485	4	233	48.6	99
	Exp #2	462	4	157	34.3	79
<b>S-carvone + BaP</b>	Exp #1	450	4	163	36.3	116
	Exp #2	519	4	146	28.4	92
<b>S-carvone + FICZ</b>	Exp #1	460	4	194	42.4	111
	Exp #2	428	4	154	36.3	81

Following AhR translocation into the nucleus, it interacts with ARNT to form a heterodimer that binds to the DRE in the promoters of target genes. This pathway, involving ARNT, is referred to as canonical AhR signaling. Carvones strongly inhibited the formation of AhR-ARNT heterodimers (Figure 41) and the binding of AhR to the CYP1A1 promoter (Figure 42) in TCDD- and BaP-stimulated cells but not with FICZ.



were analyzed on a 2% agarose gel are from the 2<sup>nd</sup> experiment (bottom). Experiments were performed at three consecutive cell passages.

A schematic summarizing the effects of carvone on the AhR function is shown in Figure 43.

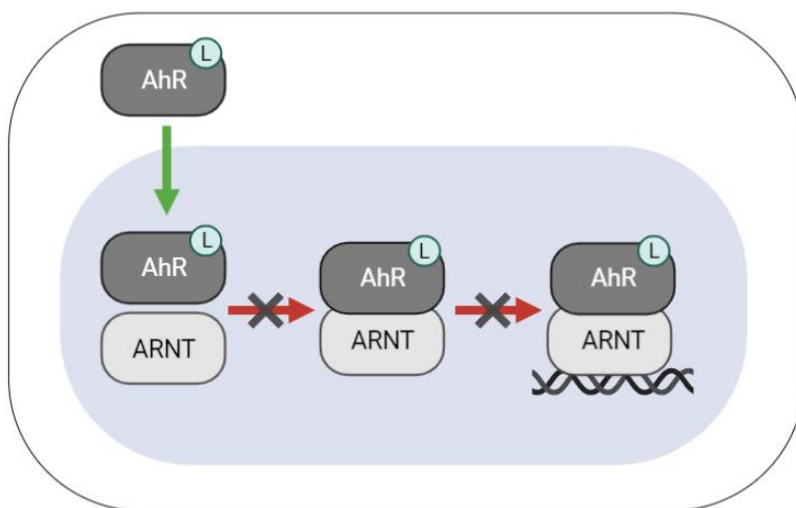


**Figure 43: Schematic depiction of the cellular effects of carvones on the AhR.**

## 9.6 Binding of carvones to the AhR

Carvones are non-competitive AhR antagonists (Figure 33) and do not inhibit ligand-elicited nuclear translocation of AhR (Figure 40), implying that they do not competitively displace ligands from binding to AhR. As a proof of concept, we performed a competitive ligand-binding assay using radiolabeled TCDD. S-carvone did not inhibit the binding to <sup>3</sup>H-TCDD in mouse hepatic AhR. However, we observed a slight decrease in <sup>3</sup>H-TCDD binding in the presence of 1000  $\mu$ M S-carvone (Figure 45). In addition, D-limonene, a deoxy analog of carvone, did not antagonize AhR (Figure 46) and did not bind to AhR(23-273) (see Chapter 9.7). These results show the importance of the oxo moiety in the carvone molecule for the interaction with AhR, tentatively through hydrogen bonds. In addition, nonspecific displacement of <sup>3</sup>H-TCDD from the mouse AhR by high concentrations of D-limonene was observed (Figure 45).

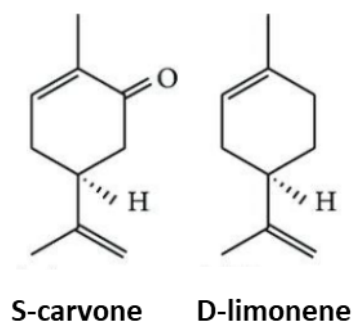


**Figure 44: Chemical structure of S-carvone and D-limonene.**

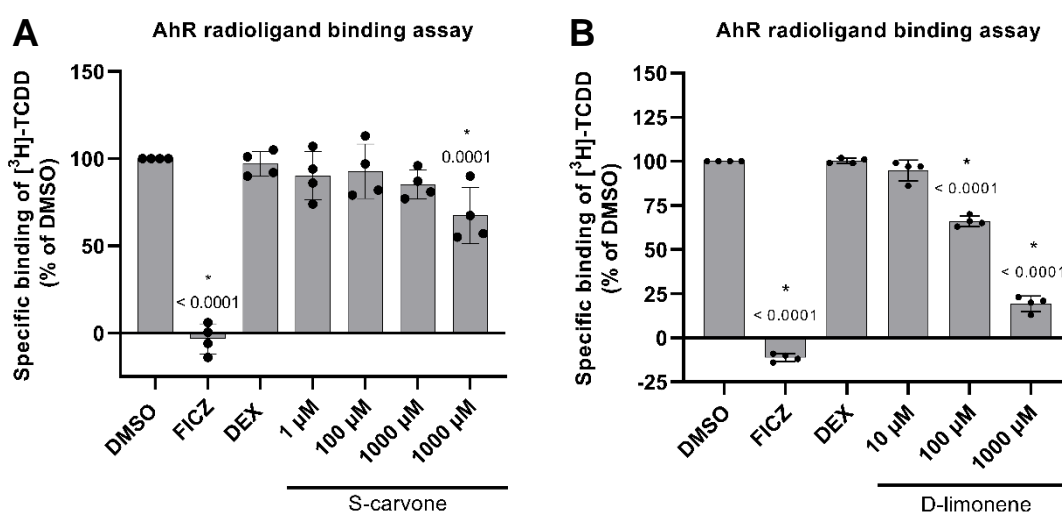


**Figure 45: Competitive radioligand-binding assays.** Specific binding of [<sup>3</sup>H]-TCDD was determined as the difference between the total and non-specific (200 nM; 2,3,7,8-tetrachlorodibenzofuran) reactions. The significance ( $p < 0.05$ ) was tested against the negative control (\*) and  $p$ -values are indicated in the graph. **PANEL A:** Non-competitive mechanism of S-carvone. Cytosolic proteins (2 mg/mL) from Hepa1c1c7 cells were incubated with S-carvone (1  $\mu$ M, 10  $\mu$ M, 100  $\mu$ M, and 1000  $\mu$ M), FICZ (10 nM), DEX (100 nM; negative control), or DMSO (0.1% v/v; corresponding to specific binding of [<sup>3</sup>H]-TCDD = 100%) in the presence of 2 nM [<sup>3</sup>H]-TCDD. Data are shown as a mean  $\pm$  SD from four independent experiments. Incubations and measurements were performed in three technical replicates. **PANEL B:** Displacement of <sup>3</sup>H-TCDD from Ahr by D-limonene. Cytosolic protein from Hepa1c1c7 cells was incubated with D-limonene (10, 100, and 1000  $\mu$ M), FICZ (10 nM), DEX (100 nM; negative control), or DMSO (0.1% v/v; corresponding to specific binding of [<sup>3</sup>H]-TCDD = 100%) in the presence of 2 nM [<sup>3</sup>H]-TCDD. Data are shown as a mean  $\pm$  S.D from four independent experiments. Incubation and measurements were performed in three technical replicates.



Fixed concentration of AhR agonists (EC<sub>80</sub>)

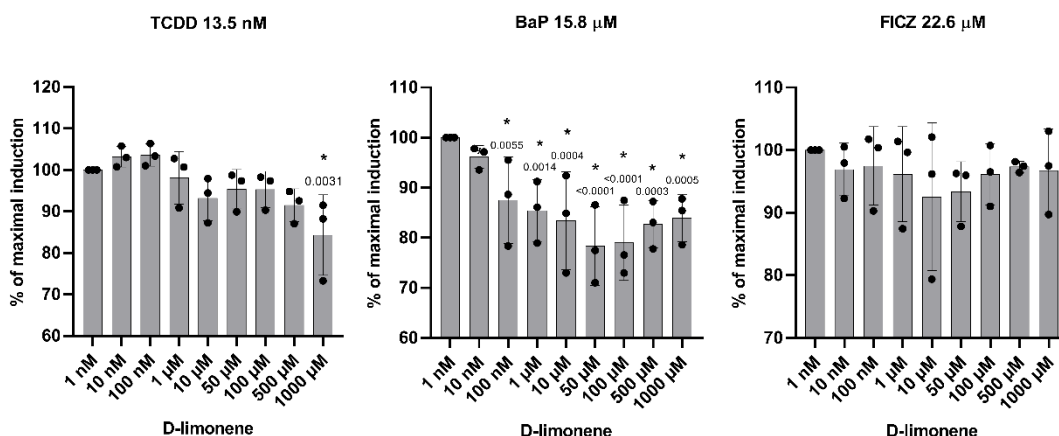


**Figure 46: D-limonene does not inhibit AhR agonists.** Reporter gene assays were carried out in AZ-AHR cells, incubated for 24 h with increasing concentrations of D-limonene in combination with the AhR agonists TCDD (13.5 nM), BaP (15.8 μM) and FICZ (22.6 μM). Incubation and measurements were performed in four technical replicates. Data are presented as the mean ± S.D. from three consecutive cell passages. The bar graph shows the percentage of maximal induction attained by the model AhR agonist. Incubation and measurements were performed in four technical replicates. \* = significantly different from AhR agonist in the absence of D-limonene ( $p < 0.05$ ).  $p$ -values are indicated in the graph.

On the basis of these results, we can assume the mechanism of antagonism. The ligand-dependent nuclear translocation of AhR was not disturbed by carvones (Figure 40); thus, the allosteric hindrance of the AhR ligand-binding pocket, which prevents proper ligand binding and AhR initiation, is unclear. Thus, irreversible competitive antagonism is unlikely to occur. An indirect mechanism could occur either at the AhR or off-target, affecting protein kinases, ARNT, etc. (see the results below). Therefore, we investigated the allosteric binding of carvones to AhR and its effects on AhR-ARNT heterodimerization. Molecular modeling was used to predict *in silico* carvone interactions with AhR protein. Molecular docking of carvones to various known binding pockets of the AhR ligands, such as TCDD, resveratrol, FICZ, BaP, and methylindoles, suggested that carvones may non-specifically bind to these sites, with an average docking score of 47.5 and 42, respectively. Unfortunately, this method also has its limitations, and because of the relatively small size of the carvone molecule, the binding could have no functional effect. Based on experimental evidence that carvones inhibit the formation of AhR-ARNT (Figure 41), we docked carvone to the heterodimerization interface of AhR

and ARNT, which spans several interdomain interactions that form the binding pocket of the DRE (Seok et al., 2017). One such interface region is the  $\alpha$ 1- $\alpha$ 2 helical region of the bHLH domain, consisting of amino acid residues Leu43, Leu47, and Leu50 from the  $\alpha$ 1 helix and Tyr76, Leu72, and Leu77 from the  $\alpha$ 2 helical region. Carvones were docked to the interface site and the AhR complex with carvones was simulated for ~250 ns to allow the ligand to stably dock to AhR. Carvones bind favorably to a site formed by residues in the bHLH domain, including close contacts with Tyr76, Pro55, Phe83, Tyr137, Leu72, Pro91, Lys80, Ala79, and Phe136 (Figure S7). More importantly, the binding of carvones to this site shifts the positions of both the  $\alpha$ 1 and  $\alpha$ 2 helical regions by 10-13 Å and causes significant unwinding of the  $\alpha$ 1 helix (Figure S7), which can affect the formation of the AhR-ARNT complex. The data suggest that carvone binds to the protein at the allosteric sites of the bHLH and PAS-A domains (Figure 47).

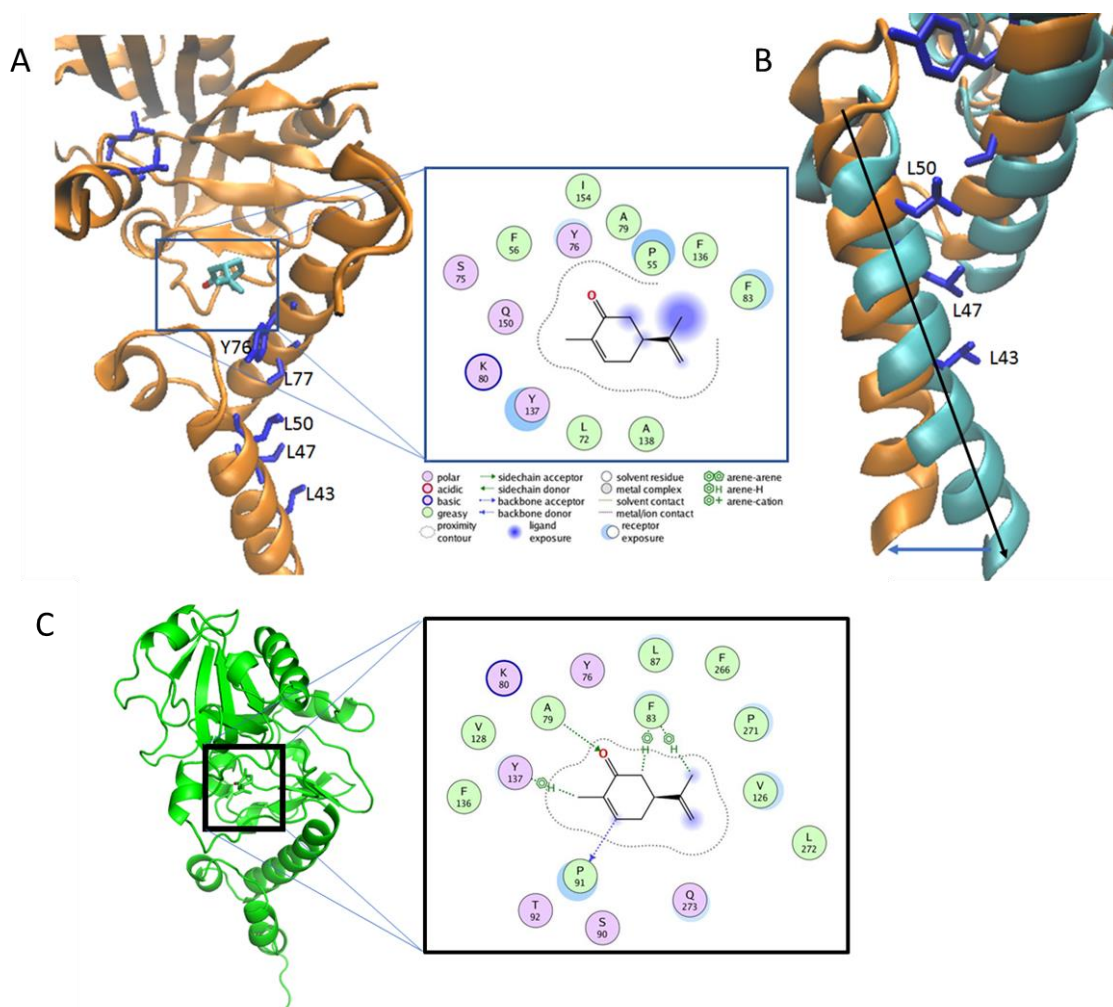


**Figure 47: Carvone binds to the protein at the allosteric sites of bHLH and PAS-A domains. PANEL A: S-carvone (licorice stick and colored atom type, carbon = cyan and oxygen = red)**

binds to a site proximal to the heterodimerization interface of AhR (depicted as orange ribbons with interface residues shown as blue licorice sticks and labeled) with residues from helices  $\alpha 1$  and  $\alpha 2$ , which contribute to binding interactions (center panel). **PANEL B:** The complex of S-carvone with AhR was simulated for 10 ns, and the resulting structure (cyan ribbons) was superimposed onto the original complex. The binding of S-carvone to this site also leads to conformational changes in the  $\alpha 1$  and  $\alpha 2$  helices (new positions are shown as cyan ribbons), thereby disrupting the formation of the AhR-ARNT interface. **PANEL C:** The complex of S-carvone with AhR was simulated for 250 ns, and the conformation of the complex is shown as green ribbons. The binding mode of S-carvone is shown in the center panel. The binding of S-carvone to this site also leads to the unwinding of the  $\alpha 1$  helix, which may further disrupt the AhR-ARNT interface.

## 9.7 Carvone binds to AhR but not ARNT

Using microscale thermophoresis and bacterially co-expressed and purified fragments of human AhR (encoding amino acid residues 23–273) and mouse Arnt, we demonstrated that carvone binds AhR but not Arnt (Figure 48 A), whereas D-limonene does not bind to AhR (Figure 48 B). Although the binding of carvone to AhR was concentration-dependent, the apparent binding constant  $K_D$  could not be determined because it lies in the low millimolar range, likely because of the artificial conditions using truncated variants of AhR and Arnt. The AhR fragment spanned amino acids 23–273, implying that the binding of carvone was localized outside the conventional ligand-binding domain but within the bHLH/PAS-A region of AhR. These data fully support the hypothesis that the non-competitive antagonism of carvones involves allosteric binding to the AhR.

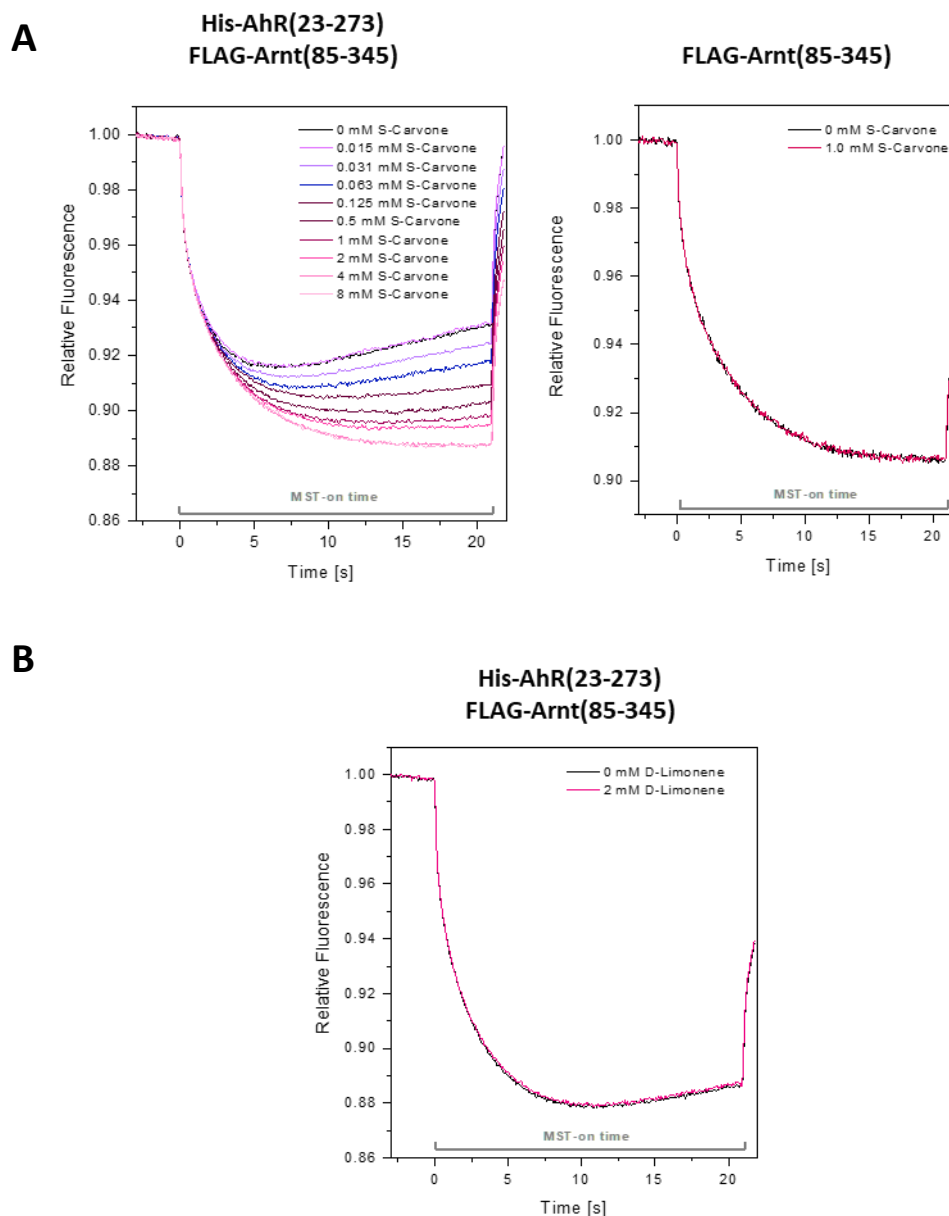


**Figure 48: Microscale thermophoresis. PANEL A:** Carvones bind to AhR in the bHLH/PAS-A region but not to Arnt (85–345). **LEFT:** Co-expressed His-AhR (23–273) and FLAG-Arnt (85–345) were incubated with S-carvone (0.25 mM, 0.5 mM, 1 mM, 2, and 4 mM). **RIGHT:** FLAG-Arnt (85–345) was incubated with vehicle or 1 mM S-carvone. **PANEL B:** D-limonene does not interact with AhR (23–273). Co-expressed His-AhR (23–273) and FLAG-Arnt (85–345) were incubated with 2 mM D-limonene.

We used several approaches to identify the AhR amino acid residues involved in the interaction with carvone. Thermal shift analyses (TSA) using the purified and cellular human AhR PAS-A domain (112–272) revealed that carvone does not interact with the PAS-A region of AhR (Figure 49). Combined with the data from microscale thermophoresis, it was suggested that the amino acid residue critical for the interaction of carvone with AhR was located in the

(23–111) region. Subsequently, using human AhR (23–273) proteins mutated at amino acid tyrosine 76 (Y76A and Y76F), we observed that the binding of carvone was completely lost or strongly diminished in the Y76A and Y76F mutants, respectively, as compared to wild-type AhR (Figure 50).

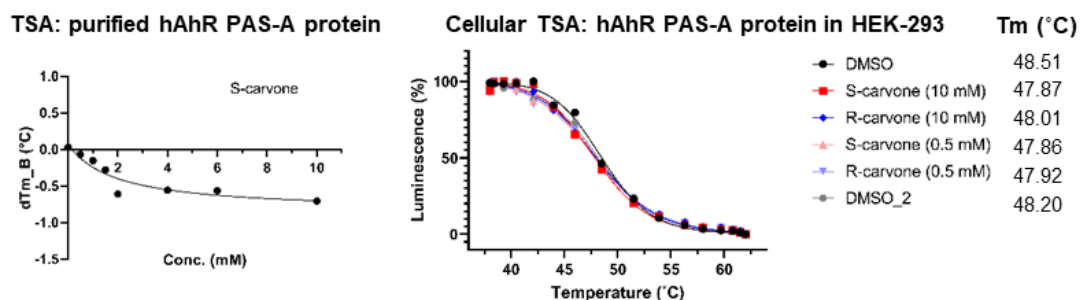


**Figure 49: Carvone does not interact with the PAS-A region of the AhR.** LEFT PANEL: Thermal shift assay with purified hAhR PAS-A (112–272) protein incubated with S-carvone (0.5 mM, 1 mM, 1.5 mM, 2 mM, 4 mM, 6 mM, and 10 mM). RIGHT PANEL: Cellular thermal shift analyses in HEK293 cells transfected with hAhR PAS-A (112–272) protein; incubations with S/R-carvones (0.5 mM and 10 mM).

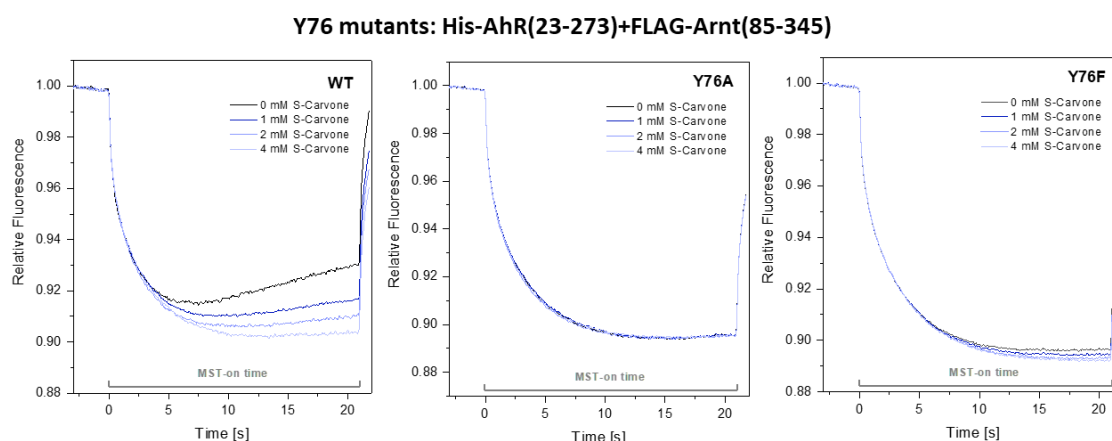


**Figure 50: Carvones bind to AhR (23–273) but not to site-directed mutated AhR.** Microscale thermophoresis: co-expressed (WT; mutY76A and mutY76F)-His-AhR (23–273) + FLAG-Arnt (85–345) incubated with S-carvone (0.25 mM, 0.5 mM, 1 mM, 2 mM, and 4 mM).

Furthermore, we used a protein cross-linking approach with a photoactivated azido-labeled ligand. We synthesized N<sub>3</sub>-S-carvone (Figure 51) and confirmed that it conserves the AhR-antagonist capability against TCDD- and BaP-activated AhR (Figure 52, right panel). Using MALDI, the recombinant AhR was identified in the control samples by 19 assigned tryptic peptides in the *m/z* range of 578.3–5207.5, which covered the regions of 33–107

and 168–250 representing a major part of the recombinant protein and approximately 17% of the full-length native AhR sequence (Swiss-Prot database accession number AHR\_HUMAN). Treatment with photoactivated N<sub>3</sub>-S-carvone resulted in a small difference in the representation of peptide peaks. Two peptides were absent in the peptide fingerprint of the AhR that reacted with N<sub>3</sub>-S-carvone compared to the control (Figure 53): *m/z* 1036.6 and 1131.5, with the amino acid sequences 72-LSVSYLRAK-80 and 41-DRLNTELDLDR-49, respectively (confirmed using MSMS sequencing). The former peptide has an alternative and preferential cleavage form, LSVSYLR, which is observable as a high peak at *m/z* 837.5, indicating a low-affinity labeling yield. A low-intensity peak at *m/z* 1199.6 corresponds to a mass difference of 163 Da, corresponding to the binding of the N<sub>3</sub>-S-carvone-derived nitrene moiety at LSVSYLRAK. However, because of low intensity, we could not perform direct confirmation using MSMS sequencing. The photoactivation process itself performed well, because N<sub>3</sub>-S-carvone, upon MALDI with a UV laser (measured in the presence of cetrimonium bromide in the matrix solution according to Guo et al. (Guo et al., 2002), provided a peak at *m/z* 164, indicating the loss of molecular nitrogen from the azido group. Overall, considering the data from molecular docking, microscale thermophoresis (S-carvone, D-limonene, mutant analysis Y76A, Y76F), and AhR covalent functionalization with photoactivated N<sub>3</sub>-S-carvone, a key role of Tyr76 in the allosteric binding of S-carvone to AhR is highly likely.

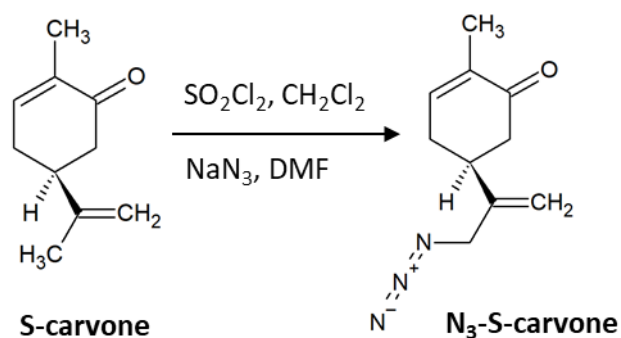


**Figure 51: Chemical synthesis of N<sub>3</sub>-S-carvone.**

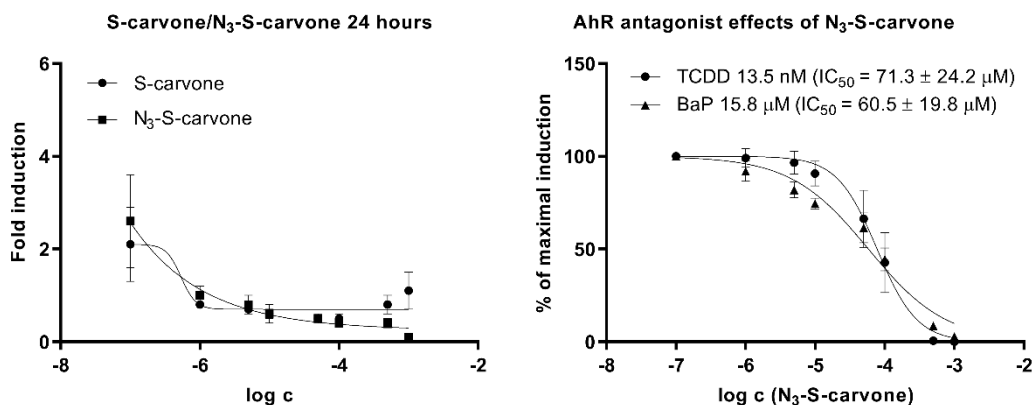


**Figure 52: Effect of S-carvone and N<sub>3</sub>-S-carvone on the transcriptional activity of AhR and agonist-inducible AhR activity.** Reporter gene assays in AZ-AHR cells. **LEFT PANEL:** AZ-AHR cells were incubated for 24 h with carvones at concentrations ranging from 100 nM to 1 mM for 24 h. Data are shown as a mean  $\pm$  SD from three independent cell passages and they are expressed as a fold increase in luciferase activity over control cells. Measurements were performed in four technical replicates. **RIGHT PANEL:** AZ-AHR cells were incubated for 24 h with N<sub>3</sub>-S-carvone in combined with TCDD (13.5 nM), and BaP (15.8  $\mu$ M). Data are shown as a mean  $\pm$  SD from three independent cell passages and they are expressed as a percentage of maximal induction attained by the model AhR agonist. Measurements were performed in four technical replicates.

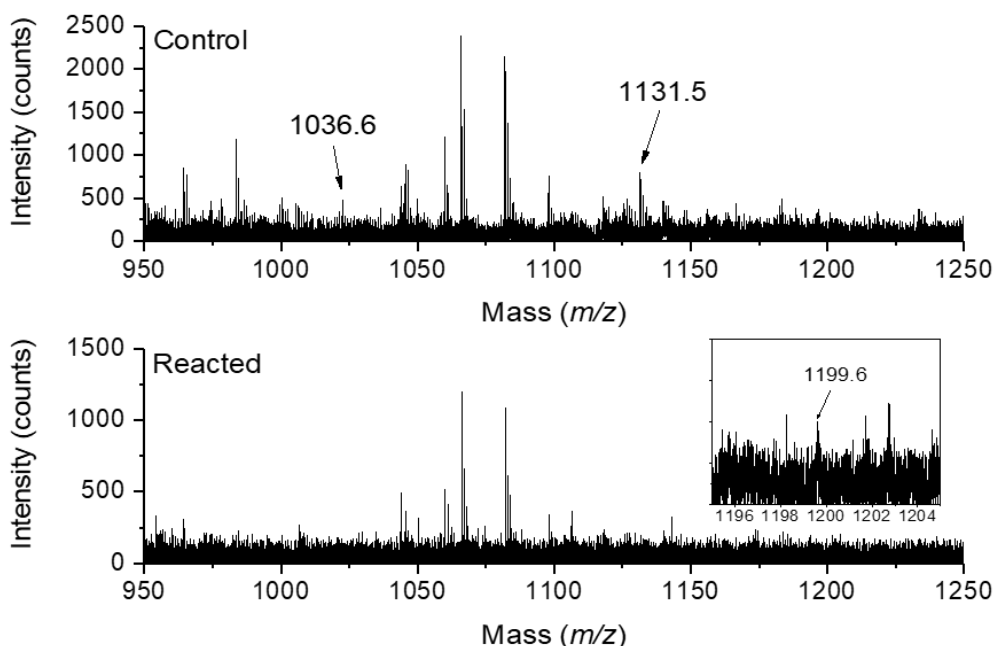


**Figure 53: MALDI-TOF/MS: photo-activated azide cross-link.** MALDI-TOF MS of peptides from AhR tryptic digests: The top panel shows the details of the control digest spectrum. The two labeled peptides ( $m/z$  1036.6 and 1131.5) were absent after the reaction of AhR with photoactivated N<sub>3</sub>-S-carvone (bottom panel). The inset shows a close-up view of the reacted AhR digest spectrum, demonstrating the presence of a putatively modified peptide at  $m/z$  1199.6, which might be related to that of the control at  $m/z$  1036.6.

## 9.8 Carvone does not inhibit the transcriptional activity of ARNT

In addition to the AhR signaling pathway, ARNT is involved in other cellular pathways, such as hypoxia signaling, which is transcriptionally mediated by the ARNT heterodimer with HIF1 $\alpha$ . Therefore, we investigated the effects of carvones on the hypoxia-mimic-inducible ARNT-dependent expression of VEGF in HaCaT keratinocytes incubated with deferoxamine. The VEGF mRNA levels were increased 5-fold by deferoxamine, and carvones at concentrations up to 1000  $\mu$ M did not influence this induction. Consistently, the hypoxia-mimic decrease in CYP1A1 mRNA levels was not affected by carvones (Figure 54). These data indicate that carvone does not inhibit the transcriptional activity of ARNT and that the disruption of AhR-ARNT complex formation is not caused by the interaction of carvones with ARNT. These observations corroborate the finding that carvones do not bind truncated recombinant Arnt (Figure 48 A).

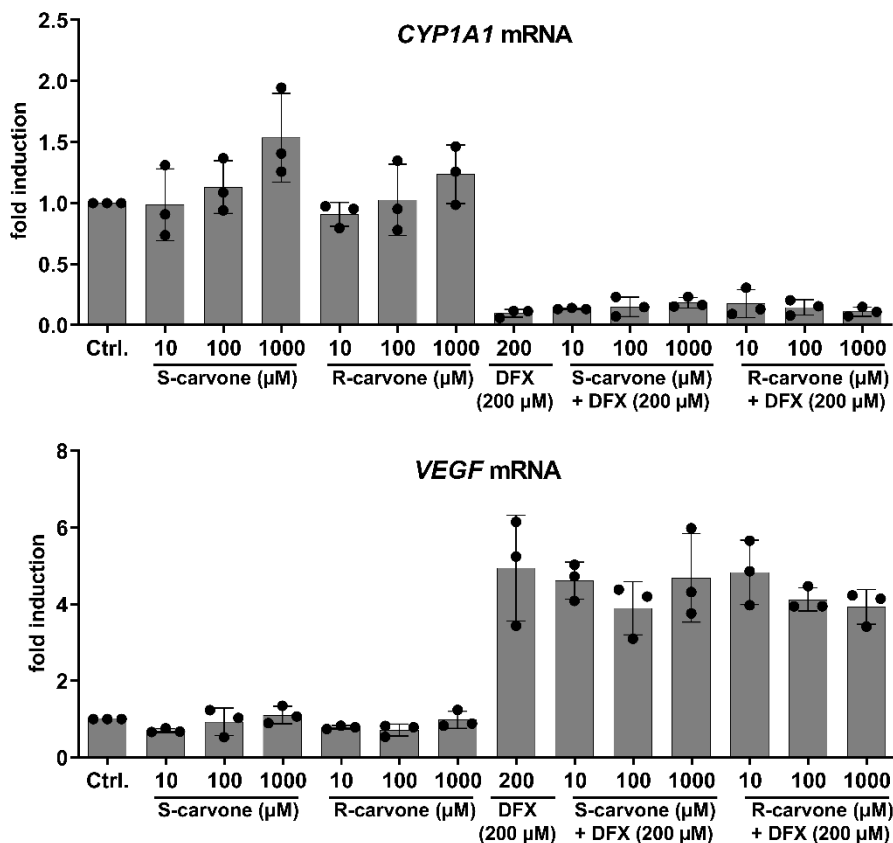


**Figure 54: Carvone did not induce VEGF mRNA expression and did not reduce hypoxia, mimicking CYP1A1 mRNA.** Hypoxia-mimic VEGF induction: HaCaT cells were incubated for 24 h with carvones (10  $\mu$ M; 100  $\mu$ M; 1000  $\mu$ M) combined with vehicle (DMSO; 0.1% v/v) or deferoxamine (DFX; 200  $\mu$ M). The mRNA expression of VEGF and CYP1A1 mRNAs was



measured using RT-PCR. Data are expressed as a mean  $\pm$  SD from three independent cell passages and are expressed as fold induction over the vehicle-treated cells. The results were normalized to GAPDH as the housekeeping gene. Measurements were performed in two technical replicates.

## 9.9 S-carvone does not inhibit protein kinases

Inhibition of PKC leads to the downregulation of CYP1A1 without blocking AhR nuclear translocation (Long et al., 1998). As carvone does not inhibit AhR nuclear translocation but inhibits all other downstream events in the AhR signaling pathway, we tested the effect of carvone on PKC activity of PKC. Carvone did not decrease PKC activity measured in HepG2 cell lysates, which precludes the involvement of PKC inhibition in the effects of carvones on AhR (Figure 55).

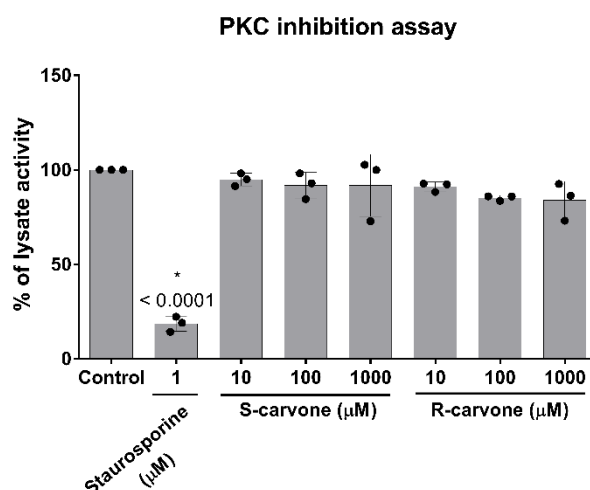


**Figure 55: Carvones do not decrease PKC activity.** PKC inhibition assay. The catalytic activity of PKC was measured in lysates from HepG2 cells incubated with vehicle (DMSO; 0.1% v/v), staurosporine (1  $\mu$ M), and carvones (10  $\mu$ M; 100  $\mu$ M; 1000  $\mu$ M). Data are presented as the mean  $\pm$  S.D. from three independent experiments. Incubation and measurements were performed in one technical replicate. \* = value significantly different from negative control ( $p < 0.05$ ) and  $p$ -value is indicated in the graph.

Subsequently, a scan of S-carvone interactions with 468 human protein kinases was performed using KINOMEScan<sup>TM</sup> (scanMAX assay), a patented active-site-directed competition binding assay (Fabian et al., 2005). The minimal inhibitory threshold used by KINOMEScan<sup>TM</sup> was 35% of control kinase activity. Among the 468 kinases tested, 467 were above the 35% cutoff value. Tyrosine kinase 2 TK2 (JH2 domain pseudokinase) activity was inhibited to 27% of the control activity, but this kinase was not relevant to the regulation

of transcriptional activity (Figure 56). Overall, we excluded the possibility that the effects of carvones on AhR signaling are caused indirectly by inhibiting the human kinome, particularly PKC.

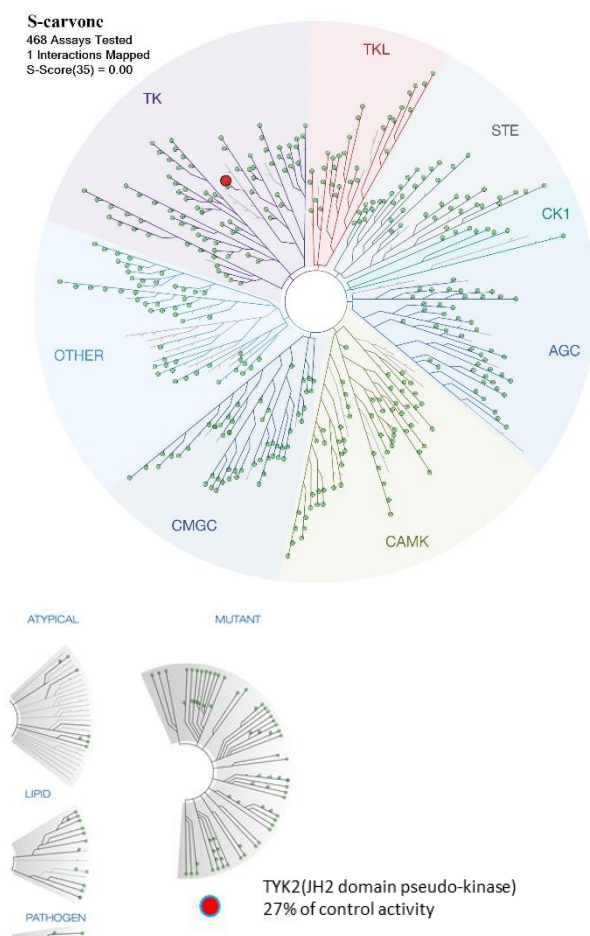


**Figure 56: Carvones have no effect on kinases related to the AhR signaling pathway.** KINOMEScan™ profiling: The interaction between 100  $\mu$ M S-carvone and 468 human protein kinases, employing KINOMEScan™ (scanMAX assay), proprietary active site-directed competition binding assay. A low-resolution interaction map is presented.

## 9.10 Carvone does not interact with AhR-related off-targets

Using radioligand-binding assays, we demonstrated that S-carvone does not bind to human nuclear and steroid receptors that transcriptionally cross-talk with AhR, including the AR, RXR $\alpha$ , GR, PR, ER $\alpha/\beta$ , and PPAR $\gamma$  (Figure 57).

### Steroid and nuclear receptor counter screen

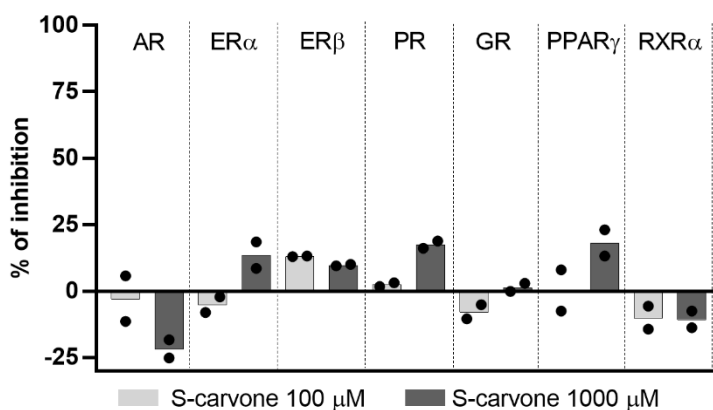


**Figure 57: S-carvone does not bind to AR, ER $\alpha/\beta$ , PR, GR, RXR $\alpha$ , or PPAR $\gamma$ .** Counter-screen radioligand binding assay with human AR, ER $\alpha/\beta$ , PR, GR, RXR $\alpha$ , and PPAR $\gamma$  receptors. The bar graph shows percentage of displacement of radioligand by S-carvone (100  $\mu$ M; 1000  $\mu$ M). Incubation was performed in two technical replicates. A value of >50% is considered indicative for interaction.

Tyrosine protein phosphatase non-receptor type PTPN11/SHP2 and PTPN6/SHP1 are critical for regulating the AhR-stress response. It was found that S-carvone did not inhibit its catalytic activity (Figure 58 A). In addition, S-carvone did not displace geldanamycin from binding to the 90 kDa heat shock protein, a cytosolic AhR binding partner (Figure 58 B).

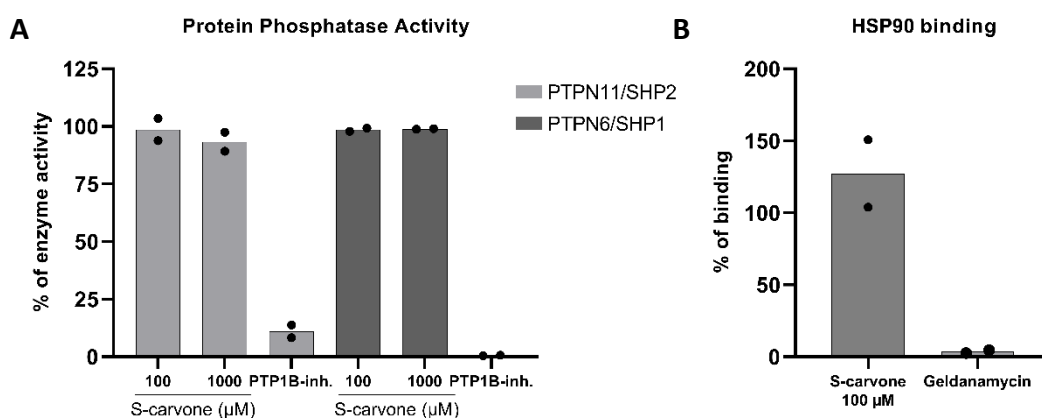


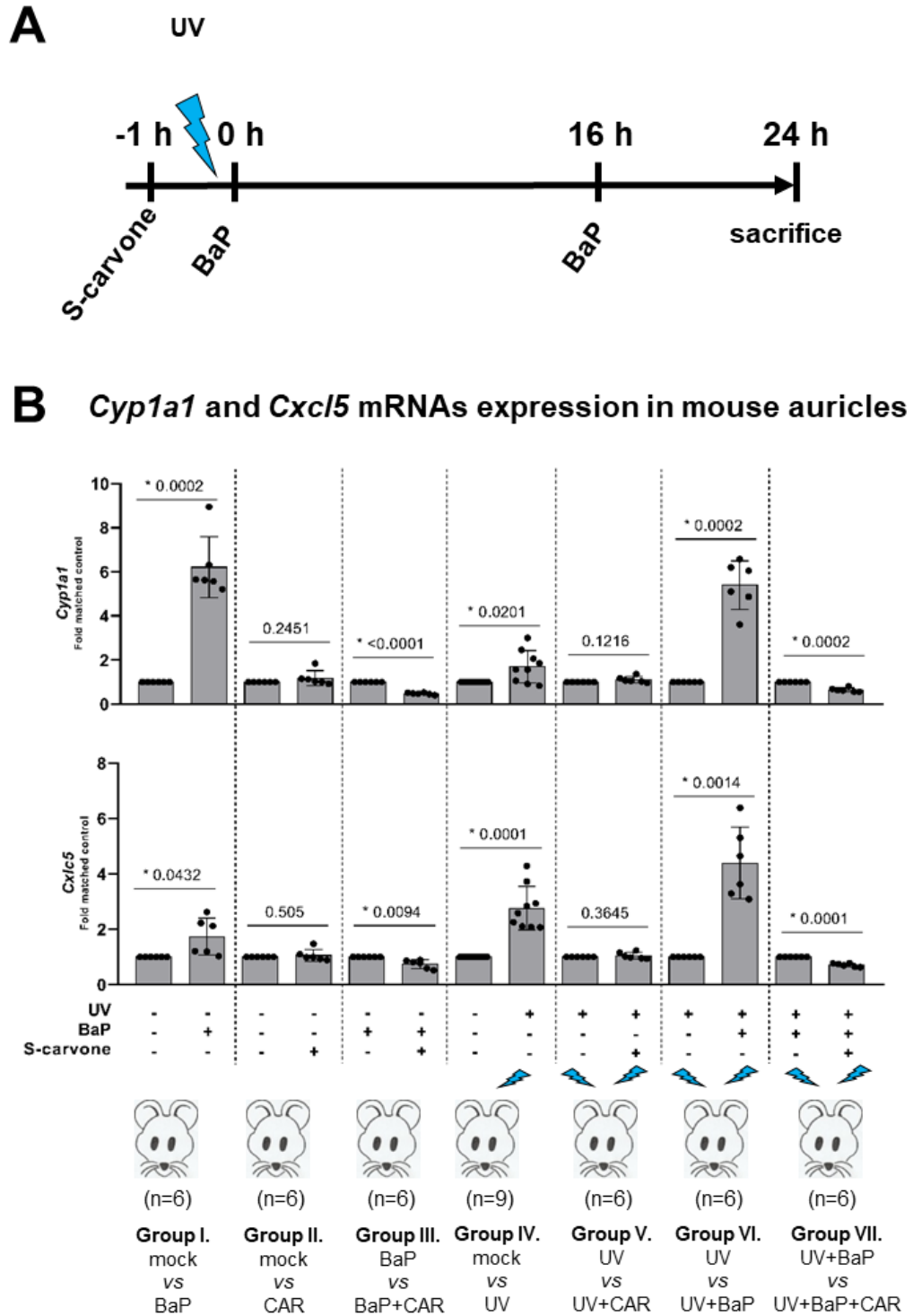
**Figure 58: S-carvone did not affect protein phosphatase or HSP90.** **PANEL A:** Protein phosphatase inhibition assay: Catalytic activity of PTPN11/SHP2 and PTPN6/SHP1 was measured with recombinant enzymes incubated with vehicle (DMSO, 0.1% v/v), PTP1B inhibitor (33.3  $\mu$ M), and S-carvone (100  $\mu$ M; 1000  $\mu$ M). Data are presented as a mean from two independent experiments. Incubation and measurements were performed in two technical replicates. **PANEL B:** Competitive fluorescence binding assay for HSP90: Bar graph shows the percentage of displacement of fluorescently labeled geldanamycin by S-carvone (100  $\mu$ M) and non-labeled geldanamycin (0.12  $\mu$ M). Data are presented as a mean from two independent experiments. Incubation and measurements were performed in two technical replicates.

## 9.11 Carvone antagonize Ahr in mouse skin

As a proof of the antagonistic effects of carvone on ligand-activated AhR, we performed an *in vivo* study in mice. The tested compounds and UV irradiation were applied to mouse auricles according in Figure 59 A. The left and right ears were exposed to different treatments, thereby providing internal individual controls for comparative treatments. Each animal represents a biological replicate. Topical application of BaP induced *Cyp1a1* mRNA expression, and this induction was inhibited (62% inhibition) in mouse ears pre-incubated with S-carvone (Figure 59 B).

AhR has been reported to be an important mediator of C-X-C motif chemokine 5 (Cxcl5) with implications for treating inflammatory skin diseases (Smith et al., 2017). Irradiation of mouse ears with UV light induced the pro-inflammatory chemokine Cxcl5, and post-radiation application of BaP further increased the levels of UV-inducible Cxcl5. Carvones reversed (38% inhibition) the induction of Cxcl5 levels by BaP in the ears of UV-irradiated mice (Figure 59), which has potential clinical relevance as Cxcl5 has been identified as a target gene associated with UV-induced inflammatory pain in sunburned mice (Dawes et al., 2011). Immunohistochemical staining with the  $\gamma$ H2AX-Ser139-P antibody confirmed extensive DNA damage (Yuan et al., 2010) in the ears of the UV-irradiated mice (Figure 60). The aggravating effect of BaP on UV-induced tissue damage was attenuated by carvone, as expressed by the number of sunburnet cells (Sheehan et Young, 2002) in the hematoxylin and eosin-stained histological samples (Figure 61). Importantly, S-carvone alone did not affect the number of UV-burned cells, regardless of whether it was applied before or after UV exposure (Figure 61). These data disprove a potential UV-shielding effect of S-carvone.

Overall, carvone inhibited BaP-inducible CYP1A1 gene expression *in vivo* in mouse skin and reversed the BaP-mediated potentiation of the UV-inducible chemokine Cxcl5. Carvones also significantly attenuated the harmful effects of BaP, as revealed by the sunburn cell count.



**$\gamma$ H2AX-Ser139-P Immunohistochemistry**

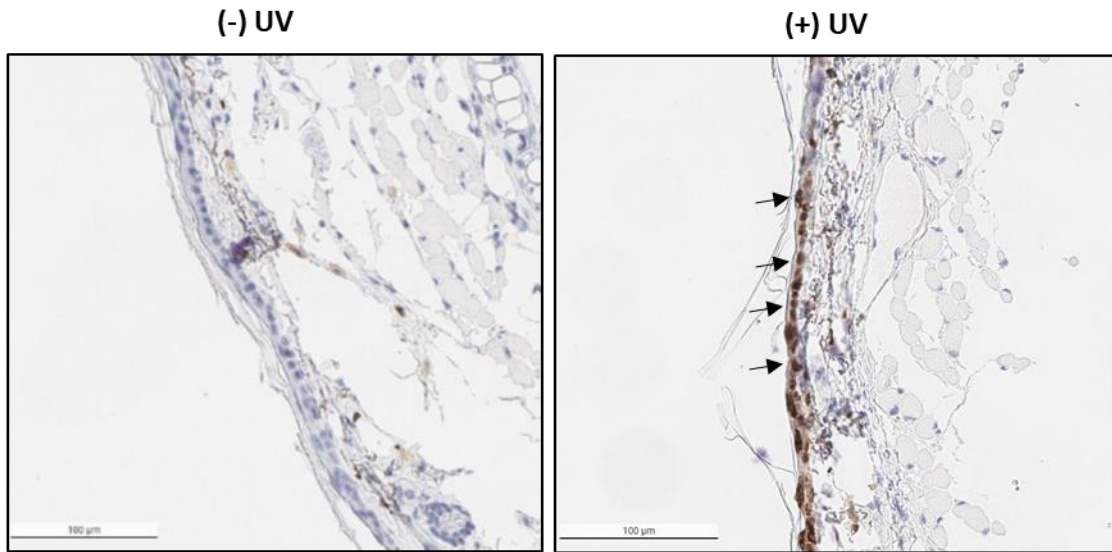


**Figure 60: Effect of UV light visualized using immunohistochemistry.** Representative control and UV-exposed mouse ear tissues stained with an antibody against  $\gamma$ H2AX-Ser-P are shown. The analyses were performed in ear tissue from six mice.

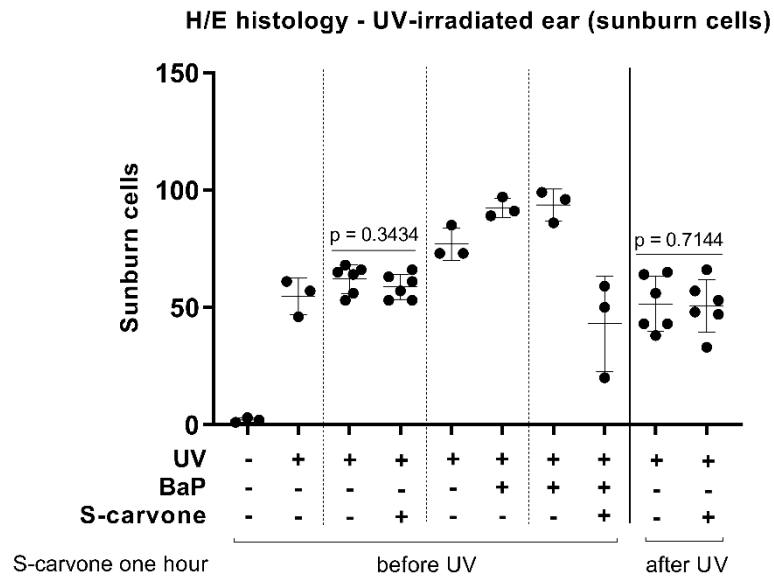


**Figure 61: UV-burned cells in mouse ears treated with S-carvone pre/post-UV exposure.** The scatter plot shows the counts of UV-burned cells in the left and right ears of individual mice. Data are presented as the mean  $\pm$  S.D. from at least three mice per treatment group. The significance was calculated using paired two-tailed t-test, and  $p$ -value is indicated for the group UV vs UV+carvone before and after UV.

## DISCUSSION

The AhR has long been considered a receptor for mediating dioxin toxicity, and recently, we observed a shift in the perception of its activation towards an attractive therapeutic target. Expanding the knowledge of its physiological and pathophysiological roles, AhR targeting can lead to cancer therapy (Wang et al., 2020), treatment of inflammatory bowel disease (Wang et al., 2018), atopic dermatitis (Furue et al., 2019; Hidaka et al., 2017), and antiviral activity (Giovannoni et al., 2021). Tranilast (an anti-allergic drug), flutamide (an anti-androgenic drug), hydroxytamoxifen (an anti-estrogen drug), and omeprazole (a proton pump inhibitor) are AhR-dependent anticancer agents (Safe et al., 2017). Furthermore, the anti-leprosy drug clofazimine and the AhR antagonist AhR-dependently suppressed the growth of multiple myeloma in transgenic mice (Bianchi-Smiraglia et al., 2018). Chemoprevention with dietary AhR-active compounds, such as I3C or DIM, is also suitable. Moreover, high-throughput screening of chemical libraries is an approach for obtaining novel AhR ligands (such as CH-223191) (Kim et al., 2006). The design and synthesis of novel AhR ligands (such as PY108 and PY109) may also be an approach for AhR targeting (Chen et al., 2020).

Majority of current drugs are designed to bind directly to the primary active orthosteric sites, resulting in modification of enzyme or receptor function, and the effectiveness of these drugs has been proven in clinical practice. However, several enzymes or receptors with related functions may possess similar active sites, leading to undesirable side effects. These substances are primarily complete inhibitors or activators rather than partial modulators. The disadvantages of these drugs can be addressed through an emerging drug design approach based on the effects of secondary binding sites (allosteric sites). Targeting allosteric sites in various biological targets is an emerging approach to drug discovery. Cinacalcet and maraviroc for treating hyperparathyroidism and AIDS, respectively, are examples of approved allosteric modulators. Other compounds are yet under patent protection, such as positive allosteric modulators of dopamine receptors for treating Parkinson's disease and schizophrenia (Pat. Appl. # WO/2014/193781; Eli Lilly&Co) and negative allosteric modulators of metabotropic glutamate receptors for treating central

nervous system disorders (Pat. Appl. # WO/2014/195311; Janssen Pharmaceutica) (Abdel-Magid, 2015; Ekins et al., 2007). Moreover, synthetic highly selective allosteric inhibitors of the hypoxia-inducible factor HIF2 $\alpha$  have been described. The PAS-B domain of the HIF-2 $\alpha$  subunit contains a large cavity within its hydrophobic pocket, which offers unique support for small-molecule regulation. Scheuermann et al. identified artificial ligands that bind within this pocket and characterized the resulting structural and functional changes caused by binding. These ligands antagonize HIF-2 heterodimerization with ARNT and its DNA-binding activity *in vitro*, resulting in reduced HIF-2 target gene expression. Selective regulation of HIF-2 may be a potential therapeutic strategy to intervene in HIF-2-driven tumors such as renal cell carcinomas (Scheuermann et al., 2013).

Applying a series of complementary mechanistic experiments, we demonstrated that carvones are non-competitive antagonists of human AhR, acting through allosteric binding in the region involved in heterodimerization with ARNT, thereby preventing the formation of functional AhR-ARNT heterodimers. Analysis of the AhR transcriptional response in reporter gene assays revealed a noncompetitive mechanism of carvone antagonism. These results were supported by the ligand-binding assay. Carvones did not displace <sup>3</sup>H-TCDD from binding at AhR and did not inhibit ligand-elicited nuclear translocation of AhR. In contrast, S/R-carvones inhibited the formation of the AhR-ARNT heterodimer and all downward events involving binding of AhR to DNA and the expression of AhR-target genes. In addition, interactions of carvone with potential off-targets, including ARNT, PKC, 468 kinases, nuclear receptors (RXR $\alpha$ , PPAR $\gamma$ ), steroid receptors (AR, ER $\alpha$ , ER $\beta$ , PR, and GR), protein phosphatases (PTPN11/SHP2, PTPN6/SHP1), and heat shock protein 90 kDa (HSP90) were excluded. Furthermore, the antagonistic effects of carvones on AhR were demonstrated *in vivo*. Carvones inhibit BaP-inducible *Cyp1a1* mRNA in the mouse skin and reverse BaP-mediated potentiation of the UV-inducible chemokine Cxcl5, which was previously found to be responsible for UVB-induced inflammatory pain (Dawes et al., 2011). Moreover, carvones significantly attenuated the harmful effects of BaP, as revealed by the sunburn cell count. In UVB-irradiated skin, AhR signaling pathways are activated by FICZ and the related Trp photoproducts,



facilitating cutaneous inflammatory responses and skin carcinogenesis (Vogeley et al., 2022). Topical application of the competitive antagonist BDDI has previously been shown to inhibit AhR-dependent signaling in UVB-irradiated human skin (Tigges et al., 2014). In this study, the application of carvones as the AhR antagonists after irradiation reduced Cxcl5 expression and may be clinically significant in relieving sunburn-induced pain.

Unfortunately, despite several efforts toward this goal, there is no complete structure for the full-length AhR protein, and thus the non-existent three-dimensional structure of AhR limits AhR research and the search for new ligands of the AhR (Uemura et al., 2020). However, structural models developed via homology modeling have allowed the characterization of the binding cavity and prediction of specific residues that play a critical role in ligand binding (Giani Tagliabue et al., 2019). Several studies have focused on deciphering the structure of AhR and understanding its three-dimensional structure. A homology model of the murine AhR-ARNT PAS domain dimer was developed using X-ray structures of other bHLH-PAS protein dimers. Mutagenesis can be used to evaluate ligand-dependent DNA-binding ability of the AhR-ARNT heterodimer (Corrada et al., 2017). The crystal structure of the mouse Ahr PAS-A domain revealed that the mouse Ahr residues Ala119 and Leu120 are critical for hydrophobic interactions at the Ahr-Arnt interface and dimerization (Wu et al., 2013). Furthermore, Corrada et al. clarified the differential roles of AhR and ARNT residues in the molecular events preceding and following the heterodimerization of AhR with ARNT (Corrada et al., 2017; Corrada et al., 2016). Recently, a high-resolution cryo-EM structure of the indirubin-bound HSP90-XAP2-AhR complex (Gruszczuk et al., 2022) and Hsp90-AhR-p23 complex with or without bound XAP (Wen et al., 2023) were solved, providing structural insights into the details of the complex assembly (Gruszczuk et al., 2022). The crystal structure of the mammalian AhR-ARNT heterodimer in complex with DRE showed that ARNT curls around AhR in a highly intertwined asymmetric architecture with extensive heterodimerization interfaces and AhR interdomain interactions. These findings also suggested that the allosteric structural pathway of AhR is crucial for sensing and transducing structural changes in its ligand-binding domain (Seok et al., 2017). Mutations in mouse AhR

residues Leu42 and Leu120 (homologous to human Leu43 and Leu122, respectively) led to the decreased binding of AhR-ARNT to the DRE, and mutation of Leu49 in mouse AhR maintained intact nuclear translocation of AhR but inhibited its transcriptional activity (Seok et al., 2017). Structural allostery has also been observed in the nuclear hormone receptors. Allosteric pathways in the PPAR $\gamma$ -RXR $\alpha$  nuclear receptor complex have been observed (Ricci et al., 2016), and changes in the dimer interfaces of GR have been found to allosterically affect DNA sequence-specific signaling (Watson et al., 2013). According to our docking data, carvone binds to the AhR protein at the allosteric site of the bHLH and PAS-A domains responsible for, among other things, binding of the dimerization partner. The binding of carvone directly affects the dimerization interface, with a helical shift of 10-13 Å and a significant unwinding of the  $\alpha$ 1 helix. Subsequently, direct binding of carvone to the AhR fragment in the range of 23–273 amino acid residues was demonstrated via microscale thermophoresis. The importance of the oxo group in the carvone molecule for its interaction with AhR, preliminarily through hydrogen bonds, has also been demonstrated in experiments with structurally similar D-limonene. Deoxy-carvone (D-limonene) does not bind to the AhR fragment or antagonize AhR. Subsequently, N<sub>3</sub>-S-carvone was synthesized for more precise determination of the binding site of carvone on AhR. Using the Achilles Blind Docking Server, target residues for the photoactivatable derivative N<sub>3</sub>-S-carvone (Leu47, Phe56, Leu72, and Tyr76) were calculated, and peptides absent in the AhR digest after reaction with N<sub>3</sub>-S-carvone contained the predicted sites.

The carvone concentrations of up to 1 mM used in this study may have potential clinical significance. However, available data showed that the tested doses were relevant. Topical application of 300 mg of R-carvone and S-carvone, used as skin permeabilizers in transdermal patches, resulted in maximum plasma concentrations of approximately 0.6  $\mu$ M and 0.2  $\mu$ M, respectively (Jager et al., 2001). The concentration of carvones in the intestine, liver, and skin after application must be an order of magnitude higher than that in plasma levels. The recommended dose of EOs in the food industry is 35–55  $\mu$ g/mL. In the case of carvone-rich EOs of dill, spearmint, and cumin (more than 50% carvone content), the concentration of carvone in food can be approximately 150  $\mu$ M

(Bartonkova et Dvorak, 2018a). Carvone distribution was tested in volunteers who were administered 100 mg cumin oil (approximately 54.5 mg carvone) in coated capsules. The carvone levels in the blood of these volunteers reached 0.1  $\mu\text{M}$  (Mascher et al., 2001). The European Food Safety Authority (EFSA) has defined an acceptable daily intake of S-carvone as 0.6 a body weight (Committee, 2014).

Overall, dietary monocyclic monoterpene carvones represent a new class of non-competitive AhR antagonists of the AhR. Carvones act through allosteric binding at the AhR, thereby blocking heterodimerization with ARNT and constraining the transcriptional function of the AhR-ARNT heterodimer. Although hundreds of orthosteric AhR ligands, including antagonists, have been described, this is the first report on the allosteric antagonism of AhR by small-molecule compounds. This study has new clinical and fundamental mechanistic implications.

## CONCLUSION

In this thesis, I examined the effects and molecular mechanisms of the monoterpenoid carvone, a component of the essential oils of caraway, dill, and spearmint, on the AhR signaling pathway. The major findings are:

1. Carvone acts as non-competitive AhR antagonist that binds allosterically to the bHLH/PAS-A region of the AhR domain. This type of atypical AhR antagonism was described for the first time.
2. Carvone inhibits heterodimerization of AhR with ARNT and inhibits all the subsequent events in the AhR signaling pathway (DNA binding and expression of AhR target genes).
3. Carvone does not interact with AhR-related off-targets.
4. Carvones antagonize the AhR *in vivo* in mice skin.

**My experimental contributions to the published work:**

Dvořák, Z., Poulíková, K., Mani, S. (2021). Indole scaffolds are a promising class of the aryl hydrocarbon receptor ligands. *Eur J Med Chem*, 215: 113231. **[IF 7.088]**. Contribution: Literature database search and figure processing.

**Ondrová K.**, Zůvalová I., Vyhlídalová B., Krasulová K., Miková E., Vrzal R., Nádvořník P., Nepal B., Kortagere S., Kopečná M., Kopečný D., Šebela M., Rastinejad F., Pu H., Sural M., Rolfes KM., Haarmann-Stemmann T., Li H., Mani S., Dvořák Z. (2023). Monoterpenoid aryl hydrocarbon receptor allosteric antagonists protect against ultraviolet skin damage in female mice. *Nat Commun* 14: 2728. **[IF<sub>2021</sub> 17.694]**. Contribution: reporter gene assay, mRNA isolation and qRT-PCR analysis, protein isolation and analysis, EROD activity assay, protein immunoprecipitation assay, collaboration on microscale thermophoresis, azido-S-carvone UV-photoactivation, and external data processing.

## REFERENCES

- Abdel-Magid, A.F. (2015). Allosteric modulators: an emerging concept in drug discovery. *ACS Med Chem Lett*, 6, 104-7.
- Abel, J., Haarmann-Stemann, T. (2010). An introduction to the molecular basics of aryl hydrocarbon receptor biology. *Biol Chem*, 391, 1235-48.
- Adachi, J., Mori, Y., Matsui, S., Takigami, H., Fujino, J., Kitagawa, H., Miller, C.A., 3rd, Kato, T., Saeki, K., Matsuda, T. (2001). Indirubin and indigo are potent aryl hydrocarbon receptor ligands present in human urine. *J Biol Chem*, 276, 31475-8.
- Ahmed, S., Bott, D., Gomez, A., Tamblyn, L., Rasheed, A., Cho, T., MacPherson, L., Sugamori, K.S., Yang, Y., Grant, D.M., Cummins, C.L., Matthews, J. (2015). Loss of the Mono-ADP-ribosyltransferase, Tiparp, Increases Sensitivity to Dioxin-induced Steatohepatitis and Lethality. *J Biol Chem*, 290, 16824-40.
- Alsanea, S., Liu, D. (2017). BITC and S-Carvone Restrain High-Fat Diet-Induced Obesity and Ameliorate Hepatic Steatosis and Insulin Resistance. *Pharm Res*, 34, 2241-2249.
- Amakura, Y., Tsutsumi, T., Sasaki, K., Nakamura, M., Yoshida, T., Maitani, T. (2008). Influence of food polyphenols on aryl hydrocarbon receptor-signaling pathway estimated by in vitro bioassay. *Phytochemistry*, 69, 3117-30.
- Angelos, M.G., Kaufman, D.S. (2018). Advances in the role of the aryl hydrocarbon receptor to regulate early hematopoietic development. *Curr Opin Hematol*, 25, 273-278.
- Angelos, M.G., Ruh, P.N., Webber, B.R., Blum, R.H., Ryan, C.D., Bendzick, L., Shim, S., Yingst, A.M., Tufa, D.M., Verneris, M.R., Kaufman, D.S. (2017). Aryl hydrocarbon receptor inhibition promotes hematolymphoid development from human pluripotent stem cells. *Blood*, 129, 3428-3439.
- Arivazhagan, L., Subramanian, S.P. (2015). Tangeretin, a citrus flavonoid attenuates oxidative stress and protects hepatocellular architecture in rats with 7, 12 - dimethylbenz(a)anthracene induced experimental mammary carcinoma. *Journal of Functional Foods*, 15, 339-353.
- Ashida, H. (2000). Suppressive effects of flavonoids on dioxin toxicity. *Biofactors*, 12, 201-6.
- Ashida, H., Fukuda, I., Yamashita, T., Kanazawa, K. (2000). Flavones and flavonols at dietary levels inhibit a transformation of aryl hydrocarbon receptor induced by dioxin. *FEBS Letters*, 476, 213-217.
- Ashida, H., Fukuda, I., Yamashita, T., Kanazawa, K. (2000). Flavones and flavonols at dietary levels inhibit a transformation of aryl hydrocarbon receptor induced by dioxin. *FEBS Lett*, 476, 213-7.
- Bakkali, F., Averbeck, S., Averbeck, D., Idaomar, M. (2008). Biological effects of essential oils--a review. *Food Chem Toxicol*, 46, 446-75.
- Barhoover, M.A., Hall, J.M., Greenlee, W.F., Thomas, R.S. (2010). Aryl hydrocarbon receptor regulates cell cycle progression in human breast cancer cells via a functional interaction with cyclin-dependent kinase 4. *Mol Pharmacol*, 77, 195-201.
- Barouki, R., Coumoul, X., Fernandez-Salguero, P.M. (2007). The aryl hydrocarbon receptor, more than a xenobiotic-interacting protein. *FEBS Lett*, 581, 3608-15.
- Bartonkova, I., Dvorak, Z. (2018a). Essential oils of culinary herbs and spices activate PXR and induce CYP3A4 in human intestinal and hepatic in vitro models. *Toxicol Lett*, 296, 1-9.
- Bartonkova, I., Dvorak, Z. (2018b). Essential oils of culinary herbs and spices display agonist and antagonist activities at human aryl hydrocarbon receptor AhR. *Food Chem Toxicol*, 111, 374-384.
- Berg, K.A., Clarke, W.P. (2018). Making Sense of Pharmacology: Inverse Agonism and Functional Selectivity. *Int J Neuropsychopharmacol*, 21, 962-977.

- Biagioli, M., Carino, A., Fiorucci, C., Annunziato, G., Marchiano, S., Bordoni, M., Roselli, R., Giorgio, C.D., Castiglione, F., Ricci, P., Bruno, A., Faccini, A., Distrutti, E., Baldoni, M., Costantino, G., Fiorucci, S. (2019). The Aryl Hydrocarbon Receptor (AhR) Mediates the Counter-Regulatory Effects of Pelargonidins in Models of Inflammation and Metabolic Dysfunctions. *Nutrients*, 11.
- Bialesova, L., Novotna, A., Macejova, D., Brtko, J., Dvorak, Z. (2015). Agonistic effect of selected isoflavones on arylhydrocarbon receptor in a novel AZ-AhR transgenic gene reporter human cell line. *Gen Physiol Biophys*, 34, 331-4.
- Bianchi-Smiraglia, A., Bagati, A., Fink, E.E., Affronti, H.C., Lipchick, B.C., Moparthy, S., Long, M.D., Rosario, S.R., Lightman, S.M., Moparthy, K., Wolff, D.W., Yun, D.H., Han, Z., Polechetti, A., Roll, M.V., Gitlin, II, Leonova, K.I., Rowsam, A.M., Kandel, E.S., Gudkov, A.V., Bergsagel, P.L., Lee, K.P., Smiraglia, D.J., Nikiforov, M.A. (2018). Inhibition of the aryl hydrocarbon receptor/polyamine biosynthesis axis suppresses multiple myeloma. *J Clin Invest*, 128, 4682-4696.
- Bjeldanes, L.F., Kim, J.Y., Grose, K.R., Bartholomew, J.C., Bradfield, C.A. (1991). Aromatic hydrocarbon responsiveness-receptor agonists generated from indole-3-carbinol in vitro and in vivo: comparisons with 2,3,7,8-tetrachlorodibenzo-p-dioxin. *Proc Natl Acad Sci U S A*, 88, 9543-7.
- Bock, K.W. (2018). From TCDD-mediated toxicity to searches of physiologic AHR functions. *Biochem Pharmacol*, 155, 419-424.
- Bock, K.W., Köhle, C. (2006). Ah receptor: Dioxin-mediated toxic responses as hints to deregulated physiologic functions. *Biochemical Pharmacology*, 72, 393-404.
- Boni, G., Feiria, S., Sant'Ana, P., Anibal, P.C., Fabiano, M., Buso-Ramos, M., Barbosa, J., Oliveira, T., Höfling, J. (2016). Antifungal and cytotoxic activity of purified biocomponents as carvone, menthone, menthofuran and pulegone from *Mentha* spp. *African Journal of Plant Science*, 10.
- Bradfield, C.A., Bjeldanes, L.F. (1987). Structure-activity relationships of dietary indoles: a proposed mechanism of action as modifiers of xenobiotic metabolism. *J Toxicol Environ Health*, 21, 311-23.
- Braeuning, A., Buchmann, A. (2009). The Glycogen Synthase Kinase Inhibitor 3-(2,4-Dichlorophenyl)-4-(1-methyl-1H-indol-3-yl)-1H-pyrrole-2,5-dione (SB216763) Is a Partial Agonist of the Aryl Hydrocarbon Receptor. *Drug Metabolism and Disposition*, 37, 1576.
- Brinchmann, B.C., Le Ferrec, E., Podechard, N., Lagadic-Gossmann, D., Shoji, K.F., Penna, A., Kukowski, K., Kubatova, A., Holme, J.A., Ovrevik, J. (2018). Lipophilic Chemicals from Diesel Exhaust Particles Trigger Calcium Response in Human Endothelial Cells via Aryl Hydrocarbon Receptor Non-Genomic Signalling. *Int J Mol Sci*, 19.
- Briolotti, P., Chaloin, L., Balaguer, P., Da Silva, F., Tomankova, V., Pascussi, J.M., Duret, C., Fabre, J.M., Ramos, J., Klieber, S., Maurel, P., Daujat-Chavanieu, M., Gerbal-Chaloin, S. (2015). Analysis of Glycogen Synthase Kinase Inhibitors That Regulate Cytochrome P450 Expression in Primary Human Hepatocytes by Activation of beta-Catenin, Aryl Hydrocarbon Receptor and Pregnane X Receptor Signaling. *Toxicol Sci*, 148, 261-75.
- Burt, S. (2004). Essential oils: their antibacterial properties and potential applications in foods--a review. *Int J Food Microbiol*, 94, 223-53.
- Casper, R.F., Quesne, M., Rogers, I.M., Shirota, T., Jolivet, A., Milgrom, E., Savouret, J.F. (1999). Resveratrol has antagonist activity on the aryl hydrocarbon receptor: implications for prevention of dioxin toxicity. *Mol Pharmacol*, 56, 784-90.
- Ćavar Zeljković, S., Schadich, E., Džubák, P., Hajdúch, M., Tarkowski, P. (2022). Antiviral Activity of Selected Lamiaceae Essential Oils and Their Monoterpenes Against SARS-Cov-2. *Frontiers in Pharmacology*, 13.
- Ciolino, H.P., Daschner, P.J., Yeh, G.C. (1998a). Resveratrol inhibits transcription of CYP1A1 in vitro by preventing activation of the aryl hydrocarbon receptor. *Cancer Res*, 58, 5707-12.

- Ciolino, H.P., Wang, T.T., Yeh, G.C. (1998b). Diosmin and diosmetin are agonists of the aryl hydrocarbon receptor that differentially affect cytochrome P450 1A1 activity. *Cancer Res*, 58, 2754-60.
- Clissold, S.P., Campoli-Richards, D.M. (1986). Omeprazole. A preliminary review of its pharmacodynamic and pharmacokinetic properties, and therapeutic potential in peptic ulcer disease and Zollinger-Ellison syndrome. *Drugs*, 32, 15-47.
- Committee, E.S. (2014). Scientific Opinion on the safety assessment of carvone, considering all sources of exposure. *EFSA Journal*, 12, 3806.
- Corrada, D., Denison, M.S., Bonati, L. (2017). Structural modeling of the AhR:ARNT complex in the bHLH-PASA-PASB region elucidates the key determinants of dimerization. *Mol Biosyst*, 13, 981-990.
- Corrada, D., Soshilov, A.A., Denison, M.S., Bonati, L. (2016). Deciphering Dimerization Modes of PAS Domains: Computational and Experimental Analyses of the AhR:ARNT Complex Reveal New Insights Into the Mechanisms of AhR Transformation. *PLoS Comput Biol*, 12, e1004981.
- Corre, S., Tardif, N., Mouchet, N., Leclair, H.M., Boussemart, L., Gautron, A., Bachelot, L., Perrot, A., Soshilov, A., Rogiers, A., Rambow, F., Dumontet, E., Tarte, K., Bessede, A., Guillemain, G.J., Marine, J.C., Denison, M.S., Gilot, D., Galibert, M.D. (2018). Sustained activation of the Aryl hydrocarbon Receptor transcription factor promotes resistance to BRAF-inhibitors in melanoma. *Nat Commun*, 9, 4775.
- Dawes, J.M., Calvo, M., Perkins, J.R., Paterson, K.J., Kiesewetter, H., Hobbs, C., Kaan, T.K., Orengo, C., Bennett, D.L., McMahon, S.B. (2011). CXCL5 mediates UVB irradiation-induced pain. *Sci Transl Med*, 3, 90ra60.
- de Sousa, D.P., de Farias Nobrega, F.F., de Almeida, R.N. (2007). Influence of the chirality of (R)-(-) and (S)-(+)-carvone in the central nervous system: a comparative study. *Chirality*, 19, 264-8.
- DeGroot, D.E., Franks, D.G., Higa, T., Tanaka, J., Hahn, M.E., Denison, M.S. (2015). Naturally occurring marine brominated indoles are aryl hydrocarbon receptor ligands/agonists. *Chem Res Toxicol*, 28, 1176-85.
- Delescluse, C., Lemaire, G., de Sousa, G., Rahmani, R. (2000). Is CYP1A1 induction always related to AHR signaling pathway? *Toxicology*, 153, 73-82.
- Denison, M., D.H., H., S.R., N., Zhao, B., D.S., B., Hayashi, A., Knockaert, M., Meijer, L. (2006). Indirubins as activators of the aryl hydrocarbon receptor signal transduction pathway.
- Denison, M.S., Faber, S.C. (2017). And Now for Something Completely Different: Diversity in Ligand-Dependent Activation of Ah Receptor Responses. *Curr Opin Toxicol*, 2, 124-131.
- Denison, M.S., Nagy, S.R. (2003). Activation of the aryl hydrocarbon receptor by structurally diverse exogenous and endogenous chemicals. *Annu Rev Pharmacol Toxicol*, 43, 309-34.
- Denison, M.S., Phelan, D., Winter, G.M., Ziccardi, M.H. (1998). Carbaryl, a carbamate insecticide, is a ligand for the hepatic Ah (dioxin) receptor. *Toxicol Appl Pharmacol*, 152, 406-14.
- Denison, M.S., Rogers, J.M., Rushing, S.R., Jones, C.L., Tetangco, S.C., Heath-Pagliuso, S. (2002). Analysis of the aryl hydrocarbon receptor (AhR) signal transduction pathway. *Curr Protoc Toxicol*, Chapter 4, Unit4 8.
- Denison, M.S., Soshilov, A.A., He, G., DeGroot, D.E., Zhao, B. (2011). Exactly the same but different: promiscuity and diversity in the molecular mechanisms of action of the aryl hydrocarbon (dioxin) receptor. *Toxicol Sci*, 124, 1-22.
- Dery, M.A., Michaud, M.D., Richard, D.E. (2005). Hypoxia-inducible factor 1: regulation by hypoxic and non-hypoxic activators. *Int J Biochem Cell Biol*, 37, 535-40.
- DiNatale, B.C., Smith, K., John, K., Krishnegowda, G., Amin, S.G., Perdev, G.H. (2012). Ah receptor antagonism represses head and neck tumor cell aggressive phenotype. *Mol Cancer Res*, 10, 1369-79.



- Dong, F., Hao, F., Murray, I.A., Smith, P.B., Koo, I., Tindall, A.M., Kris-Etherton, P.M., Gowda, K., Amin, S.G., Patterson, A.D., Perdew, G.H. (2020). Intestinal microbiota-derived tryptophan metabolites are predictive of Ah receptor activity. *Gut Microbes*, 12, 1-24.
- Dou, H., Duan, Y., Zhang, X., Yu, Q., Di, Q., Song, Y., Li, P., Gong, Y. (2019). Aryl hydrocarbon receptor (AhR) regulates adipocyte differentiation by assembling CRL4B ubiquitin ligase to target PPARgamma for proteasomal degradation. *J Biol Chem*, 294, 18504-18515.
- Dunlap, T.L., Howell, C.E., Mukand, N., Chen, S.N., Pauli, G.F., Dietz, B.M., Bolton, J.L. (2017). Red Clover Aryl Hydrocarbon Receptor (AhR) and Estrogen Receptor (ER) Agonists Enhance Genotoxic Estrogen Metabolism. *Chem Res Toxicol*, 30, 2084-2092.
- Dvorak, Z., Cvek, B. (2011). Vybrané kapitoly z buněčné biologie.
- Dvorak, Z., Kopp, F., Costello, C.M., Kemp, J.S., Li, H., Vrzalova, A., Stepankova, M., Bartonkova, I., Jiskrova, E., Poulikova, K., Vyhlidalova, B., Nordstroem, L.U., Karunaratne, C.V., Ranhotra, H.S., Mun, K.S., Naren, A.P., Murray, I.A., Perdew, G.H., Brtko, J., Toporova, L., Schon, A., Wallace, B.D., Walton, W.G., Redinbo, M.R., Sun, K., Beck, A., Kortagere, S., Neary, M.C., Chandran, A., Vishveshwara, S., Cavalluzzi, M.M., Lentini, G., Cui, J.Y., Gu, H., March, J.C., Chatterjee, S., Matson, A., Wright, D., Flannigan, K.L., Hirota, S.A., Sartor, R.B., Mani, S. (2020a). Targeting the pregnane X receptor using microbial metabolite mimicry. *EMBO Mol Med*, 12, e11621.
- Dvorak, Z., Poulikova, K., Mani, S. (2021). Indole scaffolds as a promising class of the aryl hydrocarbon receptor ligands. *Eur J Med Chem*, 215, 113231.
- Dvorak, Z., Sokol, H., Mani, S. (2020b). Drug Mimicry: Promiscuous Receptors PXR and AhR, and Microbial Metabolite Interactions in the Intestine. *Trends Pharmacol Sci*, 41, 900-908.
- Dvorak, Z., Vrzal, R., Pavek, P., Ulrichova, J. (2008). An evidence for regulatory cross-talk between aryl hydrocarbon receptor and glucocorticoid receptor in HepG2 cells. *Physiol Res*, 57, 427-435.
- Ekins, S., Chang, C., Mani, S., Krasowski, M.D., Reschly, E.J., Iyer, M., Kholodovych, V., Ai, N., Welsh, W.J., Sinz, M., Swaan, P.W., Patel, R., Bachmann, K. (2007). Human pregnane X receptor antagonists and agonists define molecular requirements for different binding sites. *Mol Pharmacol*, 72, 592-603.
- El-Shemy, H. (2020). *Essential Oils - Oils of Nature*, IntechOpen, London.
- El Gendy, M.A., El-Kadi, A.O. (2010). Harman induces CYP1A1 enzyme through an aryl hydrocarbon receptor mechanism. *Toxicol Appl Pharmacol*, 249, 55-64.
- Esser, C., Rannug, A. (2015). The aryl hydrocarbon receptor in barrier organ physiology, immunology, and toxicology. *Pharmacol Rev*, 67, 259-79.
- Fabian, M.A., Biggs, W.H., 3rd, Treiber, D.K., Atteridge, C.E., Azimioara, M.D., Benedetti, M.G., Carter, T.A., Ciceri, P., Edeen, P.T., Floyd, M., Ford, J.M., Galvin, M., Gerlach, J.L., Grotzfeld, R.M., Herrgard, S., Insko, D.E., Insko, M.A., Lai, A.G., Lelias, J.M., Mehta, S.A., Milanov, Z.V., Velasco, A.M., Wodicka, L.M., Patel, H.K., Zarrinkar, P.P., Lockhart, D.J. (2005). A small molecule-kinase interaction map for clinical kinase inhibitors. *Nat Biotechnol*, 23, 329-36.
- Faliagkas, L., Vokou, D., Theophilidis, G. (2015). Local Anaesthetic Properties vs. Neurotoxicity for (+)- and (-)-Carvone: An Ex Vivo Electrophysiological Study. *Planta Medica Letters*, 2, e6-e9.
- Filip, R., Shaw, T.A., Nishida, A., Pezacki, J.P. (2019). Fungal natural alkaloid schizocommunin activates the aryl hydrocarbon receptor pathway. *MedChemComm*, 10, 985-990.
- Foster, D.J., Conn, P.J. (2017). Allosteric Modulation of GPCRs: New Insights and Potential Utility for Treatment of Schizophrenia and Other CNS Disorders. *Neuron*, 94, 431-446.

- Franzios, G., Mirotsoy, M., Hatzia Apostolou, E., Kral, J., Scouras, Z.G., Mavragani-Tsipidou, P. (1997). Insecticidal and Genotoxic Activities of Mint Essential Oils. *Journal of Agricultural and Food Chemistry*, 45, 2690-2694.
- Froyen, E.B., Steinberg, F.M. (2016). Genistein decreases basal hepatic cytochrome P450 1A1 protein expression and activity in Swiss Webster mice. *Nutr Res*, 36, 430-9.
- Fukuda, I., Sakane, I., Yabushita, Y., Kodoi, R., Nishiumi, S., Kakuda, T., Sawamura, S., Kanazawa, K., Ashida, H. (2004). Pigments in green tea leaves (*Camellia sinensis*) suppress transformation of the aryl hydrocarbon receptor induced by dioxin. *J Agric Food Chem*, 52, 2499-506.
- Furue, M., Hashimoto-Hachiya, A., Tsuji, G. (2019). Aryl Hydrocarbon Receptor in Atopic Dermatitis and Psoriasis. *Int J Mol Sci*, 20.
- Garg, R., Gupta, S., Maru, G.B. (2008). Dietary curcumin modulates transcriptional regulators of phase I and phase II enzymes in benzo[a]pyrene-treated mice: mechanism of its anti-initiating action. *Carcinogenesis*, 29, 1022-32.
- Gasiewicz, T.A., Kende, A.S., Rucci, G., Whitney, B., Willey, J.J. (1996). Analysis of structural requirements for Ah receptor antagonist activity: ellipticines, flavones, and related compounds. *Biochem Pharmacol*, 52, 1787-803.
- Gassmann, M., Kvietikova, I., Rolfs, A., Wenger, R.H. (1997). Oxygen- and dioxin-regulated gene expression in mouse hepatoma cells. *Kidney Int*, 51, 567-74.
- Geithe, C., Protze, J., Kreuchwig, F., Krause, G., Krautwurst, D. (2017). Structural determinants of a conserved enantiomer-selective carvone binding pocket in the human odorant receptor OR1A1. *Cell Mol Life Sci*, 74, 4209-4229.
- Gentry, P.R., Sexton, P.M., Christopoulos, A. (2015). Novel Allosteric Modulators of G Protein-coupled Receptors. *J Biol Chem*, 290, 19478-88.
- Ghattamaneni, N.K., Sharma, A., Panchal, S.K., Brown, L. (2020). Pelargonidin 3-glucoside-enriched strawberry attenuates symptoms of DSS-induced inflammatory bowel disease and diet-induced metabolic syndrome in rats. *Eur J Nutr*, 59, 2905-2918.
- Ghotbaddini, M., Powell, J.B. (2015). The AhR Ligand, TCDD, Regulates Androgen Receptor Activity Differently in Androgen-Sensitive versus Castration-Resistant Human Prostate Cancer Cells. *Int J Environ Res Public Health*, 12, 7506-18.
- Giani Tagliabue, S., Faber, S.C., Motta, S., Denison, M.S., Bonati, L. (2019). Modeling the binding of diverse ligands within the Ah receptor ligand binding domain. *Scientific Reports*, 9, 10693.
- Giovannoni, F., Bosch, I., Polonio, C.M., Torti, M.F., Wheeler, M.A., Li, Z., Romorini, L., Rodriguez Varela, M.S., Rothhammer, V., Barroso, A., Tjon, E.C., Sanmarco, L.M., Takenaka, M.C., Modaresi, S.M.S., Gutierrez-Vazquez, C., Zanluqui, N.G., Dos Santos, N.B., Munhoz, C.D., Wang, Z., Damonte, E.B., Sherr, D., Gehrke, L., Peron, J.P.S., Garcia, C.C., Quintana, F.J. (2020). AHR is a Zika virus host factor and a candidate target for antiviral therapy. *Nat Neurosci*, 23, 939-951.
- Giovannoni, F., Li, Z., Remes-Lenicov, F., Davola, M.E., Elizalde, M., Paletta, A., Ashkar, A.A., Mossman, K.L., Dugour, A.V., Figueroa, J.M., Barquero, A.A., Ceballos, A., Garcia, C.C., Quintana, F.J. (2021). AHR signaling is induced by infection with coronaviruses. *Nat Commun*, 12, 5148.
- Gottel, M., Le Corre, L., Dumont, C., Schrenk, D., Chagnon, M.C. (2014). Estrogen receptor alpha and aryl hydrocarbon receptor cross-talk in a transfected hepatoma cell line (HepG2) exposed to 2,3,7,8-tetrachlorodibenzo-p-dioxin. *Toxicol Rep*, 1, 1029-1036.
- Goya-Jorge, E., Jorge Rodriguez, M.E., Veitia, M.S., Giner, R.M. (2021). Plant Occurring Flavonoids as Modulators of the Aryl Hydrocarbon Receptor. *Molecules*, 26.
- Grosskopf, H., Walter, K., Karkossa, I., von Bergen, M., Schubert, K. (2021). Non-Genomic AhR-Signaling Modulates the Immune Response in Endotoxin-Activated Macrophages After Activation by the Environmental Stressor BaP. *Front Immunol*, 12, 620270.

- Gruszczuk, J., Grandvillain, L., Lai-Kee-Him, J., Paloni, M., Savva, C.G., Germain, P., Grimaldi, M., Boulahtouf, A., Kwong, H.S., Bous, J., Ancelin, A., Bechara, C., Barducci, A., Balaguer, P., Bourguet, W. (2022). Cryo-EM structure of the agonist-bound Hsp90-XAP2-AHR cytosolic complex. *Nat Commun*, 13, 7010.
- Grycova, A., Doricakova, A., Dvorak, Z. (2015). Impurities contained in antifungal drug ketoconazole are potent activators of human aryl hydrocarbon receptor. *Toxicol Lett*, 239, 67-72.
- Grycová, A., Joo, H., Maier, V., Illés, P., Vyhliálová, B., Poulíková, K., Sládeková, L., Nádvorník, P., Vrzal, R., Zemánková, L., Pečínková, P., Poruba, M., Zapletalová, I., Večeřa, R., Anzenbacher, P., Ehrmann, J., Ondra, P., Jung, J.-W., Mani, S., Dvořák, Z. (2022). Targeting the Aryl Hydrocarbon Receptor with Microbial Metabolite Mimics Alleviates Experimental Colitis in Mice. *Journal of Medicinal Chemistry*.
- Guo, Z., Zhang, Q., Zou, H., Guo, B., Ni, J. (2002). A method for the analysis of low-mass molecules by MALDI-TOF mass spectrometry. *Anal Chem*, 74, 1637-41.
- Gupta, R., Anwer, M.M., Sharma, Y.K. (2012). 15 - Dill, in: Peter, K.V. (Ed.), *Handbook of Herbs and Spices (Second Edition)*. Woodhead Publishing, pp. 275-285.
- Gutierrez, M.A., Davis, S.S., Rosko, A., Nguyen, S.M., Mitchell, K.P., Mateen, S., Neves, J., Garcia, T.Y., Mooney, S., Perdew, G.H., Hubbard, T.D., Lamba, D.A., Ramanathan, A. (2016). A novel AhR ligand, 2AI, protects the retina from environmental stress. *Sci Rep*, 6, 29025.
- Haarmann-Stemmann, T., Sendker, J., Gotz, C., Krug, N., Bothe, H., Fritsche, E., Proksch, P., Abel, J. (2010). Regulation of dioxin receptor function by different beta-carboline alkaloids. *Arch Toxicol*, 84, 619-29.
- Hamers, T., Kamstra, J.H., Ceniijn, P.H., Pencikova, K., Palkova, L., Simeckova, P., Vondracek, J., Andersson, P.L., Stenberg, M., Machala, M. (2011). In vitro toxicity profiling of ultrapure non-dioxin-like polychlorinated biphenyl congeners and their relative toxic contribution to PCB mixtures in humans. *Toxicol Sci*, 121, 88-100.
- Hamouchene, H., Arlt, V.M., Giddings, I., Phillips, D.H. (2011). Influence of cell cycle on responses of MCF-7 cells to benzo[a]pyrene. *BMC Genomics*, 12, 333.
- Han, E.H., Hwang, Y.P., Jeong, T.C., Lee, S.S., Shin, J.G., Jeong, H.G. (2007). Eugenol inhibit 7,12-dimethylbenz[a]anthracene-induced genotoxicity in MCF-7 cells: Bifunctional effects on CYP1 and NAD(P)H:quinone oxidoreductase. *FEBS Lett*, 581, 749-56.
- Harrill, J.A., Hukkanen, R.R., Lawson, M., Martin, G., Gilger, B., Soldatow, V., Lecluyse, E.L., Budinsky, R.A., Rowlands, J.C., Thomas, R.S. (2013). Knockout of the aryl hydrocarbon receptor results in distinct hepatic and renal phenotypes in rats and mice. *Toxicol Appl Pharmacol*, 272, 503-18.
- Hawerkamp, H.C., Kislak, A., Gerber, P.A., Pollet, M., Rolfes, K.M., Soshilov, A.A., Denison, M.S., Momin, A.A., Arold, S.T., Datsi, A., Braun, S.A., Olah, P., Lacouture, M.E., Krutmann, J., Haarmann-Stemmann, T., Homey, B., Meller, S. (2019). Vemurafenib acts as an aryl hydrocarbon receptor antagonist: Implications for inflammatory cutaneous adverse events. *Allergy*, 74, 2437-2448.
- Henklova, P., Vrzal, R., Ulrichova, J., Dvorak, Z. (2008). Role of mitogen-activated protein kinases in aryl hydrocarbon receptor signaling. *Chem Biol Interact*, 172, 93-104.
- Henry, E.C., Gasiewicz, T.A. (2008). Molecular determinants of species-specific agonist and antagonist activity of a substituted flavone towards the aryl hydrocarbon receptor. *Arch Biochem Biophys*, 472, 77-88.
- Henry, E.C., Welle, S.L., Gasiewicz, T.A. (2010). TCDD and a putative endogenous AhR ligand, ITE, elicit the same immediate changes in gene expression in mouse lung fibroblasts. *Toxicol Sci*, 114, 90-100.
- Hewitson, K.S., Schofield, C.J. (2004). The HIF pathway as a therapeutic target. *Drug Discov Today*, 9, 704-11.

- Hidaka, T., Ogawa, E., Kobayashi, E.H., Suzuki, T., Funayama, R., Nagashima, T., Fujimura, T., Aiba, S., Nakayama, K., Okuyama, R., Yamamoto, M. (2017). The aryl hydrocarbon receptor AhR links atopic dermatitis and air pollution via induction of the neurotrophic factor artemin. *Nat Immunol*, 18, 64-73.
- Hoglund, E., Overli, O., Winberg, S. (2019). Tryptophan Metabolic Pathways and Brain Serotonergic Activity: A Comparative Review. *Front Endocrinol (Lausanne)*, 10, 158.
- Holme, J.A., Brinchmann, B.C., Le Ferrec, E., Lagadic-Gossmann, D., Ovrevik, J. (2019). Combustion Particle-Induced Changes in Calcium Homeostasis: A Contributing Factor to Vascular Disease? *Cardiovasc Toxicol*, 19, 198-209.
- Huang, G., Elferink, C.J. (2012). A novel nonconsensus xenobiotic response element capable of mediating aryl hydrocarbon receptor-dependent gene expression. *Mol Pharmacol*, 81, 338-47.
- Changeux, J.P., Christopoulos, A. (2016). Allosteric Modulation as a Unifying Mechanism for Receptor Function and Regulation. *Cell*, 166, 1084-1102.
- Chen, I., Safe, S., Bjeldanes, L. (1996). Indole-3-carbinol and diindolylmethane as aryl hydrocarbon (Ah) receptor agonists and antagonists in T47D human breast cancer cells. *Biochem Pharmacol*, 51, 1069-76.
- Chen, J., Haller, C.A., Jernigan, F.E., Koerner, S.K., Wong, D.J., Wang, Y., Cheong, J.E., Kosaraju, R., Kwan, J., Park, D.D., Thomas, B., Bhasin, S., De La Rosa, R.C., Premji, A.M., Liu, L., Park, E., Moss, A.C., Emili, A., Bhasin, M., Sun, L., Chaikof, E.L. (2020). Modulation of lymphocyte-mediated tissue repair by rational design of heterocyclic aryl hydrocarbon receptor agonists. *Sci Adv*, 6, eaay8230.
- Cheng, Y., Prusoff, W.H. (1973). Relationship between the inhibition constant (K<sub>1</sub>) and the concentration of inhibitor which causes 50 per cent inhibition (I<sub>50</sub>) of an enzymatic reaction. *Biochem Pharmacol*, 22, 3099-108.
- Ikuta, T., Kobayashi, Y., Kawajiri, K. (2004). Phosphorylation of nuclear localization signal inhibits the ligand-dependent nuclear import of aryl hydrocarbon receptor. *Biochem Biophys Res Commun*, 317, 545-50.
- Iwano, H., Ujita, W., Nishikawa, M., Ishii, S., Inoue, H., Yokota, H. (2014). Effect of dietary eugenol on xenobiotic metabolism and mediation of UDP-glucuronosyltransferase and cytochrome P450 1A1 expression in rat liver. *Int J Food Sci Nutr*, 65, 241-4.
- Jackson, D.P., Joshi, A.D., Elferink, C.J. (2015). Ah Receptor Pathway Intricacies; Signaling Through Diverse Protein Partners and DNA-Motifs. *Toxicol Res (Camb)*, 4, 1143-1158.
- Jager, W., Mayer, M., Reznicek, G., Buchbauer, G. (2001). Percutaneous absorption of the monoterpene carvone: implication of stereoselective metabolism on blood levels. *J Pharm Pharmacol*, 53, 637-42.
- Jia, Y., Tao, Y., Lv, C., Xia, Y., Wei, Z., Dai, Y. (2019). Tetrandrine enhances the ubiquitination and degradation of Syk through an AhR-c-src-c-Cbl pathway and consequently inhibits osteoclastogenesis and bone destruction in arthritis. *Cell Death Dis*, 10, 38.
- Jin, U.H., Park, H., Li, X., Davidson, L.A., Allred, C., Patil, B., Jayaprakasha, G., Orr, A.A., Mao, L., Chapkin, R.S., Jayaraman, A., Tamamis, P., Safe, S. (2018). Structure-Dependent Modulation of Aryl Hydrocarbon Receptor-Mediated Activities by Flavonoids. *Toxicol Sci*, 164, 205-217.
- Jones, G., Willett, P., Glen, R.C. (1995). Molecular recognition of receptor sites using a genetic algorithm with a description of desolvation. *J Mol Biol*, 245, 43-53.
- Kalmes, M., Blomeke, B. (2012). Impact of eugenol and isoeugenol on AhR translocation, target gene expression, and proliferation in human HaCaT keratinocytes. *J Toxicol Environ Health A*, 75, 478-91.
- Kalmes, M., Neumeyer, A., Rio, P., Hanenberg, H., Fritsche, E., Blomeke, B. (2006). Impact of the arylhydrocarbon receptor on eugenol- and isoeugenol-induced cell

- cycle arrest in human immortalized keratinocytes (HaCaT). *Biol Chem*, 387, 1201-7.
- Kamenickova, A., Anzenbacherova, E., Pavek, P., Soshilov, A., Denison, M.S., Anzenbacher, P., Dvorak, Z. (2013a). Pelargonidin activates the AhR and induces CYP1A1 in primary human hepatocytes and human cancer cell lines HepG2 and LS174T. *Toxicol Lett*, 218, 253-259.
- Kamenickova, A., Anzenbacherova, E., Pavek, P., Soshilov, A., Denison, M.S., Zapletalova, M., Anzenbacher, P., Dvorak, Z. (2013). Effects of anthocyanins on the AhR-CYP1A1 signaling pathway in human hepatocytes and human cancer cell lines. *Toxicol Lett*, 221, 1-8.
- Kaur, M., Badhan, R.K. (2017). Phytochemical mediated-modulation of the expression and transporter function of breast cancer resistance protein at the blood-brain barrier: An in-vitro study. *Brain Res*, 1654, 9-23.
- Kawai, S., Iijima, H., Shinzaki, S., Hiyama, S., Yamaguchi, T., Araki, M., Iwatani, S., Shiraishi, E., Mukai, A., Inoue, T., Hayashi, Y., Tsujii, M., Motooka, D., Nakamura, S., Iida, T., Takehara, T. (2017). Indigo Naturalis ameliorates murine dextran sodium sulfate-induced colitis via aryl hydrocarbon receptor activation. *J Gastroenterol*, 52, 904-919.
- Kewley, R.J., Whitelaw, M.L., Chapman-Smith, A. (2004). The mammalian basic helix-loop-helix/PAS family of transcriptional regulators. *Int J Biochem Cell Biol*, 36, 189-204.
- Kim, D.W., Gazourian, L., Quadri, S.A., Romieu-Mourez, R., Sherr, D.H., Sonenshein, G.E. (2000). The RelA NF-kappaB subunit and the aryl hydrocarbon receptor (AhR) cooperate to transactivate the c-myc promoter in mammary cells. *Oncogene*, 19, 5498-506.
- Kim, S.A., Jo, S.H., Cho, J.H., Yu, M.Y., Shin, H.C., Kim, J.A., Park, S.G., Park, B.C., Kim, S., Kim, J.H. (2020). Aryl Sulfonamides Induce Degradation of Aryl Hydrocarbon Receptor Nuclear Translocator through CRL4(DCAF15) E3 Ligase. *Mol Cells*, 43, 935-944.
- Kim, S.H., Henry, E.C., Kim, D.K., Kim, Y.H., Shin, K.J., Han, M.S., Lee, T.G., Kang, J.K., Gasiewicz, T.A., Ryu, S.H., Suh, P.G. (2006). Novel compound 2-methyl-2H-pyrazole-3-carboxylic acid (2-methyl-4-o-tolylazo-phenyl)-amide (CH-223191) prevents 2,3,7,8-TCDD-induced toxicity by antagonizing the aryl hydrocarbon receptor. *Mol Pharmacol*, 69, 1871-8.
- Knerr, S., Schrenk, D. (2006). Carcinogenicity of 2,3,7,8-tetrachlorodibenzo-p-dioxin in experimental models. *Mol Nutr Food Res*, 50, 897-907.
- Kolluri, S.K., Jin, U.H., Safe, S. (2017). Role of the aryl hydrocarbon receptor in carcinogenesis and potential as an anti-cancer drug target. *Arch Toxicol*, 91, 2497-2513.
- Lamas, B., Hernandez-Galan, L., Galipeau, H.J., Constante, M., Clarizio, A., Jury, J., Breyner, N.M., Caminero, A., Rueda, G., Hayes, C.L., McCarville, J.L., Bermudez Brito, M., Planchais, J., Rolhion, N., Murray, J.A., Langella, P., Loonen, L.M.P., Wells, J.M., Bercik, P., Sokol, H., Verdu, E.F. (2020). Aryl hydrocarbon receptor ligand production by the gut microbiota is decreased in celiac disease leading to intestinal inflammation. *Sci Transl Med*, 12.
- Lamas, B., Richard, M.L., Leducq, V., Pham, H.P., Michel, M.L., Da Costa, G., Bridonneau, C., Jegou, S., Hoffmann, T.W., Natividad, J.M., Brot, L., Taleb, S., Couturier-Maillard, A., Nion-Larmurier, I., Merabtene, F., Seksik, P., Bourrier, A., Cosnes, J., Ryffel, B., Beaugerie, L., Launay, J.M., Langella, P., Xavier, R.J., Sokol, H. (2016). CARD9 impacts colitis by altering gut microbiota metabolism of tryptophan into aryl hydrocarbon receptor ligands. *Nat Med*, 22, 598-605.
- Larigot, L., Juricek, L., Dairou, J., Coumoul, X. (2018). AhR signaling pathways and regulatory functions. *Biochim Open*, 7, 1-9.

- Levine-Fridman, A., Chen, L., Elferink, C.J. (2004). Cytochrome P4501A1 promotes G1 phase cell cycle progression by controlling aryl hydrocarbon receptor activity. *Mol Pharmacol*, 65, 461-9.
- Li, S.Y., Dougherty, J.J. (1997). Inhibitors of serine/threonine-specific protein phosphatases stimulate transcription by the Ah receptor/Arnt dimer by affecting a step subsequent to XRE binding. *Arch Biochem Biophys*, 340, 73-82.
- Ling, H., Sayer, J.M., Plosky, B.S., Yagi, H., Boudsocq, F., Woodgate, R., Jerina, D.M., Yang, W. (2004). Crystal structure of a benzo[a]pyrene diol epoxide adduct in a ternary complex with a DNA polymerase. *Proc Natl Acad Sci U S A*, 101, 2265-9.
- Lisi, G.P., Loria, J.P. (2017). Allostery in enzyme catalysis. *Curr Opin Struct Biol*, 47, 123-130.
- Long, W.P., Pray-Grant, M., Tsai, J.C., Perdew, G.H. (1998). Protein kinase C activity is required for aryl hydrocarbon receptor pathway-mediated signal transduction. *Mol Pharmacol*, 53, 691-700.
- Loub, W.D., Wattenberg, L.W., Davis, D.W. (1975). Aryl hydrocarbon hydroxylase induction in rat tissues by naturally occurring indoles of cruciferous plants. *J Natl Cancer Inst*, 54, 985-8.
- Lu, Y.F., Santostefano, M., Cunningham, B.D., Threadgill, M.D., Safe, S. (1995). Identification of 3'-methoxy-4'-nitroflavone as a pure aryl hydrocarbon (Ah) receptor antagonist and evidence for more than one form of the nuclear Ah receptor in MCF-7 human breast cancer cells. *Arch Biochem Biophys*, 316, 470-7.
- Ma, Q., Baldwin, K.T. (2000). 2,3,7,8-tetrachlorodibenzo-p-dioxin-induced degradation of aryl hydrocarbon receptor (AhR) by the ubiquitin-proteasome pathway. Role of the transcription activator and DNA binding of AhR. *J Biol Chem*, 275, 8432-8.
- Maayah, Z.H., El Gendy, M.A., El-Kadi, A.O., Korashy, H.M. (2013). Sunitinib, a tyrosine kinase inhibitor, induces cytochrome P450 1A1 gene in human breast cancer MCF7 cells through ligand-independent aryl hydrocarbon receptor activation. *Arch Toxicol*, 87, 847-56.
- MacPherson, L., Tamblyn, L., Rajendra, S., Bralha, F., McPherson, J.P., Matthews, J. (2013). 2,3,7,8-Tetrachlorodibenzo-p-dioxin poly(ADP-ribose) polymerase (TiPARP, ARTD14) is a mono-ADP-ribosyltransferase and repressor of aryl hydrocarbon receptor transactivation. *Nucleic Acids Res*, 41, 1604-21.
- Magiatis, P., Pappas, P., Gaitanis, G., Mexia, N., Melliou, E., Galanou, M., Vlachos, C., Stathopoulou, K., Skaltsounis, A.L., Marselos, M., Velegriaki, A., Denison, M.S., Bassukas, I.D. (2013). *Malassezia* yeasts produce a collection of exceptionally potent activators of the Ah (dioxin) receptor detected in diseased human skin. *J Invest Dermatol*, 133, 2023-30.
- Malorni, L., Cozzolino, R., Boscaino, F., Castaldo, D., Malorni, A. (2012). Biological and Toxicological responses to dioxins exposures. 2012, 20-30.
- Mars, R.A.T., Yang, Y., Ward, T., Houtti, M., Priya, S., Lekatz, H.R., Tang, X., Sun, Z., Kalari, K.R., Korem, T., Bhattarai, Y., Zheng, T., Bar, N., Frost, G., Johnson, A.J., van Treuren, W., Han, S., Ordog, T., Grover, M., Sonnenburg, J., D'Amato, M., Camilleri, M., Elinav, E., Segal, E., Blekhman, R., Farrugia, G., Swann, J.R., Knights, D., Kashyap, P.C. (2020). Longitudinal Multi-omics Reveals Subset-Specific Mechanisms Underlying Irritable Bowel Syndrome. *Cell*, 182, 1460-1473 e17.
- Mascher, H., Kikuta, C., Schiel, H. (2001). Pharmacokinetics of menthol and carvone after administration of an enteric coated formulation containing peppermint oil and caraway oil. *Arzneimittelforschung*, 51, 465-9.
- Matsuoka-Kawano, K., Yoshinari, K., Nagayama, S., Yamazoe, Y. (2010). TSU-16, (Z)-3-[(2,4-dimethylpyrrol-5-yl)methylidene]-2-indolinone, is a potent activator of aryl hydrocarbon receptor and increases CYP1A1 and CYP1A2 expression in human hepatocytes. *Chem Biol Interact*, 185, 33-41.

- Matthews, J. (2012). Alternative Negative Feedback Control in the Aryl Hydrocarbon Receptor Signaling Pathway. *Journal of Drug Metabolism & Toxicology*, 04.
- Matthews, J., Gustafsson, J.A. (2006). Estrogen receptor and aryl hydrocarbon receptor signaling pathways. *Nucl Recept Signal*, 4, e016.
- Mayati, A., Le Ferrec, E., Lagadic-Gossmann, D., Fardel, O. (2012). Aryl hydrocarbon receptor-independent up-regulation of intracellular calcium concentration by environmental polycyclic aromatic hydrocarbons in human endothelial HMEC-1 cells. *Environ Toxicol*, 27, 556-62.
- McDougal, A., Sethi Gupta, M., Ramamoorthy, K., Sun, G., Safe, S.H. (2000). Inhibition of carcinogen-induced rat mammary tumor growth and other estrogen-dependent responses by symmetrical dihalo-substituted analogs of diindolylmethane. *Cancer Lett*, 151, 169-79.
- Meijer, F.A., Leijten-van de Gevel, I.A., de Vries, R., Brunsveld, L. (2019). Allosteric small molecule modulators of nuclear receptors. *Mol Cell Endocrinol*, 485, 20-34.
- Merchant, M., Morrison, V., Santostefano, M., Safe, S. (1992). Mechanism of action of aryl hydrocarbon receptor antagonists: inhibition of 2,3,7,8-tetrachlorodibenzo-p-dioxin-induced CYP1A1 gene expression. *Arch Biochem Biophys*, 298, 389-94.
- Mexia, N., Gaitanis, G., Velegaki, A., Soshilov, A., Denison, M.S., Magiatis, P. (2015). Pityriazepin and other potent AhR ligands isolated from *Malassezia furfur* yeast. *Arch Biochem Biophys*, 571, 16-20.
- Mexia, N., Koutrakis, S., He, G., Skaltsounis, A.L., Denison, M.S., Magiatis, P. (2019). A Biomimetic, One-Step Transformation of Simple Indolic Compounds to *Malassezia*-Related Alkaloids with High AhR Potency and Efficacy. *Chem Res Toxicol*, 32, 2238-2249.
- Miao, W., Hu, L., Scrivens, P.J., Batist, G. (2005). Transcriptional regulation of NF-E2 p45-related factor (NRF2) expression by the aryl hydrocarbon receptor-xenobiotic response element signaling pathway: direct cross-talk between phase I and II drug-metabolizing enzymes. *J Biol Chem*, 280, 20340-8.
- Micka, J., Milatovich, A., Menon, A., Grabowski, G.A., Puga, A., Nebert, D.W. (1997). Human Ah receptor (AHR) gene: localization to 7p15 and suggestive correlation of polymorphism with CYP1A1 inducibility. *Pharmacogenetics*, 7, 95-101.
- Michaudel, C., Danne, C., Agus, A., Magniez, A., Aucouturier, A., Spatz, M., Lefevre, A., Kirchgessner, J., Rolhion, N., Wang, Y., Lavelle, A., Galbert, C., Da Costa, G., Poirier, M., Lapiere, A., Planchais, J., Nadvornik, P., Illes, P., Oeuvray, C., Creusot, L., Michel, M.L., Benech, N., Bourrier, A., Nion-Larmurier, I., Landman, C., Richard, M.L., Emond, P., Seksik, P., Beaugerie, L., Arguello, R.R., Moulin, D., Mani, S., Dvorak, Z., Bermudez-Humaran, L.G., Langella, P., Sokol, H. (2022). Rewiring the altered tryptophan metabolism as a novel therapeutic strategy in inflammatory bowel diseases. *Gut*.
- Morcia, C., Tumino, G., Ghizzoni, R., Terzi, V. (2016). Chapter 35 - Carvone (*Mentha spicata* L.) Oils, in: Preedy, V.R. (Ed.), *Essential Oils in Food Preservation, Flavor and Safety*. Academic Press, San Diego, pp. 309-316.
- Moura-Alves, P., Fae, K., Houthuys, E., Dorhoi, A., Kreuchwig, A., Furkert, J., Barison, N., Diehl, A., Munder, A., Constant, P., Skrahina, T., Gühlich-Bornhof, U., Klemm, M., Koehler, A.B., Bandermann, S., Goosmann, C., Mollenkopf, H.J., Hurwitz, R., Brinkmann, V., Fillatreau, S., Daffe, M., Tummler, B., Kolbe, M., Oschkinat, H., Krause, G., Kaufmann, S.H. (2014). AhR sensing of bacterial pigments regulates antibacterial defence. *Nature*, 512, 387-92.
- Murray, I.A., Flaveny, C.A., DiNatale, B.C., Chairó, C.R., Schroeder, J.C., Kusnadi, A., Perdew, G.H. (2010). Antagonism of aryl hydrocarbon receptor signaling by 6,2',4'-trimethoxyflavone. *J Pharmacol Exp Ther*, 332, 135-44.
- Murray, I.A., Patterson, A.D., Perdew, G.H. (2014). Aryl hydrocarbon receptor ligands in cancer: friend and foe. *Nat Rev Cancer*, 14, 801-14.
- Naderi-Kalali, B., Allameh, A., Rasaei, M.J., Bach, H.J., Behechti, A., Doods, K., Kettrup, A., Schramm, K.W. (2005). Suppressive effects of caraway (*Carum carvi*)

- extracts on 2, 3, 7, 8-tetrachloro-dibenzo-p-dioxin-dependent gene expression of cytochrome P450 1A1 in the rat H4IIE cells. *Toxicol In Vitro*, 19, 373-7.
- Neale, P.A., Leusch, F.D. (2015). Considerations when assessing antagonism in vitro: Why standardizing the agonist concentration matters. *Chemosphere*, 135, 20-3.
- Nebert, D.W., Goujon, F.M., Gielen, J.E. (1972). Aryl hydrocarbon hydroxylase induction by polycyclic hydrocarbons: simple autosomal dominant trait in the mouse. *Nat New Biol*, 236, 107-10.
- Nguyen, L.P., Bradfield, C.A. (2008). The search for endogenous activators of the aryl hydrocarbon receptor. *Chem Res Toxicol*, 21, 102-16.
- Nguyen, N., Hanieh, H., Nakahama, T., Kishimoto, T. (2013). The roles of aryl hydrocarbon receptor in immune responses. *International immunology*, 25.
- Nie, M., Blankenship, A.L., Giesy, J.P. (2001). Interactions between aryl hydrocarbon receptor (AhR) and hypoxia signaling pathways. *Environ Toxicol Pharmacol*, 10, 17-27.
- Nieves, K.M., Hirota, S.A., Flannigan, K.L. (2022). Xenobiotic receptors and the regulation of intestinal homeostasis: harnessing the chemical output of the intestinal microbiota. *Am J Physiol Gastrointest Liver Physiol*, 322, G268-G281.
- Nishiumi, S., Yamamoto, N., Kodoi, R., Fukuda, I., Yoshida, K., Ashida, H. (2008). Antagonistic and agonistic effects of indigoids on the transformation of an aryl hydrocarbon receptor. *Arch Biochem Biophys*, 470, 187-99.
- Novotna, A., Pavek, P., Dvorak, Z. (2011). Novel stably transfected gene reporter human hepatoma cell line for assessment of aryl hydrocarbon receptor transcriptional activity: construction and characterization. *Environ Sci Technol*, 45, 10133-9.
- Novotna, A., Srovnalova, A., Svecarova, M., Korhonova, M., Bartonkova, I., Dvorak, Z. (2014). Differential effects of omeprazole and lansoprazole enantiomers on aryl hydrocarbon receptor in human hepatocytes and cell lines. *PLoS One*, 9, e98711.
- Nussinov, R., Tsai, C.J. (2013). Allostery in disease and in drug discovery. *Cell*, 153, 293-305.
- O'Donnell, E.F., Jang, H.S., Pearce, M., Kerkvliet, N.I., Kolluri, S.K. (2017). The aryl hydrocarbon receptor is required for induction of p21cip1/waf1 expression and growth inhibition by SU5416 in hepatoma cells. *Oncotarget*, 8, 25211-25225.
- Ogiso, H., Kagi, N., Matsumoto, E., Nishimoto, M., Arai, R., Shirouzu, M., Mimura, J., Fujii-Kuriyama, Y., Yokoyama, S. (2004). Phosphorylation analysis of 90 kDa heat shock protein within the cytosolic arylhydrocarbon receptor complex. *Biochemistry*, 43, 15510-9.
- Ohtake, F., Baba, A., Takada, I., Okada, M., Iwasaki, K., Miki, H., Takahashi, S., Kouzmenko, A., Nohara, K., Chiba, T., Fujii-Kuriyama, Y., Kato, S. (2007). Dioxin receptor is a ligand-dependent E3 ubiquitin ligase. *Nature*, 446, 562-6.
- Ohtake, F., Fujii-Kuriyama, Y., Kato, S. (2009). AhR acts as an E3 ubiquitin ligase to modulate steroid receptor functions. *Biochem Pharmacol*, 77, 474-84.
- Paller, A.S., Stein Gold, L., Soung, J., Tallman, A.M., Rubenstein, D.S., Gooderham, M. (2021). Efficacy and patient-reported outcomes from a phase 2b, randomized clinical trial of tapinarof cream for the treatment of adolescents and adults with atopic dermatitis. *J Am Acad Dermatol*, 84, 632-638.
- Pandey, K.B., Rizvi, S.I. (2009). Plant polyphenols as dietary antioxidants in human health and disease. *Oxid Med Cell Longev*, 2, 270-8.
- Paris, A., Tardif, N., Galibert, M.D., Corre, S. (2021). AhR and Cancer: From Gene Profiling to Targeted Therapy. *Int J Mol Sci*, 22.
- Park, H., Jin, U.H., Orr, A.A., Echegaray, S.P., Davidson, L.A., Allred, C.D., Chapkin, R.S., Jayaraman, A., Lee, K., Tamamis, P., Safe, S. (2019). Isoflavones as Ah Receptor Agonists in Colon-Derived Cell Lines: Structure-Activity Relationships. *Chem Res Toxicol*, 32, 2353-2364.
- Parks, A.J., Pollastri, M.P., Hahn, M.E., Stanford, E.A., Novikov, O., Franks, D.G., Haigh, S.E., Narasimhan, S., Ashton, T.D., Hopper, T.G., Kozakov, D., Beglov, D., Vajda, S., Schlezinger, J.J., Sherr, D.H. (2014). In silico identification of an aryl



- hydrocarbon receptor antagonist with biological activity in vitro and in vivo. *Mol Pharmacol*, 86, 593-608.
- Patterson, A.D., Gonzalez, F.J., Idle, J.R. (2010). Xenobiotic metabolism: a view through the metabolometer. *Chem Res Toxicol*, 23, 851-60.
- Percie du Sert, N., Hurst, V., Ahluwalia, A., Alam, S., Avey, M.T., Baker, M., Browne, W.J., Clark, A., Cuthill, I.C., Dirnagl, U., Emerson, M., Garner, P., Holgate, S.T., Howells, D.W., Karp, N.A., Lazic, S.E., Lidster, K., MacCallum, C.J., Macleod, M., Pearl, E.J., Petersen, O.H., Rawle, F., Reynolds, P., Rooney, K., Sena, E.S., Silberberg, S.D., Steckler, T., Wurbel, H. (2020). The ARRIVE guidelines 2.0: Updated guidelines for reporting animal research. *PLoS Biol*, 18, e3000410.
- Peter Guengerich, F., Martin, M.V., McCormick, W.A., Nguyen, L.P., Glover, E., Bradfield, C.A. (2004). Aryl hydrocarbon receptor response to indigoids in vitro and in vivo. *Arch Biochem Biophys*, 423, 309-16.
- Petrovska, B., Jerabkova, H., Chamrad, I., Vrana, J., Lenobel, R., Urinovska, J., Sebela, M., Dolezel, J. (2014). Proteomic analysis of barley cell nuclei purified by flow sorting. *Cytogenet Genome Res*, 143, 78-86.
- Petrulis, J.R., Perdew, G.H. (2002). The role of chaperone proteins in the aryl hydrocarbon receptor core complex. *Chem Biol Interact*, 141, 25-40.
- Plevry, B.J. (2004). Receptors, agonists and antagonists. *Anaesthesia & Intensive Care Medicine*, 5, 350-352.
- Poland, A., Clover, E., Kende, A.S., DeCamp, M., Giandomenico, C.M. (1976). 3,4,3',4'-Tetrachloro azoxybenzene and azobenzene: potent inducers of aryl hydrocarbon hydroxylase. *Science*, 194, 627-30.
- Puga, A., Ma, C., Marlowe, J.L. (2009). The aryl hydrocarbon receptor cross-talks with multiple signal transduction pathways. *Biochem Pharmacol*, 77, 713-22.
- Puga, A., Nebert, D.W., Carrier, F. (1992). Dioxin induces expression of c-fos and c-jun proto-oncogenes and a large increase in transcription factor AP-1. *DNA Cell Biol*, 11, 269-81.
- Puga, A., Xia, Y., Elferink, C. (2002). Role of the aryl hydrocarbon receptor in cell cycle regulation. *Chem Biol Interact*, 141, 117-30.
- Puyskens, A., Stinn, A., van der Vaart, M., Kreuchwig, A., Protze, J., Pei, G., Klemm, M., Gühlich-Bornhof, U., Hurwitz, R., Krishnamoorthy, G., Schaaf, M., Krause, G., Meijer, A.H., Kaufmann, S.H.E., Moura-Alves, P. (2020). Aryl Hydrocarbon Receptor Modulation by Tuberculosis Drugs Impairs Host Defense and Treatment Outcomes. *Cell Host Microbe*, 27, 238-248 e7.
- Quadri, S.A., Qadri, A.N., Hahn, M.E., Mann, K.K., Sherr, D.H. (2000). The bioflavonoid galangin blocks aryl hydrocarbon receptor activation and polycyclic aromatic hydrocarbon-induced pre-B cell apoptosis. *Mol Pharmacol*, 58, 515-25.
- Quintana, F.J., Sherr, D.H. (2013). Aryl hydrocarbon receptor control of adaptive immunity. *Pharmacol Rev*, 65, 1148-61.
- Rang, H.P. (2001). *Pharmacology*, 4th ed. Churchill Livingstone, New York.
- Rankin, E.B., Giaccia, A.J. (2008). The role of hypoxia-inducible factors in tumorigenesis. *Cell Death Differ*, 15, 678-85.
- Rannug, A. (2020). How the AHR Became Important in Intestinal Homeostasis-A Diurnal FICZ/AHR/CYP1A1 Feedback Controls Both Immunity and Immunopathology. *Int J Mol Sci*, 21.
- Rasmussen, M.K., Balaguer, P., Ekstrand, B., Daujat-Chavanieu, M., Gerbal-Chaloin, S. (2016). Skatole (3-Methylindole) Is a Partial Aryl Hydrocarbon Receptor Agonist and Induces CYP1A1/2 and CYP1B1 Expression in Primary Human Hepatocytes. *PLoS One*, 11, e0154629.
- Reiners, J.J., Jr., Lee, J.Y., Clift, R.E., Dudley, D.T., Myrand, S.P. (1998). PD98059 is an equipotent antagonist of the aryl hydrocarbon receptor and inhibitor of mitogen-activated protein kinase kinase. *Mol Pharmacol*, 53, 438-45.
- Ricci, C.G., Silveira, R.L., Rivalta, I., Batista, V.S., Skaf, M.S. (2016). Allosteric Pathways in the PPAR $\gamma$ -RXR $\alpha$  nuclear receptor complex. *Scientific Reports*, 6, 19940.

- Riddell, N., Jin, U.-H., Safe, S., Cheng, Y., Chittim, B., Konstantinov, A., Parette, R., Pena-Abaurrea, M., Reiner, E.J., Poirier, D., Stefanac, T., McAlees, A.J., McCrindle, R. (2015). Characterization and Biological Potency of Mono- to Tetra-Halogenated Carbazoles. *Environmental Science & Technology*, 49, 10658-10666.
- Romagnolo, D.F., Papoutsis, A.J., Laukaitis, C., Selmin, O.I. (2015). Constitutive expression of AhR and BRCA-1 promoter CpG hypermethylation as biomarkers of ERalpha-negative breast tumorigenesis. *BMC Cancer*, 15, 1026.
- Roman, A.C., Carvajal-Gonzalez, J.M., Rico-Leo, E.M., Fernandez-Salguero, P.M. (2009). Dioxin receptor deficiency impairs angiogenesis by a mechanism involving VEGF-A depletion in the endothelium and transforming growth factor-beta overexpression in the stroma. *J Biol Chem*, 284, 25135-48.
- Ronnekleiv-Kelly, S.M., Nukaya, M., Diaz-Diaz, C.J., Megna, B.W., Carney, P.R., Geiger, P.G., Kennedy, G.D. (2016). Aryl hydrocarbon receptor-dependent apoptotic cell death induced by the flavonoid chrysin in human colorectal cancer cells. *Cancer Lett*, 370, 91-9.
- Rothhammer, V., Quintana, F.J. (2019). The aryl hydrocarbon receptor: an environmental sensor integrating immune responses in health and disease. *Nat Rev Immunol*, 19, 184-197.
- Safe, S. (1993). Toxicology, structure-function relationship, and human and environmental health impacts of polychlorinated biphenyls: progress and problems. *Environ Health Perspect*, 100, 259-68.
- Safe, S., Cheng, Y., Jin, U.H. (2017). The Aryl Hydrocarbon Receptor (AhR) as a Drug Target for Cancer Chemotherapy. *Curr Opin Toxicol*, 2, 24-29.
- Seifert, A., Taubert, H., Hombach-Klonisch, S., Fischer, B., Navarrete Santos, A. (2009). TCDD mediates inhibition of p53 and activation of ERalpha signaling in MCF-7 cells at moderate hypoxic conditions. *Int J Oncol*, 35, 417-24.
- Sekimoto, M., Sumi, H., Hosaka, T., Umemura, T., Nishikawa, A., Degawa, M. (2016). Aryl hydrocarbon receptor activation and CYP1A induction by cooked food-derived carcinogenic heterocyclic amines in human HepG2 cell lines. *Food Chem Toxicol*, 97, 256-264.
- Seok, S.H., Lee, W., Jiang, L., Molugu, K., Zheng, A., Li, Y., Park, S., Bradfield, C.A., Xing, Y. (2017). Structural hierarchy controlling dimerization and target DNA recognition in the AHR transcriptional complex. *Proc Natl Acad Sci U S A*, 114, 5431-5436.
- Seok, S.H., Ma, Z.X., Feltenberger, J.B., Chen, H., Chen, H., Scarlett, C., Lin, Z., Satyshur, K.A., Cortopassi, M., Jefcoate, C.R., Ge, Y., Tang, W., Bradfield, C.A., Xing, Y. (2018). Trace derivatives of kynurenine potently activate the aryl hydrocarbon receptor (AHR). *J Biol Chem*, 293, 1994-2005.
- Sheehan, J.M., Young, A.R. (2002). The sunburn cell revisited: an update on mechanistic aspects. *Photochem Photobiol Sci*, 1, 365-77.
- Shevchenko, A., Tomas, H., Havlis, J., Olsen, J.V., Mann, M. (2006). In-gel digestion for mass spectrometric characterization of proteins and proteomes. *Nat Protoc*, 1, 2856-60.
- Shimada, T. (2006). Xenobiotic-metabolizing enzymes involved in activation and detoxification of carcinogenic polycyclic aromatic hydrocarbons. *Drug Metab Pharmacokinet*, 21, 257-76.
- Shin, S., Wakabayashi, N., Misra, V., Biswal, S., Lee, G.H., Agoston, E.S., Yamamoto, M., Kensler, T.W. (2007). NRF2 modulates aryl hydrocarbon receptor signaling: influence on adipogenesis. *Mol Cell Biol*, 27, 7188-97.
- Shin, S.M., Cho, I.J., Kim, S.G. (2005). CCAAT/enhancer binding protein activation by PD98059 contributes to the inhibition of AhR-mediated 3-methylcholanthrene induction of CYP1A1. *Xenobiotica*, 35, 975-87.
- Schallreuter, K.U., Salem, M.A., Gibbons, N.C., Maitland, D.J., Marsch, E., Elwary, S.M., Healey, A.R. (2012). Blunted epidermal L-tryptophan metabolism in vitiligo

- affects immune response and ROS scavenging by Fenton chemistry, part 2: Epidermal H<sub>2</sub>O<sub>2</sub>/ONOO(-)-mediated stress in vitiligo hampers indoleamine 2,3-dioxygenase and aryl hydrocarbon receptor-mediated immune response signaling. *FASEB J*, 26, 2471-85.
- Scheuermann, T.H., Li, Q., Ma, H.W., Key, J., Zhang, L., Chen, R., Garcia, J.A., Naidoo, J., Longgood, J., Frantz, D.E., Tambar, U.K., Gardner, K.H., Bruick, R.K. (2013). Allosteric inhibition of hypoxia inducible factor-2 with small molecules. *Nat Chem Biol*, 9, 271-6.
- Schiering, C., Wincent, E., Metidji, A., Iseppon, A., Li, Y., Potocnik, A.J., Omenetti, S., Henderson, C.J., Wolf, C.R., Nebert, D.W., Stockinger, B. (2017). Feedback control of AHR signalling regulates intestinal immunity. *Nature*, 542, 242-245.
- Schulte, K.W., Green, E., Wilz, A., Platten, M., Daumke, O. (2017). Structural Basis for Aryl Hydrocarbon Receptor-Mediated Gene Activation. *Structure*, 25, 1025-1033 e3.
- Sinal, C.J., Webb, C.D., Bend, J.R. (1999). Differential in vivo effects of alpha-naphthoflavone and beta-naphthoflavone on CYP1A1 and CYP2E1 in rat liver, lung, heart, and kidney. *J Biochem Mol Toxicol*, 13, 29-40.
- Singh, K.P., Garrett, R.W., Casado, F.L., Gasiewicz, T.A. (2011). Aryl hydrocarbon receptor-null allele mice have hematopoietic stem/progenitor cells with abnormal characteristics and functions. *Stem Cells Dev*, 20, 769-84.
- Singh, N.P., Singh, U.P., Singh, B., Price, R.L., Nagarkatti, M., Nagarkatti, P.S. (2011). Activation of aryl hydrocarbon receptor (AhR) leads to reciprocal epigenetic regulation of FoxP3 and IL-17 expression and amelioration of experimental colitis. *PLoS One*, 6, e23522.
- Smelcerovic, A., Lazarevic, J., Tomovic, K., Anastasijevic, M., Jukic, M., Kocic, G., Anderluh, M. (2019). An Overview, Advantages and Therapeutic Potential of Nonpeptide Positive Allosteric Modulators of Glucagon-Like Peptide-1 Receptor. *ChemMedChem*, 14, 514-521.
- Smirnova, A., Wincent, E., Vikstrom Bergander, L., Alsberg, T., Bergman, J., Rannug, A., Rannug, U. (2016). Evidence for New Light-Independent Pathways for Generation of the Endogenous Aryl Hydrocarbon Receptor Agonist FICZ. *Chem Res Toxicol*, 29, 75-86.
- Smith, K.J., Boyer, J.A., Muku, G.E., Murray, I.A., Gowda, K., Desai, D., Amin, S.G., Glick, A.B., Perdew, G.H. (2017). Editor's Highlight: Ah Receptor Activation Potentiates Neutrophil Chemoattractant (C-X-C Motif) Ligand 5 Expression in Keratinocytes and Skin. *Toxicol Sci*, 160, 83-94.
- Smith, K.J., Murray, I.A., Tanos, R., Tellew, J., Boitano, A.E., Bisson, W.H., Kolluri, S.K., Cooke, M.P., Perdew, G.H. (2011). Identification of a high-affinity ligand that exhibits complete aryl hydrocarbon receptor antagonism. *J Pharmacol Exp Ther*, 338, 318-27.
- Song, J., Clagett-Dame, M., Peterson, R.E., Hahn, M.E., Westler, W.M., Sicinski, R.R., DeLuca, H.F. (2002). A ligand for the aryl hydrocarbon receptor isolated from lung. *Proc Natl Acad Sci U S A*, 99, 14694-9.
- Stein Gold, L., Bhatia, N., Tallman, A.M., Rubenstein, D.S. (2021). A phase 2b, randomized clinical trial of tapinarof cream for the treatment of plaque psoriasis: Secondary efficacy and patient-reported outcomes. *J Am Acad Dermatol*, 84, 624-631.
- Stejskalova, L., Dvorak, Z., Pavek, P. (2011). Endogenous and exogenous ligands of aryl hydrocarbon receptor: current state of art. *Curr Drug Metab*, 12, 198-212.
- Stepankova, M., Bartonkova, I., Jiskrova, E., Vrzal, R., Mani, S., Kortagere, S., Dvorak, Z. (2018). Methylindoles and Methoxyindoles are Agonists and Antagonists of Human Aryl Hydrocarbon Receptor. *Mol Pharmacol*, 93, 631-644.
- Stepankova, M., Krasulova, K., Dorcakova, A., Kurka, O., Anzenbacher, P., Dvorak, Z. (2016). Optical isomers of dihydropyridine calcium channel blockers display

- enantiospecific effects on the expression and enzyme activities of human xenobiotics-metabolizing cytochromes P450. *Toxicol Lett*, 262, 173-186.
- Stephensen, P.U., Bonnesen, C., Schaldach, C., Andersen, O., Bjeldanes, L.F., Vang, O. (2000). N-methoxyindole-3-carbinol is a more efficient inducer of cytochrome P-450 1A1 in cultured cells than indol-3-carbinol. *Nutr Cancer*, 36, 112-21.
- Stockinger, B., Shah, K., Wincent, E. (2021). AHR in the intestinal microenvironment: safeguarding barrier function. *Nat Rev Gastroenterol Hepatol*, 18, 559-570.
- Suresh, S., Chung, J.-W., Sung, J.-S., Cho, G.-T., Park, J.-H., Yoon, M., Kim, C.-K., Baek, H.-J. (2012). Analysis of genetic diversity and population structure of 135 dill (*Anethum graveolens* L.) accessions using RAPD markers. *Genetic Resources and Crop Evolution*, 60.
- Takeuchi, S., Iida, M., Yabushita, H., Matsuda, T., Kojima, H. (2008). In vitro screening for aryl hydrocarbon receptor agonistic activity in 200 pesticides using a highly sensitive reporter cell line, DR-EcoScreen cells, and in vivo mouse liver cytochrome P450-1A induction by propanil, diuron and linuron. *Chemosphere*, 74, 155-65.
- Taly, A., Henin, J., Changeux, J.P., Cecchini, M. (2014). Allosteric regulation of pentameric ligand-gated ion channels: an emerging mechanistic perspective. *Channels (Austin)*, 8, 350-60.
- Tanimoto, K., Hirota, K., Fukazawa, T., Matsuo, Y., Nomura, T., Tanuza, N., Hirohashi, N., Bono, H., Sakaguchi, T. (2021). Inhibiting SARS-CoV-2 infection in vitro by suppressing its receptor, angiotensin-converting enzyme 2, via aryl-hydrocarbon receptor signal. *Sci Rep*, 11, 16629.
- Tian, Y., Rabson, A.B., Gallo, M.A. (2002). Ah receptor and NF-kappaB interactions: mechanisms and physiological implications. *Chem Biol Interact*, 141, 97-115.
- Tigges, J., Haarmann-Stemann, T., Vogel, C.F.A., Grindel, A., Hubenthal, U., Brenden, H., Grether-Beck, S., Vielhaber, G., Johncock, W., Krutmann, J., Fritsche, E. (2014). The new aryl hydrocarbon receptor antagonist E/Z-2-benzylindene-5,6-dimethoxy-3,3-dimethylindan-1-one protects against UVB-induced signal transduction. *J Invest Dermatol*, 134, 556-559.
- Tomkiewicz, C., Herry, L., Bui, L.C., Metayer, C., Bourdeloux, M., Barouki, R., Coumoul, X. (2013). The aryl hydrocarbon receptor regulates focal adhesion sites through a non-genomic FAK/Src pathway. *Oncogene*, 32, 1811-20.
- Tongnuanchan, P., Benjakul, S. (2014). Essential oils: extraction, bioactivities, and their uses for food preservation. *J Food Sci*, 79, R1231-49.
- Twyman, R.M., Verpoorte, R., Memelink, J., Christou, P. (2003). GENETIC MODIFICATION OF SECONDARY METABOLISM | Alkaloids, in: Thomas, B. (Ed.), *Encyclopedia of Applied Plant Sciences*. Elsevier, Oxford, pp. 493-500.
- Uemura, S., Nakajima, Y., Yoshida, Y., Furuya, M., Matsutani, S., Kawate, S., Ikeda, S.I., Tsuji, N., Grave, E., Wakui, H., Itoh, H. (2020). Biochemical properties of human full-length aryl hydrocarbon receptor (AhR). *J Biochem*, 168, 285-294.
- Van den Berg, M., Birnbaum, L.S., Denison, M., De Vito, M., Farland, W., Feeley, M., Fiedler, H., Hakansson, H., Hanberg, A., Haws, L., Rose, M., Safe, S., Schrenk, D., Tohyama, C., Tritscher, A., Tuomisto, J., Tysklind, M., Walker, N., Peterson, R.E. (2006). The 2005 World Health Organization reevaluation of human and Mammalian toxic equivalency factors for dioxins and dioxin-like compounds. *Toxicol Sci*, 93, 223-41.
- Vogel, C.F., Matsumura, F. (2009). A new cross-talk between the aryl hydrocarbon receptor and RelB, a member of the NF-kappaB family. *Biochem Pharmacol*, 77, 734-45.
- Vogel, C.F., Sciallo, E., Li, W., Wong, P., Lazennec, G., Matsumura, F. (2007). RelB, a new partner of aryl hydrocarbon receptor-mediated transcription. *Mol Endocrinol*, 21, 2941-55.

- Vogel, C.F.A., Haarmann-Stemmann, T. (2017). The aryl hydrocarbon receptor repressor - More than a simple feedback inhibitor of AhR signaling: Clues for its role in inflammation and cancer. *Curr Opin Toxicol*, 2, 109-119.
- Vogel, C.F.A., Van Winkle, L.S., Esser, C., Haarmann-Stemmann, T. (2020). The aryl hydrocarbon receptor as a target of environmental stressors - Implications for pollution mediated stress and inflammatory responses. *Redox Biol*, 34, 101530.
- Vogeley, C., Rolfes, K.M., Krutmann, J., Haarmann-Stemmann, T. (2022). The Aryl Hydrocarbon Receptor in the Pathogenesis of Environmentally-Induced Squamous Cell Carcinomas of the Skin. *Front Oncol*, 12, 841721.
- Vorriink, S.U., Domann, F.E. (2014). Regulatory crosstalk and interference between the xenobiotic and hypoxia sensing pathways at the AhR-ARNT-HIF1 $\alpha$  signaling node. *Chem Biol Interact*, 218, 82-8.
- Vrzal, R., Zdarilova, A., Ulrichova, J., Blaha, L., Giesy, J.P., Dvorak, Z. (2005). Activation of the aryl hydrocarbon receptor by berberine in HepG2 and H4IIE cells: Biphasic effect on CYP1A1. *Biochem Pharmacol*, 70, 925-36.
- Vrzal, R., Zenata, O., Dorcakova, A., Dvorak, Z. (2015). Environmental pollutants parathion, paraquat and bisphenol A show distinct effects towards nuclear receptors-mediated induction of xenobiotics-metabolizing cytochromes P450 in human hepatocytes. *Toxicol Lett*, 238, 43-53.
- Vrzalova, A., Pecinkova, P., Illes, P., Gurska, S., Dzubak, P., Szotkowski, M., Hajduch, M., Mani, S., Dvorak, Z. (2022). Mixture Effects of Tryptophan Intestinal Microbial Metabolites on Aryl Hydrocarbon Receptor Activity. *Int J Mol Sci*, 23.
- Vyhlidalova, B., Krasulova, K., Pecinkova, P., Marcalikova, A., Vrzal, R., Zemankova, L., Vanco, J., Travniczek, Z., Vondracek, J., Karasova, M., Mani, S., Dvorak, Z. (2020a). Gut Microbial Catabolites of Tryptophan Are Ligands and Agonists of the Aryl Hydrocarbon Receptor: A Detailed Characterization. *Int J Mol Sci*, 21.
- Vyhlidalova, B., Krasulova, K., Pecinkova, P., Poulikova, K., Vrzal, R., Andrysik, Z., Chandran, A., Mani, S., Dvorak, Z. (2020b). Antimigraine Drug Avitriptan Is a Ligand and Agonist of Human Aryl Hydrocarbon Receptor That Induces CYP1A1 in Hepatic and Intestinal Cells. *Int J Mol Sci*, 21.
- Walisser, J.A., Bunger, M.K., Glover, E., Harstad, E.B., Bradfield, C.A. (2004). Patent ductus venosus and dioxin resistance in mice harboring a hypomorphic Arnt allele. *J Biol Chem*, 279, 16326-31.
- Wang, K., Lv, Q., Miao, Y.M., Qiao, S.M., Dai, Y., Wei, Z.F. (2018). Cardamonin, a natural flavone, alleviates inflammatory bowel disease by the inhibition of NLRP3 inflammasome activation via an AhR/Nrf2/NQO1 pathway. *Biochem Pharmacol*, 155, 494-509.
- Wang, S.H., Liang, C.T., Liu, Y.W., Huang, M.C., Huang, S.C., Hong, W.F., Su, J.G. (2009). Crosstalk between activated forms of the aryl hydrocarbon receptor and glucocorticoid receptor. *Toxicology*, 262, 87-97.
- Wang, Z., Snyder, M., Kenison, J.E., Yang, K., Lara, B., Lydell, E., Bennani, K., Novikov, O., Federico, A., Monti, S., Sherr, D.H. (2020). How the AHR Became Important in Cancer: The Role of Chronically Active AHR in Cancer Aggression. *Int J Mol Sci*, 22.
- Watson, L.C., Kuchenbecker, K.M., Schiller, B.J., Gross, J.D., Pufall, M.A., Yamamoto, K.R. (2013). The glucocorticoid receptor dimer interface allosterically transmits sequence-specific DNA signals. *Nat Struct Mol Biol*, 20, 876-83.
- Wei, Y.D., Helleberg, H., Rannug, U., Rannug, A. (1998). Rapid and transient induction of CYP1A1 gene expression in human cells by the tryptophan photoproduct 6-formylindolo[3,2-b]carbazole. *Chem Biol Interact*, 110, 39-55.
- Weiss, C., Kolluri, S.K., Kiefer, F., Gottlicher, M. (1996). Complementation of Ah receptor deficiency in hepatoma cells: negative feedback regulation and cell cycle control by the Ah receptor. *Exp Cell Res*, 226, 154-63.

- Wen, Z., Zhang, Y., Zhang, B., Hang, Y., Xu, L., Chen, Y., Xie, Q., Zhao, Q., Zhang, L., Li, G., Zhao, B., Sun, F., Zhai, Y., Zhu, Y. (2023). Cryo-EM structure of the cytosolic AhR complex. *Structure*, 31, 295-308 e4.
- Wille, G., Mayser, P., Thoma, W., Monsees, T., Baumgart, A., Schmitz, H.J., Schrenk, D., Polborn, K., Steglich, W. (2001). Malassezin--A novel agonist of the arylhydrocarbon receptor from the yeast *Malassezia furfur*. *Bioorg Med Chem*, 9, 955-60.
- Wilson, S.R., Joshi, A.D., Elferink, C.J. (2013). The tumor suppressor Kruppel-like factor 6 is a novel aryl hydrocarbon receptor DNA binding partner. *J Pharmacol Exp Ther*, 345, 419-29.
- Wincent, E., Amini, N., Luecke, S., Glatt, H., Bergman, J., Crescenzi, C., Rannug, A., Rannug, U. (2009a). The suggested physiologic aryl hydrocarbon receptor activator and cytochrome P4501 substrate 6-formylindolo[3,2-b]carbazole is present in humans. *J Biol Chem*, 284, 2690-2696.
- Wincent, E., Bengtsson, J., Mohammadi Bardbori, A., Alsberg, T., Luecke, S., Rannug, U., Rannug, A. (2012). Inhibition of cytochrome P4501-dependent clearance of the endogenous agonist FICZ as a mechanism for activation of the aryl hydrocarbon receptor. *Proc Natl Acad Sci U S A*, 109, 4479-84.
- Wincent, E., Shirani, H., Bergman, J., Rannug, U., Janosik, T. (2009b). Synthesis and biological evaluation of fused thio- and selenopyrans as new indolocarbazole analogues with aryl hydrocarbon receptor affinity. *Bioorg Med Chem*, 17, 1648-53.
- Winston-McPherson, G.N., Shu, D., Tang, W. (2014). Synthesis and biological evaluation of 2,3'-diindolylmethanes as agonists of aryl hydrocarbon receptor. *Bioorg Med Chem Lett*, 24, 4023-5.
- Wormke, M., Stoner, M., Saville, B., Walker, K., Abdelrahim, M., Burghardt, R., Safe, S. (2003). The aryl hydrocarbon receptor mediates degradation of estrogen receptor alpha through activation of proteasomes. *Mol Cell Biol*, 23, 1843-55.
- Wright, E.J., De Castro, K.P., Joshi, A.D., Elferink, C.J. (2017). Canonical and non-canonical aryl hydrocarbon receptor signaling pathways. *Curr Opin Toxicol*, 2, 87-92.
- Wu, D., Potluri, N., Kim, Y., Rastinejad, F. (2013). Structure and dimerization properties of the aryl hydrocarbon receptor PAS-A domain. *Mol Cell Biol*, 33, 4346-56.
- Wu, D., Su, X., Potluri, N., Kim, Y., Rastinejad, F. (2016). NPAS1-ARNT and NPAS3-ARNT crystal structures implicate the bHLH-PAS family as multi-ligand binding transcription factors. *Elife*, 5.
- Wu, H., Liu, B., Yang, K., Winston-McPherson, G.N., Leisten, E.D., Vezina, C.M., Ricke, W.A., Peterson, R.E., Tang, W. (2020). Synthesis and biological evaluation of FICZ analogues as agonists of aryl hydrocarbon receptor. *Bioorganic & Medicinal Chemistry Letters*, 30, 126959.
- Wu, Z., Uchi, H., Morino-Koga, S., Nakamura-Satomura, A., Kita, K., Shi, W., Furue, M. (2014). Z-Ligustilide inhibits benzo(a)pyrene-induced CYP1A1 upregulation in cultured human keratinocytes via ROS-dependent Nrf2 activation. *Exp Dermatol*, 23, 260-5.
- Wyatt, M., Greathouse, K.L. (2021). Targeting Dietary and Microbial Tryptophan-Indole Metabolism as Therapeutic Approaches to Colon Cancer. *Nutrients*, 13.
- Xu, B., Wang, B., Xun, W., Qiu, F.G. (2019). Total Synthesis of (-)-Daphenylline. *Angew Chem Int Ed Engl*, 58, 5754-5757.
- Yao, E.F., Denison, M.S. (1992). DNA sequence determinants for binding of transformed Ah receptor to a dioxin-responsive enhancer. *Biochemistry*, 31, 5060-7.
- Yeager, R.L., Reisman, S.A., Aleksunes, L.M., Klaassen, C.D. (2009). Introducing the "TCDD-inducible AhR-Nrf2 gene battery". *Toxicol Sci*, 111, 238-46.
- Yin, J., Sheng, B., Qiu, Y., Yang, K., Xiao, W., Yang, H. (2016). Role of AhR in positive regulation of cell proliferation and survival. *Cell Prolif*, 49, 554-60.

- Yuan, J., Adamski, R., Chen, J. (2010). Focus on histone variant H2AX: to be or not to be. *FEBS Lett*, 584, 3717-24.
- Zelante, T., Iannitti, R.G., Cunha, C., De Luca, A., Giovannini, G., Pieraccini, G., Zecchi, R., D'Angelo, C., Massi-Benedetti, C., Fallarino, F., Carvalho, A., Puccetti, P., Romani, L. (2013). Tryptophan catabolites from microbiota engage aryl hydrocarbon receptor and balance mucosal reactivity via interleukin-22. *Immunity*, 39, 372-85.
- Zhang, S., Qin, C., Safe, S.H. (2003). Flavonoids as aryl hydrocarbon receptor agonists/antagonists: effects of structure and cell context. *Environ Health Perspect*, 111, 1877-82.
- Ziello, J.E., Jovin, I.S., Huang, Y. (2007). Hypoxia-Inducible Factor (HIF)-1 regulatory pathway and its potential for therapeutic intervention in malignancy and ischemia. *Yale J Biol Med*, 80, 51-60.

# CURRICULUM VITAE

## Personal data

Name: Karolína Ondrová  
Maiden name: Poulíková  
Date of birth: 19.1.1993  
Residence: Purkyňova 1073/42, 779 00 Olomouc  
Nationality: Czech  
E-mail: ondrova.karol@gmail.com  
ORCID ID: 0000-0002-1207-6948  
Current affiliation: Department of Cell Biology and Genetics  
Faculty of Science, Palacký University Olomouc  
Šlechtitelů 27  
783 71 Olomouc  
Czech Republic  
(+420) 585 634 910

## Education

### Present study

2017-2023

Postgraduate doctoral studies

*Thesis topic:* Carvone is an atypical negative allosteric modulator of aryl hydrocarbon receptor

*Supervisor:* prof. RNDr. Zdeněk Dvořák, DrSc. et Ph.D.

### Completed studies

2015-2017

Master's program in Molecular and Cell Biology, Department of Cell Biology and Genetics, Faculty of Science, Palacký University Olomouc

*Theses topic:* The effect of selected ATR-competitive inhibitors of mTOR kinase on aryl hydrocarbon receptor (AhR)

2012 -2015

Bachelor's program in Molecular and Cell Biology, Department of Cell Biology and Genetics, Faculty of Science, Palacký University Olomouc

*Theses topic:* Interaction of mTOR signaling pathway with induced expression of biotransformation enzyme CYP1A1 in human hepatocellular carcinoma



## Teaching experience

Practical courses in Cell Biology

Practical courses in Molecular Biology

## Research internship

01/2017 – 03/2017

Internship at Leibniz-institut für umweltmedizinische forschung (IUF), Düsseldorf, Germany

01/2020

Short-term research stay at Albert Einstein College of Medicine, Department of Molecular Pharmacology, Bronx, New York City, USA

## Participation in research projects:

22-00355S – Microbial metabolite mimicry in pharmacological modulation of intestinal health (2022 – 2024)

20-00449S - Microbial catabolites of tryptophan as modulators of intestinal health via AHR (2020 - 2022)

19-00236S - The role of intestinal microbiome indole metabolites in the control of gastro-hepatic regulation of lipid and xenobiotic metabolism (2019 - 2021)

NV19-05-00220 - Activators of human aryl hydrocarbon receptor (AHR) in the therapy of inflammatory bowel disease (2019 - 2022)

Student projects IGA UP – PrF 2018-005, PrF 2019-003, PrF 2020-006, PrF 2021-005, and PrF 2022-009 of the Palacký University Olomouc

## Publications:

1. Ondrová K., Zůvalová I., Vyhlídalová B., Krasulová K., Miková E., Vrzal R., Nádvorník P., Nepal B., Kortagere S., Kopečná M., Kopečný D., Šebela M., Rastinejad F., Pu H., Sural M., Rolfes KM., Haarmann-Stemmann T., Li H., Mani S., Dvořák Z. (2023). Monoterpenoid aryl hydrocarbon receptor allosteric antagonists protect against ultraviolet skin damage in female mice. *Nat Commun* 14: 2728. **[IF<sub>2021</sub> 17.694]**.
2. Grycová, A., Joo, H., Maier, V., Illés, P., Vyhlídalová, B., **Pouliková, K.**, Sládeková, L., Nádvorník, P., Vrzal, R., Zemánková, L., Pečinková, P., Poruba, M., Zapletalová, I., Večeřa, R., Anzenbacher, P., Ehrmann, J., Ondra, P., Jung, J.-W., Mani, S. & Dvořák, Z. (2022). Targeting the aryl hydrocarbon receptor with microbial metabolite mimics alleviates experimental colitis in mice. *Journal of Medicinal Chemistry* 65(9): 6859-6868. **[IF<sub>2021</sub> 8.039]**
3. Dvorak, Z., **Poulikova, K.** & Mani, S. (2021). Indole scaffolds as a promising class of the aryl hydrocarbon receptor ligands. *Eur J Med Chem* 215: 113231 **[IF 7.088]**
4. Illes, P., Krasulova, K., Vyhlidalova, B., **Poulikova, K.**, Marcalikova, A., Pecinkova, P., Sirotova, N., Vrzal, R., Mani, S. & Dvorak, Z. (2020). Indole microbial intestinal metabolites expand the repertoire of ligands and agonists of the human pregnane X receptor. *Toxicol Lett* 334: 87-93. **[IF 4.372]**
5. Vyhlidalova, B., Krasulova, K., Pecinkova, P., **Poulikova, K.**, Vrzal, R., Andrysik, Z., Chandran, A., Mani, S. & Dvorak, Z. (2020). Antimigraine drug Avitriptan

is a ligand and agonist of human aryl hydrocarbon receptor that induces CYP1A1 in hepatic and intestinal cells. *International Journal of Molecular Sciences* 21(8):2799.

**[IF 5.923]**

6. Dvorak, Z., Kopp, F., Costello, C. M., Kemp, J. S., Li, H., Vrzalova, A., Stepankova, M., Bartonkova, I., Jiskrova, E., **Poulikova, K.**, Vyhliadalova, B., Nordstroem, L. U., Karunaratne, C. V., Ranhotra, H. S., Mun, K. S., Naren, A. P., Murray, I. A., Perdew, G. H., Brtko, J., Toporova, L., Schon, A., Wallace, W. G., Walton, W. G., Redinbo, M. R., Sun, K., Beck, A., Kortagere, S., Neary, M. C., Chandran, A., Vishveshwara, S., Cavalluzzi, M. M., Lentini, G., Cui, J. Y., Gu, H. W., March, J. C., Chatterjee, S., Matson, A., Wright, D., Flannigan, K. L., Hirota, S. A., Sartor, R. B. & Mani, S. (2020). Targeting the pregnane X receptor using microbial metabolite mimicry. *Embo Molecular Medicine* 12(4):e11621. **[IF 12.137]**
7. Vyhliadalová B., **Pouliková K.**, Bartoňková I., Krasulová K., Vančo J., Trávníček Z., Mani S. and Z. Dvořák (2019). Mono-methylindoles induce CYP1A genes and inhibit CYP1A1 enzyme activity in human hepatocytes and HepaRG cells. *Toxicology Letters* 313: 66-76. **[IF 3.569]**
8. Abbott, K. L., Chaudhury C. S., Chandran A., Vishveshwara S., Dvorak Z., Jiskrova E., **Poulikova K.**, Vyhliadalova B., Mani S. and Pondugula S. R. (2019). Belinostat, at its clinically relevant concentrations, inhibits rifampicin-induced CYP3A4 and MDR1 gene expression. *Mol Pharmacol* 95(3): 324-334. **[IF 3.664]**

#### Conference reports:

1. **Poulikova, K.**, Vyhliadalova, B., Bartonkova, I., Dvorak, Z.: Antagonists effects of carvones at human AhR [poster]. In: International Meeting on 22nd MDO and 33rd JSSX ; 2018 Oct 1-5; Kanazawa; Japan.
2. Vyhliadalova, B., **Poulikova, K.**, Bartonkova, I., Dvorak, Z.: Methylindoles activate human pregnane X receptor [poster]. International Meeting on 22nd MDO and 33rd JSSX; 2018 Oct 1-5; Kanazawa; Japan.
3. Vyhliadalova, B., Krasulova, K., **Poulikova, K.**, Bartonkova, I., Dvorak, Z.: Dual effects of methylated indoles on CYP1A1 in human hepatocytes [poster]. 12th International ISSX meeting; 2019 July 28-31; Portland; Oregon.
4. Bartonkova, I., **Poulikova, K.**, Dvorak, Z.: Thymol, carvacrol, and cuminol are ligand-specific antagonists of human aryl hydrocarbon receptor (AhR) [poster]. In: 50th International Symposium on Essential Oils; 2019 Sep 9-11; Vienna, Austria.

#### Awards:

Dean's awards to authors of prestigious scientific publications 2021 (Journal impact factor quartile Q1)

Dvořák, Z., **Pouliková, K.**, Mani, S. (2021). Indole scaffolds as a promising class of the aryl hydrocarbon receptor ligands. *Eur J Med Chem*, 215: 113231.

## APPENDIX I.

Dvořák, Z., **Pouliková, K.**, Mani, S. (2021). Indole scaffolds as a promising class of the aryl hydrocarbon receptor ligands. *Eur J Med Chem*, 215: 113231. **[IF 7.088]**.



# Indole scaffolds as a promising class of the aryl hydrocarbon receptor ligands



Zdeněk Dvořák<sup>a,\*,1</sup>, Karolína Poulíková<sup>a,1</sup>, Sridhar Mani<sup>b,\*\*</sup>

<sup>a</sup> Department of Cell Biology and Genetics, Faculty of Science, Palacký University, Šlechtitelů 27, 783 71, Olomouc, Czech Republic

<sup>b</sup> Department of Medicine and Genetics, Albert Einstein College of Medicine, Bronx, NY, USA

## ARTICLE INFO

### Article history:

Received 4 January 2021

Received in revised form

24 January 2021

Accepted 24 January 2021

Available online 4 February 2021

### Keywords:

Aryl hydrocarbon receptor

Ligands

Indoles

Rational design

## ABSTRACT

The aryl hydrocarbon receptor (AhR), deemed initially as a xenobiotic sensor, plays multiple physiological roles and is involved in various pathophysiological processes and many diseases' etiology. Therefore, the therapeutic and chemopreventive targeting of AhR is a fundamental issue. To date, thousands of structurally diverse ligands of AhR have been identified. The bottleneck in targeting the AhR is that it is a Janus-faced player with beneficial vs. harmful effects in the ligand-specific context. A distinct structural class of the AhR ligands is those with indole-based scaffolds. The present review summarizes the knowledge on the existing indole-derived AhR ligands, comprising natural and dietary compounds, synthetic compounds including clinically used drugs, endogenous intermediary metabolites, and catabolites produced by human microbiota. The examples of novel, indole ring containing, rational design based AhR ligands are presented. The molecular, *in vitro*, and *in vivo* effects are described.

© 2021 Elsevier Masson SAS. All rights reserved.

## Contents

1. Aryl hydrocarbon receptor AhR .....	1
2. Human endogenous indoles .....	2
3. Human microbiota-produced indoles .....	3
4. Xenobiotic indoles .....	3
4.1. Natural and dietary compounds .....	3
4.2. Drugs .....	3
4.3. Synthetic compounds .....	5
5. Rationally designed AhR-active indoles .....	8
6. Conclusions .....	9
Declaration of competing interest .....	9
Acknowledgements .....	9
Abbreviations .....	9
References .....	9

\* Corresponding author. Department of Cell Biology and Genetics, Faculty of Science, Palacký University Olomouc, Šlechtitelů 27; 783 71, Olomouc, Czech Republic.

\*\* Corresponding author. Department of Genetics and Department of Medicine, Albert Einstein College of Medicine, Bronx, NY 10461, USA.

E-mail addresses: [zdenek.dvorak@upol.cz](mailto:zdenek.dvorak@upol.cz) (Z. Dvořák), [sridhar.mani@einstein.yu.edu](mailto:sridhar.mani@einstein.yu.edu) (S. Mani).

<sup>1</sup> Equal contribution.

## 1. Aryl hydrocarbon receptor AhR

The aryl hydrocarbon receptor (AhR) was discovered in the early 70s' as the first xenosensor that mediated an induction of aryl hydrocarbon hydroxylase by polycyclic hydrocarbons [1] and halogenated polyaromatics [2]. The AhR belongs to the basic helix-loop-helix family of transcriptional factors. It is activated by a number of xenobiotic ligands, including environmental pollutants

(e.g., polycyclic aromatic hydrocarbons and halogenated aromatic hydrocarbons), plant polyphenolics (e.g., quercetin, genistein, curcumin), alkaloids (e.g., berberine), and many synthetic compounds such as pesticides (e.g., chlorpyrifos, carbaryl) and drugs (e.g., omeprazole, lansoprazole, primaquine) [3]. The endogenous AhR ligands are eicosanoids (e.g., leukotriene A4 metabolites, prostaglandins), indirubin and indigo, heme metabolites (bilirubin, biliverdin, hemin), tryptophan metabolites (kynurenic acid, xanthurenic acid), and 6-formylindolo[3,2-b]carbazole (FICZ), a tryptophan photoproduct generated in ultraviolet radiation-exposed skin [4]. A distinct class of the AhR ligands is produced from tryptophan by human skin and intestinal microbiota (*vide post*). Depending on their intrinsic activity, the AhR ligands are distinguished as full agonists, partial agonists, and antagonists.

In its resting state, the AhR resides in the cytoplasm in complex with several chaperone proteins such as hsp90, p23, and XAP2. Upon binding the ligand, the AhR dissociates from the multiprotein complex and undergoes translocation in the cell nucleus. In so called canonical signaling pathway, nuclear AhR forms a heterodimer with the AhR nuclear translocator (ARNT). Heterodimeric AhR/ARNT binds target DNA sequences, referred to as xenobiotic response elements (XREs), and triggers the expression of distinct class of genes, e.g. *CYP1* family. Non-canonical AhR signaling is the term referring to transcriptional functions of AhR independent of XRE. For instance, agonist-activated AhR/ARNT directly associates with estrogen receptors, which results in the recruitment of unliganded estrogen receptor and the co-activator p300 to estrogen-response elements, leading to activation of transcription and estrogenic effects [5]. Besides ARNT, other transcriptional factors including retinoblastoma protein [6], RelB subunit of NFκB [7] or Kruppel-like factor 6 [8] were identified to associate with the AhR and produce non-XRE AhR-dependent biological effects.

The AhR had been considered for a long time as a transcriptional mediator of xenoprotective and drug-metabolizing genes. Its therapeutic targeting was neglected due to the stigma of being a culprit accounting for dioxin toxicity. There is a substantial body of evidence that the AhR is a pivotal actor in various physiological processes, such as immunity [9,10], organ development [11], embryogenesis [12], hematopoiesis [13], and restorative neurogenesis [14]. On the other hand, the AhR is involved in the pathogenesis of harmful diseases, such as, but not limited to, cancer [15], intestinal inflammation [16,17], hepatic steatosis [18], and atopic dermatitis [19]. Owing to its essential roles in human physiology, pathophysiology, and disease etiology, therapeutic targeting of the AhR has emerged. For instance, off-targeting the AhR with clinically used AhR-active drugs (e.g., tranilast, flutamide, omeprazole, lansoprazole, raloxifene, flutamide, sulindac, leflunomide, nimodipine, mexeletine) was proposed as AhR-dependent chemotherapy for the treatment of breast and pancreatic cancers [20,21]. Another example is using a topical cream containing the AhR-agonist tapinarof, a bacterial stilbenoid, as an agent against atopic dermatitis [22] and plaque psoriasis [23]. Recently, antagonizing the AhR was suggested as an antiviral therapy for the Zika virus [24] and COVID-19 virus [25].

A distinct structural class of the AhR ligands is those with indole-based scaffolds. The present review summarizes the knowledge on the existing indole-derived AhR ligands, comprising natural and dietary compounds, synthetic compounds including clinically used drugs, endogenous intermediary metabolites, and catabolites produced by human microbiota. The examples of novel, indole ring containing, rational design based AhR ligands are presented, and their molecular, *in vitro*, and *in vivo* effects are described.

## 2. Human endogenous indoles

The source of endogenous AhR-active indole compounds in humans is L-tryptophan. This essential amino acid undergoes a very complex intermediary metabolism.

The serotonin pathway converts L-tryptophan into neurotransmitter serotonin (5-hydroxy-tryptamine) through consecutive 5-hydroxylation by tryptophan hydroxylases (forming 5-hydroxytryptophan), followed by decarboxylation, catalyzed by 5-hydroxytryptophan decarboxylase. This pathway is localized in intestinal epithelial enterochromaffin cells (producing 90% of serotonin), skin epidermal Merkel cells, and various brain regions. In the distinct brain areas, serotonin is further converted to N-acetylserotonin and into sleep hormone melatonin (5-methoxy-N-acetyltryptamine) is partly deacetylated in the pineal gland into 5-methoxytryptamine. The traces of tryptamine were also reported in the brain. Heath-Pagliuso et al. reported **tryptamine (I-1)** as the AhR ligand and agonist. In contrast, other serotonin pathway intermediates were inactive against the AhR [26]. A urinary metabolite of serotonin, 5-hydroxy indole acetic acid, is also the AhR inactive compound (unpublished observation from Dvorak lab).

The kynurenine pathway is localized in multiple organs. This metabolic pathway utilizes the majority of available tryptophan, which is ultimately converted into picolinic acid and nicotinamide adenine dinucleotide. The first and rate-limiting step in tryptophan conversion within the kynurenine pathway is its oxidation into kynurenine, catalyzed by indoleamine-2,3-dioxygenase and tryptophan-2,3-dioxygenase. Whereas kynurenine had a long time been deemed as a *bona fide* AhR ligand and agonist, it was recently reported that it is not kynurenine, but its trace condensation product TEACOP270 that is a highly potent agonist of the AhR ( $EC_{50} \approx 10$  pM) [27]. Notably, the indole skeleton of tryptophan is broken in this step. The whole array of resulting catabolites is not indole-based substances. Of note, two tryptophan metabolites, including kynurenic acid and xanthurenic acid, were described as the ligands and agonists of the AhR [28].

Two isomeric condensed oxindoles, **indigo (I-2)** and **indirubin (I-3)**, are highly potent endogenous activators of the AhR found in human urine [29,30]. However, the exact origin of these compounds within the human organism is not clear. They are likely produced bacterially from indoxyl-sulfate. A putative endogenous and potent indole-ligand of the AhR is **ITE (I-5)** (2-(1<sup>H</sup>-indole-3'-carbonyl)-thiazole-4-carboxylic acid methyl ester), which was isolated from porcine lungs, but not directly identified in humans, though [31]. An extremely potent endogenous agonist of the AhR is **FICZ (I-6)**, formed in the skin from tryptophan by ultraviolet irradiation. Sulfoconjugates of phenolic metabolites of FICZ were also present in human urine [32]. Interestingly, aspartate aminotransferase, an enzyme localized in several organs, including the heart, liver, skeletal muscles, kidney, and brain, was demonstrated to convert tryptophan into so called AhR pro-agonist indole-3-pyruvate [33]. Consecutive non-enzymatic oxidation and condensation of indole-3-pyruvate gave a raise two products (**1,3-di(1H-indol-3-yl)propan-2-one (I-7)** and **1-(1H-indol-3-yl)-3-(3H-indol-3-ylidene)propan-2-one (I-8)**) [34,35], which might be considered as putative endogenous AhR agonists in this context. Also, indole-3-pyruvate and other metabolites, including indole, are produced from dietary tryptophan by intestinal bacteria. Following the absorption from intestines, indole is hydroxylated and sulfated in the liver, forming **indoxyl-3-sulfate (I-4)**, a potent AhR agonist and uremic toxin [36]. Chemical structures of human endogenous AhR-active indoles are depicted in Fig. 1.

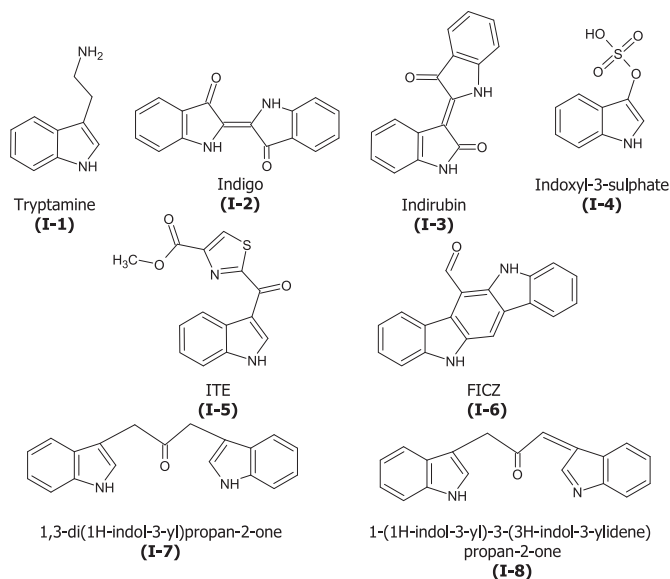


Fig. 1. Chemical structures of AhR-active human endogenous indoles

### 3. Human microbiota-produced indoles

The human microbiome produces an enormous amount of metabolites, some of which enter the systemic circulation and thereby exert systemic effects. Human microbiota-produced chemicals lay at the borderline between endogenous and xenobiotic substances. A reasonable approach to distinguishing *sensu stricto* microbiota-produced xenobiotic and endogenous compounds could be according to their origin in commensal vs. pathogenic microorganisms, respectively. The main organs where resides human microbiota, producing biologically relevant molecules, are the intestines, skin, and lungs. Intestinal microbiota produces large amounts (millimolar levels) of human selective AhR ligand **indole (II-1)** [37] through a reaction catalyzed by bacterial tryptophanase [38]. Microbial tryptophan decarboxylase forms **tryptamine (I-1)**, which is both endogenous and microbial ligand of the AhR. A series of indole-3 substituted catabolites of tryptophan are formed by intestinal and skin bacteria including **indole-3-acetate (II-2)**, **indole-3-propionate (II-3)**, **indole-3-lactate (II-4)**, **indole-3-pyruvate (II-5)**, **indole-3-acrylate (II-6)**, **indole-3-acetamide (II-7)**, **indole-3-ethanol (II-8)**, **indole-3-aldehyde (II-9)**, **indole-3-acetaldehyde (II-10)** and **3-methylindole (II-11)** (skatole) [38,39]. These metabolites displayed differential AhR activities in terms of efficacy, potency, and affinity [40]. The Perdue laboratory data recently revealed the presence of AhR agonists **2-oxindole (II-12)** and **3-methyl-2-oxindole (II-13)** in human feces [41]. Microbial production of **FICZ (I-6)** [42], **triptanthrin (II-14)** [43], **pityriazepin (II-15)** [44], and **malassezin (II-16)** (2-(1H-indol-3-ylmethyl)-1H-indole-3-carbaldehyde) [45] by opportunistic skin pathogen *Malassezia furfur* was described, implying FICZ as dual endogenous and microbial AhR ligand. Also, FICZ is produced from precursors (e.g., indole-3-pyruvate) formed by intestinal microbiota [46]. Chemical structures of AhR-active indoles produced by human microbiota are depicted in Fig. 2.

### 4. Xenobiotic indoles

#### 4.1. Natural and dietary compounds

There is an indefinite number of naturally occurring compounds

with the indole ring in their structure. Therefore, in this subchapter, only representative examples of AhR-active natural indoles are overviewed (for chemical structures ref. Fig. 3):

Cruciferous vegetables such as broccoli, cabbages, or Brussels sprouts contain glucosinolate **glucobrassicin (III-1)** and its various derivatives such as **neoglucobrassicin (III-2)**, which are dietary AhR active products [47]. In the process of digestion, glucobrassicin is converted into AhR ligand and agonist **indole-3-carbinol (III-3)**, which undergoes series of consequent condensation reactions, resulting in a production of several AhR active indole derivatives, including **3,3'-diindolylmethane (III-4)**, **indolo[3,2-b]carbazole ICZ (III-6)**, **2-(Indol-3-yl-methyl)-3,3'-diindolylmethane (III-7)** and **5,6,11,12,17,18-Hexahydrocycloona[1,2-b:4,5-b':7,8-b'']trindole (III-8)** [48,49]. Analogically, dietary neoglucobrassicin is converted into **N-methoxyindole-3-carbinol (III-5)**, which is also the agonist of the AhR [50]. **Ascorbigen (III-11)**, another indole ring-containing degradation product of glucobrassicin, was demonstrated as the AhR activator and CYP1A1 inducer in cell lines [50,51]. Cooked food-derived heterocyclic aromatic amines, including **3-amino-1,4-dimethyl-5H-pyrido[4,3-b]indole (III-9)**, **3-amino-1-methyl-5H-pyrido[4,3-b]indole (III-10)**, **2-amino-9H-pyrido[2,3-b]indole (III-12)** and **2-amino-3-methyl-9H-pyrido[2,3-b]indole (III-13)**, activated the AhR and induced AhR-regulated genes [52]. Several marine **brominated indoles** and **brominated (methylthio)indoles (III-18)**, isolated from the red alga *Laurencia brongniartii*, were identified as ligands and the agonist of the AhR, having species-selective potency [53]. Dose- and time-dependent stimulation of AhR signaling in human hepatoma cells and human keratinocytes was observed with several  $\beta$ -carboline alkaloids, including **annomontine (III-14)**, **rutaecarpine (III-15)**, and **xestomanzamine A (III-16)** [54]. Fungal alkaloid **schizocommunin (III-17)**, produced by *Schizophyllum commune*, activated the AhR and induced AhR-dependent genes in human hepatic and lung cells [55]. Interestingly, Mueller's group isolated several indole-based metabolites produced by *Myxobacterium* belonging to the *Sorangium* spp., including indothiazinone, a decarboxylated skeleton of ITE, the potent endogenous AhR agonist [56]. In parallel, Kwon et al. synthesized a series of N-alkyl, allyl, benzyl, acetyl, and benzoyl indothiazinones, employing single-step direct acetylation of indole [57]. Regrettably, neither study addressed the putative AhR effects of indothiazinones.

#### 4.2. Drugs

Many clinically used drugs contain in their chemical structure indole heterocycle. The examples comprise anti-migraine agonists of 5-HT receptor subtypes (sumatriptan, naratriptan, rizatriptan, eletriptan, frovatriptan, donitriptan, avitriptan, almotriptan, zolmitriptan), beta-blockers (pindolol, bucindolol), alpha-blockers (indoramin) anti-emetics (dolasetron, ondansetron, tropisetron), non-steroid anti-inflammatory drugs (indomethacin, pravastatin), anti-psychotics (roxindole, oxyperline), anti-virotics (umifenovir, atevirdine), anticancer drugs (panobinostat), and anti-asthma (zafirlukast). Among indole-based drugs, only a few are the AhR actives. However, possible repurposing of putative AhR active indole drugs is an underexplored area. Only a minor part of these drugs was tested for their possible AhR activity. For instance, **avitriptan (IV-1)** and **donitriptan (IV-2)** were reported as low-affinity ligands and weak agonists of the AhR, which induced AhR target genes in hepatic and intestinal cells [58]. Other existing triptans were AhR-inactive. Panobinostat enhanced AhR ligand-mediated gene induction, but the same effect was observed for vorinostat, not an indole drug. Hence, the effects of panobinostat were somewhat due to the inhibition of histone deacetylases than through indole moiety interaction with the AhR [59]. Indirect

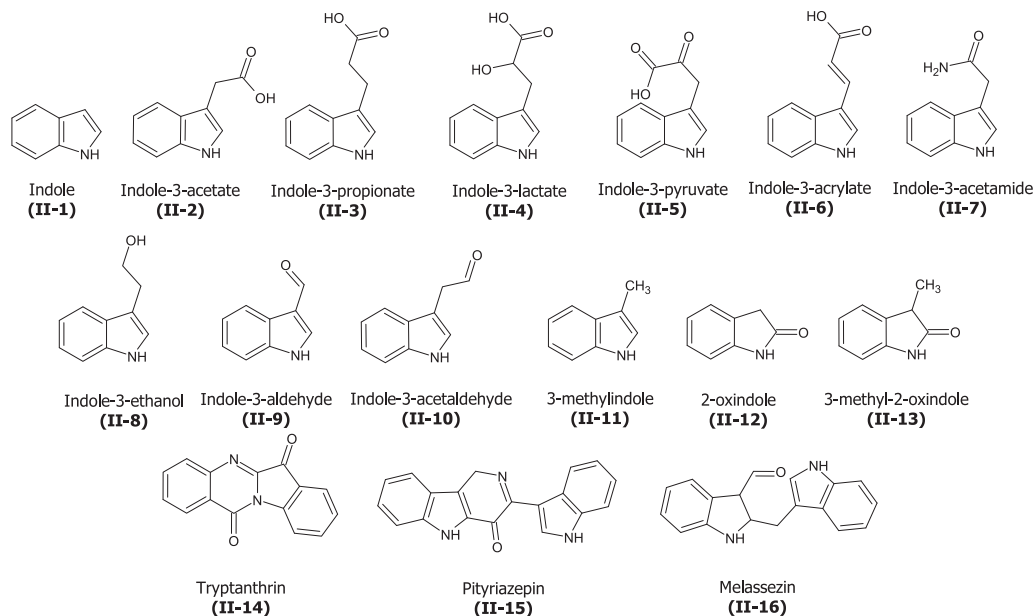


**Fig. 2.** Chemical structures of AhR-active indoles produced by human microbiota.

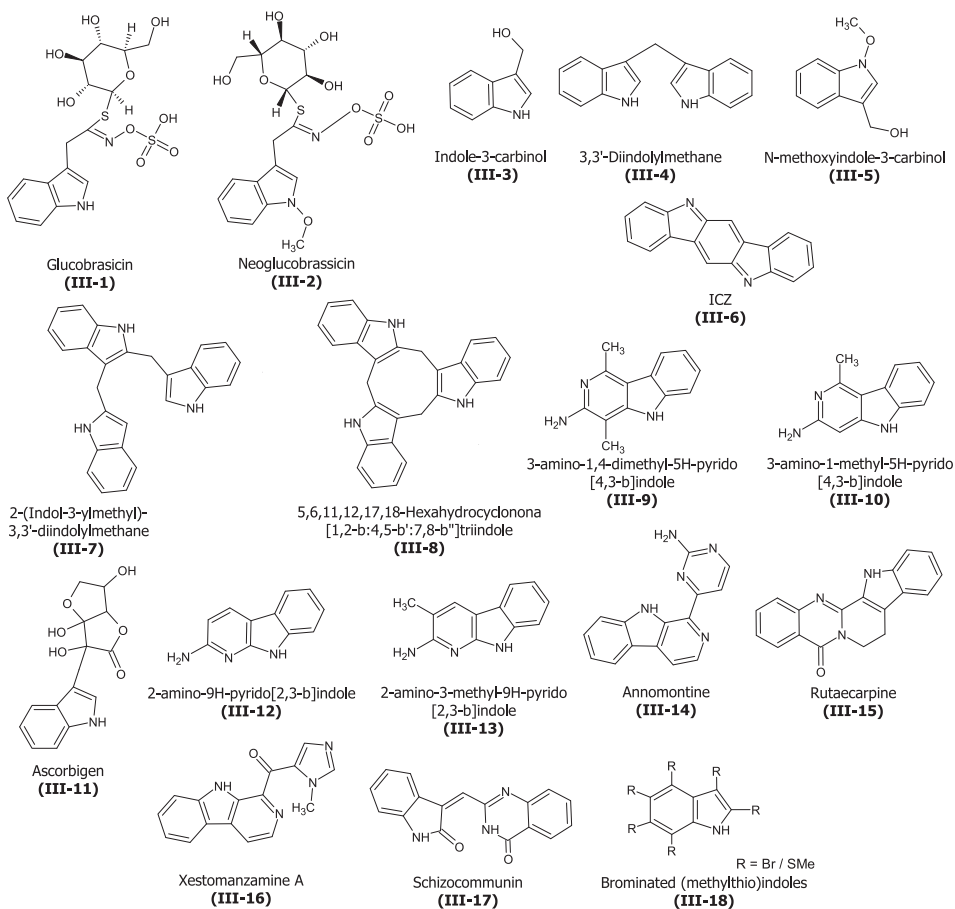


**Fig. 3.** Chemical structures of AhR-active naturally occurring and dietary indoles.



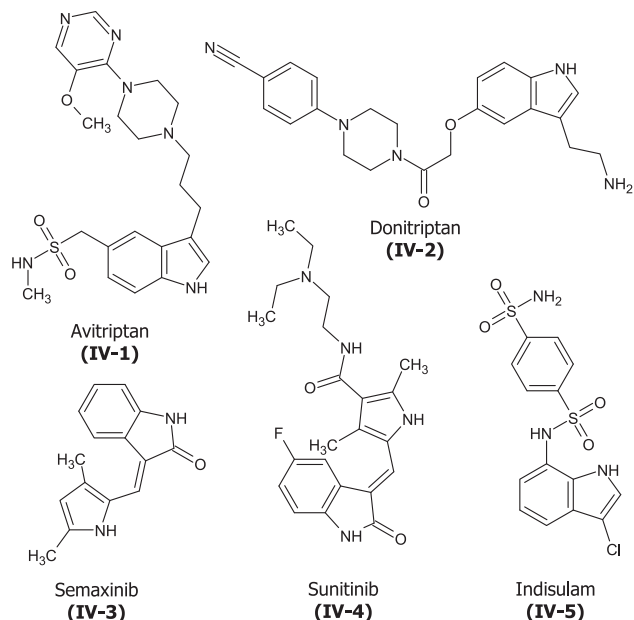


Fig. 4. Chemical structures of AhR-active drug indoles.

targeting of the AhR was proposed for aryl sulfonamides, including the indole-containing anticancer drug **indisulam (IV-5)** (E7070). These compounds induced degradation of ARNT through CRL4<sup>DCAF15</sup>E3 ligase, thereby antagonizing the AhR [60]. **Semaxinib (IV-3)** and **sunitinib (IV-4)**, two receptor tyrosine kinase inhibitors used for cancer treatment, containing 2-oxindole in their structures, were demonstrated as the AhR agonists that induce AhR-

regulated genes [61,62]. Chemical structures of AhR-active indole drugs are depicted in Fig. 4.

#### 4.3. Synthetic compounds

A series of methylated and methoxylated simple indoles displayed various AhR activities in human hepatic and intestinal cell lines, comprising full agonist, partial agonist, and antagonist effects. Intense agonist activities were observed for **4-methylindole (V-1)**, **5-methylindole (V-2)**, **6-methylindole (V-3)**, **7-methoxyindole (V-4)**, and **2,5-dimethylindole (V-5)**. Antagonist activities were demonstrated by **2,3-dimethylindole (V-6)**, **2,3,7-trimethylindole (V-7)**, **6-methoxyindole (V-8)**, and **5-methoxy-2-methylindole (V-9)**, which is a marine environmental pollutant that mimics signaling by peptide hormones in jellyfish [63]. Environmental pollutants from the halogenated carbazoles class displayed also the AhR agonist activities, the most active ( $EC_{50} < 1 \mu\text{M}$ ) being **tetra-substituted chloro/bromocarbazoles (V-16)** [64]. A frequently used inhibitor of glycogen synthase kinase (GSK), **SB216763 (V-10)**, which is structurally 3-(2,4-Dichlorophenyl)-4-(1-methyl-1H-indol-3-yl)-1H-pyrrole-2,5-dione, was reported as a partial agonist of the AhR [65]. Also, other structurally unrelated and indole-based classes of GSK inhibitors, **6BIO (V-11)** (6-bromoindirubin-30-oxime) and **GSK3iXV (V-14)** (Pyridocarbazolo-cyclopentadienyl Ruthenium complex GSK3 inhibitor XV) were described as AhR full agonists [66]. **Indirubin-3'-monoxime (V-12)** and **isoindigo (V-13)**, dual inhibitors of GSK and cyclin-dependent kinases, were about 5–10 times weaker AhR agonist than indirubin and indigo, respectively [30,67]. Using *in silico*, *in vitro*, and *in vivo* assays, **2,2'-aminophenyl indole (V-17)** was identified as a ligand and potent agonist (micromolar  $EC_{50}$ ) of AhR that protected *in vitro* retinal pigmented epithelial layer from lipid peroxidation cytotoxicity mediated by 4-hydroxynonenal as well as the retina *in vivo* from

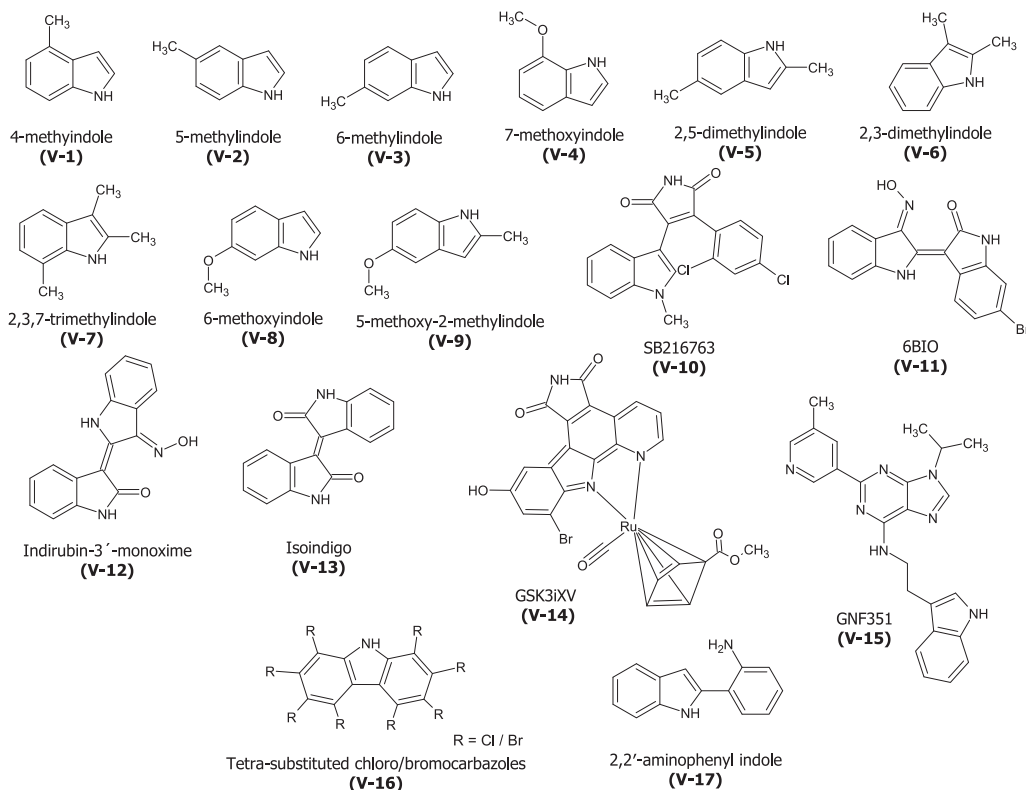
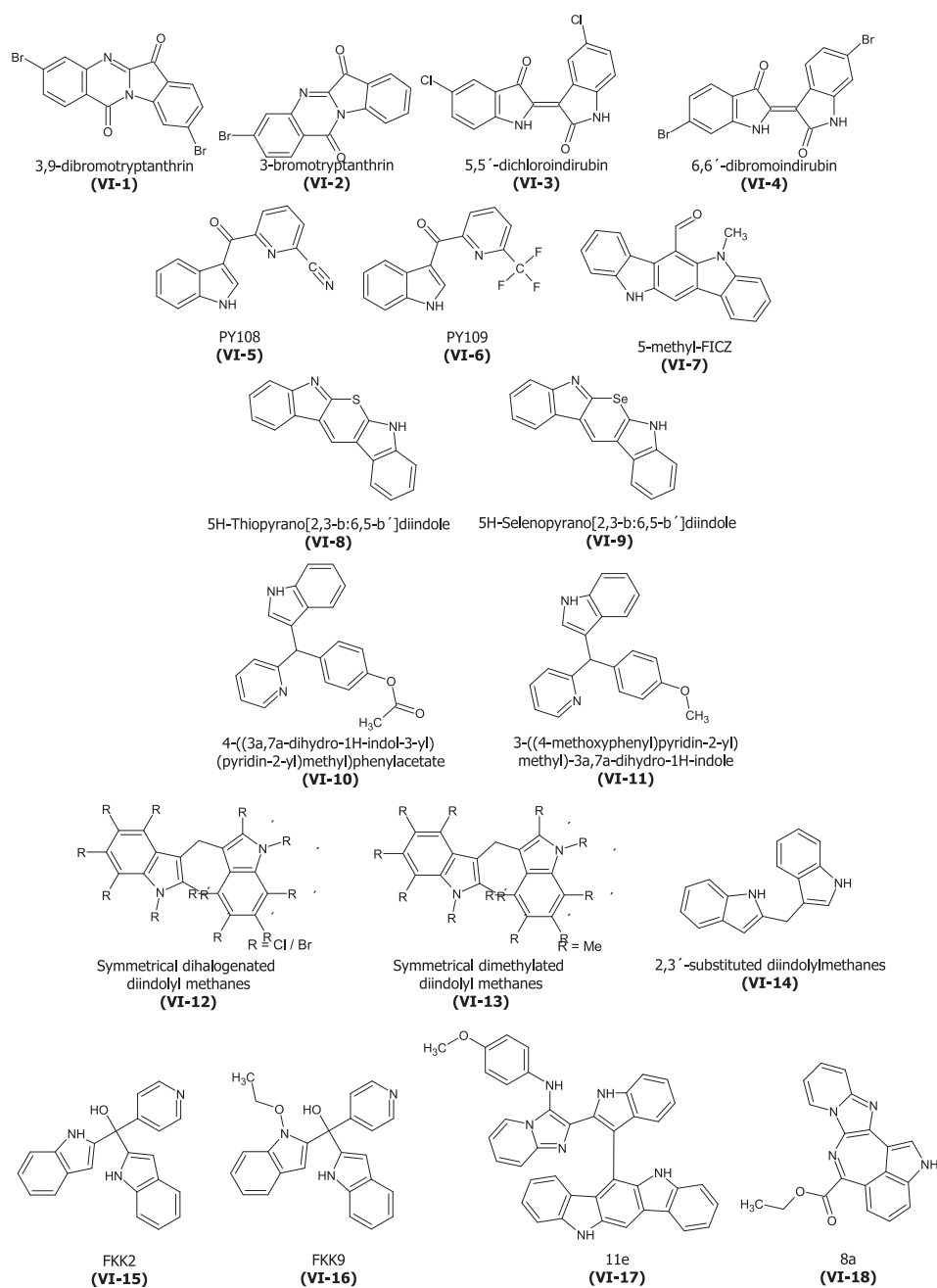


Fig. 5. Chemical structures of AhR-active synthetic indoles.





**Fig. 6.** Chemical structures of rationally designed AhR-active indoles.

**Table 1**  
Summary of experimental models used to characterize AhR-active indoles.

	AhR LIGAND	AhR FUNCTION ASSAYS	REF.
<b>Human endogenous indoles</b>			
I-1	Tryptamine	YES; Hepa1c1c7 cytosols; Guinea pig liver	reporter assay; gene expression; AhR/ARNT co-IP; ChIP; nuclear translocation [26, 40]
I-2	Indigo	YES; mouse liver cytosol	reporter assay; yeast assay; gene expression [29, 30]
I-3	Indirubin	YES; mouse liver cytosol	reporter assay; yeast assay; gene expression [29, 30, 43]
I-4	Indoxyl-3-sulfate	YES; humanized mice liver	reporter assay; gene expression [36]
I-5	ITE	YES; reticulocyte lysates; human murine	reporter assay [31]
I-6	FICZ	YES; rat liver cytosol	reporter assay; gene expression; ELISA [32, 43, 44]
I-7	1,3-di(1H-indol-3-yl)propan-2-one	not tested	reporter assay; EROD [33, 34, 35]
I-8	1-(1H-indol-3-yl)-3-(3H-indol-3-ylidene)propan-2-one	not tested	reporter assay; EROD [33, 34, 35]
<b>Human microbiota-produced indoles</b>			
II-1	Indole	YES; humanized mice liver; mice liver; Hepa1c1c7 cytosols	reporter assay; gene expression; ChIP; AhR/ARNT co-IP; nuclear translocation [37, 40]
II-2	Indole-3-acetate	YES; Hepa1c1c7 cytosols	reporter assay; gene expression [40]
II-3	Indole-3-propionate	YES; Hepa1c1c7 cytosols	reporter assay; gene expression [40]
II-4	Indole-3-lactate	YES; Hepa1c1c7 cytosols	reporter assay; gene expression [40]
II-5	Indole-3-pyruvate	YES; Hepa1c1c7 cytosols	reporter assay; gene expression; ChIP; AhR/ARNT co-IP; nuclear translocation [40]
II-6	Indole-3-acrylate	YES; Hepa1c1c7 cytosols	reporter assay; gene expression; ChIP; AhR/ARNT co-IP; nuclear translocation [40]
II-7	Indole-3-acetamide	YES; Hepa1c1c7 cytosols	reporter assay; gene expression [40]
II-8	Indole-3-ethanol	YES; Hepa1c1c7 cytosols	reporter assay; gene expression [40]
II-9	Indole-3-aldehyde	YES; Hepa1c1c7 cytosols	reporter assay; gene expression; ChIP; AhR/ARNT co-IP; nuclear translocation [40]
II-10	Indole-3-acetaldehyde	not tested	not specified [38, 42]
II-11	3-methylindole	YES; Hepa1c1c7 cytosols	reporter assay; gene expression; AhR/ARNT co-IP; ChIP; nuclear translocation [37, 39, 40, 63] 37, 39, 40, 63
II-12	2-oxindole	not tested	reporter assay; gene expression [37, 41]
II-13	3-methyl-2-oxindole	not tested	reporter assay; gene expression [41]
II-14	Tryptanthrin	not tested	reporter assay; gene expression [43, 44]
II-15	Pityriazepin	YES; Guinea pig liver	reporter assay [44]
II-16	Malassezin	not tested	reporter assay; gene expression; EROD [43, 44, 45]
<b>Natural and dietary indoles</b>			
III-1	Glucobrassicin	not tested	gene expression; EROD [47]
III-2	Neoglucobrassicin	not tested	gene expression; EROD [47]
III-3	Indole-3-carbinol	YES; mouse liver cytosol	reporter assay; gene expression; EROD; nuclear translocation [48, 49]
III-4	3,3'-Diindolylmethane	YES; mouse liver cytosol	reporter assay; gene expression; EROD; nuclear translocation [48, 49]
III-5	N-methoxyindole-3-carbinol	not tested	reporter assay; gene expression; EROD; EMSA [50]
III-6	ICZ	YES; mouse liver cytosol	reporter assay; gene expression; EROD [43, 44, 49]
III-7	2-(Indol-3-ylmethyl)-3,3'-diindolylmethane	YES; mouse liver cytosol	EROD [49]
III-8	5,6,11,12,17,18-Hexahydrocyclo[1,2-b:4,5-b':7,8-b'']trindole	YES; mouse liver cytosol	EROD [49]
III-9	3-amino-1,4-dimethyl-5H-pyrido[4,3-b]indole	not tested	reporter assay; gene expression; EROD [52]
III-10	3-amino-1-methyl-5H-pyrido[4,3-b]indole	not tested	reporter assay; gene expression; EROD [52]
III-11	Ascorbigen	not tested	reporter assay; gene expression; EROD; EMSA [50, 51]
III-12	2-amino-9H-pyrido[2,3-b]indole	not tested	reporter assay; gene expression; EROD [52]
III-13	2-amino-3-methyl-9H-pyrido[2,3-b]indole	not tested	reporter assay; gene expression; EROD [52]
III-14	Annomontine	not tested	reporter assay; gene expression; EROD [54]
III-15	Rutaecarpine	not tested	reporter assay; gene expression; EROD [54]
III-16	Xestomanzamine A	not tested	reporter assay; gene expression; EROD [54]
III-17	Schizocommunin	not tested	reporter assay; gene expression [55]
III-18	Brominated (methylthio)indoles	YES; Hepa1c1c7 cytosols	reporter assay; gene expression; EROD; EMSA [53]
<b>Drug indoles</b>			
IV-1	Avitriptan	YES; Hepa1c1c7 cytosols	reporter assay; gene expression; AhR/ARNT co-IP; ChIP; nuclear translocation [58]
IV-2	Donitriptan	YES; Hepa1c1c7 cytosols	reporter assay; gene expression; AhR/ARNT co-IP; ChIP; nuclear translocation [58]
IV-3	Semaxinib	YES; Hepa1c1c7 cytosols	reporter assay; gene expression [62]
IV-4	Sunitinib	not tested	reporter assay; gene expression; EROD [61]
IV-5	Indisulam	not tested	indirect mechanism - triggers ARNT degradation [60]
<b>Synthetic indoles</b>			
V-1	4-methylindole	not tested	reporter assay; gene expression; ChIP; nuclear translocation [63]
V-2	5-methylindole	not tested	reporter assay; gene expression [63]
V-3	6-methylindole	not tested	reporter assay; gene expression [63]
V-4	7-methoxyindole	not tested	reporter assay; gene expression; ChIP; nuclear translocation [63]
V-5	2,5-dimethylindole	not tested	reporter assay; gene expression [63]
V-6	2,3-dimethylindole	not tested	reporter assay; gene expression [63]
V-7	2,3,7-trimethylindole	not tested	reporter assay; gene expression [63]
V-8	6-methoxyindole	not tested	reporter assay; gene expression [63]
V-9	5-methoxy-2-methylindole	not tested	reporter assay; gene expression [63]
V-10	SB216763	not tested	reporter assay; gene expression [65]
V-11	6BIO	not tested	reporter assay; gene expression [66]
V-12	Indirubin-3'-monoxime	YES; mouse liver cytosol	reporter assay; <i>in vivo</i> gene expression; EROD [30]
V-13	Isoindigo	YES; mouse liver cytosol	reporter assay; gene expression; EMSA; EROD [67]
V-14	GSK3iXV	not tested	reporter assay; gene expression [66]
V-15	GNF351	YES; humanized mice liver	reporter assay; gene expression [69]
V-16	Tetra-substituted chloro/bromocarbazoles	not tested	gene expression [64]
V-17	2,2'-aminophenyl indole	YES; humanized mice liver	reporter assay; gene expression [68]

(continued on next page)

Table 1 (continued)

	AhR LIGAND	AhR FUNCTION ASSAYS	REF.
<b>Rationally designed indoles</b>			
VI-1	3,9-dibromotryptanthrin	not tested	reporter assay [71]
VI-2	3-bromotryptanthrin	not tested	reporter assay [71]
VI-3	5,5'-dichloroindirubin	not tested	reporter assay [71]
VI-4	6,6'-dibromoindirubin	not tested	reporter assay [71]
VI-5	PY108	not tested	reporter assay; gene expression; AhR/ARNT co-IP; nuclear translocation [72]
VI-6	PY109	not tested	reporter assay; gene expression; AhR/ARNT co-IP; nuclear translocation [72]
VI-7	5-methyl-FICZ	not tested	gene expression; EROD [76]
VI-8	5H-Thiopyrano[2,3-b:6,5-b']diindole	not tested	ELISA based Ah-IMMUNOASSAY [77]
VI-9	5H-Selenopyrano[2,3-b:6,5-b']diindole	not tested	ELISA based Ah-IMMUNOASSAY [77]
VI-10	4-((3a,7a-dihydro-1H-indol-3-yl)(pyridin-2-yl)methyl)phenylacetate	not tested	reporter assay [80]
VI-11	3-((4-methoxyphenyl)pyridin-2-yl methyl)-3a,7a-dihydro-1H-indole	not tested	reporter assay [80]
VI-12	Symmetrical dihalogenated diindolyl methanes	not tested	reporter assay [73]
VI-13	Symmetrical dimethylated diindolyl methanes	not tested	reporter assay; EMSA [74]
VI-14	2,3'-substituted diindolylmethanes	not tested	EROD HepG2 [75]
VI-15	FKK2	not tested	reporter assay; gene expression [78]
VI-16	FKK9	not tested	reporter assay; gene expression [78]
VI-17	11e	not tested	reporter assay; gene expression; EROD [81]
VI-18	8a	not tested	reporter assay; gene expression; EROD [81]

light-damage [68]. High-affinity ligand and complete antagonist of the AhR, devoid of partial agonist potential, **GNF351 (V-15)** (*N*-(2-(1*H*-indol-3-yl)ethyl)-9-isopropyl-2-(5-methylpyridin-3-yl)-9*H*-purin-6-amine), was identified and characterized by Perdew's group [69]. This compound suppressed both DRE-dependent and -independent AhR functions. After oral administration, its *in vivo* effects are limited to the gastrointestinal tract due to low absorption and extensive metabolism [70]. Chemical structures of synthetic AhR-active indoles are depicted in Fig. 5.

## 5. Rationally designed AhR-active indoles

Several studies, exploiting diverse approaches and strategies, were carried out to obtain highly potent and efficacious agonists or strong antagonists of the AhR, which could be potential drug candidates in the treatment of multiple diseases (for chemical structures ref Fig. 6):

A series of mono- and bisubstituted indirubins and tryptanthrins bearing halogens, alkyl, or carbomethoxy groups were synthesized from substituted indoles indole-3-aldehydes by the one-step biomimetic transformation. **3,9-dibromotryptanthrin (VI-1)**, **5,5'-dichloroindirubin (VI-3)** and **6,6'-dibromoindirubin (VI-4)** were found to be equipotent human AhR agonist to TCDD, and **3-bromotryptanthrin (VI-2)** was 10-times more potent than TCDD in the reporter cell line [71]. Chen et al. synthesized a focused library of structurally diverse indole and indazole compounds, resulting in several highly potent AHR modulators' characterization. Integrated computational and experimental studies have enabled to discover mechanisms governing ligand-receptor interaction and to identify stringent structural requirements for ligand-induced activation of AhR. The most potent ( $EC_{50} \approx 2$  nM) drug leads **PY109 (VI-6)** ((1*H*-indol-3-yl)(6-(trifluoromethyl)pyridin-2-yl)methanone) and **PY108 (VI-5)** (6-(1*H*-indole-3-carbonyl)picolinonitrile) displayed physicochemical drug-likeness properties, desirable pharmacokinetic profiles, and low toxicity. As a proof-of-concept, the anti-colitis effects of these two compounds in mouse model were demonstrated [72]. Safe's group reported **symmetrical dihalogenated diindolyl methanes (VI-12)**, including 4,4'-dichloro-, 6,6'-dichloro 5,5'-dibromo-diindolylmethane, as weak AhR agonists [73]. In the ongoing study, they observed the transformation of rat hepatic AhR into its ligand-binding form by **symmetrical dimethylated diindolyl methanes (VI-13)** (1,1' -, 2,2' -, 5,5' -, 6,6' -,

7,7'-). However, these compounds lacked AhR agonist or antagonist effects at target gene expression [74]. Tang's group synthesized series of **2,3'-substituted diindolylmethanes (VI-14)**, derived from malassezin scaffold. They found that a methyl substituent at 1'-*N* can significantly increase the AhR activity. In contrast, the 2-formyl group is not critical for some diindolylmethanes [75]. In the follow-up paper, they prepared 6- and *N*-substituted derivatives of FICZ. They identified **5-methyl-FICZ (VI-7)** as a more AhR-active substance as compared to parental FICZ [76]. Wincent et al. designed and synthesized a series of indolocarbazole-based compounds, having core structures of diindole-selenopyrans and -thiopyrans. An examples of resulting highly potent AhR agonists are **5H-Thiopyrano[2,3-b:6,5-b']diindole (VI-8)** and **5H-Selenopyrano[2,3-b:6,5-b']diindole (VI-9)** [77]. Employing an innovative microbial metabolite mimicry approach, we have recently designed and synthesized a series of AhR-active indole-containing asymmetric aromatic triarylmethanes. Besides an indole moiety, these compounds harbored pyridinyl and phenyl sulfonyl building blocks. The most active AhR agonists **FKK2 (VI-15)** (di(1*H*-indol-2-yl)(pyridin-4-yl)methanol) and **FKK9 (VI-16)** (1-(1-(ethoxymethyl)-1*H*-indol-2-yl)-2-(1*H*-indol-2-yl)-1-(pyridin-4-yl)ethan-1-ol) had relative efficacy comparable with that of TCDD and medium potency ( $EC_{50} \approx 1.6$   $\mu$ M) [78,79]. Interestingly, triarylmethanes containing unsubstituted indole group were dual agonists of the AhR and pregnane X receptor (PXR). In contrast, triarylmethanes and diarylmethanes with substituted indoles were PXR-selective agonists. Later on, Goya-Jorge et al. prepared a series of asymmetric triarylmethanes as potential ligands for the AhR. Two of these derivatives, **3-((4-methoxyphenyl)(pyridin-2-yl)methyl)-3a,7a-dihydro-1H-indole (VI-11)** and **4-((3a,7a-dihydro-1H-indol-3-yl)(pyridin-2-yl)methyl)phenylacetate (VI-10)**, contained an indole and pyridine molecules in their structure. However, their potency against the AhR was low ( $EC_{50} \approx 25$   $\mu$ M), and dual activation of the PXR is likely [80]. An approach of extended multicomponent reactions, comprising Groebke-Blackburn-Bienaymé reactions with indole aldehydes, was used to produce AhR-active indole-containing derivatives. Subsequently, a series of spontaneously triggered events led to a formation of a variety of fused and bridged polyheterocyclic scaffolds through oxidative Pickett-Spengler processes. The examples of AhR agonists resulting from indole-2-aldehyde and/or indole-3-aldehyde as starting materials, are **11e (VI-17)** (2-(3-(5,11-Dihydroindolo[3,2-b]carbazol-6-yl)-1*H*-indol-2-yl)-*N*-(4-

methoxyphenyl)imidazo[1,2-a]pyridin-3-amine) and **8a** (VI-18) (Ethyl 2H-pyrido[1',2'':1',2']imidazo[4',5':6,7]azepino[5,4,3-cd]indole-6-carboxylate), respectively [81].

## 6. Conclusions

The indole scaffold is generally well-established and of significant importance for drug discovery [82–84]. However, not all indole modifications result in better drugs. There is a need to optimize the potency and efficacy of indoles safely. Therefore, some considerations that make this feasible include host target protein specificity (versus non-specific target interactions) [85], indole pharmacophores that likely do not stray too far from non-toxic parental indole compounds [78,79,86], and metabolic liabilities that are inert [87–89]. In our current review, we argue for indole scaffolds being ideal candidates for selective targeting of AhR. In-depth chemistry is now required to optimize this scaffold minimally to achieve efficient, potent, and selective targeting of AhR and its application to AhR-related diseases [90]. Finally, a table summarizing details on the AhR assays performed for individual indoles described in this review, is presented (Table 1).

## Declaration of competing interest

The authors declare that they have no known competing financial interests or personal relationships that could have appeared to influence the work reported in this paper.

## Acknowledgements

We acknowledge financial support from the Czech Science Foundation [19-00236S]; the student grant from Palacký University in Olomouc [PrF-2021-005].

## Abbreviations

AhR	aryl hydrocarbon receptor
ARNT	AhR nuclear translocator
FICZ	6-formylindolo[3,2-b]carbazole
GSK	glycogen synthase kinase
PXR	pregnane X receptor
XRE	xenobiotic response element

## References

- [1] D.W. Nebert, F.M. Goujon, J.E. Gielen, Aryl hydrocarbon hydroxylase induction by polycyclic hydrocarbons: simple autosomal dominant trait in the mouse, *Nat. New Biol.* 236 (65) (1972) 107–110.
- [2] A. Poland, et al., 3,4,3',4'-Tetrachloro azoxybenzene and azobenzene: potent inducers of aryl hydrocarbon hydroxylase, *Science* 194 (4265) (1976) 627–630.
- [3] M.S. Denison, S.R. Nagy, Activation of the aryl hydrocarbon receptor by structurally diverse exogenous and endogenous chemicals, *Annu. Rev. Pharmacol. Toxicol.* 43 (2003) 309–334.
- [4] L. Stejskalova, Z. Dvorak, P. Pavek, Endogenous and exogenous ligands of aryl hydrocarbon receptor: current state of art, *Curr. Drug Metabol.* 12 (2) (2011) 198–212.
- [5] F. Ohtake, et al., Modulation of oestrogen receptor signalling by association with the activated dioxin receptor, *Nature* 423 (6939) (2003) 545–550.
- [6] A. Puga, et al., Aromatic hydrocarbon receptor interaction with the retinoblastoma protein potentiates repression of E2F-dependent transcription and cell cycle arrest, *J. Biol. Chem.* 275 (4) (2000) 2943–2950.
- [7] C.F. Vogel, E. Sciuillo, F. Matsumura, Involvement of ReB in aryl hydrocarbon receptor-mediated induction of chemokines, *Biochem. Biophys. Res. Commun.* 363 (3) (2007) 722–726.
- [8] S.R. Wilson, A.D. Joshi, C.J. Elferink, The tumor suppressor Kruppel-like factor 6 is a novel aryl hydrocarbon receptor DNA binding partner, *J. Pharmacol. Exp. Therapeut.* 345 (3) (2013) 419–429.
- [9] C. Gutierrez-Vazquez, F.J. Quintana, Regulation of the immune response by the aryl hydrocarbon receptor, *Immunity* 48 (1) (2018) 19–33.
- [10] V. Rothhammer, F.J. Quintana, The aryl hydrocarbon receptor: an environmental sensor integrating immune responses in health and disease, *Nat. Rev. Immunol.* 19 (3) (2019) 184–197.
- [11] P. Fernandez-Salguero, et al., Immune system impairment and hepatic fibrosis in mice lacking the dioxin-binding Ah receptor, *Science* 268 (5211) (1995) 722–726.
- [12] J.A. Walisser, et al., Gestational exposure of Ahr and Arnt hypomorphs to dioxin rescues vascular development, *Proc. Natl. Acad. Sci. U. S. A.* 101 (47) (2004) 16677–16682.
- [13] A.E. Boitano, et al., Aryl hydrocarbon receptor antagonists promote the expansion of human hematopoietic stem cells, *Science* 329 (5997) (2010) 1345–1348.
- [14] R. Di Giaino, et al., The aryl hydrocarbon receptor pathway defines the time frame for restorative neurogenesis, *Cell Rep.* 25 (12) (2018) 3241–3251 e5.
- [15] I.A. Murray, A.D. Patterson, G.H. Perdew, Aryl hydrocarbon receptor ligands in cancer: friend and foe, *Nat. Rev. Canc.* 14 (12) (2014) 801–814.
- [16] A. Metidji, et al., The environmental sensor AHR protects from inflammatory damage by maintaining intestinal stem cell homeostasis and barrier integrity, *Immunity* 49 (2) (2018) 353–362 e5.
- [17] I. Monteleone, et al., Aryl hydrocarbon receptor-induced signals up-regulate IL-22 production and inhibit inflammation in the gastrointestinal tract, *Gastroenterology* 141 (1) (2011) 237–248, 248 e1.
- [18] J.H. Lee, et al., A novel role for the dioxin receptor in fatty acid metabolism and hepatic steatosis, *Gastroenterology* 139 (2) (2010) 653–663.
- [19] T. Hidaka, et al., The aryl hydrocarbon receptor AhR links atopic dermatitis and air pollution via induction of the neurotrophic factor artemin, *Nat. Immunol.* 18 (1) (2017) 64–73.
- [20] S. Safe, Y. Cheng, U.H. Jin, The aryl hydrocarbon receptor (AhR) as a drug target for cancer chemotherapy, *Curr. Opin Toxicol.* 2 (2017) 24–29.
- [21] J.R. Baker, J.A. Sakoff, A. McCluskey, The aryl hydrocarbon receptor (AhR) as a breast cancer drug target, *Med. Res. Rev.* 40 (3) (2020) 972–1001.
- [22] J. Peppers, et al., A phase 2, randomized dose-finding study of tapinarof (GSK2894512 cream) for the treatment of atopic dermatitis, *J. Am. Acad. Dermatol.* 80 (1) (2019) 89–98 e3.
- [23] K. Robbins, et al., Phase 2, randomized dose-finding study of tapinarof (GSK2894512 cream) for the treatment of plaque psoriasis, *J. Am. Acad. Dermatol.* 80 (3) (2019) 714–721.
- [24] F. Giovannoni, et al., AHR is a Zika virus host factor and a candidate target for antiviral therapy, *Nat. Neurosci.* 23 (8) (2020) 939–951.
- [25] Y. Liu, et al., Mucus production stimulated by IFN-AhR signaling triggers hypoxia of COVID-19, *Cell Res.* 30 (12) (2020) 1078–1087.
- [26] S. Heath-Pagliuso, et al., Activation of the Ah receptor by tryptophan and tryptophan metabolites, *Biochemistry* 37 (33) (1998) 11508–11515.
- [27] S.H. Seok, et al., Trace derivatives of kynurenine potently activate the aryl hydrocarbon receptor (AHR), *J. Biol. Chem.* 293 (6) (2018) 1994–2005.
- [28] B.C. DiNatale, et al., Kynurenic acid is a potent endogenous aryl hydrocarbon receptor ligand that synergistically induces interleukin-6 in the presence of inflammatory signaling, *Toxicol. Sci.* 115 (1) (2010) 89–97.
- [29] J. Adachi, et al., Indirubin and indigo are potent aryl hydrocarbon receptor ligands present in human urine, *J. Biol. Chem.* 276 (34) (2001) 31475–31478.
- [30] F. Peter Guengerich, et al., Aryl hydrocarbon receptor response to indigo in vitro and in vivo, *Arch. Biochem. Biophys.* 423 (2) (2004) 309–316.
- [31] J. Song, et al., A ligand for the aryl hydrocarbon receptor isolated from lung, *Proc. Natl. Acad. Sci. U. S. A.* 99 (23) (2002) 14694–14699.
- [32] E. Wincent, et al., The suggested physiologic aryl hydrocarbon receptor activator and cytochrome P450 substrate 6-formylindolo[3,2-b]carbazole is present in humans, *J. Biol. Chem.* 284 (5) (2009) 2690–2696.
- [33] M.A. Bittinger, L.P. Nguyen, C.A. Bradfield, Aspartate aminotransferase generates proagonists of the aryl hydrocarbon receptor, *Mol. Pharmacol.* 64 (3) (2003) 550–556.
- [34] L.P. Nguyen, et al., D-amino acid oxidase generates agonists of the aryl hydrocarbon receptor from D-tryptophan, *Chem. Res. Toxicol.* 22 (12) (2009) 1897–1904.
- [35] G. Chowdhury, et al., Structural identification of Diindole agonists of the aryl hydrocarbon receptor derived from degradation of indole-3-pyruvic acid, *Chem. Res. Toxicol.* 22 (12) (2009) 1905–1912.
- [36] J.C. Schroeder, et al., The uremic toxin 3-indoxyl sulfate is a potent endogenous agonist for the human aryl hydrocarbon receptor, *Biochemistry* 49 (2) (2010) 393–400.
- [37] T.D. Hubbard, et al., Adaptation of the human aryl hydrocarbon receptor to sense microbiota-derived indoles, *Sci. Rep.* 5 (2015) 12689.
- [38] H.M. Roager, T.R. Licht, Microbial tryptophan catabolites in health and disease, *Nat. Commun.* 9 (1) (2018) 3294.
- [39] M.K. Rasmussen, et al., Skatole (3-methylindole) is a partial aryl hydrocarbon receptor agonist and induces CYP1A1/2 and CYP1B1 expression in primary human hepatocytes, *PLoS One* 11 (5) (2016), e0154629.
- [40] B. Vyhldalova, et al., Gut microbial catabolites of tryptophan are ligands and agonists of the aryl hydrocarbon receptor: a detailed characterization, *Int. J. Mol. Sci.* 21 (7) (2020).
- [41] F. Dong, et al., Intestinal microbiota-derived tryptophan metabolites are predictive of Ah receptor activity, *Gut Microb.* 12 (1) (2020) 1–24.
- [42] A. Smirnova, et al., Evidence for new light-independent pathways for generation of the endogenous aryl hydrocarbon receptor agonist FICZ, *Chem. Res. Toxicol.* 29 (1) (2016) 75–86.
- [43] P. Magiatis, et al., Malassezia yeasts produce a collection of exceptionally potent activators of the Ah (dioxin) receptor detected in diseased human skin,



- J. Invest. Dermatol. 133 (8) (2013) 2023–2030.
- [44] N. Mexia, et al., Pityriazepin and other potent AhR ligands isolated from *Malassezia furfur* yeast, Arch. Biochem. Biophys. 571 (2015) 16–20.
- [45] G. Wille, et al., Malassezin-A novel agonist of the arylhydrocarbon receptor from the yeast *Malassezia furfur*, Bioorg. Med. Chem. 9 (4) (2001) 955–960.
- [46] A. Rannug, How the AHR became important in intestinal homeostasis-A diurnal FICZ/AHR/CYP1A1 feedback controls both immunity and immunopathology, Int. J. Mol. Sci. 21 (16) (2020).
- [47] C. Bonnesen, et al., Modulation of cytochrome P-450 and glutathione S-transferase isoform expression in vivo by intact and degraded indolyl glucosinolates, Nutr. Canc. 33 (2) (1999) 178–187.
- [48] L.F. Bjeldanes, et al., Aromatic hydrocarbon responsiveness-receptor agonists generated from indole-3-carbinol in vitro and in vivo: comparisons with 2,3,7,8-tetrachlorodibenzo-p-dioxin, Proc. Natl. Acad. Sci. U. S. A. 88 (21) (1991) 9543–9547.
- [49] I. Chen, S. Safe, L. Bjeldanes, Indole-3-carbinol and diindolylmethane as aryl hydrocarbon (Ah) receptor agonists and antagonists in T47D human breast cancer cells, Biochem. Pharmacol. 51 (8) (1996) 1069–1076.
- [50] P.U. Stephenson, et al., N-methoxyindole-3-carbinol is a more efficient inducer of cytochrome P-450 1A1 in cultured cells than indol-3-carbinol, Nutr. Canc. 36 (1) (2000) 112–121.
- [51] P.U. Stephenson, et al., Modulation of cytochrome P4501A1 activity by ascorbigen in murine hepatoma cells, Biochem. Pharmacol. 58 (7) (1999) 1145–1153.
- [52] M. Sekimoto, et al., Aryl hydrocarbon receptor activation and CYP1A induction by cooked food-derived carcinogenic heterocyclic amines in human HepG2 cell lines, Food Chem. Toxicol. 97 (2016) 256–264.
- [53] D.E. DeGroot, et al., Naturally occurring marine brominated indoles are aryl hydrocarbon receptor ligands/agonists, Chem. Res. Toxicol. 28 (6) (2015) 1176–1185.
- [54] T. Haarmann-Stemmann, et al., Regulation of dioxin receptor function by different beta-carboline alkaloids, Arch. Toxicol. 84 (8) (2010) 619–629.
- [55] R. Filip, et al., Fungal natural alkaloid schizocommunin activates the aryl hydrocarbon receptor pathway, Medchemcomm 10 (6) (2019) 985–990.
- [56] R. Jansen, et al., Indothiazinone, an indolyl thiazolyl ketone from a novel myxobacterium belonging to the Sorangiineae, J. Nat. Prod. 77 (4) (2014) 1054–1060.
- [57] S. Kwon, Y.T. Han, J.W. Jung, Studies on the synthesis of indothiazinone and its derivatives via direct 3-acylation of indole, Synth. Commun. 45 (14) (2015) 1662–1668.
- [58] B. Vyhldalova, et al., Antimigraine drug avitriptan is a ligand and agonist of human aryl hydrocarbon receptor that induces CYP1A1 in hepatic and intestinal cells, Int. J. Mol. Sci. 21 (8) (2020).
- [59] U.H. Jin, et al., Short chain fatty acids enhance aryl hydrocarbon (ah) responsiveness in mouse colonocytes and caco-2 human colon cancer cells, Sci. Rep. 7 (1) (2017) 10163.
- [60] S.A. Kim, et al., Aryl sulfonamides induce degradation of aryl hydrocarbon receptor nuclear translocator through CRL4(DCAF15) E3 ligase, Mol. Cell. 43 (11) (2020) 935–944.
- [61] Z.H. Maayah, et al., Sunitinib, a tyrosine kinase inhibitor, induces cytochrome P450 1A1 gene in human breast cancer MCF7 cells through ligand-independent aryl hydrocarbon receptor activation, Arch. Toxicol. 87 (5) (2013) 847–856.
- [62] K. Matsuoka-Kawano, et al., TSU-16, (Z)-3-[(2,4-dimethylpyrrol-5-yl)methylidene]-2-indolinone, is a potent activator of aryl hydrocarbon receptor and increases CYP1A1 and CYP1A2 expression in human hepatocytes, Chem. Biol. Interact. 185 (1) (2010) 33–41.
- [63] M. Stepankova, et al., Methylindoles and methoxyindoles are agonists and antagonists of human aryl hydrocarbon receptor, Mol. Pharmacol. 93 (6) (2018) 631–644.
- [64] N. Riddell, et al., Characterization and biological potency of mono- to tetrahalogenated carbazoles, Environ. Sci. Technol. 49 (17) (2015) 10658–10666.
- [65] A. Braeuning, A. Buchmann, The glycogen synthase kinase inhibitor 3-(2,4-dichlorophenyl)-4-(1-methyl-1H-indol-3-yl)-1H-pyrrole-2,5-dione (SB216763) is a partial agonist of the aryl hydrocarbon receptor, Drug Metab. Dispos. 37 (8) (2009) 1576–1580.
- [66] P. Briolotti, et al., Analysis of glycogen synthase kinase inhibitors that regulate cytochrome P450 expression in primary human hepatocytes by activation of beta-catenin, aryl hydrocarbon receptor and pregnane X receptor signaling, Toxicol. Sci. 148 (1) (2015) 261–275.
- [67] S. Nishiumi, et al., Antagonistic and agonistic effects of indigoids on the transformation of an aryl hydrocarbon receptor, Arch. Biochem. Biophys. 470 (2) (2008) 187–199.
- [68] M.A. Gutierrez, et al., A novel AhR ligand, 2AI, protects the retina from environmental stress, Sci. Rep. 6 (2016) 29025.
- [69] K.J. Smith, et al., Identification of a high-affinity ligand that exhibits complete aryl hydrocarbon receptor antagonism, J. Pharmacol. Exp. Therapeut. 338 (1) (2011) 318–327.
- [70] Z.Z. Fang, et al., In vivo effects of the pure aryl hydrocarbon receptor antagonist GNF-351 after oral administration are limited to the gastrointestinal tract, Br. J. Pharmacol. 171 (7) (2014) 1735–1746.
- [71] N. Mexia, et al., A biomimetic, one-step transformation of simple indolic compounds to malassezia-related alkaloids with high AhR potency and efficacy, Chem. Res. Toxicol. 32 (11) (2019) 2238–2249.
- [72] J. Chen, et al., Modulation of lymphocyte-mediated tissue repair by rational design of heterocyclic aryl hydrocarbon receptor agonists, Sci. Adv. 6 (3) (2020), eaay8230.
- [73] A. McDougal, et al., Inhibition of carcinogen-induced rat mammary tumor growth and other estrogen-dependent responses by symmetrical dihalo-substituted analogs of diindolylmethane, Canc. Lett. 151 (2) (2000) 169–179.
- [74] A. McDougal, et al., Methyl-substituted diindolylmethanes as inhibitors of estrogen-induced growth of T47D cells and mammary tumors in rats, Breast Canc. Res. Treat. 66 (2) (2001) 147–157.
- [75] G.N. Winston-McPherson, D. Shu, W. Tang, Synthesis and biological evaluation of 2,3'-diindolylmethanes as agonists of aryl hydrocarbon receptor, Bioorg. Med. Chem. Lett. 24 (16) (2014) 4023–4025.
- [76] H. Wu, et al., Synthesis and biological evaluation of FICZ analogues as agonists of aryl hydrocarbon receptor, Bioorg. Med. Chem. Lett. 30 (5) (2020) 126959.
- [77] E. Wincent, et al., Synthesis and biological evaluation of fused thio- and selenopyrans as new indolocarbazole analogues with aryl hydrocarbon receptor affinity, Bioorg. Med. Chem. 17 (4) (2009) 1648–1653.
- [78] Z. Dvorak, et al., Targeting the pregnane X receptor using microbial metabolite mimicry, EMBO Mol. Med. 12 (4) (2020), e11621.
- [79] Z. Dvorak, H. Sokol, S. Mani, Drug mimicry: promiscuous receptors PXR and AhR, and microbial metabolite interactions in the intestine, Trends Pharmacol. Sci. 41 (12) (2020) 900–908.
- [80] E. Goya-Jorge, et al., Targeting the aryl hydrocarbon receptor with a novel set of triaryl methanes, Eur. J. Med. Chem. 207 (2020) 112777.
- [81] O. Ghazalghaei, et al., Extended multicomponent reactions with indole aldehydes: access to unprecedented polyheterocyclic scaffolds, ligands of the aryl hydrocarbon receptor, Angew Chem. Int. Ed. Engl. 60 (5) (2021) 2603–2608, <https://doi.org/10.1002/anie.202011253>.
- [82] F.R. de Sa Alves, E.J. Barreiro, C.A. Fraga, From nature to drug discovery: the indole scaffold as a 'privileged structure', Mini Rev. Med. Chem. 9 (7) (2009) 782–793.
- [83] T.P. Singh, O.M. Singh, Recent progress in biological activities of indole and indole alkaloids, Mini Rev. Med. Chem. 18 (1) (2018) 9–25.
- [84] A. Kumari, R.K. Singh, Medicinal chemistry of indole derivatives: current to future therapeutic perspectives, Bioorg. Chem. 89 (2019) 103021.
- [85] Y. Peng, et al., Identification of an irreversible PPARgamma antagonist with potent anticancer activity, Pharmacol. Res. Perspect. 8 (6) (2020), e00693.
- [86] Z. Dvorak, et al., Weak microbial metabolites: a treasure trove for using biomimicry to discover and optimize drugs, Mol. Pharmacol. 98 (4) (2020) 343–349.
- [87] R. Kato, et al., Reactive metabolite of gefitinib activates inflammasomes: implications for gefitinib-induced idiosyncratic reaction, J. Toxicol. Sci. 45 (11) (2020) 673–680.
- [88] B.H. Norman, Drug induced liver injury (DILI). Mechanisms and medicinal chemistry avoidance/mitigation strategies, J. Med. Chem. 63 (20) (2020) 11397–11419.
- [89] P.R. Bradshaw, et al., Acyl glucuronide reactivity in perspective, Drug Discov. Today 25 (9) (2020) 1639–1650.
- [90] M. Modoux, et al., Tryptophan metabolism as a pharmacological target, Trends Pharmacol. Sci. 42 (1) (2021) 60–73.

## APPENDIX II.


**Ondrová K.**, Zůvalová I., Vyhlídalová B., Krasulová K., Miková E., Vrzal R., Nádvorník P., Nepal B., Kortagere S., Kopečná M., Kopečný D., Šebela M., Rastinejad F., Pu H., Sural M., Rolfes KM., Haarmann-Stemmann T., Li H., Mani S., Dvořák Z. (2023). Monoterpenoid aryl hydrocarbon receptor allosteric antagonists protect against ultraviolet skin damage in female mice. *Nat Commun* 14: 2728. [IF<sub>2021</sub> 17.694].

# Monoterpenoid aryl hydrocarbon receptor allosteric antagonists protect against ultraviolet skin damage in female mice

Received: 27 November 2020

Accepted: 2 May 2023

Published online: 11 May 2023

 Check for updates

Karolína Ondrová<sup>1</sup>, Iveta Zůvalová<sup>1</sup>, Barbora Vyhliďalová<sup>1</sup>, Kristýna Krasulová<sup>1</sup>, Eva Miková<sup>1</sup>, Radim Vrzal<sup>1</sup>, Petr Nádvorník<sup>1</sup>, Binod Nepal<sup>2</sup>, Sandhya Kortagere<sup>2</sup>, Martina Kopečná<sup>3</sup>, David Kopečný<sup>3</sup>, Marek Šebela<sup>4</sup>, Fraydoon Rastinejad<sup>5</sup>, Hua Pu<sup>5</sup>, Miroslav Sural<sup>6</sup>, Katharina Maria Rolfes<sup>7</sup>, Thomas Haarmann-Stemmann<sup>7</sup>, Hao Li<sup>8</sup>, Sridhar Mani<sup>8</sup> ✉ & Zdeněk Dvořák<sup>1</sup> ✉

The human aryl hydrocarbon receptor (AhR) is a ligand-activated transcription factor that is a pivotal regulator of human physiology and pathophysiology. Allosteric inhibition of AhR was previously thought to be untenable. Here, we identify carvones as noncompetitive, insurmountable antagonists of AhR and characterize the structural and functional consequences of their binding. Carvones do not displace radiolabeled ligands from binding to AhR but instead bind allosterically within the bHLH/PAS-A region of AhR. Carvones do not influence the translocation of ligand-activated AhR into the nucleus but inhibit the heterodimerization of AhR with its canonical partner ARNT and subsequent binding of AhR to the promoter of *CYP1A1*. As a proof of concept, we demonstrate physiologically relevant Ahr-antagonism by carvones in vivo in female mice. These substances establish the molecular basis for selective targeting of AhR regardless of the type of ligand(s) present and provide opportunities for the treatment of disease processes modified by AhR.

The aryl hydrocarbon receptor (AhR) is a ligand-activated transcription factor that belongs to the family of basic helix-loop-helix transcription factors. In the resting state, unliganded AhR resides in the cytosol. Upon ligand binding to AhR, the ligand-receptor complex translocates to the cell nucleus. It forms a heterodimer with AhR nuclear translocator (ARNT), which binds to specific response elements in the promoters of the target genes. Typical xenobiotic ligands of AhR are environmental contaminants, such as polyaromatic hydrocarbons (e.g., benzo[*a*]pyrene - BaP) and halogenated aromatic hydrocarbons (e.g., 2,3,7,8-tetrachlorodibenzo-*p*-dioxin - TCDD), as

well as naturally occurring chemicals, such as various polyphenols. The endogenous ligands of AhR are mainly intermediary and microbial metabolites of tryptophan, such as 6-formylindolo[3,2-*b*]carbazole (FICZ)<sup>1</sup>. AhR regulates the expression of genes involved in xenoprotection, immune response, cell cycle, differentiation, lipid, and carbohydrate metabolism. Therefore, AhR is a pivotal determinant not only in human physiology (e.g., hematopoietic development)<sup>2</sup> but also in the incidence, onset, and progression of pathophysiological processes, including carcinogenesis, inflammation, infection, diabetes, and cardiovascular diseases<sup>3,4</sup>. Most AhR ligands are partial agonists.

<sup>1</sup>Department of Cell Biology and Genetics, Faculty of Science, Palacký University, Olomouc, Czech Republic. <sup>2</sup>Department of Microbiology & Immunology, Drexel University College of Medicine, Philadelphia, PA, USA. <sup>3</sup>Department of Experimental Biology, Faculty of Science, Palacký University, Olomouc, Czech Republic. <sup>4</sup>Department of Biochemistry, Faculty of Science, Palacký University, Olomouc, Czech Republic. <sup>5</sup>Target Discovery Institute Nuffield Department of Medicine Research Building Brasenose College University of Oxford, Oxford, UK. <sup>6</sup>Department of Organic Chemistry, Faculty of Science, Palacký University, Olomouc, Czech Republic. <sup>7</sup>IUF-Leibniz-Research Institute for Environmental Medicine, Düsseldorf, Germany. <sup>8</sup>Department of Medicine, Oncology, Molecular Pharmacology, and Genetics, Albert Einstein College of Medicine, Bronx, NY, USA. ✉e-mail: [sridhar.mani@einsteinmed.edu](mailto:sridhar.mani@einsteinmed.edu); [moulin@email.cz](mailto:moulin@email.cz)

Full agonists of AhR include halogenated aromatic hydrocarbons, such as TCDD, whereas AhR antagonists are scarce. For instance, the stilbenoid resveratrol or synthetic inhibitor of c-Jun-N-terminal kinase SP600125 were long deemed AhR antagonists until their minimal residual agonist activity was unveiled<sup>5</sup>. The first identified and bona fide frequently used competitive antagonist of AhR was 3'-methoxy-4'-nitroflavone (MNF)<sup>6</sup>; however, AhR-dependent enhancement of *CYP1A1* transcription by MNF was also reported<sup>7</sup>. By screening a 10 K chemical library, 2-methyl-2*H*-pyrazole-3-carboxylic acid (2-methyl-4-*o*-tolylazo-phenyl)-amide (CH223191) was identified as a ligand and potent competitive antagonist ( $IC_{50}$  - 30 nM) of AhR<sup>8</sup>. Later, a series of CH223191-based antagonists were developed, and the AhR-independent pro-proliferative properties of CH223191 were reported<sup>9</sup>. Additionally, CH223191 is a ligand-selective antagonist of AhR that preferentially inhibits the halogenated aromatic hydrocarbon class of agonists (e.g., TCDD) but not others, such as polyaromatic hydrocarbons or flavonoids<sup>10</sup>. Perdue's lab reported *N*-(2-(1*H*-indol-3-yl)ethyl)-9-isopropyl-2-(5-methyl pyridine-3-yl)-9*H*-purin-6-amine (GNF351) as a high-affinity ligand ( $IC_{50}$  - 62 nM) and competitive antagonist of AhR with the capability to inhibit both genomic and nongenomic activities of AhR<sup>11,12</sup>. There are isolated reports on the in vitro and in vivo effects of FDA-approved drugs with AhR-antagonist activity. For instance, clofazimine, an antileprosy drug and AhR antagonist, suppressed multiple myeloma in transgenic mice; however, the putative AhR-dependent mechanism was not directly evidenced<sup>13</sup>. Another example is relapse during melanoma treatment with the BRAF inhibitor vemurafenib, which was suggested to be delayed by targeting constitutively active AhR in persisting cells with antagonists<sup>14</sup>. Moreover, we identified vemurafenib as a competitive antagonist of AhR that was found to inhibit the in vitro and in vivo effects of AhR-dependent processes, including the abrogation of anti-inflammatory signaling and response<sup>15</sup>. Currently, two AhR antagonists, BAY2416964 and IK-175, have entered phase 1 clinical trials in order to assess the tolerability and toxicity of the AhR-targeting agents in patients suffering from incurable solid cancers<sup>16</sup>. Interestingly, AhR was identified as a host factor for Zika and dengue viruses, and the inhibition of AhR boosted antiviral immunity and diminished the in vivo replication of these viruses<sup>17</sup>. Recently, it was demonstrated that AhR is activated by infection with different coronaviruses and that pharmacological inhibition of AhR suppresses the in vivo replication of the viruses HCoV-229 and SARS-CoV-2, the causative agents of the common cold and COVID-19<sup>18</sup>.

We reported that the essential oils of dill, caraway, and spearmint have antagonist effects on AhR and that carvones, which are the major constituents of these oils, are responsible for AhR antagonism<sup>19</sup>. Carvone is a monocyclic monoterpenoid that exists in two enantiomers: R-carvone has a sweetish, spearmint-like odor, and S-carvone has a spicy, caraway-like odor. Human exposure to carvones occurs mainly through the dietary intake of carvone-containing foods and beverages<sup>19</sup> and via percutaneous absorption because carvones are used as skin permeabilizers in transdermal patches<sup>20</sup> and various skincare products (hair shampoos, foaming baths, body lotions, liquid soaps, foot powders, etc.).

In this study, we have significantly advanced our understanding of the mechanism by which carvones antagonize human AhR. Biochemical and cell biological studies demonstrated a specific, selective, and efficacious insurmountable and noncompetitive mechanism of AhR antagonism involving the disruption of AhR-ARNT dimerization by carvones in the cell nucleus. As a proof of concept, we showed in vivo that carvones antagonize ligand-inducible expression of AhR target genes in mouse skin, and reverse the modulation of UV-induced skin inflammatory mediators by AhR ligands. Collectively, we report small dietary monocyclic monoterpenoids as negative allosteric modulators of AhR with potential preventive and therapeutic applications.

## Results

### Carvones are noncompetitive antagonists of AhR

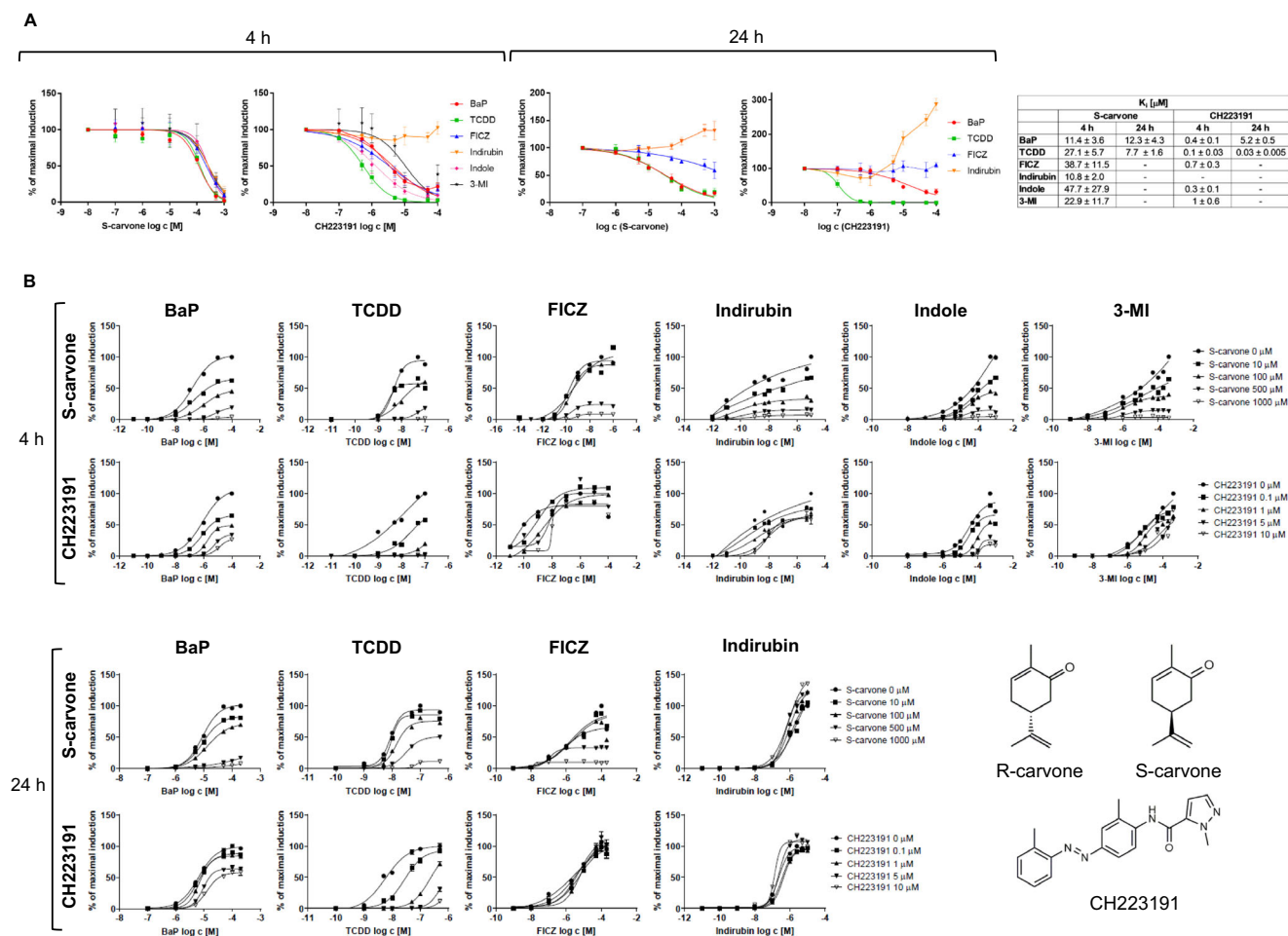
The human stably transfected reporter cell line AZ-AHR<sup>21</sup> was used to investigate the effects of carvones on the transcriptional activity of AhR. Model full agonists of AhR, including TCDD, BaP, FICZ, indirubin, indole, and 3-methylindole (3-MI), caused a concentration-dependent increase in AhR-mediated luciferase activity (Fig. S1A). Carvones did not affect the basal transcriptional activity of AhR (Fig. S1B). The antagonist effects of carvones and CH223191 (orthosteric AhR antagonist) on agonist-inducible AhR activity were examined in cells co-incubated for 4 h and 24 h with a fixed concentration of agonist ligands (corresponding to their  $EC_{80}$ ) and increasing concentrations of carvones and CH223191. After 4 h of incubation, carvones exerted concentration-dependent antagonist effects on AhR activation by all tested agonists, and the inhibitor constants  $K_i$  against all AhR agonists laid in very narrow range, which spanned from 11  $\mu$ M to 48  $\mu$ M. On the other hand, CH223191 was unable to inhibit AhR activation by indirubin. The  $K_i$  values for CH223191 were much lower than those for carvones, but they highly varied between different agonists (from 0.1  $\mu$ M to 1  $\mu$ M) (Fig. 1A). After 24 h of incubation, the antagonist effects of CH223191 against TCDD-activated AhR were much stronger as compared to carvones. Both carvones and CH223191 antagonized BaP-activated AhR to the similar extent. Neither carvones nor CH223191 inhibited FICZ-activated AhR, and both antagonists potentiated the activation of AhR by indirubin (Fig. 1A). These data support the known fact that CH223191 is a ligand-selective antagonist<sup>10</sup>, whereas carvones behave as AhR pan-antagonist. Next, we analyzed the mechanism of AhR antagonism. For this purpose, we incubated cells with fixed concentrations of carvones and CH223191, combined with increasing concentrations of AhR agonists. We observed a gradual decrease in  $E_{MAX}$  and a slight decline in  $EC_{50}$  with increasing concentrations of carvones for each tested agonist at both times of incubation (Fig. 1B, Figure S1C). The exception was indirubin, which was not antagonized by carvones, consistently with results in Fig. 1A. These data imply that carvones are primarily either (insurmountable) noncompetitive, irreversible competitive, or uncompetitive antagonists of AhR. Since the same concentration of carvones antagonized both high and low concentrations of all agonists used to a comparable degree (Table S2), the uncompetitive mechanism was ruled out<sup>22</sup>. We also excluded inhibition of luciferase catalytic activity (Figure S1D) and cytotoxicity (Figure S1E), as culprits of inhibition of AhR activity by carvones. The orthosteric ligand of AhR, CH223191, displayed competitive antagonist behavior against TCDD-activated AhR, as it caused typical rightward shift of sigmoid curves (Fig. 1B). The antagonist effects of CH223191 against other AhR agonists were ambiguous. Of note, whereas CH223191 displayed much lower  $K_i$  values than carvones, the relative strength of antagonism is hereby manifested against the agonists at their  $EC_{80}$  concentration (Fig. 1A). Carvones were much stronger AhR antagonists as compared to CH223191, when applied against high concentrations of agonists ( $\sim 100 \times EC_{80}$ ) (Fig. 1B).

Finally, we have examined AhR-antagonist activities of different cyclic monoterpenoids as the carvones structural analogs. We found that (+)-dihydrocarvone, R/S-pulegones, piperitone, piperitenone, carvacrol and thymol dose-dependently inhibited TCDD- and BaP-activated AhR. On the other hand (+)/(-)-menthones, (+)/(-)-isomenthones, cuminol, cuminal and *p*-cymene did not display AhR antagonist activity (Figure S2).

### Carvones downregulate AhR target genes

The effects of carvones on the ligand-inducible expression of the prototypical AhR target gene *CYP1A1*<sup>23</sup> were examined in a complementary set of AhR-competent human cell lines, including primary human hepatocytes, HepG2 hepatocarcinoma cells, LS180 colon adenocarcinoma cells, and HaCaT immortal keratinocytes<sup>23</sup>. Carvones inhibited the ligand-inducible mRNA and protein expression of *CYP1A1* in cell type-specific and ligand-selective manner. Induction of *CYP1A1* by TCDD was





incubations with a fixed concentration of antagonists (carvones and CH223191) and increasing concentrations of AhR agonists. Experiments were performed in three independent cell passages (n = 3). Representative plots from one experiment are shown. Abbreviations: BaP, benzo[*a*]pyrene; FICZ, 6-formylindolo[3,2-*b*]carbazole; 3-MI, 3-methylindole; TCDD, 2,3,7,8-tetrachlorodibenzo-*p*-dioxin. Source data are provided as a Source Data file.

inhibited by carvones in all cell types, by BaP in LS180, HaCaT, and hepatocytes, and by FICZ in HaCaT cells and human hepatocytes (Fig. 2, Figure S3). In addition, TCDD-inducible, AhR receptor-regulated 7-ethoxyresorufin-*O*-deethylase (EROD) catalytic activity<sup>3</sup> was strongly decreased by S-carvone in AZ-AHR cells (Figure S4A). Carvones also downregulated AhR ligand-inducible canonical genes *CYP1A2* (Figure S3) and *AhRR* (AhR repressor) (Figure S4B) and the noncanonical AhR target gene *PAI-1* (plasminogen activator inhibitor 1) (Figure S4C).

### Carvones influence the cellular functions of AhR

We analyzed in detail the effects of carvones on individual cellular events throughout the AhR signaling pathway. The AhR agonists TCDD, BaP, and FICZ triggered the translocation of AhR from the cytosol to the nucleus, and carvones did not influence this process. Additionally, carvones alone did not induce AhR nuclear translocation (Fig. 3A; Table S3). Nuclear, ligand-bound AhR forms a heterodimer with ARNT, which in turn binds specific dioxin-response elements in the promoters of target genes. This pathway, involving ARNT, is referred to as canonical AhR signaling. Carvones strongly inhibited the formation of AhR-ARNT heterodimers (Fig. 3B) and the binding of AhR to the *CYP1A1* promoter (Fig. 3C) in cells stimulated with TCDD- and BaP- but not with FICZ. We also observed that structural analogs of carvone (monocyclic monoterpenoids) with AhR antagonist activity

(Figure S2) do not inhibit TCDD- and BaP-inducible nuclear translocation of AhR (Figure S5A), but inhibit formation of AhR-ARNT heterodimer (Figure S5B). A scheme summarizing the effects of carvones on canonical AhR signaling is depicted in Fig. 3D.

### Binding of carvones to AhR

A reporter gene assay revealed that carvones are noncompetitive antagonists of AhR (Fig. 1, Figure S1), implying that they should not competitively displace ligands from binding to AhR. This assumption was corroborated by a competitive radioligand binding assay, which showed that S-carvone did not inhibit the binding of <sup>3</sup>H-TCDD to mouse hepatic AhR. However, we observed a slight, concentration-independent decrease in <sup>3</sup>H-TCDD binding in the presence of 1000 μM S-carvone (Fig. 4A). Noncompetitive antagonism may occur through the following potential mechanisms. (i) Allosteric hindrance (direct or involving conformational change) of the ligand binding pocket of AhR would prevent proper binding of the ligand and switching on of AhR. This scenario is unlikely because the ligand-dependent nuclear translocation of AhR was not disturbed by carvones (Fig. 3A). For this reason, irreversible competitive antagonism is also unlikely. (ii) An indirect mechanism could occur either at AhR or off-target, affecting protein kinases, ARNT, etc. (*vide infra*). Therefore, we investigated the allosteric binding of carvones to AhR and their effects on AhR-ARNT

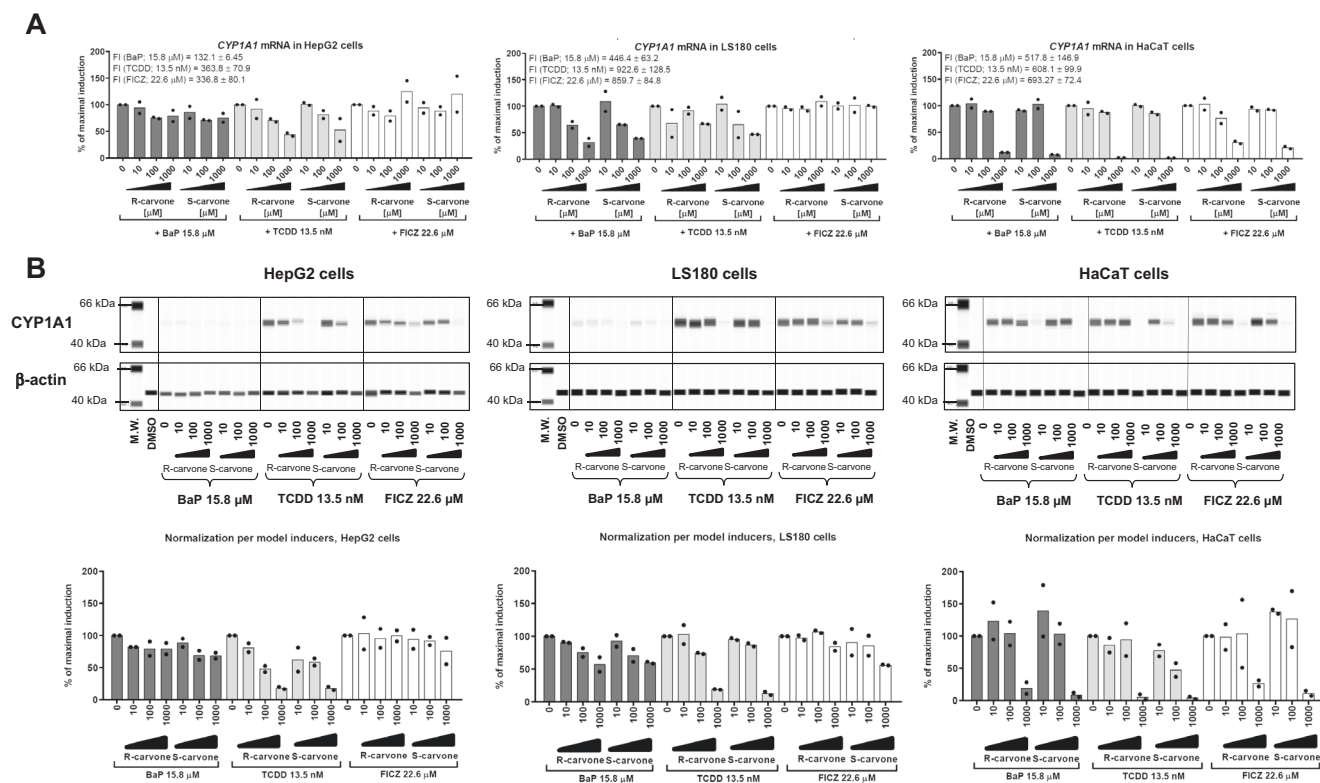


**Fig. 2 | Downregulation of CYP1A1 in human cell lines by carvones.** HepG2, LS180, and HaCaT cells were incubated for 24 h with carvones (0  $\mu$ M – 1000  $\mu$ M) in the presence of the AhR agonists TCDD, BaP and FICZ at their  $EC_{50}$  concentrations. Incubations and measurements were performed in triplicate (technical replicates). **(A)** RT-PCR analyses of CYP1A1 mRNA; results expressed relative to the agonist in the absence of carvones (100%). Data are the mean from two independent cell passages ( $n = 2$ ). The results were normalized using GAPDH as a housekeeping gene. The absolute values of CYP1A1 mRNA fold inductions (F.I.) by model agonists are

indicated in the text inserted in the bar graphs from each cell line. **(B)** Quantitative automated Western blot analysis by SallySue of CYP1A1 protein. Representative SallySue records from one cell passage are shown. Bar graphs at the bottom show quantified CYP1A1 protein normalized per  $\beta$ -actin; data are expressed relative to agonist in the absence of carvones (100%) and are the mean  $\pm$  S.D. from two independent cell passages ( $n = 2$ ). Abbreviations: BaP, benzo[a]pyrene; FICZ, 6-formylindolo[3,2-*b*]carbazole; TCDD, 2,3,7,8-tetrachlorodibenzo-*p*-dioxin. Source data are provided as a Source Data file.

heterodimerization. The molecular docking of carvones to various known binding pockets of AhR ligands, such as TCDD, resveratrol, FICZ, BaP, and methylindoles, suggested that carvones may nonspecifically bind to these sites with average docking scores of 47.5 and 42, respectively. However, this binding could be due to their relatively small size and could have no functional effect. Based on the experimental evidence that carvones inhibit the formation of AhR-ARNT (Fig. 3B), we docked these molecules to the heterodimerization interface of AhR and ARNT. This interface spans several interdomain interactions that also form the dioxin-responsive element binding pocket<sup>24</sup>. One such interface region is the  $\alpha 1$ - $\alpha 2$  helical region of the bHLH domain consisting of residues Leu43, Leu47, and Leu50 from the  $\alpha 1$  helix and Tyr76, Leu72, and Leu77 from the  $\alpha 2$  helical region. Carvones were docked to the interface site, and the complex of AhR with carvones was simulated for ~250 ns to allow the ligand to dock stably to AhR (Figure S7). Carvones bind favorably at a site formed by residues from the bHLH domain, including close contacts with Tyr76, Pro55, Phe83, Tyr137, Leu72, Pro91, Lys80, Ala79 and Phe136 (Figure S7). More significantly, the binding of carvones to this site shifts the position of both the  $\alpha 1$  and  $\alpha 2$  helical regions by 10–13 Å and significant unwinding of  $\alpha 1$  helix (Figure S7), which can affect the formation of the AhR-ARNT complex. By means of microscale thermophoresis using bacterially coexpressed fragments of human AhR (23–273) and mouse Arnt, we showed that carvones bind AhR but not Arnt (Fig. 4B). Although the binding of carvones to AhR was concentration dependent, the apparent binding constant  $K_D$  could not be determined since it lays in the low millimolar range, probably due to artificial conditions using truncated variants of AhR and Arnt. The interaction of carvones with AhR fragment spanning from amino acids

23 to 273, implies that the binding of carvones was localized outside the conventional ligand binding domain but within the bHLH/PAS-A region of AhR. These data fully support the hypothesis that carvones' non-competitive antagonism involves allosteric binding to AhR. In addition, D-limonene (deoxo analog of carvone) did not display AhR antagonism and did not bind human AhR (23–273), which reveals the importance of the oxo moiety in the carvone molecule for interaction with AhR, tentatively through hydrogen bonds (Figure S6A–C). We also observed non-specific displacement of <sup>3</sup>H-TCDD from mouse AhR by high concentrations of D-limonene (Figure S6D). To identify AhR amino acid residues involved in the interaction with carvones, we employed multiple approaches: (i) Thermal shift analyses using purified and cellular human AhR PAS-A domain (112–272) showed that carvones do not interact with PAS-A region of AhR (Fig. 4C). Since carvones bind AhR (23–273) fragment, as showed by microscale thermophoresis (Fig. 4B), it is likely that amino acid residue critical for carvone interaction with AhR is located in the region (23–111); (ii) Therefore, and taking in account the candidate residues identified by docking, we bacterially expressed and purified His-AhR (23–273) proteins mutated at Tyrosine 76 (Y76A, Y76F). Using microscale thermophoresis, we observed that binding of carvones was completely lost or strongly diminished in Y76A and Y76F mutants, respectively, as compared to wild type AhR (Fig. 4D); (iii) Finally, we used a technique of protein cross-linking with a photo-activated azido-labeled ligand. We synthesized N<sub>3</sub>-S-carvone (Figure S6E) and confirmed that it still exhibits AhR-antagonist capability against TCDD- and BaP-activated AhR (Figure S6F). By using MALDI, the recombinant AhR was identified in the control samples by 19 assigned tryptic peptides in the *m/z* range of 578.3–5207.5, which covered the

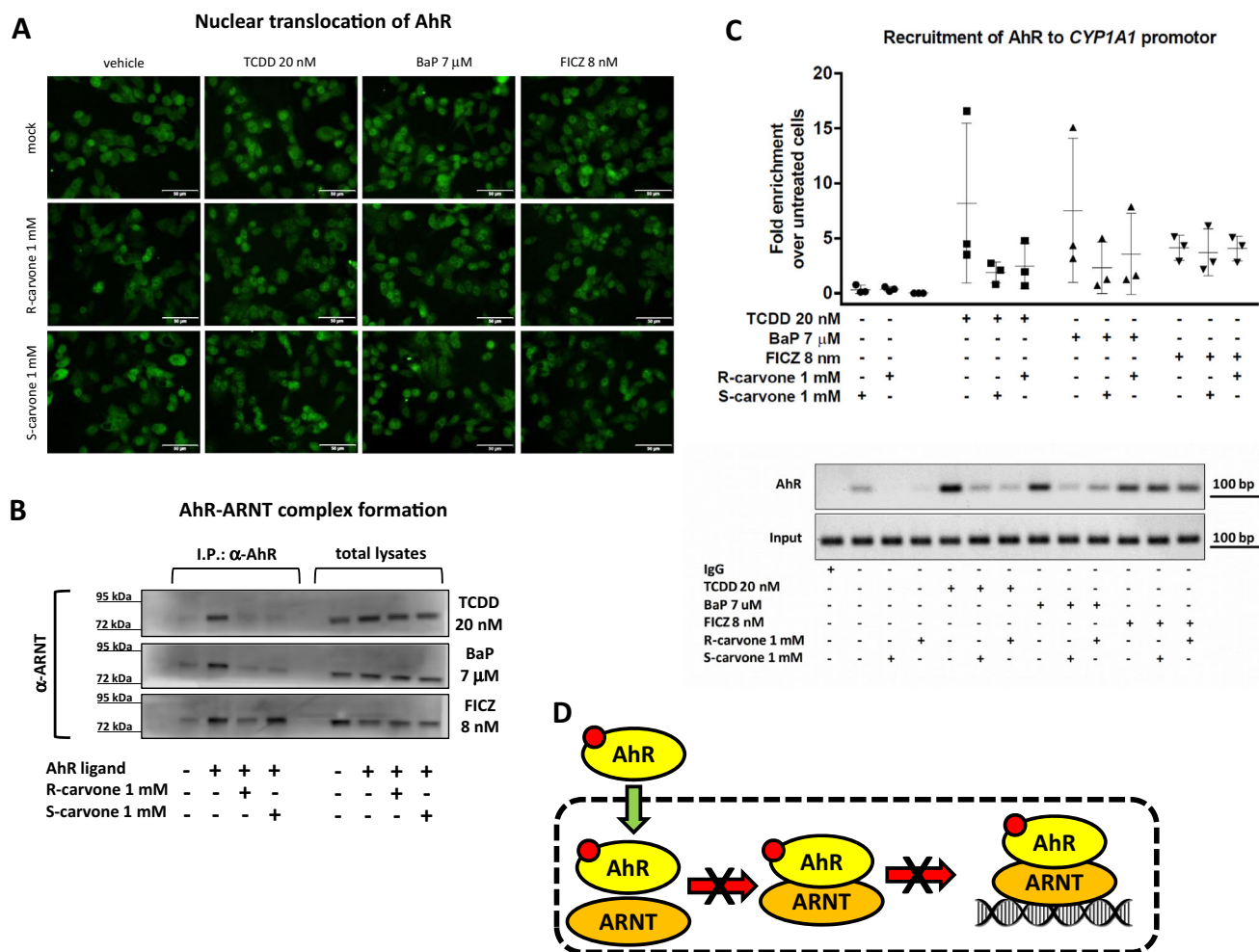


**Fig. 3 | Carvones influence the cellular functions of AhR.** Cells were incubated for 90 min with carvones (1000 μM) in combination with vehicle (0.1% DMSO) or AhR agonists TCDD (20 nM), BaP (7 μM), or FICZ (8 nM). **(A)** The nuclear translocation of AhR is not influenced by carvones. Microscopic specimens from LS180 cells were prepared using Alexa Fluor 488-labeled primary antibody against AhR and DAPI. AhR was visualized and evaluated using a fluorescence microscope. Experiments were performed in two consecutive cell passages (n = 2) with all tested compounds in duplicate. Representative images are shown. Scale bar = 50 μm. **(B)** Carvones inhibit the formation of AhR-ARNT heterodimers. Protein coimmunoprecipitation – formation of AhR-ARNT heterodimers in LS180 cells. Representative immunoblots of immunoprecipitated protein eluates and total cell lysates are shown.

Experiments were performed in three consecutive cell passages (n = 3). **(C)** Carvones inhibit the binding of AhR to the *CYP1A1* promoter. Chromatin immunoprecipitation ChIP – binding of AhR to the *CYP1A1* promoter in HepG2 cells. The bar graph (top) shows enrichment of the *CYP1A1* promoter with AhR compared to vehicle-treated cells. Representative DNA fragments amplified by PCR analyzed on a 2% agarose gel are from the 2<sup>nd</sup> experiment (bottom). Experiments were performed in three consecutive cell passages (n = 3). Data are shown as mean ± SD. **(D)** Schematic depiction of the cellular effects of carvones binding to AhR. Abbreviations: BaP, benzo[*a*]pyrene; FICZ, 6-formylindolo[3,2-*b*]carbazole; TCDD, 2,3,7,8-tetrachlorodibenzo-*p*-dioxin. Source data are provided as a Source Data file.

regions of 33–107 and 168–250, representing a major part of the recombinant protein and approximately 17% of the full-length native AhR sequence (Swiss-Prot database accession number AHR\_HUMAN P35869). Treatment with photoactivated N<sub>3</sub>-S-carvone yielded a tiny difference in the representation of peptide peaks. Two peptides were absent in the peptide fingerprint of AhR reacted with N<sub>3</sub>-S-carvone compared to the control (Fig. 4D): *m/z* 1036.6 and 1131.5, with the amino acid sequences 72-LSVSYLRAK-80 and 41-DRLNTELDLDR-49, respectively (confirmed by MS/MS sequencing). The former peptide has an alternative and preferred cleavage form, LSVSYLR, observable as a high peak at *m/z* 837.5, indicating a low affinity-labeling yield. A low-intensity peak at *m/z* 1199.6 corresponded to a mass difference of 163 Da, reflecting to the binding of the N<sub>3</sub>-S-carvone-derived nitrene moiety at LSVSYLRAK. However, due to the low intensity, we could not obtain direct confirmation by MS/MS sequencing. The photoactivation process itself performed well because N<sub>3</sub>-S-carvone, upon MALDI with the UV laser (measured in the presence of cetrimonium bromide in the matrix solution according to Guo et al.<sup>25</sup>), exhibited a peak at *m/z* 164,

indicating the loss of molecular nitrogen from the azido group. Altogether, considering data from molecular docking, microscale thermophoresis (S-carvone, D-limonene) and AhR covalent functionalization with photoactivated N<sub>3</sub>-S-carvone, Tyr76 is highly likely to play a key role in the allosteric binding of S-carvone to AhR.

#### S-carvone does not inhibit a random panel of protein kinases, including PKC

Blocking protein kinase C (PKC) activity was reported to inhibit the transcription of *CYP1A1* but to exert no effect on the nuclear translocation of AhR<sup>26</sup>, which was also the case here with carvones. Therefore, we tested whether carvones inhibit PKC catalytic activity. We did not observe any decline in PKC activity measured in lysates from HepG2 cells incubated with carvones at concentrations up to 1000 μM, which rules out the involvement of PKC inhibition in the effects of carvones on AhR (Fig. 5A). We also evaluated the interaction between 100 μM S-carvone and 468 human protein kinases, employing KINOMEScan™ (scanMAX assay), a proprietary active site-directed competition



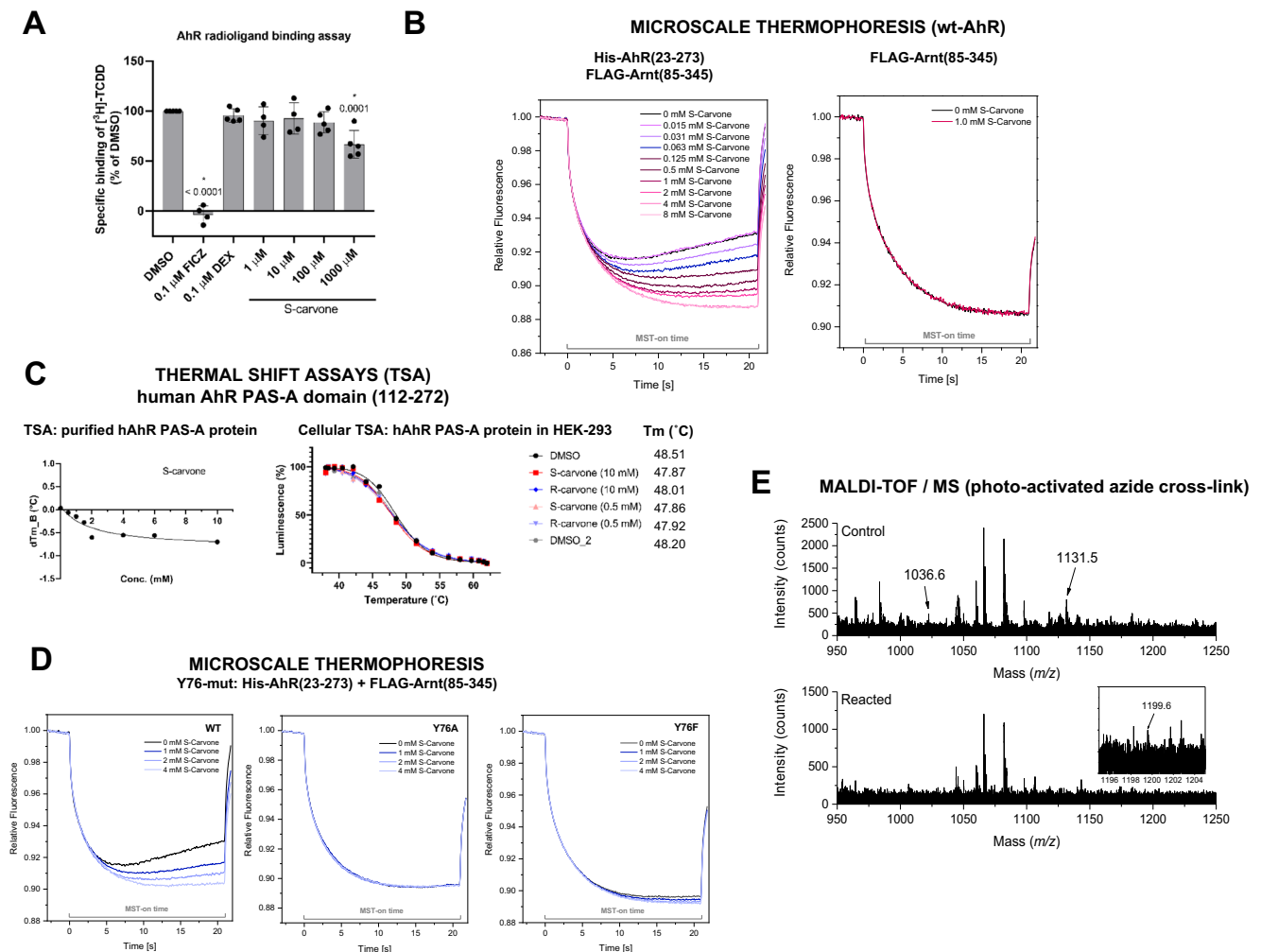


**Fig. 4 | Binding of S-carvone to AhR.** **A** Competitive radioligand binding assay: Cytosolic protein (2 mg/mL) from Hepa1c1c7 cells was incubated with S-carvone (1  $\mu$ M, 10  $\mu$ M, 100  $\mu$ M, 1000  $\mu$ M), FICZ (10 nM), DEX (100 nM; negative control) or DMSO (0.1% V/V); corresponding to *specific binding of [<sup>3</sup>H]-TCDD = 100%* in the presence of 2 nM [<sup>3</sup>H]-TCDD. Specific binding of [<sup>3</sup>H]-TCDD was determined to be the difference between total and nonspecific (200 nM; 2,3,7,8-tetrachlorodibenzofuran) reactions. The significance was calculated using 1way ANOVA multiple comparison test, and *p*-values are indicated in the graph. Four independent experiments (*n* = 4) were performed, and the incubations and measurements were performed in triplicate in each experiment (technical replicates). The error bars represent the mean  $\pm$  SD. **B** Microscale thermophoresis; *Left panel*: coexpressed His-AhR(23-273) + FLAG-Arnt(85-345) incubated with S-carvone (0.25 mM, 0.5 mM, 1 mM, 2 mM, 4 mM); *right panel*: FLAG-Arnt(85-345) incubated with vehicle or 1 mM S-carvone. **C** *Left panel*:

Thermal shift assay with purified hAhR PAS-A (112-272) protein incubated with S-carvone (0.5 mM, 1 mM, 1.5 mM, 2 mM, 4 mM, 6 mM, 10 mM); *right panel*: Cellular thermal shift analyses in Hek293 cell transfected with hAhR PAS-A (112-272) protein; incubations with S/R-carvones (0.5 mM and 10 mM). **D** Microscale thermophoresis: coexpressed (WT; mutY76A; mutY76F)-His-AhR(23-273) + FLAG-Arnt(85-345) incubated with S-carvone (0.25 mM, 0.5 mM, 1 mM, 2 mM, 4 mM). **E** MALDI-TOF MS of peptides from AhR tryptic digests: The top panel shows a detail of the control digest spectrum. The two labeled peptides (*m/z* 1036.6 and 1131.5) were absent after the reaction of AhR with photoactivated N<sub>3</sub>-S-carvone (bottom panel). The inset shows a close-up view of the reacted AhR digest spectrum to demonstrate the presence of a putatively modified peptide at *m/z* 1199.6, which might be related to that at *m/z* 1036.6 in the control. FICZ 6-formylindolo[3,2-*b*]carbazole, DEX dexamethasone, DMSO dimethylsulfoxide. Source data are provided as a Source Data file.

binding assay<sup>27</sup>. The minimal inhibitory threshold used by the screening platform KINOMEScan™ is 35% of the control kinase activity. Among 468 kinases tested, 467 were above the 35% cutoff. Tyrosine kinase 2 TK2 (JH2 domain pseudokinase) activity was inhibited to 27% of the control activity, but this kinase is not relevant to the regulation of transcription activity (Fig. 5B; Figure S9). Overall, we excluded the possibility that the effects of carvones on AhR signaling are caused indirectly by the inhibition of the human kinome, particularly PKC.

### Carvones do not inhibit ARNT transcriptional activity

ARNT is involved in other cellular pathways in addition to AhR, such as hypoxia signaling, which is transcriptionally mediated by the ARNT heterodimer with hypoxia-inducible factor 1 $\alpha$  (HIF1 $\alpha$ ). Therefore, we investigated the effects of carvones on the hypoxia-mimic inducible, ARNT-dependent expression of vascular endothelial

growth factor (*VEGF*) in HaCaT keratinocytes incubated with deferroxamine. The levels of *VEGF* mRNA were increased 5-fold by deferroxamine, and carvones at concentrations up to 1000  $\mu$ M did not influence this induction. Consistently, the hypoxia-mimic decrease in *CYP1A1* mRNA was not affected by carvones (Fig. 5C). These data imply that carvones do not inhibit ARNT transcriptional activity and that disruption of AhR-ARNT complex formation is not due to the interaction of carvones with ARNT. These observations corroborate the finding that carvones do not bind truncated recombinant Arnt (Fig. 4B).

### Carvones do not interact with AhR-related off-targets

Using radioligand binding assays, we showed that S-carvone (up to 1000  $\mu$ M) does not bind to human nuclear and steroid receptors that transcriptionally cross-talk with AhR, including androgen receptor

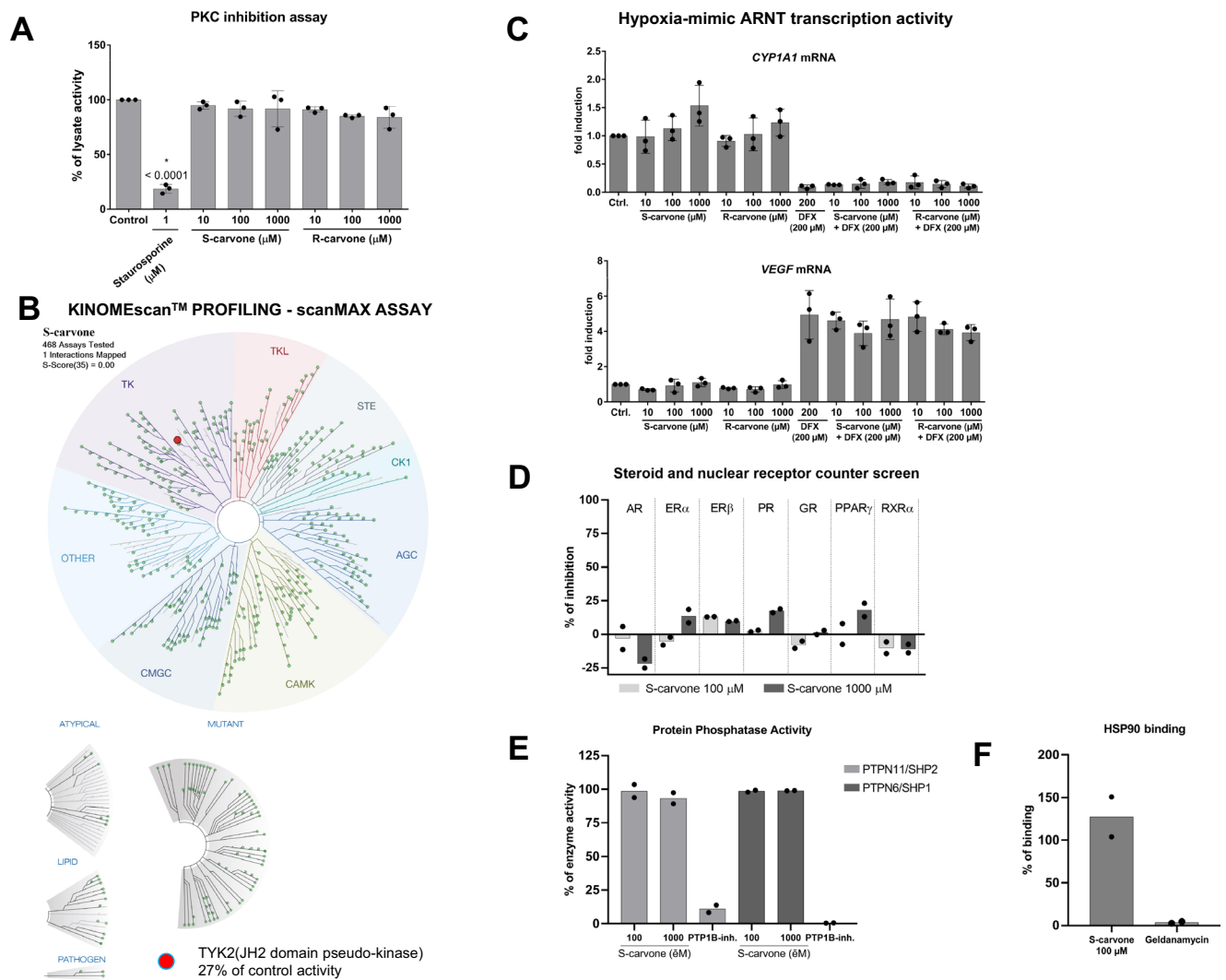


**Fig. 5 | Evaluation of off-target effects of carvones.** **A** PKC inhibition assay: The catalytic activity of PKC was measured in lysates from HepG2 cells incubated with vehicle (DMSO, 0.1% V/V), staurosporine (1 μM), and carvones (10 μM; 100 μM; 1000 μM). Data are the mean ± SD from three independent experiments ( $n = 3$ ). The significance was calculated using 2-way ANOVA multiple comparison test, and  $p$ -values are indicated in the graph. Incubations and measurements were performed in uniplicate (technical replicates). **B** KINOMEScan™ profiling: The interaction between 100 μM S-carvone and 468 human protein kinases, employing KINOMEScan™ (scanMAX assay), a proprietary active site-directed competition binding assay. A low-resolution interaction map is shown. **C** Hypoxia-mimic *VEGF* induction: HaCaT cells were incubated for 24 h with carvones (10 μM; 100 μM; 1000 μM) in combination with vehicle (0.1% DMSO) or deferoxamine (DFX; 200 μM). The expression of *VEGF* and *CYP1A1* mRNAs was measured using RT-PCR. Incubations and measurements were performed in duplicate (technical replicates). Data are the mean ± SD from three independent cell passages ( $n = 3$ ) and are expressed as fold induction over the vehicle-treated cells. The results were normalized using *GAPDH* as a housekeeping gene. **D** Counterscreen radioligand binding assay with human AR, ERα, ERβ, PR, GR, RXRα, and PPARγ receptors. The

bar graph shows the percentage of displacement of the radioligand by S-carvone (100 μM; 1000 μM). The data are mean from two independent incubations ( $n = 2$ ). A value >50% is considered to indicate interaction. **E** Protein phosphatase inhibition assay: The catalytic activity of PTPN11/SHP2 and PTPN6/SHP1 was measured with recombinant enzymes incubated with vehicle (DMSO, 0.1% V/V), PTP1B inhibitor (33.3 μM), and S-carvone (100 μM; 1000 μM). Data are the mean from two independent experiments ( $n = 2$ ). Incubations and measurements were performed in duplicate (technical replicates). **F** Competitive fluorescence binding assay for HSP90: The bar graph shows the percentage displacement of fluorescently labeled geldanamycin by S-carvone (100 μM) and nonlabeled geldanamycin (0.12 μM). Data are the mean from two independent experiments ( $n = 2$ ). Incubations and measurements were performed in duplicate (technical replicates). AR androgen receptor, ARNT AhR nuclear translocator, DFX deferoxamine, ERα/β estrogen receptor alpha/beta, GR glucocorticoid receptor, HSP90 heat shock protein 90 kDa, PKC protein kinase C, PPARγ peroxisome proliferator-activated receptor gamma, PR progesterone receptor, PTPN6(11)/SHP1(2) tyrosine-protein phosphatases non-receptor type 6(11), RXRα retinoid X receptor alpha, VEGF vascular endothelial growth factor. Source data are provided as a Source Data file.

(AR), retinoid X receptor alpha (RXRα), glucocorticoid receptor (GR), progesterone receptor (PR), estrogen receptors alpha/beta (ERα/β) and peroxisome proliferator-activated receptor gamma (PPARγ) (Fig. 5D). S-carvone did not inhibit the catalytic activity of the non-receptor-type tyrosine-protein phosphatases PTPN11/SHP2 and PTPN6/SHP1, which are critical in regulating the AhR stress response (Fig. 5E). Finally, S-carvone did not displace geldanamycin from binding to heat shock protein 90 kDa, which is a cytosolic binding partner of AhR (Fig. 5F).

### Carvones antagonize AhR in mouse skin

We carried out a study on live mouse skin to determine the antagonistic effects of carvones on ligand-activated AhR (Fig. 6A). The topical application of BaP to mouse outer ears (auricles) induced *Cyp1a1* mRNA expression, and this induction was inhibited (62% inhibition) in mouse ears preincubated with S-carvone (Fig. 6B). The involvement of AhR in skin inflammation and the modulation of inflammatory mediators by AhR ligands has been reported<sup>28</sup>. Irradiation of mouse ears with ultraviolet (UV) light caused the induction of

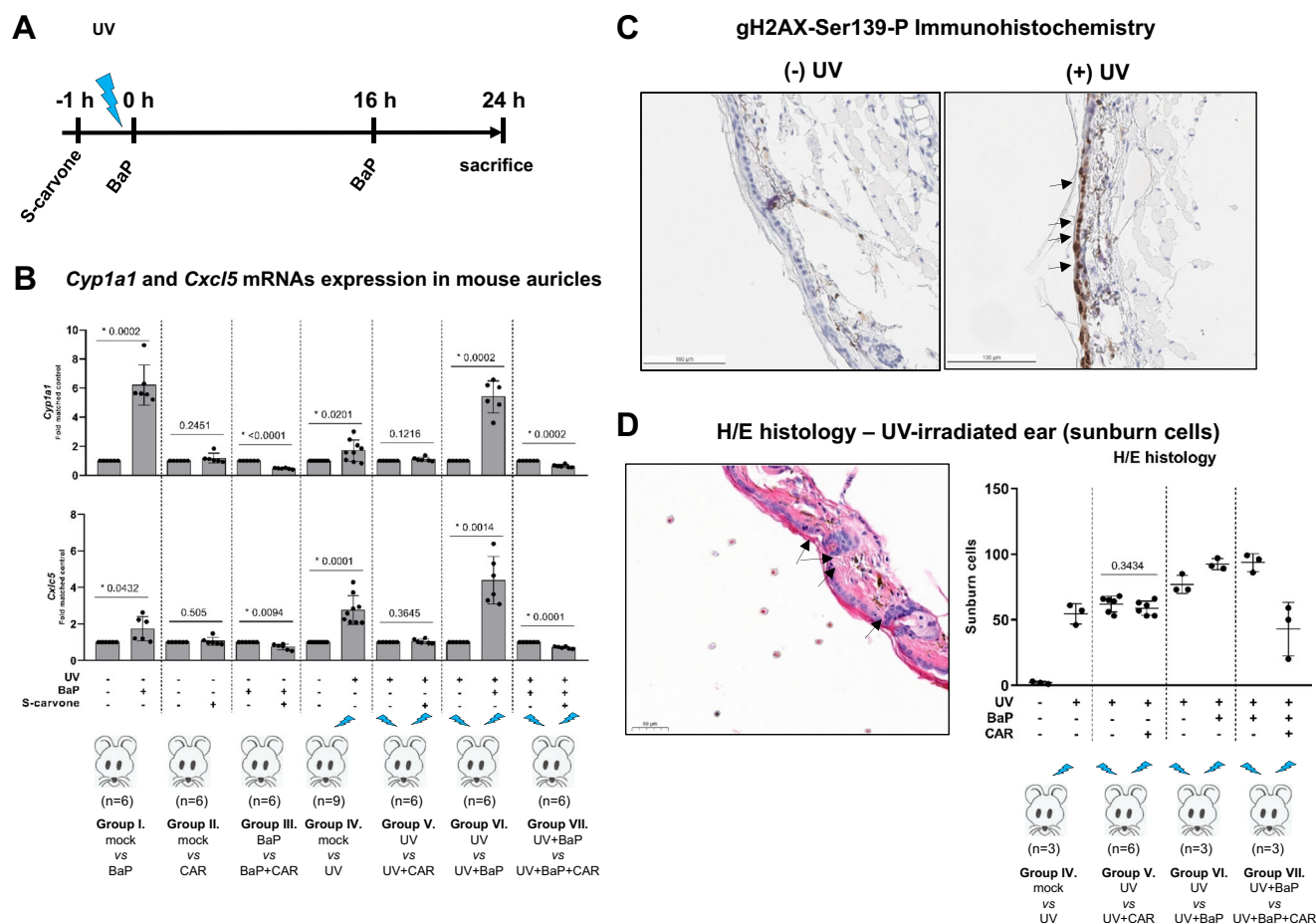


**Fig. 6 | Carvones antagonize AhR in vivo.** Tested compounds and UV irradiation were applied to C57BL/6 mouse auricles as described in the Methods section. The left and right ears were exposed to different treatments, thereby providing internal individual controls for comparative treatments, and each animal represents a biological repeat. **A** Scheme of the treatment. **B** RT-PCR analyses of *Cyp1a1* and *Cxcl5* mRNAs were performed in quadruplicate. The results are expressed as a ratio between the left and right ears of an individual mouse. Data are the mean  $\pm$  SD from at least six mice *per* treatment group. The results were normalized using *Rplp0* as a housekeeping gene. The data normality was tested by Shapiro-Wilk test. The significance was calculated using one-sample two-tailed t-test, and *p*-values are indicated in the graph. **C** Immunohistochemistry: Representative control and UV-

exposed mouse ear tissues stained with an antibody against  $\gamma$ H2AX-Ser-P are shown. The analyses were performed in ear tissue from six mice ( $n = 6$ ). Scale bar = 100  $\mu$ m. **D** Histology: Representative UV-exposed mouse ear tissue stained with hematoxylin & eosin is shown. The scatter plot shows the count of UV-burned cells in the left and right ears of an individual mouse. Data are the mean  $\pm$  SD from three mice *per* treatment group. The significance was calculated using paired two-tailed t-test, and *p*-value is indicated in the group UV *vs* UV+carvone group ( $n = 6$ ). Scale bar = 50  $\mu$ m. BaP benzo[a]pyrene, CAR S-carvone, *CYP1A1* cytochrome P450 1A1, *CXCL5* C-X-C motif chemokine 5, H/E hematoxylin/eosin stain. Source data are provided as a Source Data file.

the proinflammatory chemokine *Cxcl5*, and postirradiation application of BaP further increased the levels of UV-inducible *Cxcl5*. Carvones reversed (38% inhibition) the induction of *Cxcl5* levels by BaP in UV-irradiated mouse ears (Fig. 6B), which is of potential clinical importance because *Cxcl5* was identified as a target gene associated with UV irradiation-induced inflammatory pain in sunburn subjects<sup>29</sup>. Immunohistochemical staining with  $\gamma$ H2AX-Ser139-P antibody confirmed widespread DNA damage<sup>30</sup> in UV-irradiated mouse ears (Fig. 6C). The aggravating effect of BaP on UV-induced tissue damage was attenuated by carvones, as revealed by the sunburn cell count<sup>31</sup> of hematoxylin/eosin-stained histology samples (Fig. 6D). Of note, S-carvone itself did not influence the number of UV-burned cells, regardless of its application prior (Fig. 6D) or post (Figure S8) UV-exposure. These data disprove potential shielding effect of S-carvone against UV-irradiation.

## Discussion

Therapeutic targeting of AhR has long been neglected, mainly due to the negative impression of AhR being a receptor mediating TCDD toxicity. With increasing knowledge of the physiological and pathophysiological roles of AhR, attempts to target AhR have emerged,

including the therapy of cancer, inflammatory bowel disease, and atopic dermatitis. The following strategies are employed: (i) repositioning of clinically used AhR-active drugs (e.g., tranilast, flutamide, omeprazole); (ii) chemoprevention with dietary AhR-active compounds (e.g., indole-3-carbinol, diindolylmethane); and (iii) the application of novel AhR ligands identified by screening chemical libraries (e.g., CH223191)<sup>8</sup> or by rational design (e.g., PY109)<sup>32</sup>.

The interactions between small-molecule compounds and AhR signaling may occur directly (ligand-dependent) or indirectly through off-targets such as PKC<sup>26</sup>, protein tyrosine kinases<sup>33</sup>, or cAMP<sup>34</sup>. To date, all reported AhR ligands, both agonists and antagonists, are orthosteric ligands, i.e., ligands that bind to a conventional discrete site on the AhR protein, referred to as the ligand binding pocket. Recently, three structurally distinct groups of AhR orthosteric ligands were defined according to the mode of their interactions with residues within the AhR ligand binding site<sup>35</sup>. Functionally, the effects of AhR ligands comprise full agonists, partial agonists, and competitive antagonists. This report describes small-molecule compounds acting as allosteric antagonists of human AhR, which may potentially be of clinical importance. Allosteric approaches to inhibiting receptors

circumvent any dependence on ligand binding or the nature of the ligand involved<sup>36</sup>.

Applying a series of complementary mechanistic experiments, we demonstrated that carvones are noncompetitive antagonists of human AhR, acting through allosteric binding in the region of the AhR involved in heterodimerization with ARNT, thereby preventing the formation of functional AhR-ARNT heterodimers. In brief, detailed analyses of the AhR transcriptional response in reporter gene assays revealed a noncompetitive mechanism of carvone antagonism. This is consistent with the finding that carvones did not displace <sup>3</sup>H-TCDD from binding AhR and did not inhibit the ligand-elicited nuclear translocation of AhR. On the other hand, carvones inhibited the formation of AhR-ARNT heterodimers, and all downstream events involving the binding of AhR to DNA and the expression of AhR target genes. We excluded the interactions of carvones with potential off-targets, including ARNT, PKC, a panel of 468 kinases, steroid receptors (AR, ER $\alpha$ , ER $\beta$ , PR, GR), nuclear receptors (RXR $\alpha$ , PPAR $\gamma$ ), protein phosphatases (PTPN11/SHP2, PTPN6/SHP1) and heat shock protein 90 kDa (HSP90). As a proof of concept, we demonstrated the AhR antagonist effects of carvones in vivo. First, carvones inhibited the BaP-inducible xenobiotic-metabolizing *Cyp1a1* in mouse skin. Second, carvones reversed the BaP-mediated potentiation of the UV-inducible chemokine *Cxcl5*, which was previously found to be accountable for UVB irradiation-induced inflammatory pain<sup>29</sup>. In our exploratory proof-of-concept and hypothesis generation experiment, carvones also attenuated the harmful effects of BaP, as revealed by the sunburn cell count. In UVB-irradiated skin, AhR signaling pathways are activated by FICZ and related tryptophan photoproducts and facilitate cutaneous inflammatory responses and skin carcinogenesis<sup>37</sup>. We have earlier shown that a topical application of the competitive antagonist BDDI inhibits AHR dependent signaling in UVB-irradiated human skin<sup>38</sup>. Our current data indicate that the topical application of carvones to sunburned skin might reduce *Cxcl5*-related inflammatory symptoms and pain.

Differential roles of the AhR and ARNT residues in molecular events preceding and following heterodimerization of AhR with ARNT were determined by Corrada et al.<sup>39,40</sup>. The crystal structure of the mouse Ahr PAS-A domain revealed that mouse Ahr residues Ala119 and Leu120 are critically crucial for hydrophobic interactions at the Ahr-Arnt interface and dimerization<sup>41</sup>. Seok et al. determined the crystal structure of a mouse Ahr-Arnt heterodimer in complex with DRE, showing that Arnt curls around Ahr into a highly intertwined asymmetric architecture, with extensive heterodimerization interfaces and interdomain interactions within Ahr. They proposed the phenomenon of ligand-selective structural hierarchy for complex scenarios of Ahr activation<sup>24</sup>. Mutations in mouse Ahr residues Leu42 and Leu120 (homologous to human Leu43 and Leu122) led to decreased binding of Ahr-Arnt to DRE<sup>24</sup>, which corroborates the findings of Wu et al.<sup>41</sup>. The mutation of Leu49 in mouse Ahr maintained the nuclear translocation of Ahr but inhibited its transcriptional activity<sup>24</sup>, which was mimicked by the binding of carvones to AhR. According to our docking data, carvones interact with residues in the bHLH domain, and the proposed docking models show that the binding of carvones directly affects the dimerization interface with a helical shift of 10–13 Å and significant unwinding of the  $\alpha$ 1 helix (Figure S7). This assumption was experimentally confirmed, and direct binding of carvones at the AhR fragment spanning from amino acids 23 to 273 was demonstrated using microscale thermophoresis. The significance of the oxo moiety in the carvone molecule for interaction with AhR, tentatively through hydrogen bonds, was demonstrated because deoxy-carvone (D-limonene) did not bind the AhR fragment and did not antagonize AhR. By using the Achilles Blind Docking Server (<http://bio-hpc.eu/software/blind-docking-server/><sup>42</sup>), we calculated that the target residues for the photoactivable derivative N<sub>3</sub>-S-carvone include Leu47, Phe56, Leu72

and Tyr76. Indeed, we demonstrated that the peptides absent from the AhR digest after the reaction with N<sub>3</sub>-S-carvone contained the predicted sites (Fig. 4E). Microscale thermophoresis using Y76A and Y76F mutants of AhR(23-273) revealed the importance of tyrosine Y76 for interaction with carvones. The biological effects of carvones against AhR were attained at concentrations spanning from 100  $\mu$ M to 1000  $\mu$ M, which might appear high; however, the available data suggest that these concentrations are relevant. The topical application of 300 mg of R-carvone or S-carvone, which are used as skin permeabilizers in transdermal patches, resulted in maximal plasma concentrations of  $\sim$ 0.6  $\mu$ M and  $\sim$ 0.2  $\mu$ M, respectively<sup>20</sup>. Moreover, the local concentrations of carvones in the skin, after topical application must be orders of magnitude higher than the plasma levels. The blood levels of carvone in volunteers who received 100 mg of caraway oil ( $\sim$ 54.5 mg carvone) in coated capsules reached approx. 0.1  $\mu$ M<sup>43</sup>. However, local concentrations of carvones in the intestines (intestinal first-pass) and liver (hepatic first-pass) must be much higher than those reached in the plasma. The concentration of carvones in foods is approximately 150  $\mu$ M, implying the exposure of enterocytes to such concentrations when consuming food containing EOs of caraway, spearmint, or dill<sup>44</sup>. The European Food Safety Authority EFSA defined the acceptable daily intake of S-carvone as 0.6 mg/kg of body weight. In addition, a recent estimate based on the recommended dose and the published fecal excreted fraction of 200 marketed drugs reported a median expected colon concentration of 80  $\mu$ M for drugs having a median serum concentration of 0.6  $\mu$ M, implying globally >100-fold higher drug concentrations in the gut compared to blood<sup>45</sup>. Collectively, the potential clinical or preventive use of carvones as AhR antagonists is indicated by their local (not systemic) effects on the skin (topical application) or in the intestines (*per os* intake).

In summary, we report dietary monocyclic monoterpenoid carvones, as noncompetitive antagonists of AhR that act through allosteric binding to AhR, thereby blocking heterodimerization with ARNT and constraining the transcriptional functions of AhR-ARNT. While hundreds of orthosteric AhR ligands, including antagonists, have been described, here we report the allosteric antagonism of AhR by small-molecule compounds, which might be of both clinical and fundamental mechanistic importance.

## Methods

The research complied with all relevant ethical regulations; (i) Human hepatocytes cultures—the tissue acquisition protocol issued by the “Ethical Committee of the Faculty Hospital Olomouc, Czech Republic”; (ii) Animal experiments—approved by the Institutional Animal Care and Use Committee of the Albert Einstein College of Medicine (New York, NY, USA; Protocol #00001405).

## Chemicals and materials

S-carvone (sc-239480, purity 99.4%, Lot L0613), R-carvone (sc-293985, purity 99.7%, Lot H1015), indole (sc-257606, purity 98.4%, Lot J0918), 3-methylindole (sc-256535, purity 99.9%, Lot E0418), indirubin (sc-201531A, purity 96.5%, Lot B1513), and D-limonene (sc-205283, Lot F1314) were purchased from Santa Cruz Biotechnology. BaP (B1760, Lot SLBS0038V, purity 99%), FICZ (SML1489, Lot 0000026018, purity 99.5%), staurosporine (S4400, purity 98%), deferroxamine mesylate (DFX; D9533, purity 92.5%), cuminal (W293318, purity 99.7%, Lot MKCF1644), p-cymene (C121452, purity 99.4%, Lot MKCG5957), cuminaldehyde (#135178, purity 99.6%, Lot MKCC7110), (+)-dihydrocarvone (#218286, purity 99.9%, Lot MKBN2588v), R-pulegone (#376388, purity 99.7%, Lot MKCF5536), S-pulegone (#328847, purity 98.0%, Lot 1433568), thymol (T0501, purity 99.5%, Lot SLBZ9699), carvacrol (W224511, purity 99.9%, Lot MKCG2266), (+)-menthone (#63675, purity 98.6%, Lot BCCCI798), (-)-menthone (W266701, purity 98.7%, Lot STBH6314), piperitone (#79899, purity 98.3%, Lot BCBZ9676), and dexamethasone (DEX; D4902, Lot 112K12845, purity 98%) were obtained



from Sigma-Aldrich (Prague, Czech Republic). TCDD (RPE-029) was purchased from Ultra Scientific, and 2,3,7,8-tetrachlorodibenzofuran (TCDF; AmbI7620425, Lot 51207-31-9) was obtained from Ambinter. (+)-isomenthone (MI99545, purity 96.7%, Lot 1-NKM-85-3), and (-)-isomenthone (MI99560, purity 80%, Lot 1-NKM-97-3) were obtained from Toronto Research Centre Inc. (Toronto, Canada). Piperitenone (#491-09-8, purity 95.0%, Lot BS17ZJ05212) was acquired from BOC Sciences (Shirley, NY, USA). Radiolabeled [<sup>3</sup>H]-TCDD (ART 1642, Lot 181018, purity 98.6%) was purchased from American Radiolabeled Chemicals. Bio-Gel® HTP hydroxyapatite (1300420, Lot 64079675) was obtained from Bio-Rad Laboratories.

### Cell lines and hepatocytes

The human hepatoma cell line HepG2 (ECACC No. 85011430), the intestinal human colon adenocarcinoma cell line LS180 (ECACC No. 87021202), the human immortalized keratinocyte line HaCaT (kindly donated by P. Boukamp, IUF Düsseldorf, Germany), and the mouse hepatoma cell line Hepa1c1 (ECACC No. 95090613) were cultured as recommended by the supplier. The primary human hepatocytes LH75 (female, 78 years, Caucasian) were prepared at the Faculty of Medicine, Palacky University Olomouc. The tissue acquisition protocol complied with the regulation issued by the “Ethical Committee of the Faculty Hospital Olomouc, Czech Republic” and Transplantation law #285/2002 Coll (which implies presumed consent from donor). The primary human hepatocytes Hep200571 (male, 77 years, unknown ethnicity) and Hep220993 (female, 76 years, Caucasian) were purchased from Biopredic International (Rennes, France). Mycoplasma Detection Kit-Digital Test v2.0 Cat. No. B39132 (Biotool) was used to survey mycoplasma infection. The study involving human tissue samples was conducted in accordance with the declaration of Helsinki.

### Reporter gene assays

The stably transfected gene reporter cell line AZ-AHR, derived from the human hepatoma cell line HepG2, expressing endogenous AhR and transfected with a construct containing several AhR binding sites upstream of a luciferase reporter gene, was used to evaluate the transcriptional activity of AhR<sup>21</sup>. Cells were seeded in 96-well culture plates, and after 16 h of stabilization, they were incubated for 4 h and 24 h with the tested compounds or their combinations. Thereafter, the cells were lysed, and luciferase activity was measured on a Tecan Infinite M200 Pro plate reader (Schoeller Instruments, Czech Republic). The half-maximal inhibitory concentrations (IC<sub>50</sub>), half-maximal effective concentrations (EC<sub>50</sub>), and concentrations of EC<sub>80</sub> were calculated using GraphPad Prism 8 software (GraphPad Software, San Diego, U.S.A.). Experiments were performed in three independent cell passages. Incubations and measurements were performed in quadruplicate (i.e., four technical replicates).

### Inhibition of luciferase catalytic activity

Stably transfected AZ-AHR cells and COS-7 cells transiently transfected with DRE-luc reporter plasmid were incubated for 24 h with 20 nM TCDD. Cells were lysed and the lysate containing luciferase was incubated for 30 min with carvones (1000 μM) or vehicle (control). Luciferase activity was measured on a 446 Tecan Infinite M200 Pro plate reader (Schoeller Instruments, Czech Republic).

### Cell viability—MTT test

Cells were incubated for 24 h with carvones, vehicle (DMSO; 0.1% v/v) and Triton X-100 (1%, v/v), using multi-well culture plates of 96 wells. MTT test was performed and absorbance was measured spectrophotometrically at 540 nm on Infinite M200 (Schoeller Instruments, Prague, Czech Republic). The data were expressed as the percentage of cell viability, where 100% and 0% represent the treatments with the vehicle and Triton X-100, respectively.

### Quantitative real-time polymerase chain reaction qRT-PCR

Total RNA from cultured cells was isolated using TRI Reagent® (Sigma-Aldrich). cDNA was synthesized from 1 μg of total RNA using M-MuLV Reverse Transcriptase and Random Primers 6 (both New England Biolabs) at 42 °C for 60 min and diluted at a 1:4 ratio with PCR grade water. qRT-PCR was carried out on a Light Cycler® 480 Instrument II (Roche). Data were processed by the delta-delta C<sub>t</sub> method and normalized to *GAPDH* as a housekeeping gene. In animal experiments, cDNA was synthesized from 2 μg of total RNA using a High Capacity cDNA Reverse Transcription Kit (Thermo Fisher Scientific, #4368814). qRT-PCR was performed using PowerUp SYBR Green Master Mix (Thermo Fisher, #A25742) on a ViiA Y Real-Time PCR System (Thermo Fisher Scientific, USA). The levels of individual mRNAs were determined using the probes and primers listed in Table S1.

### Simple Western blotting by Sally Sue™

The total protein extract was isolated by using ice-cold lysis buffer (150 mM NaCl; 10 mM Tris pH 7.2; 1% (v/v) Triton X-100; 0.1% (w/v) SDS; 1% (v/v) sodium deoxycholate; 5 mM EDTA; anti-protease cocktail; anti-phosphatase cocktail), and the protein concentration was determined using Bradford reagent. CYP1A1 and β-actin proteins were detected by the Sally Sue™ Simple Western System (ProteinSimple™) using Compass Software version 2.6.5.0 (ProteinSimple™). Immunodetection was performed using primary antibodies against CYP1A1 (mouse monoclonal, sc-393979, A-9, dilution 1:100, Santa Cruz Biotechnology) and β-actin (mouse monoclonal, 3700 S, dilution 1:100, Cell Signaling Technology). Detection was performed by horseradish-conjugated secondary antibody followed by a reaction with a chemiluminescent substrate. Full scan blots are available at <https://doi.org/10.5281/zenodo.7764002>.

### 7-Ethoxyresorufin-O-deethylase activity (EROD)

AZ-AHR cells plated in 96-well culture dishes were incubated for 24 h with vehicle (DMSO; 0.1% v/v), TCDD (13.5 nM) and/or S-carvone (1 mM) + TCDD (13.5 nM). After washing with PBS, medium containing 7-ethoxyresorufin (8 μM) and dicoumarol (10 μM) was applied to the cells. Culture plates were incubated at 37 °C for 30 min. After that, an aliquot of 75 μl of the medium was mixed with 125 μl of methanol, and fluorescence was measured in a 96-well plate with 530 nm excitation and 590 nm emission filters using a Tecan Infinite M200 Pro plate reader (Schoeller Instruments, Czech Republic).

### Radioligand binding assays

**Aryl hydrocarbon receptor.** Cytosol from murine hepatoma Hepa1c1c7 cells was isolated as described<sup>46</sup>. Cytosolic protein (2 mg/ml) was incubated for 2 h at room temperature in the presence of 2 nM [<sup>3</sup>H]-TCDD with S-carvone (1 μM, 10 μM, 100 μM, 1000 μM), D-limonene (10 μM, 100 μM, 1000 μM), FICZ (10 nM; positive control), DEX (100 nM; negative control) or vehicle (DMSO; 0.1% V/V; corresponds to *specific binding of [<sup>3</sup>H]-TCDD = 100%*). Ligand binding to the cytosolic proteins was determined by the hydroxyapatite binding protocol and scintillation counting. The specific binding of [<sup>3</sup>H]-TCDD was determined as the difference between total and nonspecific (TCDF; 200 nM) reactions. Five independent experiments were performed, and the incubations and measurements were performed in triplicate (three technical replicates) in each experiment.

A radioligand binding assay counterscreen (with 100 μM and 1000 μM S-carvone) was carried out in a series of human recombinant steroid and nuclear receptors at Eurofins Panlabs Discovery Services Taiwan (New Taipei City, Taiwan) and Eurofins Cerep SA (Poitiers, France):

**Glucocorticoid receptor (GR; NR3C1).** Endogenous receptor from IM-9 cells. The model ligand was 1.5 nM [<sup>3</sup>H]-dexamethasone, and the nonspecific competitor was 10 μM triamcinolone. The incubation time was 6 h at 4 °C.



**Androgen receptor (AR; NR3C4).** Endogenous receptor from LNCaP cells. The model ligand was 1 nM [<sup>3</sup>H]-methyltrienolone, and the non-specific competitor was 1 μM testosterone. The incubation time was 24 h at 4 °C.

**Progesterone receptor (PR; NR3C3).** Endogenous receptor from T47D cells. The model ligand was 0.5 nM [<sup>3</sup>H]-progesterone, and the nonspecific competitor was 1 μM promegestone. The incubation time was 20 h at 4 °C.

**Estrogen receptor alpha (ERα; NR3A1).** Recombinant receptor expressed in sf9 cells. The model ligand was 0.5 nM [<sup>3</sup>H]-estradiol, and the nonspecific competitor was 1 μM diethylstilbestrol. The incubation time was 2 h at room temperature.

**Estrogen receptor beta (ERβ; NR3A2).** Recombinant receptor expressed in sf9 cells. The model ligand was 0.5 nM [<sup>3</sup>H]-estradiol, and the nonspecific competitor was 1 μM diethylstilbestrol. The incubation time was 2 h at 25 °C.

**Peroxisome proliferator-activated receptor gamma (PPARγ; NR1C3).** Recombinant receptor expressed in *E. coli*. The model ligand was 5 nM [<sup>3</sup>H]-rosiglitazone, and nonspecific competitor was 10 μM rosiglitazone. The incubation time was 2 h at 4 °C.

**Retinoid X receptor alpha (RXRα; NR2B1).** Recombinant receptor expressed in sf9 cells. The model ligand was 5 nM [<sup>3</sup>H]-9-cis-retinoic acid, and nonspecific competitor was 3 μM 9-cis-retinoic acid. The incubation time was 1 h at 4 °C.

#### Intracellular distribution of AhR

An immunofluorescence assay was performed as recently described<sup>47</sup>. Briefly, LS180 cells were seeded on chamber slides (ibidi GmbH, Germany) and cultured for two days. Then, the cells were treated for 90 min with tested compounds in combination with vehicle (0.1% DMSO) or the AhR agonists TCDD (20 nM), BaP (7 μM), and FICZ (8 nM). After treatment, washing, fixation, permeabilization, and blocking, the cells were incubated with Alexa Fluor 488-labeled primary antibody against AhR (sc-133088, Santa Cruz Biotechnology, U.S.A.) diluted 1:500 in 0.5% bovine serum albumin at 4 °C overnight. The next day, nuclei were stained with 4',6-diamino-2-phenylindole (DAPI), and cells were mounted in VectaShield® Antifade Mounting Medium (Vector Laboratories Inc., USA). AhR translocation into the nucleus was visualized and evaluated using an IX73 fluorescence microscope (Olympus, Japan). The whole staining protocol was performed in two independent experiments in technical duplicates (with all tested compounds). AhR translocation was evaluated visually depending on the distinct signal intensity of the AhR antibody in the nucleus and cytosol. For percentage calculation, approximately one hundred cells from at least four randomly selected fields of view in each replicate were used.

#### Protein immunoprecipitation assay

The effects of carvones on the ligand-dependent heterodimerization of AhR with ARNT were studied in cell lysates from LS180 cells incubated with tested compounds in combination with vehicle (0.1% DMSO) or the AhR agonists TCDD (20 nM), BaP (7 μM) and FICZ (8 nM) for 90 min at 37 °C. Pierce™ Co-Immunoprecipitation Kit (Thermo Fisher Scientific) was used. In brief, 25 μg of AhR antibody (mouse monoclonal, sc-133088, A-3, Santa Cruz Biotechnology) was covalently coupled to resin for 120 min at room temperature. The antibody-coupled resin was incubated with cell lysate overnight at 4 °C. In parallel with total parental lysates, eluted protein complexes were diluted in delivered sample buffer and resolved on 8% SDS-PAGE gels followed by Western blot analysis and immunodetection with ARNT 1 antibody (mouse monoclonal, sc-17812, G-3, Santa Cruz Biotechnology). Chemiluminescent

detection was performed using horseradish peroxidase-conjugated anti-mouse secondary antibody (7076S, Cell Signaling Technology) and WesternSure® PREMIUM Chemiluminescent Substrate (LI-COR Biotechnology) by a C-DiGit® Blot Scanner (LI-COR Biotechnology). Full scan blots are available at <https://doi.org/10.5281/zenodo.7764002>.

#### Chromatin immunoprecipitation assay

The assay was performed as recently described<sup>47</sup>. Briefly, HepG2 cells were seeded in a 60-mm dish, and the following day, they were incubated with carvones (1000 μM) in combination with vehicle (0.1% DMSO) or the AhR agonists TCDD (20 nM), BaP (7 μM), and FICZ (8 nM) for 90 min at 37 °C. The procedure followed the manufacturer's recommendations for the SimpleChIP Plus Enzymatic Chromatin IP kit (Magnetic Beads) (Cell Signaling Technology; #9005). Anti-AhR rabbit monoclonal antibody was purchased from Cell Signaling Technology (D5S6H; #83200). *CYP1A1* promoter primers were (fw: AGCTAGGC-CATGCCAAAT, rev: AAGGGTCTAGGTCTGCGTGT-3'). Experiments were performed in three consecutive cell passages. Full scan gels are available at <https://doi.org/10.5281/zenodo.7764002>.

#### Protein kinase C inhibition assay

Protein kinase C (PKC) inhibition was assayed in HepaG2 cell lysates using a PKC Kinase Activity Assay Kit (ab139437; Abcam). Cells were grown to 90% confluency in a 60 mm dish. After removal of the medium, 1 mL of lysis buffer (E4030, Promega) was applied for 10 min on ice. Cells were scraped, sonicated, and centrifuged at 15,900 × g/15 min/4 °C (Eppendorf Centrifuge 5415 R; Eppendorf, Stevenage, U.K.). Then, 3 μL of cell lysate was mixed with 297 μL of kinase assay buffer, and 40 μL aliquots were transferred into 0.5 mL microtubes. These aliquots were mixed with 1/100 stock solutions of carvones to obtain final concentrations of 10 μM, 100 μM, and 1000 μM. DMSO (1% V/V) and staurosporine (1 μM) were used as negative and positive controls, respectively. The reaction was initiated by the addition of 10 μL of reconstituted ATP, and the rest of the procedure was performed as described in the manufacturer's recommendations. Absorbance was measured at 450 nm using an Infinite M200 microplate reader (TECAN, Austria). The results are expressed as a percentage of the negative control. The cell lysate was stored at -80 °C and used in performing three independent experiments.

#### KINOMEScan™ profiling

The KINOMEScan™ screening platform (scanMAX assay) employs a proprietary active site-directed competition binding assay that quantitatively measures the interactions between test compounds (here 100 μM S-carvone) and 468 human protein kinases<sup>27</sup>. The assay was performed at Eurofins DiscoverX Corp. (Fremont, CA, USA).

#### Tyrosine-protein phosphatase non-receptor-type inhibition assays

The catalytic activity of PTPN11/SHP2 and PTPN6/SHP1 was measured with recombinant enzymes incubated with vehicle (DMSO, 0.1% V/V), PTP1B inhibitor (33.3 μM), and S-carvone (100 μM; 1000 μM). The phosphatase activities were monitored as a time-course measurement of the increase in the fluorescence signal from the fluorescent substrate (6,8-difluoro-4-methylumbelliferyl phosphate), and the initial linear portion of the slope (signal/min) was analyzed. Two independent experiments were performed, and the incubations and measurements were performed in duplicate (technical replicates). The assays were carried out at Reaction Biology Corp. (Malvern, PA, USA).

#### Heat shock protein 90 kDa fluorescence competitive binding assay

This assay is based on the competition of fluorescently labeled geldanamycin for binding to HSP90. The fluorescent substrate binds to the ATP binding pocket of HSP90; therefore, an ATP-competitive

inhibitor was found by this assay. The assay was carried out at Reaction Biology Corp. (Malvern, PA, USA).

### Molecular modeling and docking

The full-length three-dimensional structure of human AhR has not been resolved. The structure available from alpha fold database consists of several unstructured regions that are unsuitable for understanding the binding mode of carvones. Further, a recent effort by Bourguet's group has resulted in a high resolution cryo EM structure of indirubin bound HSP90-XAP2-AhR complex<sup>48</sup> but could not be used for understanding the binding mode of carvones as the cryo EM studies failed to resolve the coordinates for the 270 residues from the N-terminal region. The crystal structure complex of a construct of human AhR with a truncated mouse ARNT has been solved (PDB code: 5NJ8)<sup>49</sup>. Since the solved structure does not contain the LBD of AhR, it was modeled based on neuronal PAS-1 protein (PDB code: 5SY5)<sup>47,50</sup>. The molecular structures of carvones were modeled using the ligand builder module of Molecular Operating Environment (MOE ver 2018; Chemical Computing Group; Montreal, Canada). The molecules were energy minimized and geometry optimized for docking studies. Since carvones occupy a small volume and have the potential to bind nearly any binding pocket, we utilized a triage-based approach to finalize the predicted binding pocket. We screened the PAS-B domain of AhR containing the binding pockets for TCDD, FICZ, BaP, CH-223191, vemurafenib, dabrafenib, PLX7904, PLX8394, and resveratrol as detailed in<sup>14</sup> and our newly developed methylindoles<sup>47</sup>. Pockets including TCDD were used as a control for each of these dockings. All docking screening experiments were performed using GOLD version 5.2 (Cambridge Crystallographic Data Centre, Cambridge, UK)<sup>51</sup>. The complexes were ranked using the default option of GOLD SCORE, and the best-ranking complexes were visualized in MOE. The molecules were also docked to AhR derived from the AhR-ARNT complex. S-carvone-bound AhR was then energy minimized and subjected to molecular dynamics simulation with a production run of 10 ns. The docked protein complex of AhR protein with S-carvone was incorporated into an aqueous rectangular box having a dimension of 106 nm × 106 nm × 106 nm. Potassium chloride (0.15 M) was added with extra ions to neutralize the excess charges. The water molecules were modeled as TIP3P water. The initial minimization and equilibration were carried out in our local server using the NAMD software (Version 2.15) and CHARMM36 forcefield. The force field for the ligand was generated using CHARMM General Force Field (CGenFF) program version 2.5.1. The production simulation was carried out on the Anton2 supercomputer at the Pittsburgh Supercomputing Center for 400 ns with a 2.5 fs time step. Simulations were run in the NPT ensemble at 310 K and 1 bar using the Nose-Hoover thermostat and the MTK barostat. The cutoff distances for nonbonded interactions were determined automatically by Anton2. Structural snapshots were taken at 10 ns, 100 ns, and 250 ns timepoints and the binding mode of carvone was assessed for the specificity of binding.

### Thermal shift assay

Human AHR 112-272 aa (domain PASA) was subcloned into pMKH vector to produce a his6-TEV-hAHR(PASA) construct. The plasmid was transformed into Rosetta (DE3) cells, and protein was expressed in LB media. Cells were dissolved in lysis buffer containing 20 mM Tris, pH 8.0, 500 mM NaCl, 5% Glycerol, 5 mM imidazole, protease inhibitor cocktail (#5056489001, Sigma Aldrich). Supernatant was collected after sonication and centrifugation, and then flowed through Ni-NTA His-bind resin (#70666-5, Millipore). Resin was washed 3 times with lysis buffer, and protein was eluted with 200 mM imidazole in lysis buffer. The purified protein was passed through a gel filtration column (Cytiva, HiLoad 16/600 Superdex 75) to remove aggregated protein and imidazole. His tag was removed by TEV cleavage and final hAHR(PASA) protein was pooled in size-exclusion chromatography with a Bis-Tris Propane buffer (20 mM Bis-Tris Propane, pH 8.0,

150 mM NaCl). For thermal shift assay, 50 nl of compound was transferred into 384-well plate by Echo 555 liquid handler (Labcyte), and then 5  $\mu$ l of protein solution was added into each well in a microplate dispenser (#5840300, Thermo Scientific). Protein solution was prepared by diluting hAHR(PASA) protein to 0.1 mg/mL in Bis-Tris Propane buffer, and then add SYPRO orange dye (S6650, Invitrogen) to a final concentration of 8 $\times$ . Plate was spun at 1000  $\times$ g for 10 s and incubated at room temperature for 30 min before transferring into QuantStudio 7 Flex real-time PCR machine (Applied Biosystems). Melt curve was generated by heating the plate from 25 °C to 95 °C applying a gradient of 0.1 °C/s. Data was analyzed in protein thermal shift software v1.4 (Applied Biosystems).

### Cellular thermal shift assay

Human AHR 112-272 aa (domain PASA) was subcloned into pBit3.1-N vector to produce a HiBiT-hAHR(PASA) construct. HEK293T cells were cultured in DMEM media (#31966-021, Gibco) at 37 °C, 5% CO<sub>2</sub>. The plasmid was transfected into HEK293T cells with lipofectamine 3000 (L3000001, Invitrogen), and the cells were grown to 60–80% confluence. Cells were harvested 3 days after transfection. Cells were washed two times with ice-cold PBS, scraped and suspended in Bis-Tris Propane buffer containing protease inhibitor cocktail (#5056489001, Sigma). Cells were sonicated and supernatant was collected after centrifugation. The cell lysate was diluted to 0.3 mg/mL for further analysis. 50 nl of compound solution (in DMSO) was transferred into 384-well plate with Echo 555 liquid handler (Labcyte), and 5  $\mu$ l of cell lysate was added to each well. Plate was spun at 1000  $\times$ g for 10 s and incubated at room temperature for 30 min. The plate was heated in PCR thermal cycler (Bio-Rad, C1000 Touch) at a gradient of 38–62 °C for 3 min. Denatured protein was removed by spinning plate at 4300  $\times$ g for 15 min, and soluble HiBiT-hAHR(PASA) protein was detected by Nano-Glo HiBiT lytic detection system (N3040, Promega) according to the manufacturer protocol.

### Microscale thermophoresis

A codon-optimized fragment of human AhR (Swiss-Prot database accession number AHR\_HUMAN P35869) encoding amino acid residues 23–273 was synthesized and cloned into pET28b(+) using NdeI and BamHI restriction sites to express an N-terminally fused 6 $\times$ His-tag. A codon-optimized fragment of mouse Arnt encoding amino acid residues 85–345 was synthesized and cloned into pETDuet-1 using BamHI and HindIII restriction sites, expressing N-terminally fused 6 $\times$ His-tag or using NcoI and HindIII restriction sites, expressing N-terminally FLAG-tag (GenScript, Leiden, Netherlands). A selection of truncated versions of AhR and Arnt was performed based on published data<sup>49,52</sup>. Both constructs were coexpressed in Rosetta 2 (DE3) *E. coli* cells (Novagen). Protein production was induced with 1 mM isopropyl- $\beta$ -thiogalactopyranoside, and cells were grown at 20 °C in LB medium overnight. Cells were lysed at 30 kpsi using a One-Shot cell lyser (Constant Systems Ltd.) and the addition of EDTA-free cOmplete™ protease inhibitor cocktail (Roche). B-PER complete bacterial protein extraction reagent (Thermo) and Denerase (c-Lecta) were added to the lysate. Protein heterodimers were partially purified using HisPur Cobalt columns (Thermo Fisher Scientific) to obtain solutions in the final buffer containing 20 mM HEPES, pH 7.0, 300 mM NaCl, and 5% (w/v) glycerol. The presence of AhR and Arnt proteins was verified by Western blot using anti-His-tag (mouse monoclonal, MA1-21315, dilution 1:1000, Invitrogen) and anti-FLAG-tag (rabbit monoclonal, 14793 S, dilution 1:1000, Cell Signaling Technology) antibodies, respectively. In parallel, lysates from *E. coli* were separated by electrophoresis using precast NuPAGE Bis-Tris protein gels (Thermo Fisher Scientific) and visualized by Coomassie Brilliant Blue staining. Excised gel pieces with protein bands corresponding to the expected molecular masses of recombinant AhR and Arnt were processed using in-gel digestion and peptide extraction protocols<sup>53</sup>, and

the recombinant proteins were identified by nanoflow liquid chromatography of peptides coupled to tandem mass spectrometry<sup>54</sup>.

The protein fractions were concentrated to 2 mg mL<sup>-1</sup> using 10 kDa filters (Amicon) and stored at 5 °C for 10 days. Microscale thermophoresis was used to determine S-carvone and D-limonene binding to human 6×His-tagged AhR in a complex with FLAG-Arnt. The protein (200 nM) was fluorescently labeled using a RED-tris-NTA 2<sup>nd</sup> generation dye (NanoTemper Technologies GmbH) and a 1:1 dye/protein molar ratio in the reaction buffer: 20 mM Tris-HCl, pH 7.4, supplemented with 150 mM NaCl and 0.075% Tween-20. Ligands were dissolved in ethanol (max. 0.5% final concentration in the reaction mixture). Measurements were performed on a Monolith NT.115 instrument (NanoTemper Technologies GmbH) at 25 °C with 3 s/22 s/2 s laser off/on/off times and continuous sample fluorescence recording in premium capillaries and using an excitation power of 90% and a high MST power mode. The normalized fluorescence  $\Delta F_{\text{norm}}$  [%] as a function of the ligand concentration was analyzed and concluded to reflect a ligand binding interaction.

In experiments using AhR mutants (Y76A and Y76F), the above-described procedure was applied, using wt-His-hAhR(23-273) plasmid as a template for site-directed mutagenesis (GenScript, Leiden, Netherlands).

### Covalent functionalization of AhR with azido-S-carvone

N<sub>3</sub>-S-carvone was synthesized according to a published procedure (Fig. S4D)<sup>55</sup>. His-AhR(23-273)/FLAG-Arnt(85-345) were coexpressed in T7 Express *E. coli* cells (Novagen) as described above and reconstituted (0.5 mg/mL) in 20 mM phosphate buffer (pH 7.0) using 10 kDa filters (Amicon). The protein was mixed with 10 mM N<sub>3</sub>-S-carvone and photoactivated by a 3UV Lamp (Thermo Fisher Scientific) for 1 h at 365 nm and 2 mW cm<sup>-2</sup> intensity. The reaction mixture was resolved by SDS-PAGE, and the gel was stained with QC Colloidal Coomassie S stain (Bio-Rad, Hercules, CA, USA). The protein bands of the recombinant His-AhR(23-273) segment were excised from the gel slab, and their content was subjected to in-gel digestion by SOLu trypsin (Merck, Steinheim, Germany) after a reduction followed by the carbamidomethylation of thiol groups<sup>53</sup>. Peptides from the digests were purified on ZipTip-C18 pipette tips (Merck-Millipore, Carrigtwohill, Ireland) and analyzed by MALDI-TOF/TOF MS and MSMS on an ultrafleXtreme instrument equipped with a Smartbeam II Nd:YAG laser (Bruker Daltonik, Bremen, Germany). Peptide samples (0.5 μL) were deposited on an MTP AnchorChip 384 BC MALDI target (Bruker Daltonik) by a standard dried droplet technique with α-cyano-4-hydroxycinnamic acid matrix (5 mg/mL in 50% acetonitrile containing 0.1% trifluoroacetic acid). The calibration spots on the target were made with Peptide Calibration Standard II (Bruker Daltonik) and the same matrix. The instrumental setups for acquiring mass spectra and tandem mass spectra were as described<sup>54</sup>. MS and MSMS data were processed by flexAnalysis 3.4 and BioTools 3.1 (Bruker Daltonik). Database searches (against the Swiss-Prot protein sequence database) were performed by ProteinScape 3.1 (Bruker Daltonik) and Mascot Server 2.4 (Matrix Science, London, UK) or using PEAKS Studio X (Bioinformatics Solutions, Waterloo, ON, Canada). The mass error tolerances for the MS and MSMS data-based searches were 25 ppm and 0.5 Da, respectively.

### Animal experiments

Six-week-old female C57BL/6 mice were obtained from The Jackson Laboratory (Bar Harbor, ME, USA; #000664) and housed for two weeks in the institutional vivarium before experimentation. They were co-housed for acclimatization at the vivarium for one week prior to experiments. Housing conditions: 14 h light/10 h dark cycle; temperature: 20–22 °C; humidity: 30–70%; diet: LAB Diet #5058. All clinical inspections were performed by laboratory personnel. On our animal protocol, mice were clinically inspected daily (with particular attention to ear and body skin conditions at 6–8 h intervals within a

single day). For irradiation studies, there is potential for ear bleeding, ulceration, and infection. These could result in poor movement or feeding although this was not observed in any mice over a 24 h period of observation. Mice were to be euthanized if they exhibited—poor feeding, ulcerated skin on ears, cachexia, weight loss >20% of highest basal weight, and poor drinking—mice were to be hydrated for loss of fluids (50–100 μL in 0.9% saline/PBS every 3–4 h to look for signs of reversal), shallow breathing. None of the mice in the study met any criteria for euthanasia. At the end of the experiment, all mice were euthanized by CO<sub>2</sub> asphyxiation.

The experiments were approved by the Institutional Animal Care and Use Committee of the Albert Einstein College of Medicine (New York, NY, USA; Protocol #00001405). They were performed with the following institutional and national guidelines<sup>56</sup>. Since all mice are inbred, active, and had nearly equivalent starting weights/overall body habitus, mice were randomly picked without prior knowledge of baseline weight from each cage and assigned to control versus treatment group(s) in a consecutive manner. No randomization software was used. Since this is an exploratory analysis to generate the hypothesis that carvones protect against AhR mediated UV-damage as an in vivo “proof-of-concept” for its antagonist actions on ligand-activated AhR, a priori sample size calculations for the treatment groups and controls were not conducted. Instead, given the technical difficulty of managing more than 3 mice per treatment group for the UV studies, we performed all the experimental groups in two installments spread over time using  $n = 3$ /treatment group. Thus, in total, we obtained  $n = 6$  mice/treatment, which was included in the analyses. Experiments with RT-qPCR analysis endpoints were performed separately from experiments with H&E endpoints. No mice died or had sickness to preclude and replace the sample. Mouse ears were irradiated with short-wave UV 254 nm light (distance: ~1 cm; absorbed dose: 360 mJ/cm<sup>2</sup>) using a Spectronics ENF-240C Handheld UV Lamp (Spectronics Corp., Melville, NY, USA). Chemicals were dissolved in acetone and topically applied to the skin (mouse ear). (i) BaP (1 μg) was applied in two doses (0 h, 16 h); (ii) S-carvone (960 μg) was applied 1 h before the first BaP dose; (iii) UV irradiation was applied at 0 h and –1 h. In each mouse, the left and right ears were exposed to different treatments, thereby providing internal individual controls for comparative treatments, and each animal then represents a biological repeat. The ears were collected at 24 h, and RNA was isolated using TRI Reagent® (Carlsbad, CA, USA, #1596026). Note: In these experiments, mouse positioning relative to the UV lamp is critical to get even exposures across entire ear, so this was optimized individually for each mouse. Adjustments of distance from the source and time of exposure will also need to be optimized for a given mouse since that natural ear positioning and curvature is different from each mouse.

**Ear histology & immunohistochemistry.** Following auriclectomy, the ear tissue was rinsed, fixed in 10% buffered formalin for 24 h, and embedded in paraffin. Slices (3 mm) were cut and, for sun (UV)-burned cell scoring purposes, stained with hematoxylin-eosin. The sunburn cell count was performed by HL in a single-blinded manner; the slides were decoded only after the cell count was determined. Immunohistochemical staining against gamma-H2AX-Ser139-P was performed using P-Histone H2AX primary antibody (Cell Signaling, CST9718, 1:800). Bond Polymer Refine Detection (Leica Biosystems) was used according to the manufacturer’s protocol. After staining, sections were dehydrated, and film cover-slipped using a TissueTek-Prisma and Coverslipper (Sakura). Whole-slide scanning (40×) was performed on an Aperio AT2 (Leica Biosystems). Immunohistochemistry was carried out at HistoWiz, Inc. (New York City, NY, USA). Note: In these studies, ear embedding needs to be adjusted and the cut level appropriate to obtain an accurate representation of the entire “continuous” auricular epithelium. This was optimized for each mouse ear through repeated embedding and cuts adjusted to obtain a continuous epithelial layer.



## Statistics

All statistical analyses, as well as the calculations of half-maximal effective concentration (EC<sub>50</sub>), EC<sub>80</sub>, and half-maximal inhibitory concentration (IC<sub>50</sub>) values, were performed using GraphPad Prism 8 for Windows (GraphPad Software, La Jolla, CA, USA).

The numbers of independent repeats and technical replicates are stated in the corresponding figure legends for all the experiments. Where appropriate, data were processed by one-way analysis of variance (ANOVA) followed by Dunnett's test or Student's t test. The results with *p* values lower than 0.05 were considered significant. The EC<sub>50</sub>, EC<sub>80</sub>, and IC<sub>50</sub> values were calculated using nonlinear regression by the least-square fitting method. The R-squared value was checked in all of the calculations and did not drop below 0.9. The inhibition constant (K<sub>i</sub>) was calculated using the Cheng-Prusoff equation<sup>57</sup>. In an animal experiment, the normality of the data was analyzed by Shapiro-Wilk test, the outliers were detected by Grubbs test, and the significance was determined by Mann-Whitney non-parametric test.

## Reporting summary

Further information on research design is available in the Nature Portfolio Reporting Summary linked to this article.

## Data availability

All data needed to evaluate the paper's conclusion are presented in the paper or the Supplementary Materials. Source data are available with this manuscript and have also been deposited in a publicly accessible repository: <https://doi.org/10.5281/zenodo.7764002>. Source data are provided in this paper.

## References

1. Stejskalova, L., Dvorak, Z. & Pavek, P. Endogenous and exogenous ligands of aryl hydrocarbon receptor: current state of art. *Curr. Drug. Metab.* **12**, 198–212 (2011).
2. Angelos, M. G. & Kaufman, D. S. Advances in the role of the aryl hydrocarbon receptor to regulate early hematopoietic development. *Curr. Opin. Hematol.* **25**, 273–278 (2018).
3. Bock, K. W. From TCDD-mediated toxicity to searches of physiologic AHR functions. *Biochem. Pharmacol.* **155**, 419–424 (2018).
4. Gutierrez-Vazquez, C. & Quintana, F. J. Regulation of the immune response by the aryl hydrocarbon receptor. *Immunity* **48**, 19–33 (2018).
5. Dvorak, Z. et al. JNK inhibitor SP600125 is a partial agonist of human aryl hydrocarbon receptor and induces CYP1A1 and CYP1A2 genes in primary human hepatocytes. *Biochem. Pharmacol.* **75**, 580–588 (2008).
6. Lu, Y. F. et al. Identification of 3'-methoxy-4'-nitroflavone as a pure aryl hydrocarbon (Ah) receptor antagonist and evidence for more than one form of the nuclear Ah receptor in MCF-7 human breast cancer cells. *Arch. Biochem. Biophys.* **316**, 470–477 (1995).
7. Zhou, J. & Gasiewicz, T. A. 3'-methoxy-4'-nitroflavone, a reported aryl hydrocarbon receptor antagonist, enhances Cyp1a1 transcription by a dioxin responsive element-dependent mechanism. *Arch. Biochem. Biophys.* **416**, 68–80 (2003).
8. Kim, S. H. et al. Novel compound 2-methyl-2H-pyrazole-3-carboxylic acid (2-methyl-4-o-tolylazo-phenyl)-amide (CH-223191) prevents 2,3,7,8-TCDD-induced toxicity by antagonizing the aryl hydrocarbon receptor. *Mol. Pharmacol.* **69**, 1871–1878 (2006).
9. Choi, E. Y. et al. Development of novel CH223191-based antagonists of the aryl hydrocarbon receptor. *Mol. Pharmacol.* **81**, 3–11 (2012).
10. Zhao, B. et al. CH223191 is a ligand-selective antagonist of the Ah (Dioxin) receptor. *Toxicol. Sci.* **117**, 393–403 (2010).
11. Smith, K. J. et al. Identification of a high-affinity ligand that exhibits complete aryl hydrocarbon receptor antagonism. *J. Pharmacol. Exp. Ther.* **338**, 318–327 (2011).
12. Fang, Z. Z. et al. In vivo effects of the pure aryl hydrocarbon receptor antagonist GNF-351 after oral administration are limited to the gastrointestinal tract. *Br. J. Pharmacol.* **171**, 1735–1746 (2014).
13. Bianchi-Smiraglia, A. et al. Inhibition of the aryl hydrocarbon receptor/polyamine biosynthesis axis suppresses multiple myeloma. *J. Clin. Invest.* **128**, 4682–4696 (2018).
14. Corre, S. et al. Sustained activation of the aryl hydrocarbon receptor transcription factor promotes resistance to BRAF-inhibitors in melanoma. *Nat. Commun.* **9**, 4775 (2018).
15. Hawerkamp, H. C. et al. Vemurafenib acts as an aryl hydrocarbon receptor antagonist: implications for inflammatory cutaneous adverse events. *Allergy* **74**, 2437–2448 (2019).
16. Paris, A. et al. AhR and cancer: from gene profiling to targeted therapy. *Int. J. Mol. Sci.* **22**, <https://doi.org/10.3390/ijms22020752> (2021).
17. Giovannoni, F. et al. AHR is a Zika virus host factor and a candidate target for antiviral therapy. *Nat. Neurosci.* **23**, 939–951 (2020).
18. Giovannoni, F. et al. AHR signaling is induced by infection with coronaviruses. *Nat. Commun.* **12**, 5148 (2021).
19. Bartonkova, I. & Dvorak, Z. Essential oils of culinary herbs and spices display agonist and antagonist activities at human aryl hydrocarbon receptor AhR. *Food Chem. Toxicol.* **111**, 374–384 (2018).
20. Jager, W. et al. Percutaneous absorption of the monoterpene carvone: implication of stereoselective metabolism on blood levels. *J. Pharm. Pharmacol.* **53**, 637–642 (2001).
21. Novotna, A., Pavek, P. & Dvorak, Z. Novel stably transfected gene reporter human hepatoma cell line for assessment of aryl hydrocarbon receptor transcriptional activity: construction and characterization. *Environ. Sci. Technol.* **45**, 10133–10139 (2011).
22. Chen, H. S. V. et al. Open-channel block of N-methyl-D-aspartate (Nmda) responses by memantine - therapeutic advantage against nmda receptor-mediated neurotoxicity. *J. Neurosci.* **12**, 4427–4436 (1992).
23. Mescher, M. & Haarmann-Stemmann, T. Modulation of CYP1A1 metabolism: from adverse health effects to chemoprevention and therapeutic options. *Pharmacol. Ther.* **187**, 71–87 (2018).
24. Seok, S. H. et al. Structural hierarchy controlling dimerization and target DNA recognition in the AHR transcriptional complex. *Proc. Natl Acad. Sci. USA* **114**, 5431–5436 (2017).
25. Guo, Z. et al. A method for the analysis of low-mass molecules by MALDI-TOF mass spectrometry. *Anal. Chem.* **74**, 1637–1641 (2002).
26. Long, W. P. et al. Protein kinase C activity is required for aryl hydrocarbon receptor pathway-mediated signal transduction. *Mol. Pharmacol.* **53**, 691–700 (1998).
27. Fabian, M. A. et al. A small molecule-kinase interaction map for clinical kinase inhibitors. *Nat. Biotechnol.* **23**, 329–336 (2005).
28. Smith, K. J. et al. Editor's highlight: Ah receptor activation potentiates neutrophil chemoattractant (C-X-C Motif) ligand 5 expression in keratinocytes and skin. *Toxicol. Sci.* **160**, 83–94 (2017).
29. Dawes, J. M. et al. CXCL5 mediates UVB irradiation-induced pain. *Sci. Transl. Med.* **3**, 90ra60 (2011).
30. Yuan, J., Adamski, R. & Chen, J. Focus on histone variant H2AX: to be or not to be. *FEBS Lett.* **584**, 3717–3724 (2010).
31. Sheehan, J. M. & Young, A. R. The sunburn cell revisited: an update on mechanistic aspects. *Photochem. Photobiol. Sci.* **1**, 365–377 (2002).
32. Chen, J. et al. Modulation of lymphocyte-mediated tissue repair by rational design of heterocyclic aryl hydrocarbon receptor agonists. *Sci. Adv.* **6**, eaay8230 (2020).
33. Backlund, M. & Ingelman-Sundberg, M. Regulation of aryl hydrocarbon receptor signal transduction by protein tyrosine kinases. *Cell Signal* **17**, 39–48 (2005).
34. Oesch-Bartlomowicz, B. et al. Aryl hydrocarbon receptor activation by cAMP vs. dioxin: divergent signaling pathways. *Proc. Natl Acad. Sci. USA* **102**, 9218–9223 (2005).

35. Giani Tagliabue, S. et al. Modeling the binding of diverse ligands within the Ah receptor ligand binding domain. *Sci. Rep.* **9**, 10693 (2019).
36. Scheuermann, T. H. et al. Allosteric inhibition of hypoxia inducible factor-2 with small molecules. *Nat. Chem. Biol.* **9**, 271–276 (2013).
37. Vogeley, C. et al. The aryl hydrocarbon receptor in the pathogenesis of environmentally-induced squamous cell carcinomas of the skin. *Front Oncol.* **12**, 841721 (2022).
38. Tigges, J. et al. The new aryl hydrocarbon receptor antagonist E/Z-2-benzylindene-5,6-dimethoxy-3,3-dimethylindan-1-one protects against UVB-induced signal transduction. *J. Invest. Dermatol.* **134**, 556–559 (2014).
39. Corrada, D. et al. Deciphering dimerization modes of PAS domains: computational and experimental analyses of the AhR:ARNT complex reveal new insights into the mechanisms of AhR transformation. *PLoS Comput. Biol.* **12**, e1004981 (2016).
40. Corrada, D., Denison, M. S. & Bonati, L. Structural modeling of the AhR:ARNT complex in the bHLH-PASA-PASB region elucidates the key determinants of dimerization. *Mol. Biosyst.* **13**, 981–990 (2017).
41. Wu, D. et al. Structure and dimerization properties of the aryl hydrocarbon receptor PAS-A domain. *Mol. Cell Biol.* **33**, 4346–4356 (2013).
42. Sanchez-Linares, I. et al. High-throughput parallel blind virtual screening using BINDSURF. *BMC Bioinformatics* **13**, S13 (2012).
43. Mascher, H., Kikuta, C. & Schiel, H. Pharmacokinetics of menthol and carvone after administration of an enteric coated formulation containing peppermint oil and caraway oil. *Arzneimittelforschung* **51**, 465–469 (2001).
44. Bartonkova, I. & Dvorak, Z. Essential oils of culinary herbs and spices activate PXR and induce CYP3A4 in human intestinal and hepatic in vitro models. *Toxicol Lett.* **296**, 1–9 (2018).
45. Maier, L. et al. Extensive impact of non-antibiotic drugs on human gut bacteria. *Nature* **555**, 623–628 (2018).
46. Denison, M. S. et al. Analysis of the aryl hydrocarbon receptor (AhR) signal transduction pathway. *Curr. Protoc. Toxicol.* <https://doi.org/10.1002/0471140856.tx0408s11> (2002).
47. Stepankova, M. et al. Methylindoles and methoxyindoles are agonists and antagonists of human aryl hydrocarbon receptor. *Mol. Pharmacol.* **93**, 631–644 (2018).
48. Gruszczyk, J. et al. Cryo-EM structure of the agonist-bound Hsp90-XAP2-AHR cytosolic complex. *Nat. Commun.* **13**, 7010 (2022).
49. Schulte, K. W. et al. Structural basis for aryl hydrocarbon receptor-mediated gene activation. *Structure* **25**, 1025–1033.e3 (2017).
50. Wu, D. et al. NPAS1-ARNT and NPAS3-ARNT crystal structures implicate the bHLH-PAS family as multi-ligand binding transcription factors. *Elife*, **5** <https://doi.org/10.7554/eLife.18790> (2016).
51. Jones, G., Willett, P. & Glen, R. C. Molecular recognition of receptor sites using a genetic algorithm with a description of desolvation. *J. Mol. Biol.* **245**, 43–53 (1995).
52. Puyskens, A. et al. Aryl hydrocarbon receptor modulation by tuberculosis drugs impairs host defense and treatment outcomes. *Cell Host Microbe* **27**, 238–248.e7 (2020).
53. Shevchenko, A. et al. In-gel digestion for mass spectrometric characterization of proteins and proteomes. *Nat. Protoc.* **1**, 2856–2860 (2006).
54. Petrovska, B. et al. Proteomic analysis of barley cell nuclei purified by flow sorting. *Cytogenet. Genome Res.* **143**, 78–86 (2014).
55. Xu, B. et al. Total Synthesis of (-)-Daphenylline. *Angew. Chem. Int. Ed. Engl.* **58**, 5754–5757 (2019).
56. Percie du Sert, N. et al. The ARRIVE guidelines 2.0: updated guidelines for reporting animal research. *BMJ Open Sci.* **4**, e100115 (2020).
57. Cheng, Y. & Prusoff, W. H. Relationship between the inhibition constant (K1) and the concentration of inhibitor which causes 50 per cent inhibition (I50) of an enzymatic reaction. *Biochem. Pharmacol.* **22**, 3099–3108 (1973).

## Acknowledgements

Financial support from the Czech Health Research Council [NV19-05-00220] (to Z.D.), the Czech Science Foundation [23-04662S] (to Z.D.), the National research council at the National Academies of Science and Pittsburgh supercomputing facility for use of Anton2 with grant [MCB210021P] (to S.K.), and the Juergen Manchot Foundation (to K.M.R.) are acknowledged. We thank Dr. Radka Končítiková for assistance with the microscale thermophoresis experiments and Dr. David Vanda for support with the synthesis of azidocarvone.

## Author contributions

Participated in research design: Z.D., T.H.S., S.M. Conducted experiments: K.O., B.V., I.Z., K.K., E.M., R.V., P.N., K.M.R., S.K., D.K., M.K., M.Š., H.L., M.S., H.P., B.N. Contributed new reagents and analytic tools: Z.D., T.H.S., S.K. Performed data analysis: K.O., B.V., I.Z., K.K., E.M., R.V., P.N., K.M.R., S.K., Z.D., D.K., M.K., M.Š., H.L., H.P., F.R., B.N. Wrote or contributed to the writing of the manuscript: Z.D., T.H.S., S.M., S.K.

## Competing interests

The authors declare no competing interests.

## Additional information

**Supplementary information** The online version contains supplementary material available at <https://doi.org/10.1038/s41467-023-38478-6>.

**Correspondence** and requests for materials should be addressed to Sridhar Mani or Zdeněk Dvořák.

**Peer review information** *Nature Communications* thanks Sandro Cosconati and the other, anonymous, reviewer(s) for their contribution to the peer review of this work. A peer review file is available.

**Reprints and permissions information** is available at <http://www.nature.com/reprints>

**Publisher's note** Springer Nature remains neutral with regard to jurisdictional claims in published maps and institutional affiliations.

**Open Access** This article is licensed under a Creative Commons Attribution 4.0 International License, which permits use, sharing, adaptation, distribution and reproduction in any medium or format, as long as you give appropriate credit to the original author(s) and the source, provide a link to the Creative Commons license, and indicate if changes were made. The images or other third party material in this article are included in the article's Creative Commons license, unless indicated otherwise in a credit line to the material. If material is not included in the article's Creative Commons license and your intended use is not permitted by statutory regulation or exceeds the permitted use, you will need to obtain permission directly from the copyright holder. To view a copy of this license, visit <http://creativecommons.org/licenses/by/4.0/>.

© The Author(s) 2023